CANADIAN THESES

THÈSES CANADIENNES

NOTICE

The quality of this microfiche is heavily dependent upon the quality of the original thesis submitted for microfilming. Every effort has been made to ensure the highest quality of reproduction possible.

If pages are missing, contact the university which granted the degree.

Some pages may have indistinct print especially if the original pages were typed with a poor typewriter ribbon or if the university sent us an inferior photocopy.

Previously copyrighted materials (journal articles, published tests, etc.) are not filmed.

Reproduction in full or in part of this film is governed by the Canadian Copyright Act, R.S.C. 1970, c. C-30.

AVIS

La qualité de cette microfiche dépend grandement de la qualité de la thèse soumise au microfilmage. Nous avons tout fait pour assurer une qualité supérieure de reproduction.

S'il manque des pages, veuillez communiquer avec l'université qui a conféré le grade.

La qualité d'impression de certaines pages peut laisser à désirer, surtout si les pages originales ont été dactylographiées à l'aide d'un ruban usé ou si l'université nous a fait parvenir une photocopie de qualité inférieure.

Les documents qui font déjà l'objet d'un droit d'auteur (articles de revue, examens publiés, etc.) ne sont pas microfilmés.

La reproduction, même partielle, de ce microfilm est soumise à la Loi canadienne sur le droit d'auteur, SRC 1970, c. C-30.

THIS DISSERTATION HAS BEEN MICROFILMED EXACTLY AS RECEIVED

LA THÈSE A ÉTÉ MICROFILMÉE TELLE QUE NOUS L'AVONS REÇUE

Lateral Stability and Steady-State Curving Behaviour of Railway Freight Car System with Elasto-Damper-Coupled Wheelset

Abul Karam Waizuddin Ahmed

A Thesis

in

The Department

of

Mechanical Engineering

Presented in Partial Fulfillment of the Requirements
for the degree of Doctor of Philosophy at
Concordia University
Montréal, Québec, Canada

March 1986

ISBN 0-315-30690-4

ABSTRACT

Lateral Stability and Steady-State Curving Behaviour
of Railway Freight Car System
with Elasto-Damper Coupled Wheelset

Abul Karam Waizuddin Ahmed, Ph.D
Concordia University, 1986

Conventional railway freight car systems, in general, exhibit hunting phenomenon due to self induced oscillations of the wheelsets. The hunting phenomenon increases component wear, and imposes limitation on the operating speeds. Alternatively, independently rotating wheels (IRW) within an axle eliminate hunting, however, the hunting performance of IRW is improved at the expense of wheelset guiding capabilities. In this study, an elasto-damper coupling is introduced between the IRW, and its potential to improve the critical speed of freight car system are investigated. The concept of Elasto-Damper Coupled Wheelset (EDCW) can offer a compromise between the excellent guiding capability of rigid wheelset and improved hunting performance of IRW.

This dissertation primarily investigates the influence of an elasto-damper coupling on the stability and steady-state curving behaviour of a freight car system. The evaluation of stability and curving performance of EDCW is carried out in three phases. In the initial phase of the investigation, an analytical model of a single EDCW is developed and analysis of its stability behaviour on tangent track is presented. A truck model with pseudo-car body is developed in the second phase, where the initial wheelset model is extended to incorporate truck

dynamics. Tangent track stability analysis of the truck model is carried out, and the optimal wheelset coupler parameters to maximize critical speed are established. Finally a steady-state curving model of the truck incorporating EDCW is formulated, and the influence of wheelset coupler on the curving performance is investigated.

In all phases of this study, only linearized models are considered, and the analytical models are validated in their limiting case against simulated and experimental results of conventional system. A comprehensive parametric study is carried out to examine the influence of various parameters on the stability and curving performance of an EDCW and truck incorporating EDCW systems. The results of the investigations show, that a speed dependent optimal coupler damper can provide over 100% improvement of tangent track critical speed in comparison to a conventional system. However, the steady-state curving performance of the truck with an optimal coupler is deteriorated in terms of lateral response to track curvature, when compared to that of conventional system. Since curved track may be negotiated under the guidance of flange, based on the results of this study, the concept of EDCW appears to be a strong candidate for the high speed freight cars of the future.

ACKNOWLEDGEMENTS

The author would like to thank professor S. Sankar for suggesting the topic, and providing encouragement, guidance, support, and friendship during the course of this investigation, and throughout the author's graduate career.

The author gratefully acknowledges useful discussions, and informations supplied by Dr. R.V. Dukkipati of the Railway Laboratory of National Research Council of Canada. Sincere thanks are extended to several colleagues for their valuable discussions.

The financial supports provided by NSERC and FCAC post graduate scholarship, Concordia University fellowship, and the NSERC grant: number A3685 are gratefully acknowledged.

The author is grateful to Mrs. Vicky Pelletier for her sincere effort in typing the manuscript, and to Mr. Claude Voisard for his help in preparing the figures.

Finally, the author would like to express his appreciation for the patience, faith, and encouragement of his wife, Sharmeen, and that of their parents. Last and least the author wishes to mention his daughter, Meghan, whose innocent demands made the last part of the work even tougher, who also provided a lot of enjoyment during the enormous task of completing the thesis.

TABLE OF CONTENTS

Page

APPENDIX C

SIMPLIFICATION OF WHEELSET LONGITUDINAL, ROLL, AND VERTICAL EQUATIONS

LIST OF FIGURES

Figure

Figure

Figure

Figures

Figure

Figure

Figure

LIST OF TABLES

NOMENCLATURE

a	one-half track gage, m (ft)
CG	centre of gravity
$C_{D_{AX}}$	coefficient of speed dependent coupler torsional damping as defined in Equation (5.2), N.m^2/rad (lb.ft^2/rad)
[D]	matrix containing damping elements
D_{AX}	wheelset coupler damping coefficient, N.m.s/rad (lb.ft.s/rad)
D^*_{AX}	optimal coupler damping of an EDCW to maximize critical speed of truck model, N.m.s/rad (lb.ft.s/rad)
D_{cp}	centre plate connection damping coefficient, N.m.s/rad (lb.ft.s/rad)
DOF	degrees-of-freedom
D_y	secondary suspension lateral damping coefficient, N.s/m (lb.s/ft)
D_{x_p}	primary suspension longitudinal damping coefficient, N.s/m (lb.s/ft)
D_{y_p}	primary suspension lateral damping coefficient, N.s/m (lb.s/ft)
D_{ψ_p}	primary suspension effective yaw damping coefficient, N.m.s/rad (lb.ft.s/rad)
D_{θ_w}	secondary suspension warp damping coefficient, N.m.s/rad (lb.ft.s/rad)
D_z	secondary suspension vertical damping coefficient, N.s/m (N.s/m)
d	one-half distance between side frames, m (ft)
$\bar{e}_{1_L}, \bar{e}_{2_L}, \bar{e}_{3_L}$	unit vectors at the left wheel contact point
$\bar{e}_{1_R}, \bar{e}_{2_R}, \bar{e}_{3_R}$	unit vectors at the right wheel contact point
EDCW	elasto-damper coupled wheelset
$\bar{F}_{s_p}$	force acting on wheelset model due to primary suspension, N (lb)

F_{ϕ_d}	cant deficiency (lateral unbalance) force, as defined in Equation (6.3), N (lb)
$\bar{F}_L, \bar{F}_R$	creep force on left and right wheels, respectively, N (lb)
f_{11}, f_{22}	longitudinal and lateral creep coefficients, N/wheel (lb/wheel)
f_{23}	lateral/spin creep coefficient, N.m/wheel (lb.ft/wheel)
f_{33}	spin creep coefficient, $N.m^2$/wheel ($lb.ft^2$/wheel)
g	acceleration due to gravity, m/s^2 (ft/s^2)
h	distance between bolster and car body controid, m (ft)
h_{CG}	distance between rail and centroid of the truck model, m (ft)
$\bar{H}_G$	angular momentum of wheelset about its centroid, $kg.m^2/s$ ($slug.ft^2/s$)
$\bar{H}_{G_L}, \bar{H}_{G_R}$	angular momentum of left and right wheels about the wheelset centroid, $kg.m^2/s$ ($slug.ft^2/s$)
I_{B_1}, I_{B_3}	bolster mass moment of inertia about longitudinal and vertical axes, kg. m^2 ($slug.ft^2$)
I_{C_1}	car body centroid mass moment of inertia about longitudinal axis, $kg.m^2$ ($slug.ft^2$)
$I_{w_1}, I_{w_2}, I_{w_3}$	wheelset centroid mass moment of inertia about longitudinal, lateral and vertical axes, kg m^2 ($slug.ft^2$)
I_{s_3}	side frame centroid mass moment of inertia about vertical axis in yaw, $kg.m^2$ ($slug.ft^2$)
$\hat{i}', \hat{j}', \hat{k}'$	unit vectors for wheelset body axes
$\hat{i}''', \hat{j}''', \hat{k}'''$	unit vectors for wheelset fixed reference axes
[K]	matrix containing stiffness elements
k_{AX}	wheelset coupler torsional stiffness in parallel N.m/rad (lb.ft/rad)

k'_{AX}	wheelset coupler torsional stiffness in series, N.m/rad (lb.ft/rad)
k_{cp}	centre plate connection stiffness coefficient, N.m/rad (lb.ft/rad)
k_y	secondary suspension lateral stiffness coefficient, N/m (lb/ft)
k_{x_p}	primary suspension longitudinal stiffness coefficient, N/m (lb/ft)
k_{y_p}	primary suspension lateral stiffness coefficient, N/m (lb/ft)
k_z	secondary suspension vertical stiffness coefficient, N/m (lb/ft)
k_{ψ_p}	primary suspension effective yaw stiffness coefficient, N.m/rad (lb.ft/rad)
k_{θ_w}	secondary syspension warp stiffness coefficient, N.m/rad (lb.ft/rad)
l	one-half distance between wheelsets, m (ft)
m_B	bolster mass, kg (slugs)
m_c	car body mass, kg (slugs)
m_s	mass of each side frame, kg (slugs)
m_w	wheelset mass, kg (slugs)
$[M]$	matrix containing inertia elements
$\bar{M}_L, \bar{M}_R$	moment due to creep on left and right wheel, respectively, N.m (lb.ft)
$\bar{M}_{AX}$	moment due to wheelset coupler, N.m (lb.ft)
$\bar{M}_{AX_L}, \bar{M}_{AX_R}$	moment due to wheelset coupler on left and right wheels, respectively, N.m (lb.ft)
$\bar{M}_{cp}$	moment due to centre plate connection, N.m (lb.ft)
$\bar{M}_{s_p}$	moment due to primary suspension, N.m (lb.ft)
$\bar{N}_L, \bar{N}_R$	normal force on left and right wheels, respectively, N (lb)

R	radius of track curvature, m (ft)
$\bar{r}_{CG}$	position vector of wheelset centroid
r_L, r_R	instantaneous rolling radii of left and right wheels, m (ft)
$\bar{r}_{L_C}$, $\bar{r}_{R_C}$	position vector of left and right wheel point of contact, respectively
r_o	wheel rolling radius at equilibrium, m (ft)
t	time, s
V	forward velocity, m/s (ft/s)
W_{APP}	axle load, N (lb)
W_{APP}	applied load to wheelset, N (lb)
x, y, z	longitudinal, lateral, and vertical displacements of wheelset model, m (ft)
y_c	lateral displacement of pseudo-car body, m (ft)
y_T	lateral displacement of truck frame, m (ft)
y_{w_1}, y_{w_2}	lateral displacement of leading and trailing wheelsets w.r.t. truck, m (ft)
y_1, y_2	lateral displacement of leading and trailing wheelsets, respectively, m (ft)
y_1^*, y_2^*	lateral displacement of leading and trailing wheelsets from pure rolling line (curved track), m (ft)
α_i	real part of i-th eigenvalue
β	half the differential spin between left and right wheels, rad
β_L, β_R	spin displacement of left and right wheels, respectively, rad
β_i	intermediate spin variable between coupler stiffness and damper in series, rad
β_1, β_2	relative spin between β_L and β_i, and β_R and β_i as defined after Equation (2.41), rad

β_{1_w}, β_{2_w}	half the differential spin between left and right wheels of leading and trailing wheelsets, respectively, rad
Γ	wheelset roll angle coefficient
δ_0	wheel/rail contact angle at equilibrium, rad
δ_L, δ_R	wheel/rail contact angle of left and right wheels, respectively, rad
Δ	wheel/rail contact angle coefficient
ζ	damping ratio
η_i	immaginary part of i-th eigenvalue
θ_w	warp displacement of truck frame, rad
λ	effective wheel conicity
μ_i	eigenvalue corresponding to i-th mode
ϕ	wheelset roll angle, rad
ϕ_c	roll displacemtnt of pseudo-car body, rad
ϕ_d	cant deficiency as defined in Equation (6.2)
ϕ_{se}	track superelevation, rad
ϕ_T	roll displacement of truck frame, rad
ψ	yaw displacement of wheelset model, rad
ψ_T	yaw displacement of truck frame, rad
ψ_{w_1}, ψ_{w_2}	yaw displacement of leading and trailing wheelstes with respect to truck frame, rad
ψ_1, ψ_2	yaw displacement of leading and trailing wheelsets, respectively, rad
ψ_1^*, ψ_2^*	yaw displacement of leading and trailing wheelsets from radial alignment on curved track, rad
Ω	angular velocity of wheelset at equilibrium, rad/s
$\bar{\omega}_L$, $\bar{\omega}_R$	angular velocity of left and right wheels, respectively, rad/s

$\bar{\omega}_{L_c}$, $\bar{\omega}_{R_c}$	angular velocity of left and right wheel contact point, respectively, rad/s
ω_n	natural frequency, rad/s
ω_d	damped natural frequency, rad/s
$\dot{}$	first derivative with respect to time
$\ddot{}$	second derivative with respect to time

CHAPTER 1

INTRODUCTION AND LITERATURE REVIEW

1.1 General

The importance of railways around the world for commerce and development is self-evident. In the modern days, rail transportation system provides dependable, and economical movement for both freight and passengers. In the light of ever increasing energy requirements and limited supplies of fossil fuels, there is every chance that there will be a compelling cost benefit derived from a switch of road to rail transport. For heavy freight, railway always has been the most energy-efficient overland mover.

The rail-vehicle has been in existence for over 150 years, and still operates on the same basic principle, as when the first railway system was designed. It uses rigid steel wheel-axle set, where each wheel have conical tread with flange, and runs on a set of steel track. This di-cone configuration of wheelset was a brilliant concept, that simultaneously provides guidance, support, and traction. This conventional rigid axle wheelset, as shown in Figure 1.1, acts as a restoring mechanism by providing lateral guidance on the track, whenever they are deviated from central position. This arrangement also aids in curve negotiation, where lateral displacement of wheelset effectively increases and reduces the rolling radius of outer and inner wheels respectively, in an attempt to allow pure rolling motion of the wheelsets.

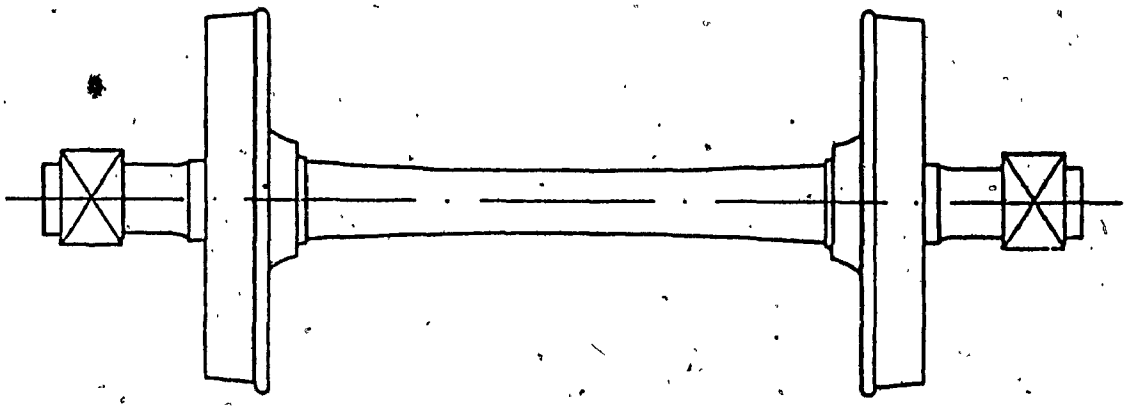

Figure 1.1 Conventional rail vehicle wheelset.

Although, the concept is very simple, the dynamics of the resulting motion is of highly complex nature. Over the years, researchers were challenged with the understanding of the railway wheels and vehicle motion resulting from complex interaction among the system components. In practice, the conventional wheelsets are well known to exhibit lateral oscillations about the center of the track in an unstable manner. The dynamics resulting from the moving contact points between wheel and rail are of as much concern today as they were, when the system was first designed. When a wheelset under load, rolls over the rails a contact region is formed at the point of contact, where the actual forward velocity is not the same as pure rolling forward velocity. These deviations generate creepages and result in creep forces at the contact point. At sufficiently high speeds, the creep forces absorb energy from the propulsion force and allow the amplitude of oscillation to grow. This motion limited by the flange of the wheel is severe at critical speed, which for some cars can be as low as 72 km/h (45 mph) [1]. This can result in axles slamming from rail to rail with impacting flange, and may lead to derailment, if unchecked.

In general, the wheelsets for all rail vehicles are identical , but the types of rail vehicle are countless. In broad sense, beside locomotive, there are two types of railway cars, i.e. passenger and freight cars. Over the years, considerable attention has been given to the development of passenger vehicles and resulted in considerable improvement in terms of speed, safety, and comfort. This however, has been achieved through innovative design of vehicle components to isolate the problem and not by tackling the problem itself, i.e. wheelset oscillations. On the other hand, practically nothing has been done for

the physical development of freight cars.

For both freight and passenger cars, the weight of vehicle is transmitted to the rails through trucks or bogies via secondary suspension. Normally, there is a truck at each end of the vehicle, where each truck consists of two wheel-axle sets, that are connected to the truck frame through primary suspension. A typical North American freight car is shown in Figure 1.2. Figure 1.3 shows a conventional three-piece truck assembly consisting of two side frames and a bolster. The main difference between freight truck and passenger truck is that in case of freight truck, the frame is relatively less rigid, and there are no intentional primary suspensions between the wheelsets and truck frame. Also for freight truck, dry friction is present in secondary suspension.

During operation, the lateral oscillations of the wheelset result in truck following a sinusoidal path on a tangent track. This phenomenon commonly known as "hunting", first becomes apparent as damped response and then as a dramatic increase at a threshold speed known as "critical speed". Continued operation near the critical speed causes severe hunting and may lead to derailment. In practice, two different and distinct hunting modes are commonly observed, i.e. body hunting or primary hunting, and truck hunting or secondary hunting. The primary hunting mode occurs over a limited speed range with lower and upper bounds, and is initiated when truck oscillation frequency coincides with natural frequency of car body lateral mode. This can be viewed as a resonance behaviour, and can be taken care of by proper design of secondary suspension. The secondary or truck hunting, on the other hand is inherent in the system, and once starts at the critical speed, it

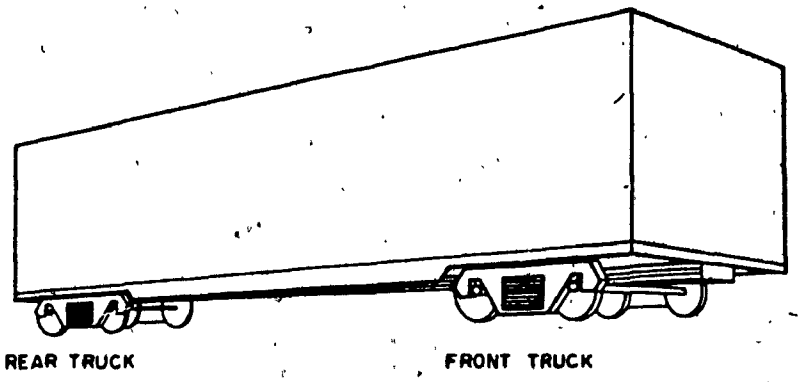

Figure 1.2 A typical North American freight car [2].

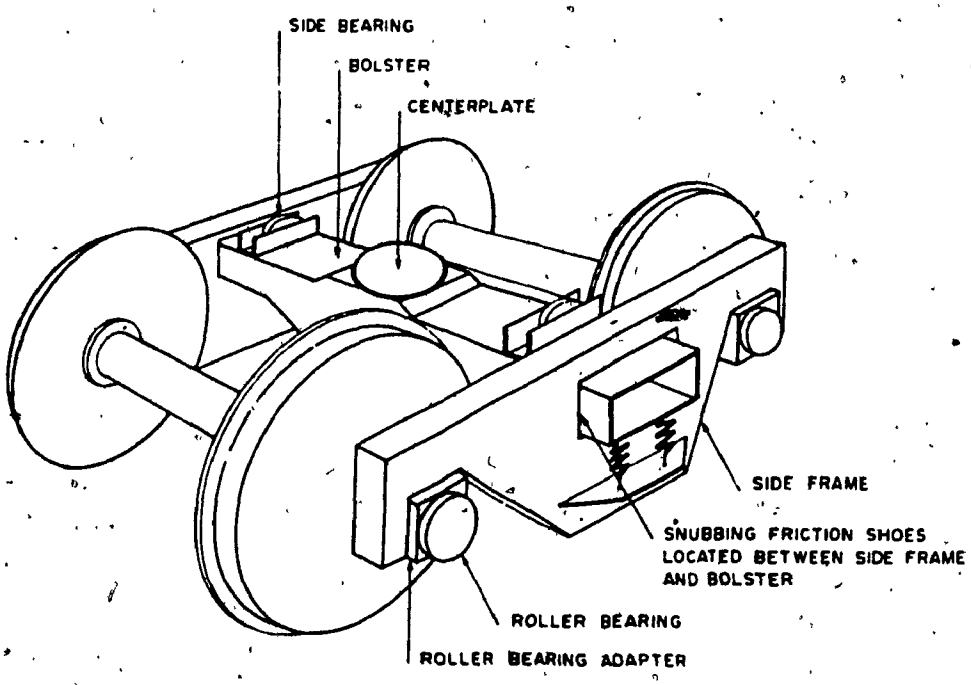

Figure 1.3 Three-piece truck configuration [2].

continues to worsen as the vehicle speed is increased. The truck hunting critical speed is therefore, of prime concern for increasing operating speed.

This investigation is primarily concerned with the railway freight car dynamics, more specifically, the effect of elasto-damper coupled wheelset on the dynamics of freight car. In such a investigation, the various aspects that need to be considered are: stability, curving and vibration response. Since the lateral instability is the critical problem, this study mainly deals with lateral stability analysis of freight car system with elasto-damper coupled wheelset. Further, it is known, that stability performance on tangent track and curving performance of conventional system have conflicting requirements. This study hence, includes both tangent track and curving analyses. Only linearized models of a single wheelset and truck with pseudo-car body are considered for lateral stability analysis on a tangent track. For steady-state curving analysis, the truck model with pseudo-car body is considered. Conventional models of same complexity are also considered to aid in model validation and comparison.

1.2 Literature Review

In the last two decades, extensive research work has been carried out in the field of railway vehicle dynamics, with prime objective of increasing operating speed, improving safety, improving ride quality, and reducing wear and maintenance. A good number of these were devoted to understanding the complex dynamic behaviour of conventional rail vehicle system. An excellent survey of rail vehicle dynamic research prior to

1974 was published by Law and Cooperrider [1]. This report presented an outline of major analytical efforts with special emphasis on lateral dynamics of conventional system. Very recently, Garg and Dukkipati [2] have published a book entitled "Dynamics of Railway Vehicle Systems". This book presents wide aspects of rail vehicle dynamic analysis through mathematical modeling of conventional system.

Based on the understanding of the conventional system behaviour and limitations, over the years, researchers have also directed their attention towards modified or "unconventional" systems. For the sake of easy understanding, in this thesis the conventional and unconventional systems are defined as follows:

- Conventional system:
  - Is a freight car system with conventional three-piece truck, and rigid axle di-cone wheelset.

- Unconventional system:
  - Is a freight car system with conventional three-piece truck, and with independently rotating wheelset (IRW), or IRW with torsional coupling between the wheels.

In the following sub-sections a review of the literature is presented under the heading of conventional and unconventional systems. Under the first heading, work on various aspects of conventional railway vehicle dynamic study are discussed with emphasis on those pertaining to this study. Under the second heading only the aspects of unconventional systems (modified version of conventional system) are discussed in a sequence so as to develop the scope of the present study.

1.2.1 Conventional System

In the case of conventional system, railway vehicle dynamics research includes a diversity of subjects. Study of all aspects by a single investigation would be a very long task if not impossible. Generally, studies are directed toward one or two specific areas. The various subjects or areas can be grouped under track and track/wheel interaction, vibration response, lateral stability, and curving. Previous investigations in these areas are briefly discussed in the following sub-sections.

1.2.1.1 Track and Track/Wheel Interaction

As the vehicle travels forward, the track irregularities cause displacement of the wheelsets and act as one of the major inputs. Therefore, the knowledge of track irregularities is important for response analysis of rail vehicles. The track geometry is commonly defined in terms of four irregularities, namely; surface, cross-level, alignment, and gage irregularities. Depending on the irregularity, tracks are divided into six classes in the United States. A well compiled review of these can be found in [2, 3]. Useful analytical expressions and statistical characterization of railway track irregularities have been developed [4, 5], which is necessary for quantitative evaluation of vehicle response. The rail road track has also been considered for the study of stress level and stability behaviour [6]. Grassie et al. carried out both analytical and experimental investigations of track response to lateral excitation [7], as well as longitudinal excitation [8]. Other studies include dynamics

of track at high vehicle speeds [9], and prediction of load environment [10]. There has also been studies investigating bridge-vehicle interactions [11].

Track/wheel studies dealing with interaction between wheel and rail is a highly important subject. The wheel-rail interaction forces have significant effect on the dynamic behaviour of railway vehicle. The various studies in this area are based on rolling contact theories, and has been considered for over 50 years, by Carter [12], Johnson and Vermenlen [13], and Kalker [14] among others. Detailed survey of research and results are not presented here, as it is to be discussed later in the thesis, where the wheel/rail forces are developed for the model under consideration. An excellent survey of wheel/rail rolling contact theories has been given by Kalker [15, 16].

1.2.1.2 Vibration Response

This area of vehicle dynamics study is concerned with the vehicle response due to track irregularities. A common assumption of linearity and symmetry allow the vertical response to be treated as independent from the lateral plane oscillation. Although response analysis is not one of the objectives in this study, the work in this area are briefly discussed here.

Vertical response of rail vehicle has been a concern to railway industry, because excessive rock and roll motion of cars are caused due to movement over half-staggered track. This problem was encountered as early as 1926 by Leffler [17]. Later through investigations [18, 19, 20], to prevent 100 ton hopper cars from frequent derailing, it was found

that when travelling at certain low speed range, the vertical track profile irregularities coincide with car's natural frequency in the rocking mode. This initiates rocking, violent enough to lift the wheels off the tangent as well as curved tracks. It was also found that cars will rock singly or as a series of cars indicating negligible effect of car to car coupling. Remedies of this problem has been sought through linear [17, 18] as well as non-linear studies [21, 22, 23] of vertical response model subjected to periodic and random rail inputs. The work at AAR [24] and Illinois Institute of Technology [25] use extremely complicated digital computer simulation program to obtain the rocking responses in the time domain under cross-level track variations. These models and others [26] represent high degree of modeling details, and require evaluation of 20 to 30 degrees-of-freedom system. The application of study in this area are primarily aimed at determining vertical and rock and roll responses of the vehicle, suspension design, and suspension optimization [23, 27].

The lateral response of rail vehicle or response to lateral and cross-level track irregularities are important to evaluate ride quality. Appropriately, the models for this study are often referred to as ride quality model [27]. Although, lateral response falls under the category of vibration response analysis it is more convenient here to discuss them together with lateral stability studies, as presented in the following sub-section.

1.2.1.3 Lateral Stability

In rail vehicle dynamic study, the prime concern is in the area of

lateral stability, due to the obvious hunting phenomenon inherent in the conventional system. A limitation on the operating speed is imposed by the critical speed of the system where hunting begins. In 1928, Carter [28] was one of the first to find, that hunting occurs above certain critical speed. The mathematical models used by various researchers to represent the actual complex system have varied considerably depending on the objective of the individual investigation. Generally, for lateral stability analysis, the track is considered to be perfectly smooth, straight, and rigid. Usually aerodynamic forces are neglected and the vehicle is assumed to be travelling at constant speed, with no braking or traction.

The simplest model considered to describe lateral stability behaviour, is a single wheelset model. Such studies have been presented by Brann [29], Wickens [30, 31], Law and Brand [32], as well as Law [33]. Although hunting of wheelset is qualitatively similar to that of complete truck, truck hunting is the critical mode in railway car lateral dynamics. Therefore, in order to predict vehicle critical speed it is necessary to consider truck or complete vehicle model. Investigations concerning lateral dynamics of truck model consisting of truck frames and two wheelsets include the studies by Wickens [30], Clark and Law [34], Cooperrider [35, 36] and Matsudaira [37]. Besides the study of suspension influence on hunting [38], extensive studies have also been carried out to determine the effect or influence of other model parameters on the lateral stability. Hannebrink et al. [39], examined the influence of axle load, track gage and wheel profile, whereas Tuten et al. [40], examined the effect of asymmetric loading and different wheel profile within one vehicle. Non-linear lateral response analysis

of wheelset [41], truck [42], and car [43], to track irregularities have also been carried out. Other previous analytical study of complete vehicle model are reported in [35, 37, 44]. There are also reports of experimental investigation of freight car lateral dynamics, using scaled model [45], as well as full-size vehicles [46]. Some studies attempted optimization of conventional system suspension [47, 48] for maximizing critical speed.

Over the years, several complex computer softwares have been developed for lateral dynamic study of railway freight cars. A recent survey of these are presented by Ramachandran et al. [49]. These softwares include, a 17-DOF linear model for frequency domain lateral stability analysis developed by Law et al. [50], a 21 DOF non-linear model for time domain response and stability analysis called HUNCT developed at Wyle Laboratories, as well as a linear model with up to 50-DOF [51], developed for both frequency and time domain analysis of response and stability, called DYNALIST.

In developing a model, the considerations mainly depend on the objective. When car body response is of concern a complete vehicle model with flexible car body should be included. But when stability is of main concern, a simplified truck model with laterally fixed body is adequate [52], since the critical truck hunting frequency is considerably above the body hunting frequency. In the study by Hadden [44], a single truck and pseudo-car body having lateral and roll motions was considered. This model can effectively show both primary and secondary hunting behaviour of freight car.

Railway freight car components, such as suspensions, as well as

wheel/rail geometry and resulting creep forces have non-linear characteristics. The model, however, can be linearized with assumption of small displacements, and using equivalent damping constants. In general, a critical speed is predicted by linearized study. Non-linear models on the other hand exhibit limit cycle behaviour. Investigations [32, 33, 35, 36], that have included flange contact force, showed that if flange contact takes place before linear critical speed is reached, there may be stable limit cycle oscillations. In another study with test vehicle, Pearce and May [53], found no limit cycle oscillation below linear critical speed. By including the effect of track flexibility and gyroscopic effect, Wickens [54] concluded that while gyroscopic force has stabilizing effect, increase in track flexibility tends to reduce the critical speed. However, the effect is negligible for current value of lateral track stiffnesses.

It is a well known fact, that the scope of limited improvement in the lateral stability or critical speed of conventional system lie mainly in reducing effective wheel conicity and increasing primary yaw stiffness. But as this investigation as well as other studies [27, 55] have shown, the opposite is necessary for improving curving performance. Due to this conflicting requirement between stability and curving performance, some studies [27, 55, 56] consider both these aspects together to evaluate performance.

1.2.1.4 Curving

The first practical curving theory for rail vehicle was reported by Mackenzie [57] in 1883. In those days, it had been generally supposed

that centrifugal force caused all axles to run in flange contact with the outer rails of the curves. But through experiments, Mackenzie showed that this is not necessarily the case. Early analytical model of rail vehicle curve negotiation were reported over fifty years ago [57, 58]. The work assumed rigid framed vehicle, and lacked appropriate treatment of wheel/rail interactions.

With better understanding of creep forces between wheel and rail, useful approach was developed by Newland [60, 61], and Boocock [62, 63]. Both considered wheelsets with flexible primary suspension and coned wheels. By linearized steady-state analysis, each developed efficient computational tool, which allows evaluation of railway car curving performance. Since then, a number of studies have been carried out using the steady-state approach. Bell et al. [55], and Hedrick et al. [27] carried out linear steady-state curving analysis of conventional rail vehicle system. This approach has also been used for non-linear models by Nagurka et al. [64], Law and Cooperrider [56], and Hedrick et al. [65] for investigating different aspects of curving behaviour. Generally, in steady-state method, the radius of curvature is assumed to be a constant with constant vehicle speed.

Another breed of curving models has been developed using quasi-steady-state approach. In this case, acceleration is ignored for a general curve negotiation. The response of the model is determined at discrete points along the track by applying the kinematic constraints. Among the studies that used this approach, are those by Elkins and Gostling [66] and Matsui [67], requiring iterative procedures. There are also reported studies that consider dynamic curving model of conventional

rail vehicle. Such studies have been carried out by Muller [68], Smith [69] as well as Law and Cooperrider [56]. In the dynamic time domain approach, the complete equations of motion are used to account for arbitrary track curvature, speed and track inputs, and needs numerical integration techniques for solutions. This approach is necessary to study curve entry and exit response, effect of track irregularities, as well as other dynamic effects.

Like any other study, the appropriate approach depends on the specific situation and need for the study. In the absence of track irregularities, all major forces and moments between vehicle components and rail may easily be obtained under steady-state condition [2]. Furthermore, linearized models provide useful qualitative behaviour and parametric sensitivity. Therefore, during a design phase or in evaluating performance of a given configuration, linear steady-state curving analysis is a reasonable approach.

Over the years, various performance indices have been developed to determine vehicles' curving ability. Survey of this is presented later in the thesis. In general, it is desirable to negotiate a curve without flange contact or wheel slip. Through investigations [60 - 63] on curving behaviour of conventional model, it has been shown that when a conventional free wheelset rolls around a curve, the wheelset displaces radially outward to assume a pure rolling line. At the same time, longitudinal creep forces generate a moment necessary to maintain the yawed position for radial alignment with the track. For restrained wheelset, as Boocock [62] notes, "... increasing the longitudinal stiffness (yaw stiffness), leads to greater lateral displacement before

sufficient longitudinal creep force are produced to yaw the wheelset by the required amount". Therefore, with larger restraints in yaw, greater lateral displacement of the wheelset takes place to generate the creep force required for equilibrium, and consequently flange contact takes place at a less tighter curve. If the creep force on the other hand is greater than maximum friction force available, the wheelset will slip [61]. However, as Newland [61] and Boocock [63] both indicated, there exists a minimum radius curve that may be negotiated by a given vehicle without wheelset slip or flanging.

As evident from the literature, curving analysis has been given less attention than response and stability analyses on tangent track. Although mainline radius of track curvature are large, considerable proportion of track is curved, and as pointed out earlier, both stability and curving analysis should be carried out to determine performance of a design.

1.2.2 Unconventional System

As defined earlier, an unconventional system is referred to as a modified conventional system, rather than new systems such as magnetically levitated trains. Due to performance limitation of conventional system, in recent years, much attention has been directed towards unconventional system with modified design of rail vehicle components, in attempt to improve operating speed. In this area of study, most attention perhaps has been given to the design of truck structure [70 - 77]. These trucks are referred to as radial trucks, where constraints are introduced between wheelsets by diagonal elastic

connections. Among various designs that have received considerable attention are: Scheffel's [70 - 73] and Scale's [74], radial truck design for passenger cars, and List's [75, 76] radial truck design for freight cars. In general, these designs provide high shear stiffness between wheelsets for stability, and low yaw (bending) stiffness between wheels to allow radial position on curves. Due to performance limitation of both conventional and radial truck vehicles [78], use of trucks which employ active control [79 - 82] has been emphasized in recent years. Active control, however, requires a power source, sensors, and actuators requiring increased maintenance. A detailed survey of these areas are outside the scope of this study, which can be found in [78] and [83].

The studies with unconventional systems discussed above are primarily aimed at isolating the inherent problem of conventional wheelset. Alternatively, limited studies have seen carried out to exploit the concept of independently rotating wheels, as well as wheels within an axle coupled through stiffness and/or damper elements. In the following sub-sections, a survey of previous studies in this area are presented and discussed.

1.2.2.1 Independently Rotating Wheelset (IRW)

The idea of IRW, where each wheel within an axle can rotate independently has been around since the mid 60's. There are some reports of adaptational, analytical, and experimental work carried out in this field, in Japan, Italy, Germany, Spain, Great Britain, United States and Canada. A brief review of these are presented in reference [84].

In 1968, a 100 tons freight car fitted with IRW was tested at

Quebec Cartier Mining Company [84], details of which are not available. A theoretical discussion on the kinematics of rail vehicle wheelset with a review of tests made on individually supported IRW system was presented by Becker [85]. This report as well as investigation carried out by Hadden and Law [86] arrived at the same conclusion. The studies showed that IRW in fact reduces the longitudinal slip and creep force drastically, reducing wheel/rail wear and energy absorbtion. As a result they do not develop lateral oscillations, and have less vibration and consequently runs quieter. However, the studies have also showed that IRW eliminates guidance capability of the wheelset along the track, which is conventionally provided by rigid di-cone wheelset. This means, that IRW do not have preferred equilibrium point, and that they may wander randomly from side to side in response to track irregularities and curves. Consequently, there exist the possibilities of greater flange wear and increased proneness to derailment as the wheels tend to run against a flange.

There are however, examples of operating systems that use the principle of IRW, such as high speed Spanish Talgo passenger trains (230 Km/h) [85]. The success of Talgo train is perhaps due to the fact that the trucks are coupled together in a form of a draw bar chain forming an articulated train system as shown in Figure 1.4. The draw bar chain system provides a manner of guidance for the wheels. Thus, it overcomes the major guidance incapability problem of IRW system. Although the Talgo train can adapt IRW, the disadvantages of this arrangement are that the train is unable to operate in reverse direction and an individual car cannot stand alone.

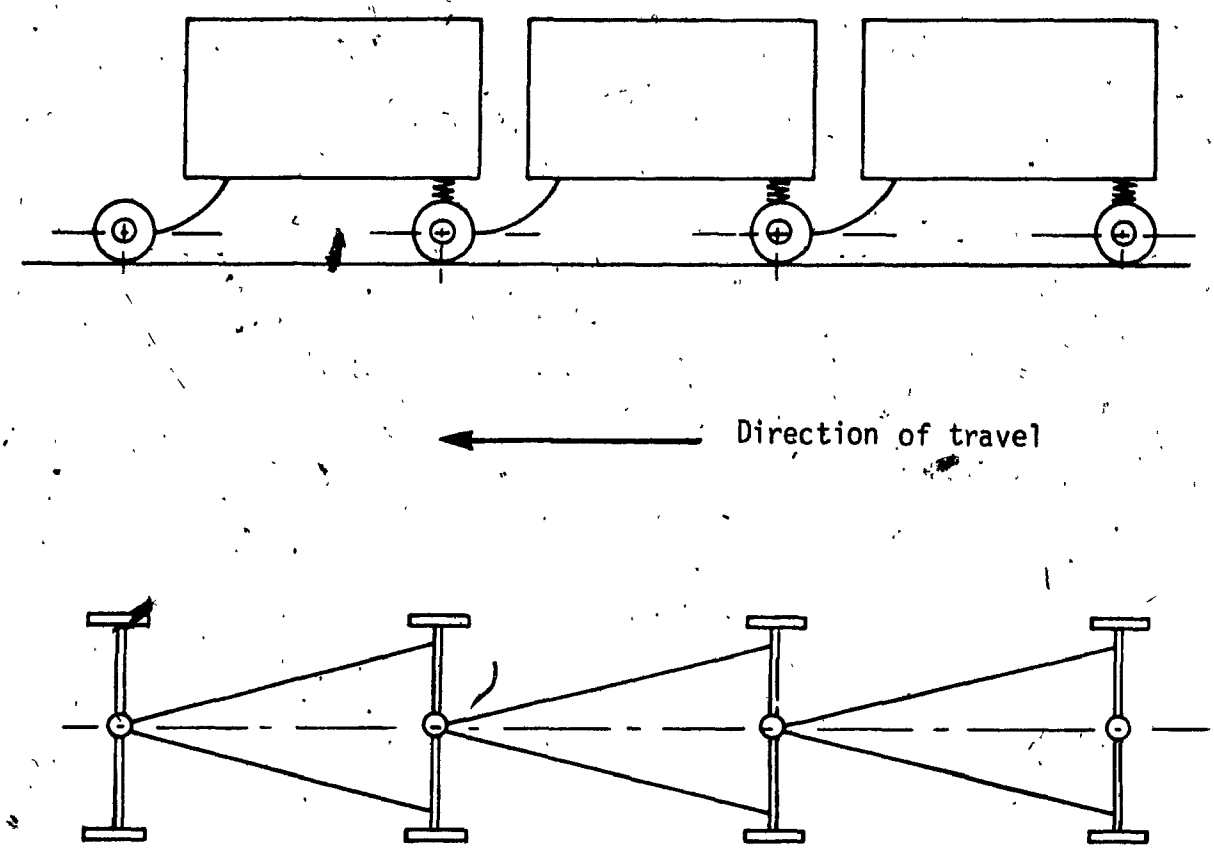

Figure 1.4 Configuration of Spanish Talgo Train with IRW [85].

In the United States, Kaplan et al. [87] carried out a feasibility study of high speed passenger rail vehicle (tube system). Their study included mathematical modeling and analysis of single wheel-axle set and two-axle truck model with IRW in an attempt to improve the conventional system. Since IRW do not have guidance capability, they suggested the use of concave wheel contact surface with single or double contact as shown in Figure 1.5, to introduce guidance. The results of the analysis indicated that the lateral response of the system can be improved significantly in comparison to conventional system. Similar idea of guidance as shown in Figure 1.6, has been in use in Germany on slowspeed Wuppertal Monorail [85]. The most obvious disadvantage of these wheel profiles is the problem of switching track as the outer arc of the wheel extends over the rail acting effectively as a flange. Furthermore, this arrangement is likely to generate excessive force on the wheels due to irregular track, and on curves.

An alternative idea of providing guidance was explored in Japan by Koyanagi [88, 89, 90], where a guide rail laid in the center of the track was used as a restoring mechanism for axle with IRW, as shown in Figure 1.7. The guidance in this arrangement is provided by a guiding carriage with suitable links, where the guiding carriage moves along the guide rail. Stability analysis of single wheel-axle set [88, 89], and two-axle track model [90] indicated, that the system is stable beyond the speed limits for hunting motion of conventional system. The analytical results were also confirmed experimentally on a one-fifth scale model to some degree of success. However, any arrangement of this nature involves major addition on the truck as well as an extra guide carriage and rail requiring maintenance. Further, this arrangement will require a

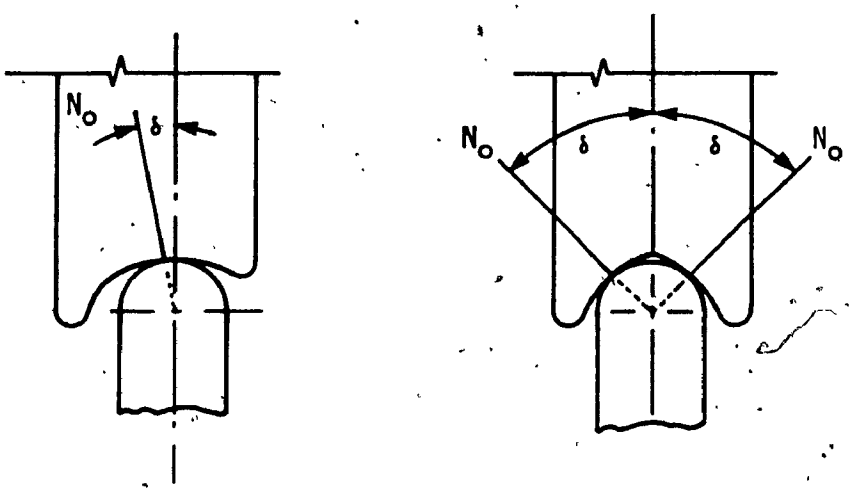

Figure 1.5 Possible contact contours for IRW [87].

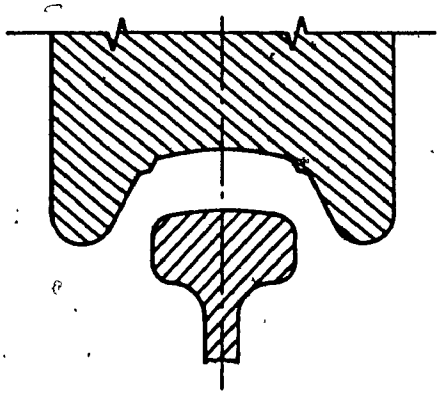

Figure 1.6 Rail and wheel profile of Wuppertal monorail [85].

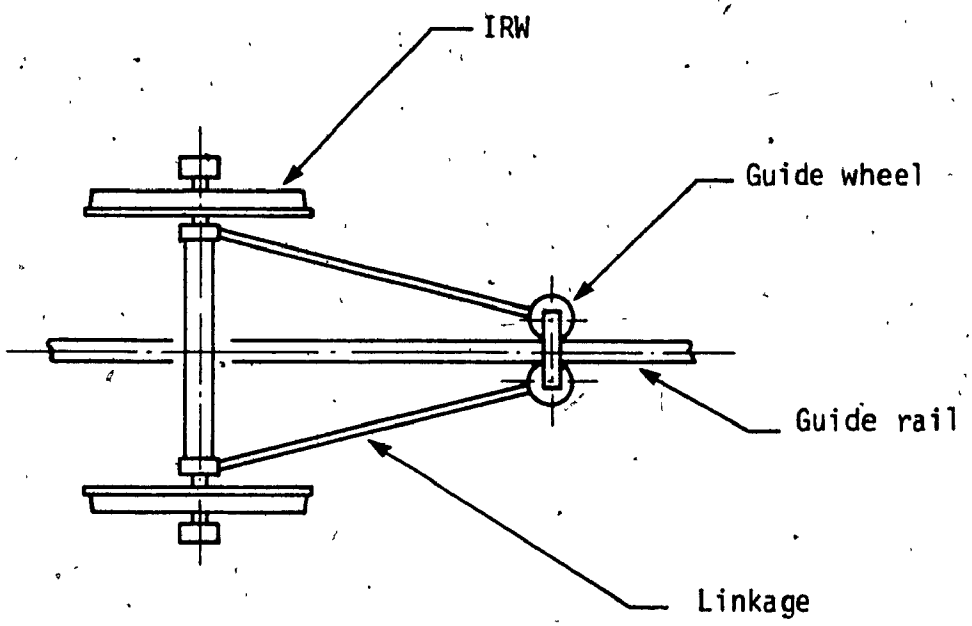

Figure 1.7 Guidance mechanism for an IRW system [89].

difficult solution to the problem of switching, and will be subjected to additional inputs from the guide rail.

Since the merits of conventional wheelset with conical wheels are very high, perhaps a more practical and effective way to provide guidance to an IRW would be through some means of coupling between two independently rotating conical wheels. In the past there has been some reports of studies in this general area, as presented in the following section.

1.2.2.2 Torsionally Coupled Wheelset

There are very few reports of published work that considers the concept of torsional coupling between independently rotating wheels as a means of improving conventional system. Since both IRW and conventional rigid axle system have their own merits, it may be possible to utilize the benefits of both these extreme cases by introducing torsional coupling between the wheels of an axle, through a stiffness and damper combination.

In an analytical investigation, Benington [91] studied a simplified single wheel-axle set, where the wheels are coupled through a damper element. The study suggested the use of a coupler that can slip at a predetermined torque. With limited study, this investigation concluded, that a damper-coupled wheelset effectively reduces the creep force, and that unlike conventional wheelset, in this case the conflict between stability and curving is not so sharp. In a later study, Benington and Greenhorn [92] considered truck model with two damper-coupled wheelsets. From the analysis of this model they note "... The basic obstacles to

correspondingly improved behaviour of the complete vehicle are very similar to those which confront the suspension designer of conventional vehicle...". In this study, no attempt was made in exploring the performance range of the system. In a much recent study Dukkipati et al. [93] used the Benington [91] single-axle model to investigate sensitivity of wheelset and suspension parameters on the stability. They found the concept of damper-coupled wheelset is useful to provide overall superior performance over the conventional rigid axle wheelset.

A more detailed model of a wheelset, studied by Hadden [44], included coupling between wheels through stiffness and damper in parallel. His investigation on the other hand, showed negligible effect of damping on the stability of wheelset hunting mode. However, damping was found effective for highly flexible axle where instability is in the wheelset spin mode. Hadden and Law [86] as well as Doyle and Prause [94] studied the effect of torsional stiffness between wheels, on the lateral stability of truck and vehicle models, respectively. Both these independent studies produced similar results. The general trend of this result [86] as shown in Figure 1.8 indicates, that the critical speed is zero until a certain torsional stiffness is reached. For torsional stiffness greater than this, critical speed increases as the torsional stiffness is increased further, where maximum critical speed is provided by a rigid axle. These studies [86, 94], however, did not explore the effect of axle torsional damping on the vehicle critical speed. Further, the study by Hadden [49] that included both single wheelset and truck model showed the effect of torsional stiffness on the stability of wheelset to be significantly different from those obtained from the truck model.

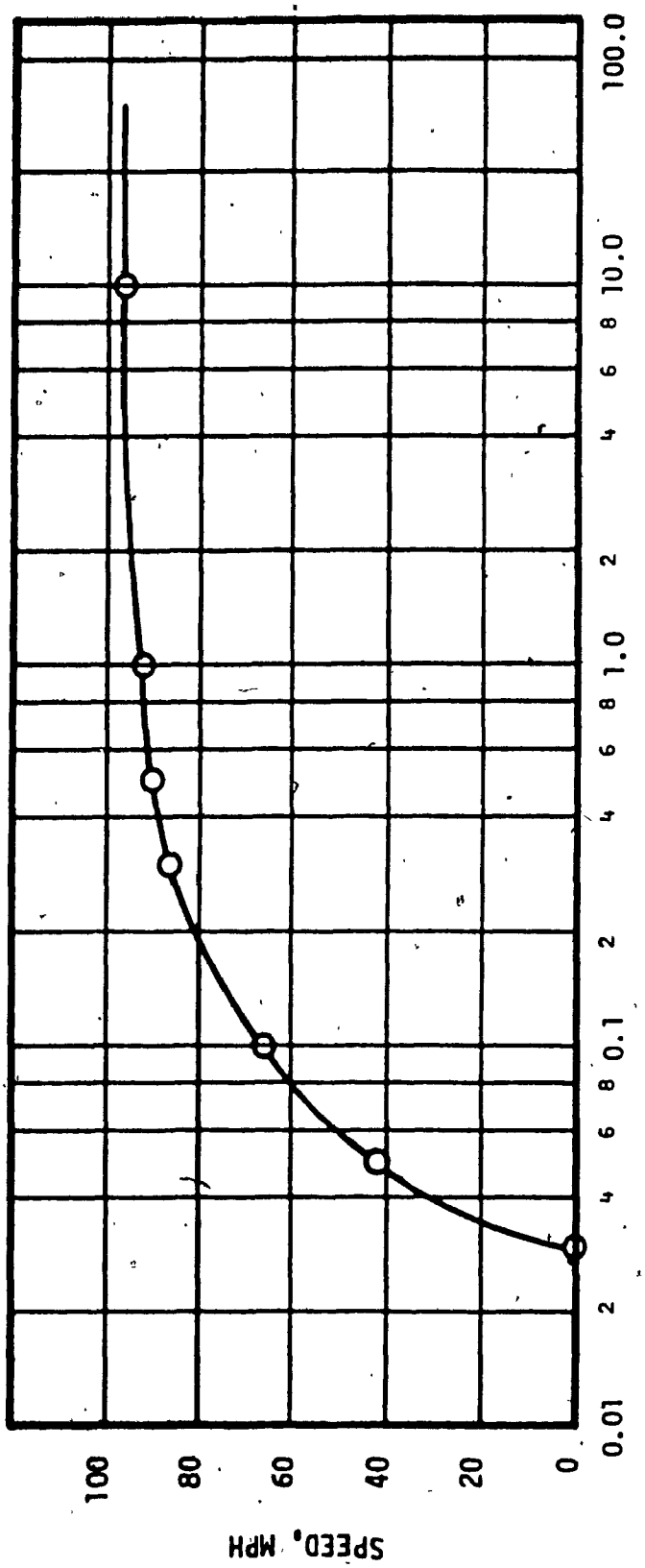

Figure 1.8 Effect of axle torsional stiffness on the critical speed of freight car system [86].

Previous studies that employed coupling between the wheels, to investigate lateral stability of wheelset, truck and freight car produced different and sometimes conflicting results. Only one previous investigation [44] considered wheelset coupling through stiffness as well as a damper. Complete investigation of the influence of this concept on the stability of freight car system, however, was not within the scope of that study. Furthermore, curving study of freight car system with such concept have never been reported.

Study of such concept, however, would not be of any use, unless the concept of coupling between the wheels can be practically implemented. Therefore, it is necessary to survey possible design of wheel-axle set that allows each wheel to rotate at different speeds and can support large loads. One such wheelset designed and manufactured for tests on passengers coaches in Italy [95], is shown in Figure 1.9. The wheelset in this design consists of two half shafts, with one wheel rigidly mounted on each shaft. The half shaft are in turn held and supported by a sleeve, through a set of bearings.

An alternative design, which consists of two wheel assembly mounted on a shaft through bearings, is shown in Figure 1.10. This arrangement was considered for study of IRW by Malavasi and Scarponi [96]. In comparing these two (Figures 1.9 and 1.10) designs, the design of wheelset in Figure 1.10 is superior in terms of simplicity, number of bearings required, and load carrying capacity. This arrangement of IRW can also be modified to incorporate coupling elements between the wheels. The modeling of elasto-damper coupled wheelset in this study is primarily based on this design.

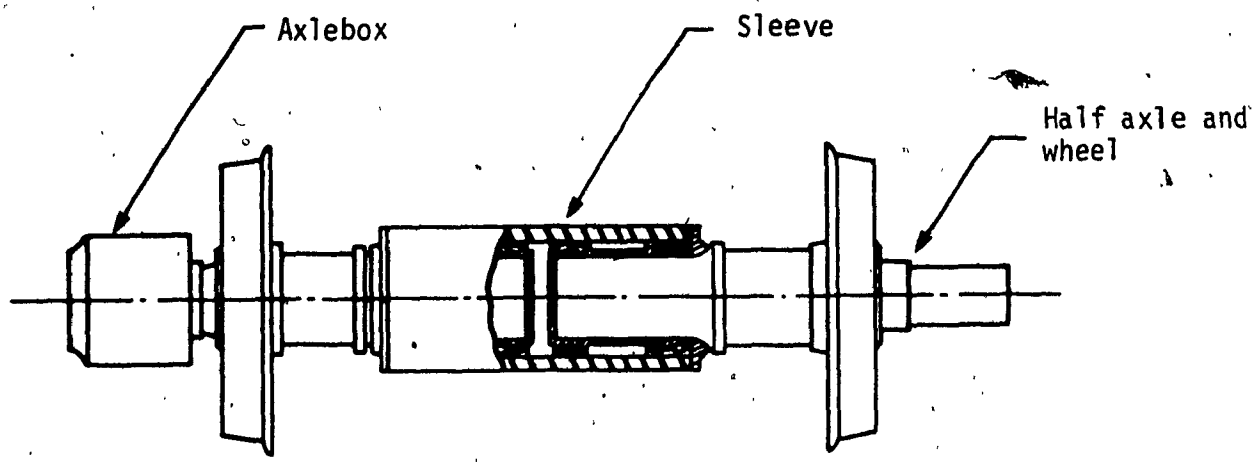

Figure 1.9 Wheelset assembly for IRW system with two part axle [95].

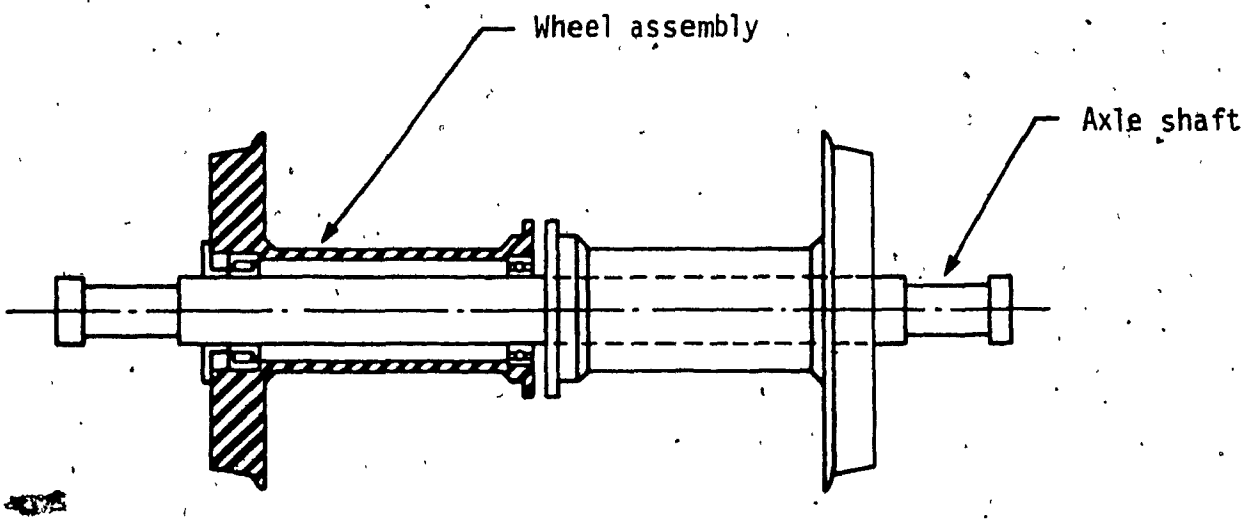

Figure 1.10 Wheelset assembly for IRW system with single axle [96].

1.3 Scope of the Present Investigation

From the literature survey of past experiences, it is evident that operating speed of conventional freight car system is primarily restricted by the truck hunting critical speed, and the root of the problem is wheelset dynamics. The scope of improving the stability behaviour or critical speed of freight car system with conventional wheelset is limited. The lateral instability (hunting) problem of conventional rigid axle wheelset can be overcome by utilizing IRW system. An IRW system, however,has its serious drawback of guiding incapability.

The existence of conventional rigid axle di-cone wheelset for so long is due to the overwhelming merits of the system. It can provide traction guidance and ability to negotiate a curve at the same time. Moreover, the di-cone arrangement of the wheelset with inner flange is convenient for switching tracks. Therefore, it would be ideal if wheelset of conventional configuration can be improved in terms of lateral stability behaviour.

The scope of this study is therefore, aimed at employing an elasto-damper coupling between independently rotating wheels of conventional shape. Such concept should yield a compromise between the excellent guiding and switching capabilities of conventional wheelset and improved hunting performance of IRW. The various benefits that may be derived from an elasto-damper coupled wheelset (EDCW) can be summarized as follows:

- reduction in longitudinal component of creep force;
- reduction in wheel/rail wear, as well as lower energy absorption;
- significant reduction in hunting phenomenon, and consequent

improved ride quality and operating speeds;

- reduction in the conflict between stability and curving that exists in conventional system.

From the review of limited previous studies that considered EDCW, evidently no constructive conclusion can be drawn regarding the influence of EDCW on the stability behaviour of freight car system. Furthermore, there are no reports of studies evaluating curving performance of freight car system with EDCW. As stated earlier, considerable portion of track length is comprised of curved track, and there are conflicting parametric requirements between stability and curving performance of freight car system. It is therefore, necessary to evaluate stability as well as curving performance for completeness.

The primary objectives of this investigation are to study the influence of elasto-damper coupling between the wheels, on the lateral stability and steady-state curving performance of freight car system. The study of stability and curving performance is carried out in three phases. An analytical model of a single EDCW is first developed and studied for stability behaviour on tangent track. As a representative of freight car system, a comprehensive truck model with pseudo-car body is formulated in the second phase, where the initial EDCW model is extended to incorporate truck motions. Tangent track stability analysis of the truck model is carried out, and optimal coupler parameters to maximize critical speed are established. Finally, a steady-state curving model of the truck incorporating EDCW is developed, and the influence of wheelset coupler on the curving performance is investigated.

In all phases of the study, only linearized models are considered,

and the analytical models are validated in their limiting case by comparing with models of conventional system. For each model considered, comprehensive parametric study is carried out to examine the influence of various system parameters.

In Chapter 2, various modeling considerations pertaining to single wheelset model are discussed. Various elements of the model are identified, and analytical expressions for each element are derived. Finally in this section, equations of motion for a single EDCW are formulated, and the assumptions made in the formulations are outlined.

Chapter 3 primarily presents the stability analysis of the EDCW model on tangent track. Results are obtained here for EDCW with three possible coupler configurations. The results are compared with those corresponding to conventional rigid axle wheelset. Influence of model parameters on the stability of EDCW in comparison to conventional wheelset are also presented and discussed in this section.

In Chapter 4, a freight truck model with a set of EDCW and pseudo-car body is developed. The wheelset model developed in Chapter 2, is extended here to include truck motions. Various elements of the truck model, and assumptions made pertaining to the formulation of truck model are discussed. Finally the equations to describe the motion of the truck on tangent track are obtained in this section.

Chapter 5 deals with the stability analysis of truck model on tangent track. Extensive study to investigate the effect of EDCW on the stability behaviour of each mode are carried out here. The optimal wheelset coupler parameter to maximize the critical speed is determined.

Limited parametric study is carried out to examine the influence of model parameters on the critical speed, as well as on the optimal coupler parameter. In all cases, results are compared with those corresponding to truck system with rigid axle wheelsets.

In Chapter 6, steady-state curving model of the truck with EDCW is presented. The model is identical to that of truck model developed in Chapter 4. In this section, various modeling considerations pertaining to curved track simulation are discussed. By introducing additional effects of a curved track, steady-state curving equations of motion for the truck model with EDCW as well as conventional wheelset are developed. Various assumptions made in the formulation of steady-state curving model are also discussed.

Chapter 7 primarily deals with steady-state curving analysis of the truck model. The indices used in determining the curving performance are discussed. Extensive analysis is carried out to study the effects of EDCW on the curving performance, in comparison to rigid axle wheelset system. This section also presents a parametric study, to determine the influence of selected model parameters on the curving performance of the truck model. Results are obtained to identify the conflicts in the parametric requirements between stability and curving performance.

Finally, in Chapter 8, the thesis is concluded with discussions on the highlights of the study. And recommendations are made for possible future work.

CHAPTER 2

ELASTO-DAMPER COUPLED WHEELSET MODELING CONSIDERATIONS AND APPROACH

2.1 Introduction

The lateral dynamic behaviour of railway vehicles is primarily dominated by wheel/rail interactions and dynamic behaviour of the wheelset itself. It is therefore, necessary to devote considerable attention in carrying out a comprehensive study of a single Elasto-Damper Coupled Wheelset (EDCW) model, and to establish an understanding of the wheelset dynamics. A single EDCW model can be considered as the initial "block" in a "building block" approach to develop comprehensive truck and complete vehicle models.

During the modeling stage, it is usually desirable to develop a simple and credible model such that the motion of a dynamical system is fully described. The simplicity of a model, in general can be determined by the number of Degrees-of-Freedom (DOF) selected to simulate a given physical system. Often increased complexity of the model in terms of increased DOF does not necessarily improve the validity of the model and may lead to difficulties in interpretations of the system behaviour. Moreover, the simulation of a complex model with large numbers of DOF is extremely demanding on computer time. The credibility of a model is determined in part by its capability to simulate the system behaviour realistically within the desired accuracy. Simplified model with essential DOF is often adequate to study the qualitative behaviour of the system. Alternatively, it may be necessary to include large numbers of DOF in the model such that the quantitative behaviour of the system can

be obtained.

In the case of railway vehicles, the prediction from the mathematical model of wheelset lateral dynamics, primarily depends on the valid data and characterization of the forces. In developing the mathematical model of EDCW, it is necessary first to identify all the forces and moments acting on the wheelset. Hence, the primary objective of this chapter is to identify and develop analytical representation of various components of EDCW system. In the following sub-sections the analytical model of a EDCW is developed, and the various considerations and assumptions associated with the modeling process are discussed. The equations of motion of the EDCW model are established to carry out its lateral stability analysis on a tangent track.

2.2 Description of an Elasto-Damper Coupled Wheelset Model

An elasto-damper coupled wheelset (EDCW) primarily consists of an axle with two independently rotating wheels, coupled through an elasto-damper combination. A possible arrangement of the wheelset is shown in Figure 2.1. Such an EDCW configuration can be modeled similar to a conventional wheelset, where each wheel experiences independent rotation, The axle of the wheelset is supported at each end through stiffness and damping in lateral, longitudinal and vertical directions, and can move in each direction with respect to the truck frame. For the single wheelset model, the truck is assumed to be the fixed reference frame that moves along the track. A schematic of the EDCW model is shown in Figure 2.2. The various degrees-of-freedom for the model are lateral, longitudinal, vertical, yaw, roll and spin. In general conventional wheelset lateral

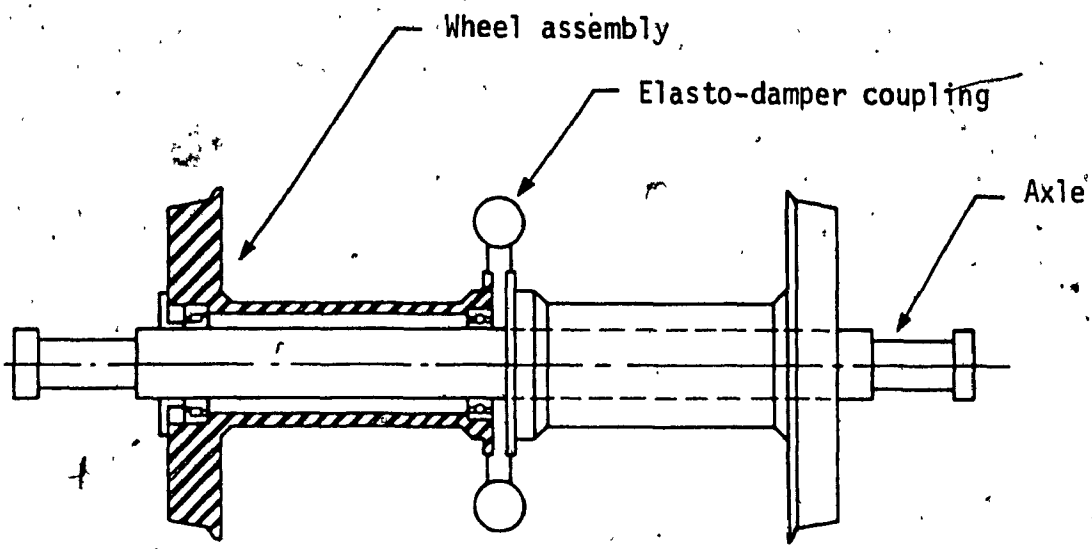

Figure 2.1 Elasto-damper coupled wheelset (EDCW) model

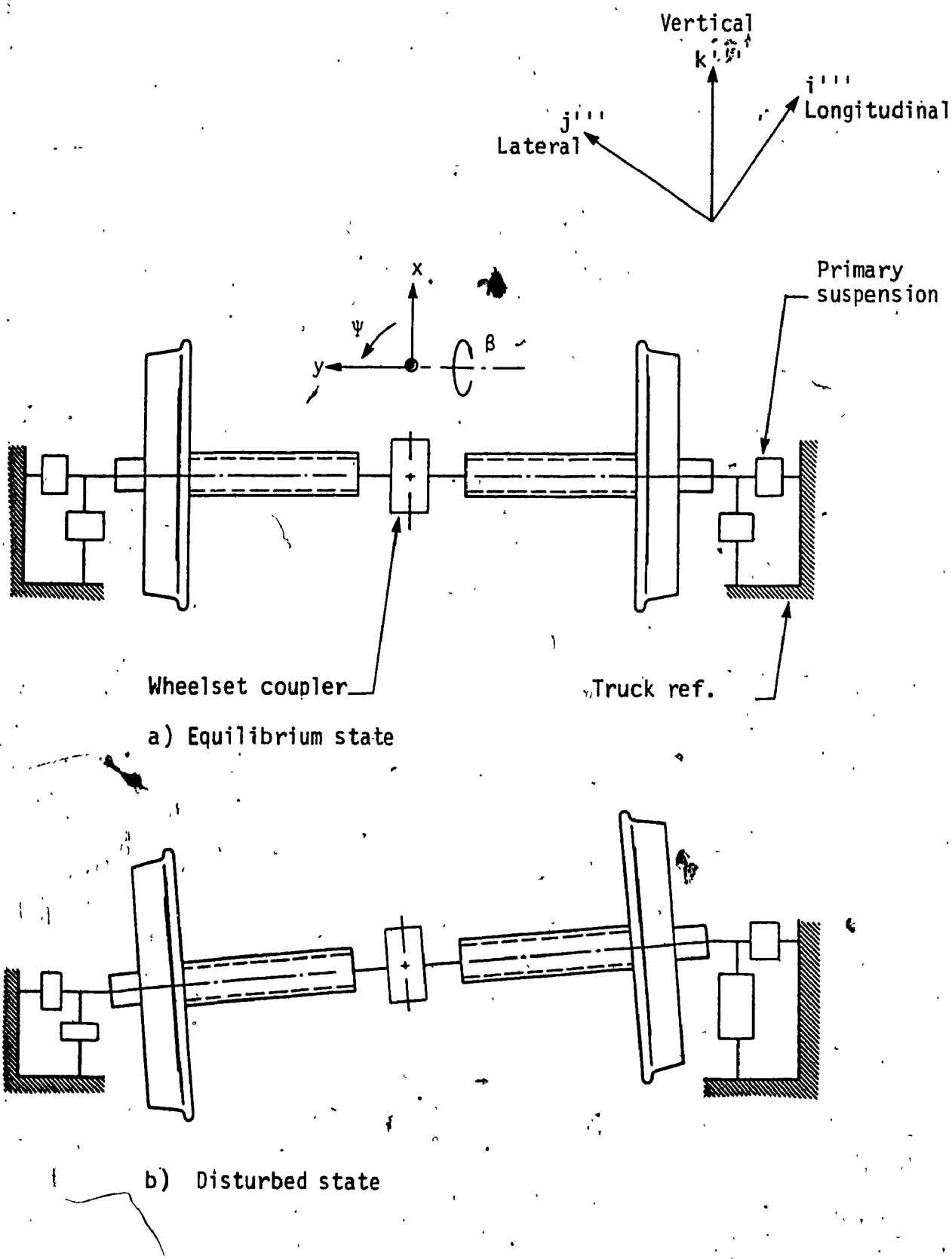

Figure 2.2 Schematic of the EDCW model (plan view)

dynamic study, considers only the lateral and yaw modes to describe the motion of the wheelset for small oscillations about its equilibrium position. In the case of an EDCW model, additional spin DOF are required to describe the motion of the system. The number of spin DOF depends on the configuration of the wheelset coupler elements. In this study three specific configurations of the coupler elements are considered. In the following section, characteristics of various components of the EDCW are identified and discussed in detail.

2.3 Modeling Considerations

The modeling task as applied to EDCW can be addressed under four areas, which are: wheel/rail interaction creep forces, normal forces, primary suspension forces, and moments due to wheelset coupler elements. The objective of this section is to discuss, identify and develop analytical expressions for the forces and moments arising from the various components of an EDCW.

2.3.1 Creep and Creep Forces

Carter [12] was among the first to establish that when a wheelset rolls over the rails, a contact region is formed at the point of contact, where the actual forward velocity is not the same as pure rolling forward velocity. The above finding by Carter [12] initiated a series of studies into the phenomenon of creep and creep forces, on the basis of rolling contact theories. Creep force on creepage are developed due to the difference in strain rates of two bodies in the contact region. Creepages are defined in both lateral (ξ_y) and longitudinal (ξ_x)

directions, as the relative velocity in each direction between the wheels and rails at contact, normalized by the forward velocity. There is another term, spin creep (ξ_{sp}) which is defined as the ratio of the relative angular velocity about the normal to the contact area and forward velocity. In Figure 2.3 these creepages at the contact plane are shown. For small values of creepage, there is a linear relationship between creepage quantities and applied creep force. However, as the creepage increases, there is a departure from linearity until ultimately there is a gross sliding of the wheels on the rails, giving a general creep characteristics as shown in Figure 2.4 [52].

As discussed briefly in literature review, the importance of creep forces to the dynamic stability of rail vehicle has been acknowledged and investigated by several researchers during the past half century. The most significant advancement in the phenomenon of creep can be attributed to Kalker [14,97] who developed linear and non-linear creep theories. Kalker's linear creepage-creep force relationship for the longitudinal and lateral creep forces are given as:

$$F_x = - f_{11}\xi_x \tag{2.1}$$

$$F_y = - f_{22}\xi_y - f_{23}\xi_{sp} \tag{2.2}$$

and the spin-creep moment as:

$$M_z = f_{23}\xi_y - f_{33}\xi_{sp} \tag{2.3}$$

where f_{ij} are creep coefficients defined as functions of normal load, the modulus of rigidity, and Poisson's ratio.

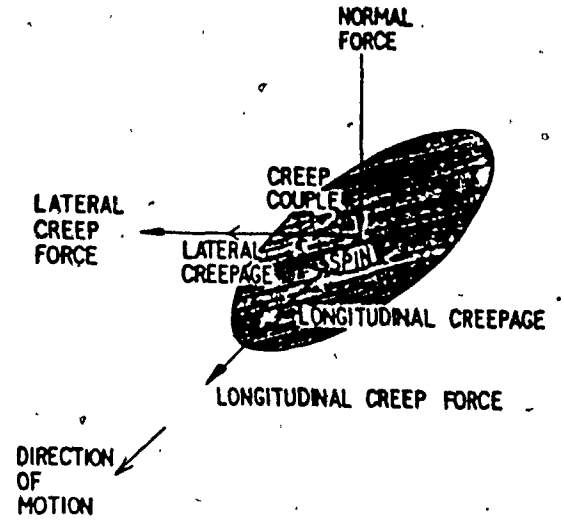

Figure 2.3 Deviation from pure rolling described in terms of creepages, that give rise to corresponding creep forces and couple [52].

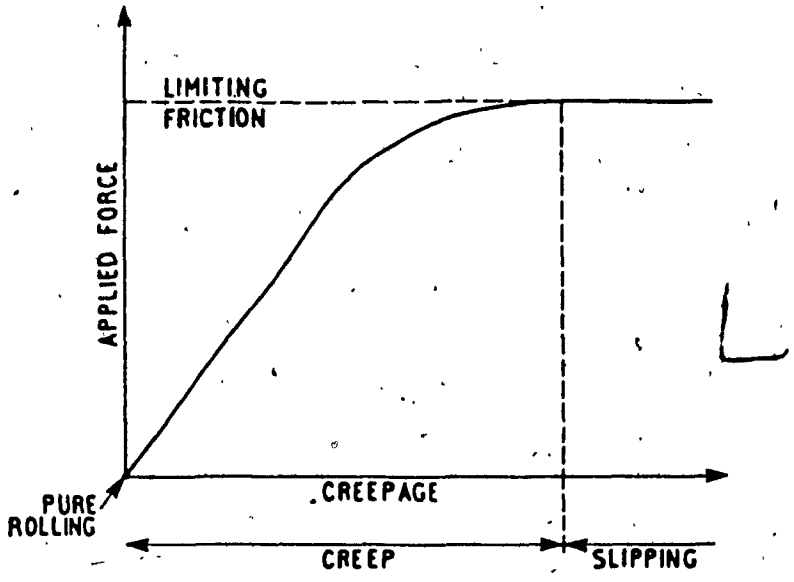

Figure 2.4 The relationship between creepage and creep force [52].

For linearized analysis these coefficients appear as values that exist when wheelset is in equilibrium position. In case of symmetrical wheelset and loading, these values of creep coefficients associated with left and right wheels are equal. The total creep force and moment acting on the wheelset, given by expressions (2.1) to (2.3) can be defined as components of the following terms [41];

- The longitudinal component consists of a single term due to longitudinal creep.
- The lateral component comprised of a term due to lateral creep and a term due to spin creep, the former is called the lateral creep force and the latter is called lateral/spin creep force.
- The moment about an axis normal to the contact area is comprised of a term due to lateral creep and a term due to spin creep. The former is called the lateral/spin creep moment and the latter is called the spin creep moment.

In the past, experimental work to determine creep coefficients were carried out by Illingworth [98] and Brickle [99], using single wheelset on a roller rig. For clean and dry wheel-roller surface, both the studies obtained creep coefficients that were in good agreement with those predicted by Kalker's linear theory. However, large deviations have been reported for contaminated surfaces. For example, Hobbs [100] reported experiments performed using a full scale railway wheelset traversing a short length of track at low speeds. The results showed good agreement with Kalker's prediction for various axle loads. However, the creep coefficients were reduced by over 30% for smaller axle loads when the surface was sprayed with water. Experimental evidences suggest that changes in surface conditions, like work hardening, contamination

and wetness can significantly affect the creep force characteristics. However, the effect of varying surface conditions cannot be predicted from the theories presently available. The wide range of variations in the wheel and rail surface conditions, and track environment make it very difficult to model the creep forces accurately. Thus, only "reasonable" approximations of the magnitude of the creep coefficients can be made. It is concluded in [15], that the creep coefficients and forces based on Kalker's simplified theory are sufficient for all practical problems in railway vehicle dynamics.

In the vast majority of the railway vehicle dynamic models developed to-date, the creep forces are modeled according to the linear creep theory. Typical experimental results [101] obtained from a three-piece truck model on the Arizona State roller rig is shown in Figure 2.5. The theoretical results obtained using 50% and 100% of Kalker values for creep coefficients are also included. Based on this, the nominal creep coefficients are taken as 50% of the calculated value as most reasonable approximation of actual creep phenomenon.

One set of values for creep coefficients, however, cannot be representative of the wide range of wheel/rail loading conditions encountered in practice. In order to account for such variation in wheel/rail loading, the typical values of creep coefficients used by various researchers [39, 40, 44] are shown in Table 2.1 for three different axle loading conditions. These values based on Kalker's linear theory are considered as nominal parameters in this study. Further in this investigation the effect of variations in creep coefficients over a range of values which may be encountered in practice are also examined.

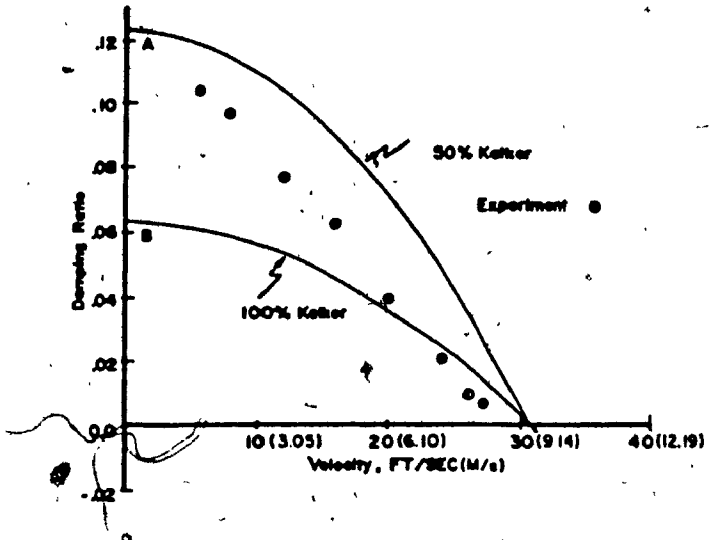

a) Damping ratio versus forward velocity.

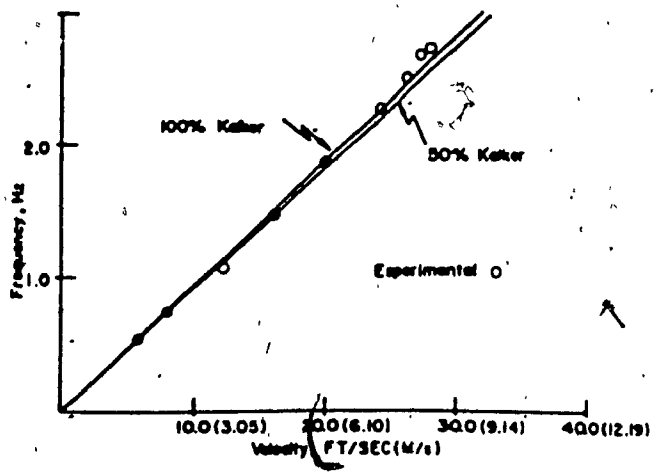

b) Frequency of oscilation versus forward velocity.

Figure 2.5 Theoretical and experimental results from tests on Arizona State University roller rig [101].

Table 2.1 Creep Coefficients as Function of Axle Load [39, 40, 44]

Loading Condition	Axle Load	Longitudinal f_{11}	Lateral f_{22}	Lateral/Spin f_{23}	Spin f_{33}
	N (lb)	N/wheel (lb/wheel)	N/wheel (lb/wheel)	N.m/wheel (lb.ft/wheel)	$N.m^2$/wheel ($lb.ft^2$/wheel)
Empty	5.6×10^4 (1.26×10^4)	2.56×10^6 (5.763×10^5)	2.212×10^6 (4.973×10^5)	3.12×10^3 (2.30×10^3)	16.01 (38.75)
Half Load	1.49×10^5 (3.35×10^4)	5.92×10^6 (1.33×10^6)	5.69×10^6 (1.28×10^6)	1.42×10^4 (1.05×10^4)	40.80 (98.70)
Full Load	2.42×10^5 (5.43×10^4)	7.72×10^6 (1.736×10^6)	7.12×10^6 (1.60×10^6)	2.11×10^4 (1.56×10^4)	69.40 (168.00)

(The values are from Kalker's linear theory and are 50% of the value.)

Derivation of Creep Forces and Moments

In deriving the expressions for creep forces and moments similar approach as in [44] and [102] are followed. The derivation of analytical expressions for creep forces and moments for the EDCW are very similar to that of conventional wheelset, except for the differential spin associated with each wheel in an axle. The creep forces are the tangential forces generated at the wheel/rail contact plane, which when resolved along the lateral and longitudinal directions, and their moment about the normal axis to the plane are given by Equations (2.1) to (2.3).

When the axis system for wheel/rail contact surface is defined as shown in Figure 2.6, the total creep force and moment on the left and right wheel can be given as:

$$\bar{F}_L = F_{x_L}\hat{e}_{1_L} + F_{y_L}\hat{e}_{2_L} \tag{2.4}$$

$$\bar{M}_L = M_{z_L}\hat{e}_{3_L} \tag{2.5}$$

$$\bar{F}_R = F_{x_R}\hat{e}_{1_R} + F_{y_R}\hat{e}_{2_R} \tag{2.6}$$

$$\bar{M}_R = M_{z_R}\hat{e}_{3_R} \tag{2.7}$$

where:

F_{x_L}, F_{x_R} are longitudinal components of creep force at the left and right wheels respectively.

F_{y_L}, F_{y_R} are the lateral components of creep force at the left and right wheels respectively.

M_{z_L}, M_{z_R} are the spin creep moments at the left and right wheels respectively.

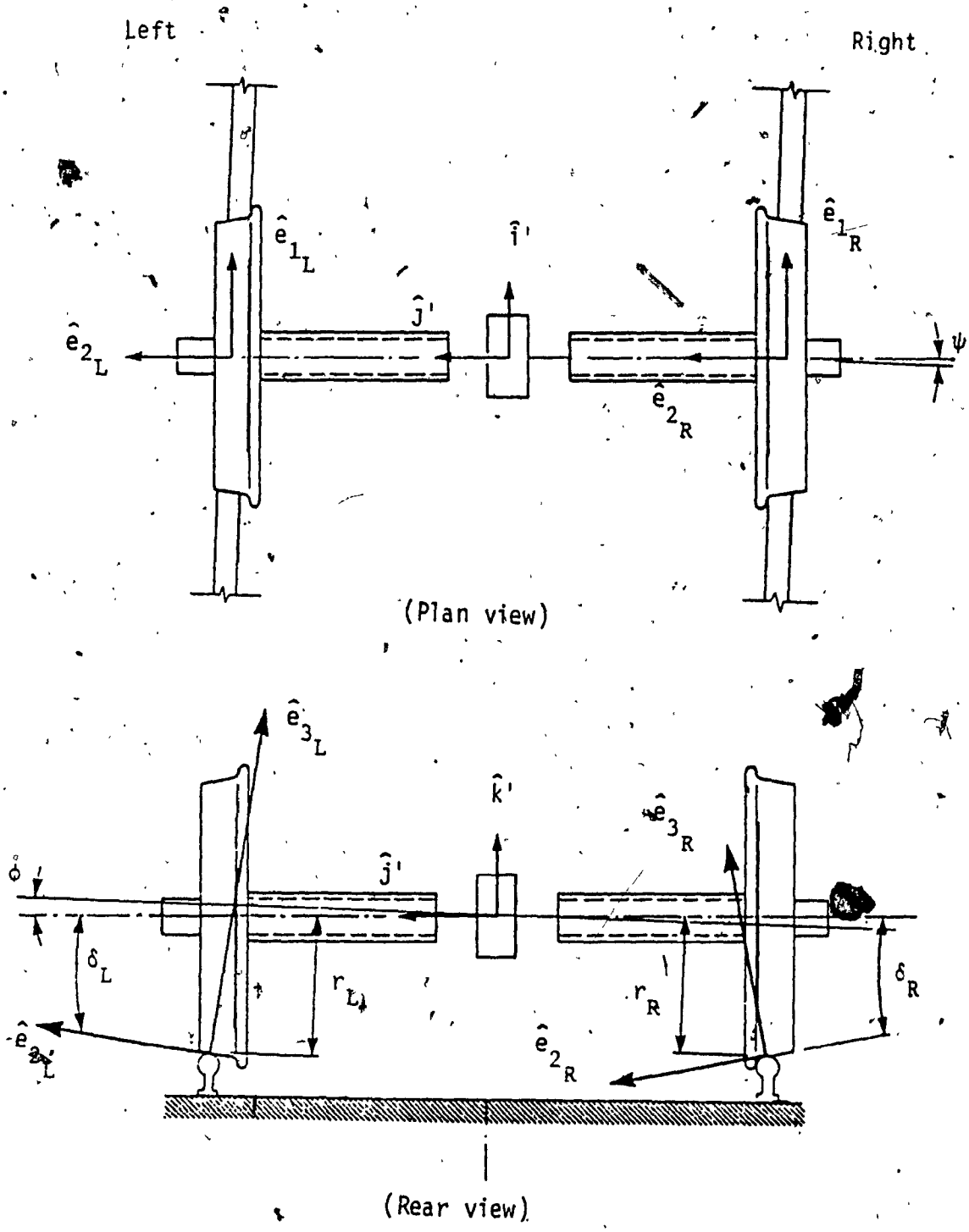

Figure 2.6 Axis system at wheel/rail contact plane

$\hat{e}_{1_L}, \hat{e}_{2_L}, \hat{e}_{3_L}$ the unit vectors defined with respect to plane of left wheel/rail contact as tangent in the longitudinal, lateral, and normal directions respectively.

$\hat{e}_{1_R}, \hat{e}_{2_R}, \hat{e}_{3_R}$ are the unit vectors defined with respect to plane of right wheel/rail contact as tangent in the longitudinal, lateral, and normal directions respectively.

When the rails or tracks are assumed rigid, and fixed to the ground, the creepage terms in Equations (2.1) to (2.3) can be simply obtained by dividing the total velocity of each wheel at contact point by the forward velocity. Therefore, defining the velocities as:

$\dot{\bar{r}}_{L_C}$ = velocity of left wheel at the wheel/rail contact point,

$\dot{\bar{r}}_{R_C}$ = velocity of right wheel at the wheel/rail contact point,

$\bar{\omega}_{L_C}$ = angular velocity at the point of left wheel/rail contact,

$\bar{\omega}_{R_C}$ = angular velocity at the point of right wheel/rail contact,

and substituting Equations (2.1) to (2.3) into (2.4) to (2.7) leads to the following expressions for total creep force and moment at the wheel/rail contact point of left and right wheels:

$$\bar{F}_L = \frac{f_{11}}{V}(-\dot{\bar{r}}_{L_C} \cdot \hat{e}_{1_L})\hat{e}_{1_L} + \frac{f_{22}}{V}(-\dot{\bar{r}}_{L_C} \cdot \hat{e}_{2_L})\hat{e}_{2_L} + \frac{f_{23}}{V}(-\bar{\omega}_{L_C} \cdot \hat{e}_{3_L})\hat{e}_{2_L} \quad (2.8)$$

$$\bar{M}_L = \frac{f_{23}}{V}(\dot{\bar{r}}_{L_C} \cdot \hat{e}_{2_L})\hat{e}_{3_L} + \frac{f_{33}}{V}(-\bar{\omega}_{L_C} \cdot \hat{e}_{3_L})\hat{e}_{3_L} \quad (2.9)$$

$$\bar{F}_R = \frac{f_{11}}{V}(-\dot{\bar{r}}_{R_C} \cdot \hat{e}_{1_R})\hat{e}_{1_R} + \frac{f_{22}}{V}(-\dot{\bar{r}}_{R_C} \cdot \hat{e}_{2_R})\hat{e}_{2_R} + \frac{f_{23}}{V}(-\bar{\omega}_{L_C} \cdot \hat{e}_{3_R})\hat{e}_{2_R} \quad (2.10)$$

$$\bar{M}_R = \left[\frac{f_{33}}{V}(\dot{\bar{r}}_{R_C} \cdot \hat{e}_{2_R})\hat{e}_{3_R} + \frac{f_{33}}{V}(-\bar{\omega}_{R_C} \cdot \hat{e}_{3_R})\hat{e}_{3_R}\right] \quad (2.11)$$

For the EDCW model, the axis system is defined, and the expressions for the terms $\dot{\bar{r}}_{L_c}$, $\dot{\bar{r}}_{R_c}$, $\bar{\omega}_{L_c}$ and $\bar{\omega}_{R_c}$ are derived in terms of wheelset axis system in Appendix A. Substitution of these expressions into Equations (2.8) to (2.11) lead to the final expressions for the creep forces and moments in terms of the wheelset reference axis system. These derivations are shown in Appendix B, where the final expressions for the EDCW model on tangent track are obtained as follows:

Left wheel:

$$\bar{F}_L = \left[-\frac{f_{11}}{V}\left(\dot{x}+V-r_L\Omega-r_L\dot{\beta}_L-a\dot{\psi}\right)\hat{i}''' + \left[-\frac{f_{22}}{V}\left(\dot{y}+r_L\dot{\phi}-V\psi\right)\right.\right.$$

$$\left.\left. -\frac{f_{23}}{V}\left(\dot{\psi}-\delta_L\Omega\right) - \frac{f_{11}}{V}\left(V\psi-r_L\Omega\psi\right)\right]\hat{j}''' \qquad (2.12)$$

$$\bar{M}_L = \left[\frac{f_{23}}{V}\left(\dot{y}-V\psi+r_L\dot{\phi}\right) - \frac{f_{33}}{V}\left(\dot{\psi}-\delta_L\Omega\right)\hat{k}''' \qquad (2.13)$$

Right wheel:

$$\bar{F}_R = \left[-\frac{f_{11}}{V}\left(\dot{x}+V-r_R\Omega-r_R\dot{\beta}_R+a\dot{\psi}\right)\hat{i}''' + \left[-\frac{f_{22}}{V}\left(\dot{y}+r_R\dot{\phi}-V\psi\right)\right.\right.$$

$$\left.\left. -\frac{f_{23}}{V}\left(\dot{\psi}+\delta_R\Omega\right) - \frac{f_{11}}{V}\left(V\psi-r_R\Omega\psi\right)\right]\hat{j}''' \qquad (2.14)$$

$$\bar{M}_R = \left[\frac{f_{23}}{V}\left(\dot{y}-V\psi+r_R\dot{\phi}\right) - \frac{f_{33}}{V}\left(\dot{\psi}+\delta_R\Omega\right)\right]\hat{k}''' \qquad (2.15)$$

where, $\hat{i}'''$, $\hat{j}'''$ and $\hat{k}'''$ are unit vectors in longitudinal, lateral and vertical directions for the wheelset in equilibrium.

2.3.2 Gravitational Stiffness Force

In addition to creep forces at the wheel/rail contact point, there are normal forces exerted in the direction perpendicular to the plane of contact. Due to the taper or conicity of the wheels, the normal forces acting on the wheelset have both lateral and vertical components as shown in Figure 2.7. The net effect of the lateral component of the normal force acting on the wheelset is often referred to as the "gravitational stiffness effect". The gravitational stiffness force is a function of the axle load, the wheelset roll angle, and the difference in contact angle between the left and right wheels.

In dynamic study of wheelset with light axle load, the gravitational stiffness term is often neglected. However, as axle load increases, this term becomes increasingly important. For axle loads typical of heavy freight cars, this effect may be strong as outlined by Cooperrider et al, [103]: "... the gravitational stiffness effect can provide more restoring force than the vehicle suspension for heavily loaded wheelset". This is due to the fact that lateral component of the normal force on the left and right wheels of a wheel-axle-set acts in the opposite direction and thus effectively provide guidance for the wheelset.

Tuten et al. [40] examined lateral stability of freight car with axles having different wheel profiles. The study showed that the wheel profile had significant effect on the critical speed, due to gravitational effect. Cooperrider et al. [103] developed analytical and experimental methods for determining kinematic function for given wheel and rail profile, and rail gage, as function of wheelset lateral

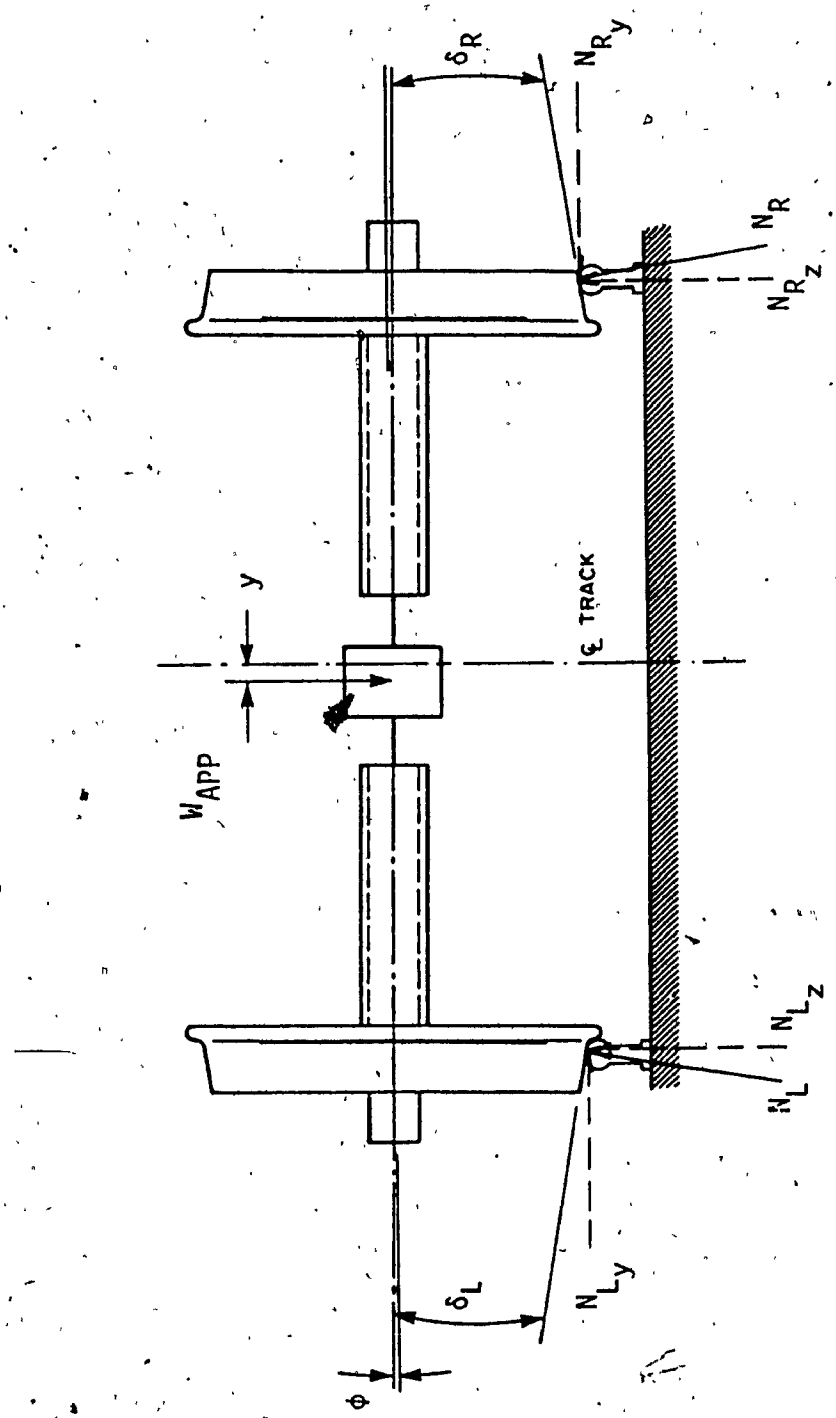

Figure 2.7 Components of normal force acting on a wheelset.

displacement. The results showed that for new conical wheels or slightly worn wheels, the function can be well approximated by linear relation, when amplitude of lateral oscillation is less than that for flange contact. But as the wheels wear with use, the profile may become quite non-linear, as shown in Figure 2.8. Furthermore, this change in profile may be different from axle to axle or within an axle of a given car. Thus it is not possible to develop a model of worn wheel profile which gives accurate characteristics of all worn profiles. In this study, linearized model of EDCW is considered, where the wheel profile are taken to be conical. The effect of variation in effective wheel conicity is however examined.

Derivation of Gravitational Stiffness Force

When a symmetric wheelset is centered on a symmetric track, the normal forces on the left and right wheels are equal in magnitude and slightly inclined inward from the vertical. The sum of the vertical components of the two normal forces are equal to the axle load, and the lateral components act in the opposite direction with zero lateral resultant force on the wheelset. When the wheelset is displaced laterally by small distance y, the normal reaction forces between the rails and wheels change their direction depending on the contact angle as shown in Figure 2.7. With reference to wheelset axis system defined in Appendix A, for small angle assumptions, the normal forces at the left and right wheels are:

$$\bar{N}_L = -N_L(\delta_L+\phi)\hat{j}''' + N_L\hat{k}''' \qquad (2.16)$$

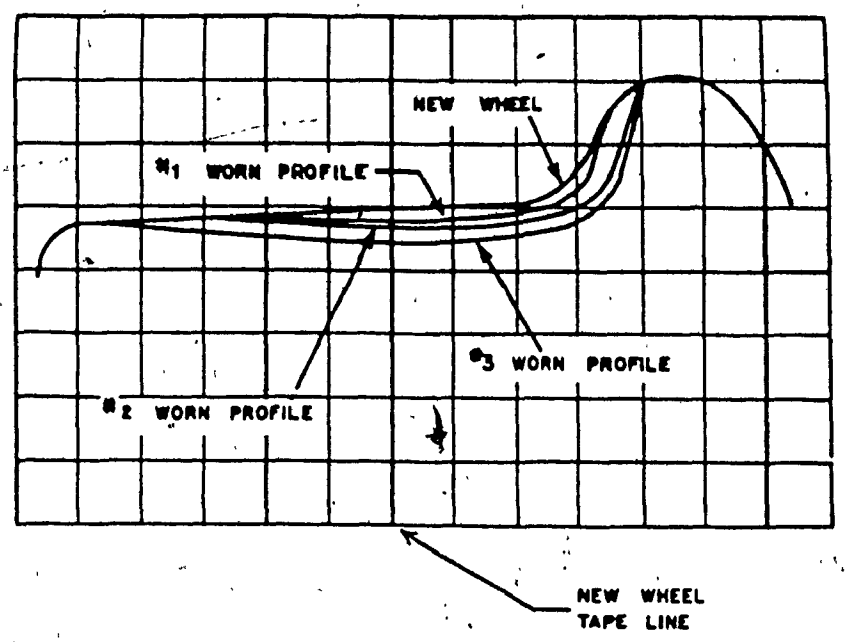

Figure 2.8 Changes in wheel profile with use [44].

$$\bar{N}_R = N_R(\delta_R - \phi)\hat{j}''' + N_R\hat{k}''' \tag{2.17}$$

The magnitude of the lateral component on the gravitational stiffness force (GSF) can be found by summing the lateral components of Equations (2.16) and (2.17). On tangent track, assuming that the vertical force at each wheel are equal to the proportionate share of the axle load ($W_{APP}/2 = N_L = N_R$), the GSF can be expressed as:

$$GSF = -W_{APP}\left(\frac{\delta_L - \delta_R}{2} + \phi\right)\hat{j}''' \tag{2.18}$$

This expression only represents the effect of gravity where there is no dynamic effect.

2.3.3 Primary Suspension Forces and Moments

The wheelset suspension or the primary suspension of railway vehicle is defined as the mechanism which connects the wheelset to the truck frame. The primary suspension for the EDCW can be modeled similar to conventional model, where suspension elements provide stiffness and damping to the system. A typical North American three-piece freight truck is shown in Figure 2.9. The truck consists of two side frames, two wheelsets and a bolster. The bolster supports the car body, the ends of which rests on a vertical spring group, which in turn rests on the side frames. The frame of the truck can deform so that the wheelsets and side frames assume a sort of parallelogram shape, called "warping". The warping motion is resisted by friction between the bolster and side frames.

As mentioned previously, for conventional freight car there are no

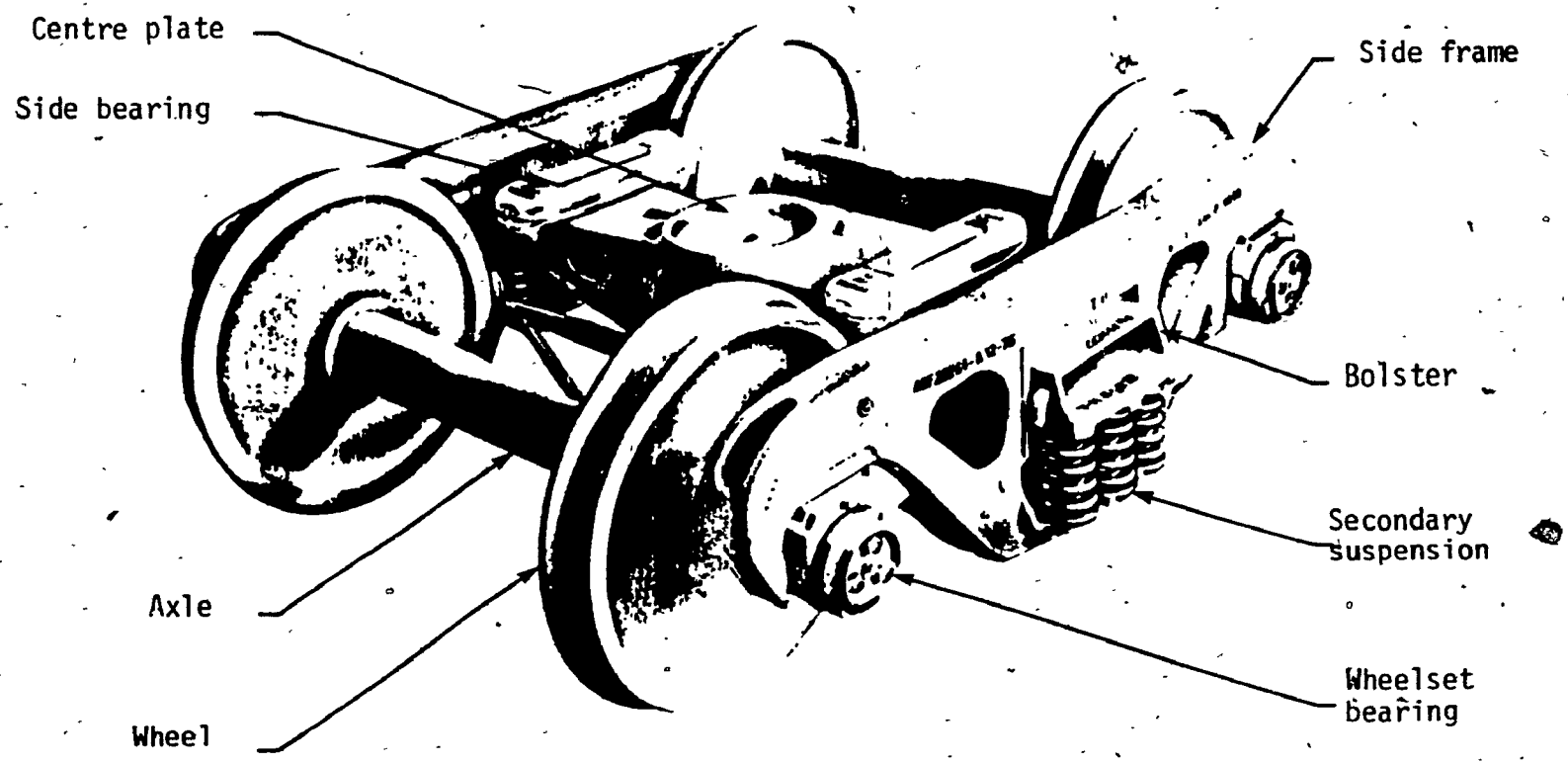

Figure 2.9 Typical North American three-piece freight truck

intentional primary suspension. However, in modeling wheelsets, the compliance of truck frame and wheelset bearings that support the wheelset are accounted for through representation as primary suspension.

The conventional wheelsets are connected to the side frames through either plain or roller bearings. In plain journal bearings, the wheelset lateral motion is relatively unrestricted until the allowed clearance is taken up and the axle hits the limit stop. Also with plain bearings, longitudinal or yaw motion of the wheelset is virtually eliminated. Roller bearings on the other hand permit less lateral motion, as well as some yaw motion. As the two bearing types constrain wheelset motion differently, the wheelset hunting motion differs for roller and plain bearing trucks. For roller bearings, the hunting mode usually consists of large motion of the truck. For plain bearing, the lateral motion of the wheelset can be large with respect to the truck. The critical speed for freight car with plain bearings have been observed to be about 16 km/h (10 mph.) lower than that of freight car with roller bearings [44]. For freight trucks, the superiority of the roller bearings over the plain bearings is well recognized [104].

In this investigation, there is no intention to study the effect of different bearing supports. Here the nominal parameters for primary suspension are taken according to a conventional freight truck model with roller bearings. The effect of variations in these primary suspension parameters are also studied.

Realistically, conventional primary suspension exhibit non-linear characteristics due to clearance and coulomb friction. For linearized

study, with the assumption of small clearance, the primary suspension elements can be modeled as linear stiffness and equivalent viscous damping in parallel. In some studies with conventional freight truck model [39, 40], the effect of axle load on the primary suspension is also included. In Table 2.2, primary lateral and yaw stiffnesses as function of axle load are shown [39].

Derivation of Primary Suspension Forces and Moments

For the wheelset model considered, the restoring force provided by primary suspension can be resolved at the wheelset centroid. For linearized model, with reference to Figure 2.10 and wheelset axis system defined in Appendix A. The expressions for total force and moment due to primary suspension can be summarized as:

$$\bar{F}_{s_p} = -2(D_{x_p}\dot{x} + k_{x_p}x)\hat{i}''' - 2(D_{y_p}\dot{y} + k_{y_p}y)\hat{j}''' \tag{2.19}$$

$$\bar{M}_{s_p} = (-2D_{x_p}a^2\dot{\psi} - 2k_{x_p}a^2\psi)\hat{k}''' = -(D_{\psi_p}\dot{\psi} + k_{\psi_p}\psi)\hat{k}''' \tag{2.20}$$

Where D_{ψ_p} and k_{ψ_p} are effective wheelset yaw damping and stiffness constants, respectively.

2.3.4 EDCW Coupler Moment

In this section, the spin moment acting on each wheel of the wheel-axle set due to coupling between the wheels are discussed, and for which expressions are derived. In this study, primarily three different arrangements for coupling are considered, which are referred to as Configuration 1, 2, and 3, as shown in Figure 2.11. The coupling

Table 2.2 Primary Suspension Stiffness as Function of Axle Load

Loading Condition	Axle Load, W_{App}	Primary lateral Stiffness, k_{y_p}	Primary Yaw Stiffness, k_{ψ_p}
	N (lb)	N/m lb/ft	N.m/rad (lb.ft/rad)
Empty	5.60×10^4 1.26×10^4	7.30×10^5 (5.00×10^4)	1.69×10^6 (1.25×10^6)
Half Load	1.49×10^5 (3.35×10^4)	1.02×10^6 (7.00×10^4)	2.03×10^6 $(1.50 \times 10^6$
Full Load	2.42×10^5 (5.43×10^4)	1.36×10^6 (9.30×10^4)	2.31×10^6 (1.70×10^6)

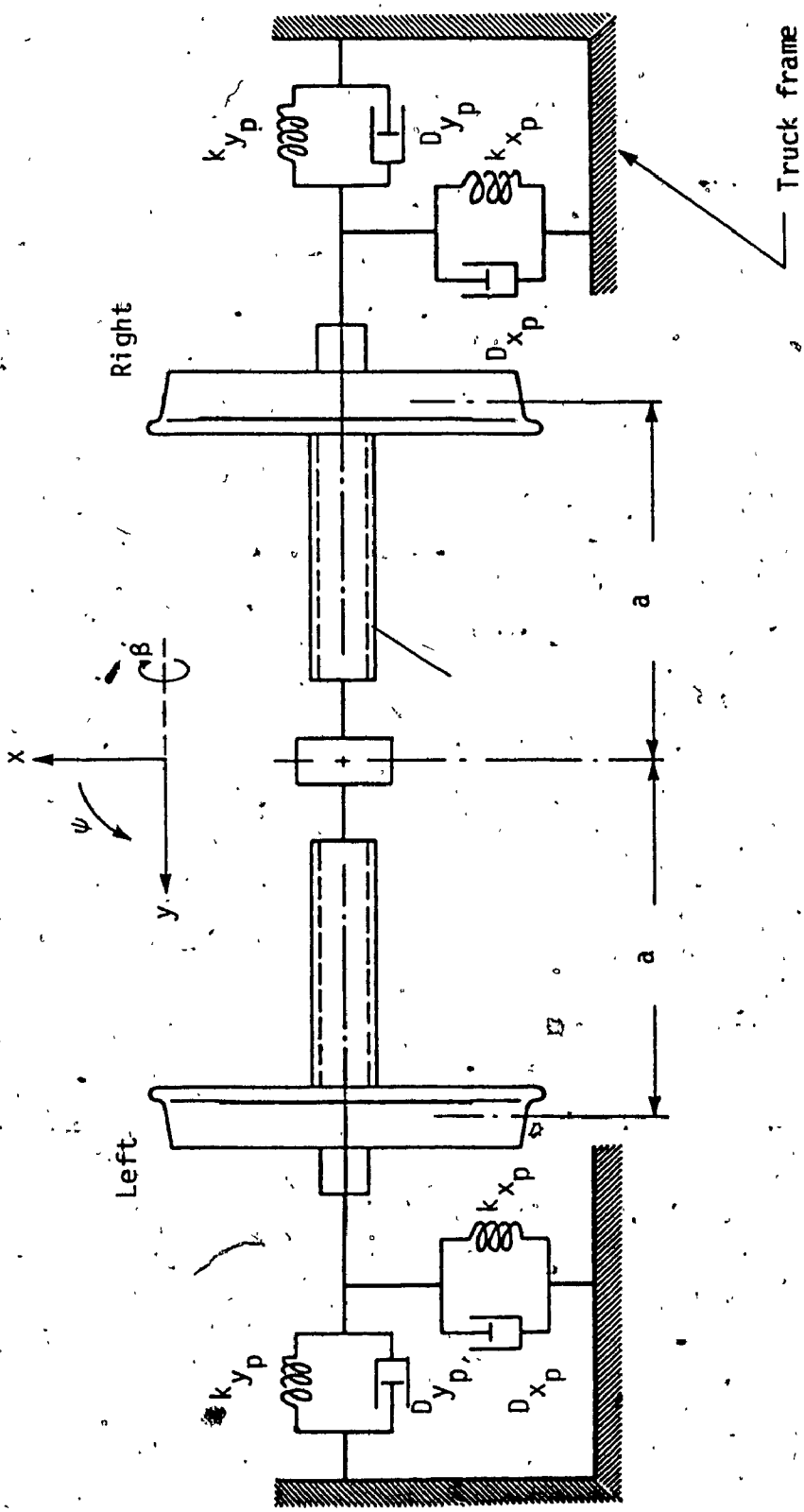

Figure 2.10 Schematic of an EDCW model with primary suspension

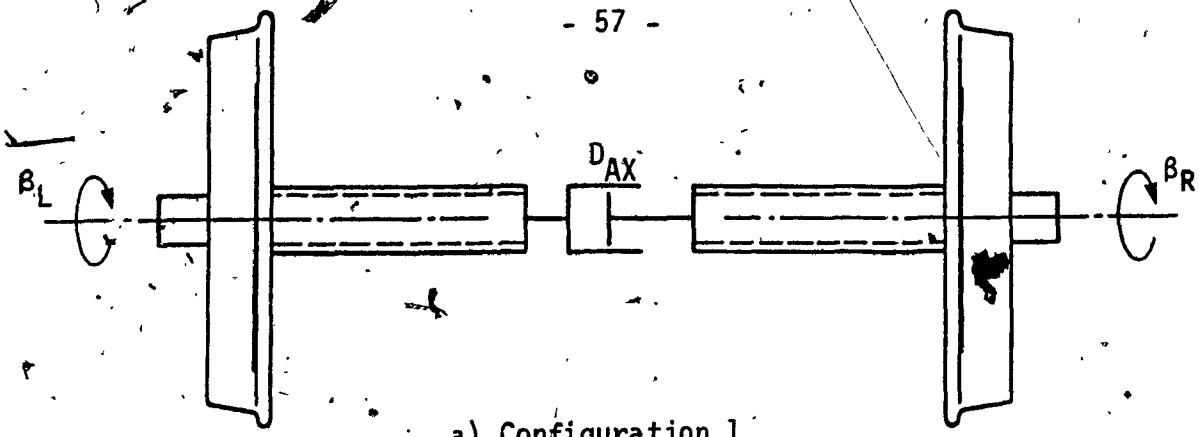

a) Configuration 1

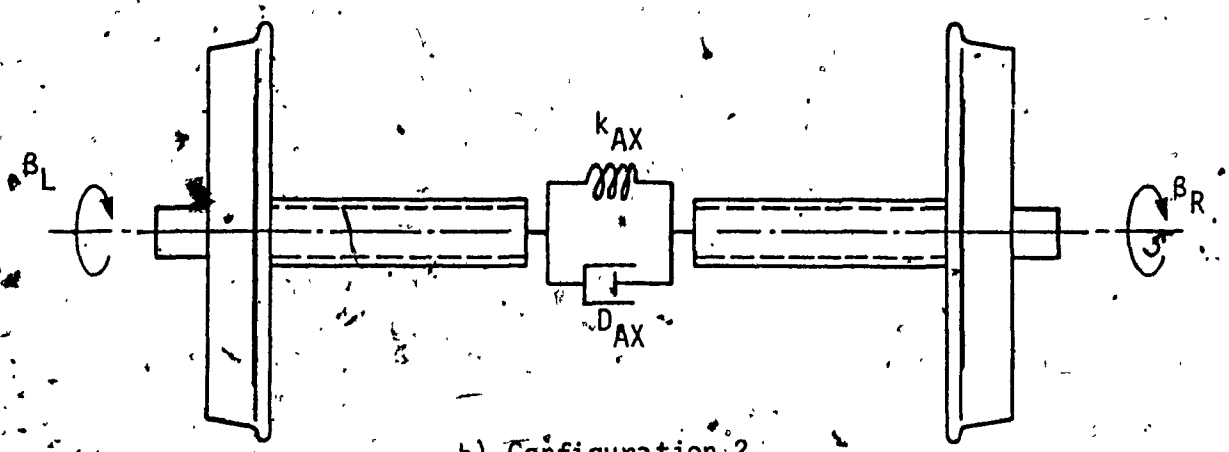

b) Configuration 2

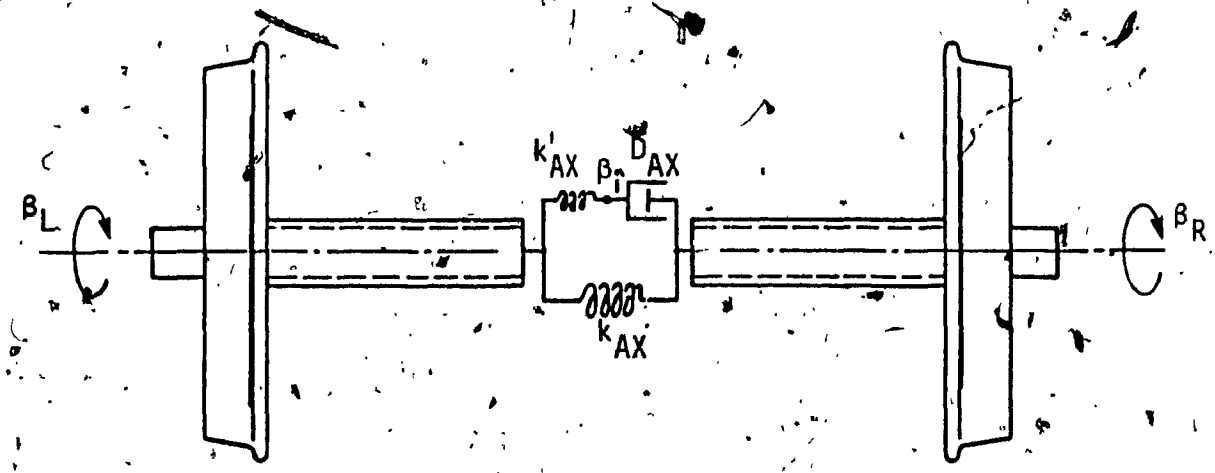

c) Configuration 3

Figure 2.11 Coupler configurations for the EDCW model

arrangement in Configuration 1, is simply a torsional viscous damper element. In Configuration 2, the coupling element consists of a linear torsional stiffness and torsional viscous damper in parallel. The coupling element in Configuration 3 consists of a linear torsional stiffness and viscous damper in series, as well as a linear torsional stiffness in parallel. Configurations 2 and 3 are referred to as elasto-damper coupled wheelset (EDCW).

Although, Configuration 3 alone can be used to study the effect of all the three configurations, in this study, both Configurations 2 and 3 are considered separately for comparison of results and to aid in model validation. In this investigation, equations of motion for EDCW of Configurations 2 and 3 are to be developed. In Configuration 2, by setting k_{AX} to zero, Configuration 1 can be obtained, and by setting k_{AX} to rigid conventional rigid axle can be simulated. In Configuration 3, by setting k'_{AX} to rigid Configuration 2 can be obtained, and by setting k'_{AX} to rigid and k_{AX} to zero, Configuration 1 can be obtained. Further in Configuration 3, by setting k_{AX} to zero a series arrangement of stiffness-damper can be obtained, and by setting k_{AX} to rigid conventional rigid axle can be simulated.

In the modeling of the EDCW it is assumed that, besides wheel/rail interaction, coupling provides the only spin moment about the axis of the wheelset axle, and that there are no moments due to bearing friction. It is further assumed that the coupling does not allow relative motion between the left and right wheels in lateral or yaw directions. In other words, the only difference between the conventional and EDCW is that in the latter case, the left and right wheels within an axle can have

differential spin resisted by coupling moment.

Derivation of Coupler Moment

The coupling elements between the two wheels are modeled as torsional spring and damper combination. The coupling moment depends on the relative spin rotation and velocity between left and right wheels. The expression for coupler moment that act about wheelset axle axis (j'), can be summarized as:

Configuration 1.

$$\bar{M}_{AX} = [D_{AX}(\dot{\beta}_L - \dot{\beta}_R)]\hat{j}' \qquad (2.21)$$

Configuration 2.

$$\bar{M}_{AX} = [D_{AX}(\dot{\beta}_L - \dot{\beta}_R) + k_{AX}(\beta_L - \beta_R)]\hat{j}' \qquad (2.22)$$

Configuration 3.

$$\bar{M}_{AX_L} = [k'_{AX}(\beta_L - \beta_i) + k_{AX}(\beta_L - \beta_R)]\hat{j}' \qquad (2.23)$$

$$\bar{M}_{AX_R} = [D_{AX}(\dot{\beta}_R - \dot{\beta}_i) + K_{AX}(\beta_R - \beta_L)]\hat{j}' \qquad (2.24)$$

and $$[K'_{AX}(\beta_i - \beta_L) + D_{AX}(\dot{\beta}_i - \dot{\beta}_R)]\hat{j}' = 0 \qquad (2.25)$$

2.4 Assumptions and Limitations

There are a number of assumptions made during modeling of the physical arrangement of a wheelset on a freight car. The applicability

of the model is primarily determined by such assumptions, and the implications of the assumptions must be fully understood before the results obtained from the model can be interpreted and used. The assumptions made in the modeling process, together with limitations of the model are summarized as follows.

For the analysis of lateral dynamic behaviour of the EDCW, it is assumed that the excitation acting on the wheelset is only due to track irregularities, however, the excitation is set to zero for stability analysis. While modeling a single wheelset, the wheelset motions are assumed to be with respect to fixed truck reference frame. The coupling between the wheelsets within a truck, and the clearance between the wheelset and truck frames are neglected.

The external forces applied at the wheel/rail contact are assumed only to be gravitational stiffness and creep forces. In obtaining the equations of motion, the motions of the wheelset are assumed to be small, and hence the effect of flange contact and corresponding flange force is not included. As pointed out in the literature review, inclusion of flange contact non-linearity basically exhibits stable or unstable limit cycle behaviour near the linear critical speed, depending on the flange contact. The critical speed on the other hand can be predicted from linearized analysis.

The dynamic analysis of conventional wheelset carried out by Law [41], indicated that gyroscopic effects are stabilizing, while the spin creep effects are destabilizing. Hence, in this study both the gyroscopic and spin creep terms are included.

In modeling the coupler of an EDCW, it is assumed that the coupler between the wheels within an axle allow only relative motion in the spin direction. Therefore, the only difference between conventional and EDCW is the additional spin degree-of-freedom. The wheels are also assumed to run freely without bearing friction.

For stability analysis, the track is assumed to be smooth and rigid. This assumptions is supported by Wickens [54] study, which reported that flexibility of track in-use has a very small effect on the stability behaviour of a rail vehicle.

The models developed in this investigation are primarily for linear lateral dynamic study, where the objective is to study the effect of elasto-damper coupler on the stability behaviour of the wheelset. In deriving the equations of motion for the EDCW, the effects of longitudinal, vertical and roll motions are eliminated by simplification and substitution. These simplifications are valid for a symmetrical wheelset travelling at a constant forward velocity.

The primary limitation of the single wheelset model in simulating freight car stability behaviour is that it neglects the effects of truck dynamics, which in this case is assumed to serve as a fixed reference that moves along the track. In the forth-coming Chapter 4, the EDCW model is incorporated with freight truck system in developing a representative model of freight car system.

2.5 Elasto-Damper Coupled Wheelset Equations of Motion

Based on the modeling considerations and assumptions discussed in

the previous sections, in this section the equation of motion for the EDCW model are established for tangent track. Expressions for various forces and moments acting on the wheelset due to creep, gravitational effect, primary suspension, and coupling are derived in the previous sections. The axis system and derivation of expressions for velocity, angular velocity, and angular momentum for the wheelset are presented in Appendix A. Newton's second Law is applied in all cases, where the expressions derived for each force and moment terms are substituted. In arriving at the final equations, small displacement assumption is made, and the product of perturbation quantities are neglected as second order terms in the equations. The equations of motion, from force balance in each direction are:

Longitudinal Motion:

The summations of forces at the wheelset centre of gravity in the longitudinal direction ($\hat{i}'''$) of the equilibrium coordinate system yields,

$$F_{L_x} + F_{R_x} + F_{s_{p_x}} = m_w \ddot{\bar{r}}_{CG} \hat{i}''' \tag{2.26}$$

Substituting respective component of $\bar{F}_L$, $\bar{F}_R$, and $\ddot{\bar{r}}_{CG}$ from Equations (2.12), (2.14), and (A.10) respectively, results in the longitudinal equation of motion, as:

$$m_w \ddot{x} + \frac{f_{11}}{V}\left[\dot{2x} + 2V - \Omega(r_L + r_R) - r_L \dot{\beta}_L - r_R \dot{\beta}_R\right] + F_{s_{p_x}} = 0 \tag{2.27}$$

Vertical Motion:

The summation of forces at the wheelset centre of gravity in the

vertical direction (k''') of the equilibrium coordinate system yields,

$$F_{L_z} + F_{R_z} + N_{L_z} + N_{R_z} - m_w g - W'_{APP} - F_{s_{p_z}} = m_w \ddot{\bar{r}}_{CG} \hat{k}''' \qquad (2.28)$$

Since vertical component of $\bar{F}_L$ and $\bar{F}_R$ are zero, substituting respective components of $\bar{N}_L$, $\bar{N}_R$ and $\ddot{\bar{r}}_{CG}$ from Equations (2.16), (2.17), and (A-10) respectively, the equation of motion for vertical direction is:

$$m_w \ddot{z} + m_w g + W'_{APP} + F_{s_{p_z}} - (N_L + N_R) = 0 \qquad (2.29)$$

Lateral Motion:

The summation of forces at the wheelset centre of gravity in the lateral direction ($\hat{j}'''$) of the equilibrium coordinate system yields,

$$F_{L_y} + F_{R_y} + F_{s_{p_y}} + N_{L_y} + N_{R_y} = m_w \ddot{\bar{r}}_{CG} \hat{j}''' \qquad (2.30)$$

Substituting respective components of $\bar{F}_L$, $\bar{F}_R$, $\bar{N}_L$, $\bar{N}_R$, $\bar{F}_{s_p}$, and $\ddot{\bar{r}}_{CG}$ from Equations (2.12), (2.14), (2.16), (2.17), (2.19), and (A-10) respectively, leads to the lateral equation as:

$$m_w \ddot{y} + 2\frac{f_{22}}{V}(\dot{y} + r_0\dot{\phi} - V\psi) + \frac{f_{23}}{V}(2\dot{\phi} - \delta_L\Omega + \delta_R\Omega)$$

$$+2(D_{y_p}\dot{y} + k_{y_p}y) + N_L(\delta_L + \phi) - N_R(\delta_R - \phi) = 0 \qquad (2.31)$$

Roll Motion:

The roll equation of motion is obtained by summing moments about the longitudinal equilibrium coordinate (i'''), which yields a general expression:

$$\{[a\hat{j}' - r_L\hat{k}']x[(F_{L_x})\hat{i}''' + (N_{L_y} + F_{L_y})\hat{j}''' + (N_{L_z} + F_{L_z})\hat{k}''']$$

$$[-a\hat{j}' - r_R\hat{k}']x[(F_{R_x})\hat{i}''' + (N_{R_y} + F_{R_y})\hat{j}''' + (N_{R_z} + F_{R_z})\hat{k}''']\}\hat{i}'''$$

$$+ M_{s_{p_x}} = \dot{\bar{H}}_G\hat{i}''' \qquad (2.32)$$

Transforming wheelset axis system to reference axis system, performing the vectorial cross and dot products, and substituting for creep and normal forces, and $\dot{\bar{H}}_G$ from Equations (2.12), (2.14), (2.16), (2.17) and (A-18), respectively, leads to the roll equation as:

$$I_{w_1}\ddot{\phi} - I_{w_2}\Omega\dot{\psi} + \frac{2f_{22}r_0}{V}(\dot{y} + r_0\dot{\phi} - V\psi) + f_{23}(\frac{2r_0\dot{\psi}}{V} + \delta_R - \delta_L)$$

$$- M_{s_{p_x}} - a(N_L - N_R) = 0 \qquad (2.33)$$

Yaw Motion:

Similar to roll motion, yaw equation of motion is obtained by summing moments about the k''' axis through the wheelset centroid. In doing so, the moment equilibrium equation is:

$$M_{L_z} + M_{R_z} + M_{s_{p_z}} + \{[a\hat{j}' - r_L\hat{k}']x[F_{L_x}\hat{i}''' + (N_{L_y} + F_{L_y})\hat{j}'''$$

$$+ (N_{L_z} + F_{L_z})\hat{k}'''] + [-a\hat{j}' - r_R\hat{k}']x[F_{R_x}\hat{i}''' + (N_{R_y} + F_{R_y})\hat{j}'''$$

$$+ (N_{R_z} + F_{R_z})\hat{k}''']\}\hat{k}''' = \dot{\bar{H}}_G\hat{k}''' \qquad (2.34)$$

Following the same steps as in the roll equation, the equation for yaw motion can be obtained as:

$$I_{w_1}\ddot{\phi} + I_{w_2}\Omega\dot{\phi} + \frac{2f_{33}}{V}\left[\dot{\phi} - \Omega\left(\frac{\delta_L - \delta_R}{2}\right)\right] - \frac{2f_{23}}{V}\left(\dot{y} - V\psi + r_0\dot{\phi}\right)$$

$$+ \frac{2f_{11}a^2}{V}\left[\dot{\phi} + \Omega\left(\frac{r_L - r_R}{2a}\right) + \frac{r_0}{2a}\left(\dot{\beta}_L - \dot{\beta}_R\right)\right] - a\phi W_{APP}\left(\frac{\delta_L + \delta_R}{2}\right)$$

$$+ \left(D_{\psi_p}\dot{\phi} + k_{\psi_p}\phi\right) = 0 \qquad (2.35)$$

Spin Motion:

The spin equation of motion for the EDCW is obtained by summing moments about the spin axis (j') of each wheel. Therefore, two equations are obtained for the wheelset spin motion. The summation of moments at the left wheel gives:

$$M_{L_y} + M_{L_z}\phi - M_{AX} + \left\{-r_L\hat{k}' \times \left[F_{L_x}\hat{i}''' + (N_{L_y} + F_{L_y})\hat{j}'''\right.\right.$$

$$\left.\left. + (N_{L_z} + F_{L_z})\hat{k}'''\right]\hat{j}'\right\} = \dot{\bar{H}}_{G_L}\hat{j}' \qquad (2.36)$$

Performing the cross and dot products and substituting for $\dot{\bar{H}}_{G_L}$ from Equation (A-20), the expression for left wheel spin motion is:

$$\tfrac{1}{2}I_{w_2}\ddot{\beta}_L + M_{AX} - M_{L_z}\phi - M_{L_y} + r_L\left[(N_{L_y} + F_{L_y})\phi + F_{L_x}\right] = 0 \qquad (2.37)$$

Similarly for the right wheel, the equation of motion is:

$$\tfrac{1}{2}I_{w_2}\ddot{\beta}_R - M_{AX} - M_{R_z}\phi - M_{L_y} + r_R\left[(N_{R_y} + F_{R_y})\psi + F_{R_x}\right] = 0 \qquad (2.38)$$

Subtracting Equation (2.38) from (2.37), and substituting for creep forces and moments from Equations (2.12) to (2.15), and substituting for

M_{AX} from Equation (2.22), leads to the wheelset spin equation of motion as:

$$I_{w_2}\ddot{\beta} + 4D_{AX}\dot{\beta} + 4k_{AX}\beta + \frac{2f_{11}r_0^2}{V}\dot{\beta} + \frac{2f_{11}r_0 a\dot{\psi}}{V} + f_{11}(r_L - r_R) - \frac{2f_{33}}{r_0}\left(\frac{\delta_L + \delta_R}{2}\right)\phi = 0 \qquad (2.39)$$

where product of small quantities are neglected, and $(\beta_L - \beta_R)/2$ is substituted by β, which is half the differential spin between left and right wheels. The spin Equation (2.39) corresponds to the Configuration 2, from which Configuration 1, can be obtained by setting k_{AX} to zero.

For Configuration 3, an additional equation is required due to an intermediate spin at the node point between stiffness and damper arranged in series. In this case, equations of motion for spin are obtained following the same steps as above, except in this case, expressions for M_{AX_L} and M_{AX_R} are substituted from Equations (2.23) and (2.24) for left and right wheel spin equations, respectively. In doing so, the differential spin equation between left and right wheels is obtained as:

$$I_{w_2}\ddot{\beta} + \frac{2f_{11}r_0^2}{V}\dot{\beta} + 2k'_{AX}\beta + 2D_{AX}\dot{\beta}_2 - 2k'_{AX}\beta_2 + 4k_{AX}\beta + \frac{2f_{11}a\dot{\psi}\,r_0}{V} + f_{11}(r_L - r_R) - \frac{2f_{33}}{r_0}\left(\frac{\delta_L + \delta_R}{2}\right)\phi = 0 \qquad (2.40)$$

And the additional equation required is identical to that of Equation (2.25), which can be written as:

$$2D_{AX}\dot{\beta}_2 + 2k'_{AX}\beta_2 - 2k'_{AX}\beta = 0 \qquad (2.41)$$

where β is half the differential spin between the left and right wheels defined as:

$$\beta = \frac{\beta_L - \beta_R}{2} = \beta_1 + \beta_2$$

$$\text{where, } \beta_1 = \frac{\beta_L - \beta_i}{2}$$

$$\beta_2 = \frac{\beta_i - \beta_R}{2}$$

The equations of motion derived above for the EDCW describe its motion in all possible six modes. However, as shown in Appendix C.1, the longitudinal Equation (2.27), simply shows that, for symmetric wheelset, rolling radius of one wheel will increase by the same amount the other decreases. Further more, vertical and roll Equations (2.29) and (2.33) can be used to obtain an explicit expression for normal forces in the lateral equation (2.31). The steps in obtaining this, is shown in Appendix C.2, where the following expression is obtained:

$$(N_L + N_R)\phi + (N_L\delta_L - N_R\delta_R) = W_{APP}(\phi + \frac{\delta_L - \delta_R}{2}) - I_{w_2}\Omega\dot{\psi}(\frac{\delta_L + \delta_R}{2a}) \qquad (2.42)$$

Substituting the above result into the wheelset lateral Equation (2.31) leads to the final expression for lateral equation as:

$$m_w\ddot{y} + 2(\frac{f_{22}}{V} + n_{y_p})\dot{y} + 2k_{y_p}y + W_{APP}(\phi + \frac{\delta_L - \delta_R}{2}) - \frac{2f_{23}}{r_0}(\frac{\delta_L - \delta_R}{2})$$

$$+ [\frac{2f_{23}}{V} - \frac{I_{w_2}V}{r_0 a}(\frac{\delta_L + \delta_R}{2})]\dot{\psi} - 2f_{22}\phi + \frac{2f_{22}r_0}{V}\dot{\phi} = 0 \qquad (2.43)$$

Therefore, the above lateral Equation (2.43) along with yaw Equation (2.35) and spin Equation (2.39) (for Configurations 1 and 2) or spin Equations (2.40) and (2.41) (for Configuration 3), fully describe the motion of the EDCW. In these equations the terms representing wheel radii (r_L, r_R) contact angle (δ_L, δ_R) of left and right wheels, and wheelset roll angle (ϕ) are non-linear functions of lateral displacement (y). As mentioned earlier, for conical wheels and lateral displacement less than those corresponding to flange contact, the wheel/rail geometry may be approximated by linear relationships. The linear relationships for symmetric wheelset are given by [44, 103].

$$\begin{aligned}
\frac{r_L - r_R}{2a} &= \lambda y/a \\
\frac{\delta_L - \delta_R}{2} &= \Delta y/a \\
\phi &= \Gamma y/a \\
\frac{\delta_L + \delta_R}{2} &= \delta_0 \\
\frac{r_L + r_R}{2} &= r_0
\end{aligned} \tag{2.44}$$

where λ, Δ, and Γ represent the coefficients of the first-order term in the series expansion of the kinematic expression represented as function of lateral motion. The above expressions are result of neglecting higher-order terms (product of perturbation quantities). For conical wheelset, these coefficients are approximately constant for all amplitudes of wheelset lateral displacements less than those corresponding to flange contact [103].

Substituting the expressions (2.44) into wheelset equations of motion and rearranging, the EDCW equations of motion are obtained for the three basic modes as:

Lateral:

$$m_w\ddot{y} + 2[D_{y_p} + \frac{f_{22}}{V}(1 + \frac{r_0\Gamma}{a})]\dot{y} + [2k_{y_p} + \frac{W_{APP}}{a}(\Gamma + \Delta) - \frac{f_{23}}{r_0 a}\Delta]y + [\frac{2f_{23}}{V} - \frac{I_{w_2}V\delta_0}{r_0 a}]\dot{\psi} - 2f_{22}\psi = 0 \quad (2.45)$$

Yaw:

$$I_{w_1}\ddot{\psi} + (D_{\psi_p} + \frac{2f_{33}}{V} + \frac{2f_{11}a^2}{V})\dot{\psi} + (k_{\psi_p} + 2f_{23} - W_{APP}a\delta_0)\psi + (\frac{I_{w_2}V\Gamma}{ar_0} - \frac{f_{23}}{V} - \frac{2f_{23}\Gamma r_0}{Va})\dot{y} + (\frac{2f_{11}a\lambda}{r_0} - \frac{2f_{33}\Delta}{r_0 a})y + \frac{2f_{11}ar_0}{V}\beta = 0 \quad (2.46)$$

Spin:

$$I_{w_2}\ddot{\beta} + [4D_{AX} + \frac{2f_{11}r_0^2}{V}]\dot{\beta} + 4k_{AX}\beta + \frac{2f_{11}r_0 a}{V}\dot{\psi} + 2f_{11}\lambda y - \frac{2f_{33}\delta_0\Gamma}{r_0 a}y = 0 \quad (2.47)$$

where

$k_{AX} = 0$, for Configuration 1.

$k_{AX} = k_{AX}$, for Configuration 2.

Configuration 3:

$$I_{w_2}\ddot{\beta} + \frac{2f_{11}r_0^2}{V}\dot{\beta} + (2k'_{AX} + 4k_{AX})\beta + 2D_{AX}\dot{\beta}_2 - 2k'_{AX}\beta_2 + \frac{2f_{11}r_0 a}{V}\dot{\psi} + 2f_{11}\lambda y - \frac{2f_{33}\delta_0\Gamma}{r_0 a}y = 0 \qquad (2.48)$$

$$2D_{AX}\dot{\beta}_2 + 2k'_{AX}\beta_2 - 2k'_{AX}\beta = 0 \qquad (2.49)$$

where β and β_2 are defined in Equation (2.41)

2.6 Summary

In this chapter, various aspects of modeling an EDCW for a railway freight car are discussed. The model basically characterizes a conventional wheelset system, where the rigid axle is replaced by an elasto-damper coupling. Various forces and moments acting on the wheelset due to creep, gravitational stiffness, primary suspension, and wheelset coupler are identified, and analytical expressions for forces and moment due to each element are derived. In modeling the coupler between the wheels within an axle, three different arrangements are considered. Various assumptions made in the modeling approach are discussed. This is, subsequently followed by derivation of the equations of motion for the EDCW.

Equations are first obtained for all six possible modes, which are then simplified and combined to obtain three final equations of motion in the lateral, yaw, and spin directions. For the coupling arrangement

Therefore, the above lateral Equation (2.43) along with yaw Equation (2.35) and spin Equation (2.39) (for Configurations 1 and 2) or spin Equations (2.40) and (2.41) (for Configuration 3), fully describe the motion of the EDCW. In these equations the terms representing wheel radii (r_L, r_R) contact angle (δ_L, δ_R) of left and right wheels, and wheelset roll angle (ϕ) are non-linear functions of lateral displacement (y). As mentioned earlier, for conical wheels and lateral displacement less than those corresponding to flange contact, the wheel/rail geometry may be approximated by linear relationships. The linear relationships for symmetric wheelset are given by [44, 103].

$$\begin{aligned}
\frac{r_L - r_R}{2a} &= \lambda y/a \\
\frac{\delta_L - \delta_R}{2} &= \Delta y/a \\
\phi &= \Gamma y/a \\
\frac{\delta_L + \delta_R}{2} &= \delta_0 \\
\frac{r_L + r_R}{2} &= r_0
\end{aligned} \tag{2.44}$$

Where λ, Δ, and Γ represent the coefficients of the first-order term in the series expansion of the kinematic expression represented as function of lateral motion. The above expressions are result of neglecting higher-order terms (product of perturbation quantities). For conical wheelset, these coefficients are approximately constant for all amplitudes of wheelset lateral displacements less than those corresponding to flange contact [103].

Substituting the expressions (2.44) into wheelset equations of motion and rearranging, the EDCW equations of motion are obtained for the three basic modes as:

Lateral:

$$m_w\ddot{y} + 2[D_{y_p} + \frac{f_{22}}{V}(1 + \frac{r_0\Gamma}{a})]\dot{y} + [2k_{y_p} + \frac{W_{APP}}{a}(\Gamma + \Delta) - \frac{f_{23}}{r_0 a}\Delta]y + [\frac{2f_{23}}{V} - \frac{I_{w_2}V\delta_0}{r_0 a}]\dot{\phi} - 2f_{22}\phi = 0 \quad (2.45)$$

Yaw:

$$I_{w_1}\ddot{\phi} + [D_{\phi_p} + \frac{2f_{33}}{V} + \frac{2f_{11}a^2}{V})\dot{\phi} + (k_{\phi_p} + 2f_{23} - W_{APP}a\delta_0)\phi + (\frac{I_{w_2}V\Gamma}{ar_0} - \frac{f_{23}}{V} - \frac{2f_{23}\Gamma r_0}{Va})\dot{y} + (\frac{2f_{11}a\lambda}{r_0} - \frac{2f_{33}\Delta}{r_0 a})y + \frac{2f_{11}ar_0}{V}\dot{\beta} = 0 \quad (2.46)$$

Spin:

$$I_{w_2}\ddot{\beta} + [4D_{AX} + \frac{2f_{11}r_0^2}{V}]\dot{\beta} + 4k_{AX}\beta + \frac{2f_{11}r_0 a}{V}\dot{\phi} + 2f_{11}\lambda y - \frac{2f_{33}\delta_0\Gamma}{r_0 a}y = 0 \quad (2.47)$$

where

$k_{AX} = 0$, for Configuration 1.

$k_{AX} = k_{AX}$, for Configuration 2.

Configuration 3:

$$I_{w_2}\ddot{\beta} + \frac{2f_{11}r_0^2}{V}\dot{\beta} + (2k'_{AX} + 4k_{AX})\beta + 2D_{AX}\dot{\beta}_2 - 2k'_{AX}\beta_2 + \frac{2f_{11}r_0 a}{V}\dot{\psi} + 2f_{11}\lambda y - \frac{2f_{33}\delta_0 \Gamma}{r_0 a}y = 0 \qquad (2.48)$$

$$2D_{AX}\dot{\beta}_2 + 2k'_{AX}\beta_2 - 2k'_{AX}\beta = 0 \qquad (2.49)$$

where β and β_2 are defined in Equation (2.41)

2.6 Summary

In this chapter, various aspects of modeling an EDCW for a railway freight car are discussed. The model basically characterizes a conventional wheelset system, where the rigid axle is replaced by an elasto-damper coupling. Various forces and moments acting on the wheelset due to creep, gravitational stiffness, primary suspension, and wheelset coupler are identified, and analytical expressions for forces and moment due to each element are derived. In modeling the coupler between the wheels within an axle, three different arrangements are considered. Various assumptions made in the modeling approach are discussed. This is, subsequently followed by derivation of the equations of motion for the EDCW.

Equations are first obtained for all six possible modes, which are then simplified and combined to obtain three final equations of motion in the lateral, yaw, and spin directions. For the coupling arrangement

consisting of stiffness and damper in series, one additional spin equation is required to describe the motion of the wheelset. Finally in this chapter, linearized wheel/rail geometric constraint functions are used to obtain a set of linear homogeneous second-order differential equations of motion for the single EDCW. In the following chapter, these equations are used to carry out detailed stability analysis of the wheelset model on a tangent track.

CHAPTER 3

LATERAL STABILITY ANALYSIS OF ELASTO-DAMPER COUPLED WHEELSET ON TANGENT TRACK

3.1 Introduction

One of the most interesting aspects of rail vehicle dynamic behaviour concerns the stability of rail vehicle motion. From the view point of running stability, the primary problem is that of lateral stability. The lateral stability problem of freight car system may be illustrated by the lateral dynamic behaviour of a single wheelset.

In this chapter, lateral stability analysis of an Elasto-Damper Coupled Wheelset (EDCW) is carried out using the models developed in Chapter 2. A study of a simplified and linearized model is desirable to obtain qualitative results through simple solution techniques. This allows the basic concepts to emerge more clearly and aids in the interpretation of results. Furthermore, linear models, because of simplicity are very efficient for parametric study.

The primary objective of this section is to carry out the model validation to gain confidence in the developed model, and to investigate the effects of wheelset coupler on the stability behaviour of the wheelset. In the following sub-sections, stability performance criterion is discussed, and the method of solution is outlined. The results of the stability analysis are also presented, and discussed to highlight the following:

1) Validation of the EDCW model by comparing its limiting case

with that of a conventional model of same complexity.

2) The effect of coupling parameters and configurations on the stability behaviour of the baseline wheelset.

3) Influence of other model parameters on the critical speed of an EDCW.

In all cases, results of EDCW system are compared to those corresponding to rigid axle conventional wheelset system.

3.2 Stability Performance Criterion

The condition of lateral instability or wheelset hunting has traditionally been described in terms of forward speed, or critical speed at which eigenvalue changes sign from negative to positive, or damping in the least damped eigenvalue goes to zero. A linear study can predict the critical speed at which wheelset will oscillate with an amplitude depending on the initial conditions. For speeds higher than the critical speed the wheelset will become unstable.

The predicted critical speed or stability boundary is however, not a direct measure of the operating speed of the wheelset or a railway car. This is simply because of the fact that ride quality is also one of the factors in determining operating speed, for which certain amount of damping must be present for satisfactory dynamic response on poor track. However, for qualitative investigation and comparison, critical speed is an effective measure of stability performance.

3.3 Method of Solution

In Section 2.5, the equations of motion for the EDCW are obtained as a set of homogeneous second-order differential equations. These equations of motion can be represented in a matrix form as:

$$[M]\{\ddot{X}\} + [D]\{\dot{X}\} + [K]\{X\} = 0 \qquad (3.1)$$

where $\{X\}^T$ is a vector of variables $\{y, \psi, \beta\}$ for Configurations 1 and 2, and $\{y, \psi, \beta, \beta_2\}$ for Configuration 3. $\{\dot{X}\}$ and $\{\ddot{X}\}$ are vectors representing velocities and accelerations respectively. [M] represents inertia matrix, and [D] and [K] represent damping and stiffness matrices, respectively. These matrices are (3 x 3) for Configurations 1 and 2, and (4 x 4) for Configuration 3.

The wheelset stability problem involves the determination of critical velocity, at which a perturbation on the system will cause divergent mode of oscillations. One of the most convenient ways of obtaining stability and mode shapes of the system is by solving the eigenvalue problem associated with Equation (3.1). The general solution to a second-order homogeneous linear differential equation with constant coefficient is given by:

$$X = \sum_{i=1}^{n} X_{0_i} e^{\mu_i t} \qquad (3.2)$$

where i is the mode number, X_{0_i} is a constant depending on the initial condition, μ_i is the corresponding eigenvalue, and t is time. Substitution of Equation (3.2) into Equation (3.1) and rearranging results in the state equation:

$$[[A] + \mu[I]]\{Z\} = 0 \tag{3.3}$$

where, $$[A] = \begin{bmatrix} [M]^{-1}[D] & [M]^{-1}[K] \\ -[I] & [0] \end{bmatrix}, \quad \{Z\} = \begin{Bmatrix} \dot{X} \\ X \end{Bmatrix}$$

In general, the solution of Equation (3.3) will produce complex eigenvalues of the form:

$$\mu_i = \alpha_i + j\eta_i \tag{3.4}$$

From the real and imaginary components of the eigenvalues, useful information such as natural frequency, damped natural frequency, and damping ratio can be defined, respectively, as:

$$\omega_{n_i} = [\alpha_i^2 + \eta_i^2]^{\frac{1}{2}} \tag{3.5}$$

$$\omega_{d_i} = |\eta_i| \tag{3.6}$$

$$\zeta_i = -\alpha_i / \omega_{n_i} \tag{3.7}$$

Substitution of Equations (3.5) to (3.7) in the expression for solution given by Equation (3.3), illustrates the stability of any mode by:

$$X_i = X_{o_i} e^{-\zeta\omega_n t} \cos(\omega_{d_i} t + N_i) \tag{3.8}$$

where N_i is a phase angle dependent on initial condition. In the

solution of the form (3.8), the factor $e^{-\zeta\omega_n t}$ determines the behaviour of the wheelset transient oscillation. When the system is stable (convergent), ζ_i will be positive, which implies that real part of eigenvalue (α_i) must be negative. As the forward speed of the model is increased, damping ratio of one of the modes will decrease to zero, indicating instability of that mode and wheelset critical speed.

3.4 Results and Discussion

The solution to eigenvalue problem is accomplished using IMSL* subroutine EIGRF, which computes the eigenvalues and eigenvectors of the given general real matrix [A], defined in Equation (3.3). Results are obtained as a series of solutions as the wheelset speed is increased. For each speed, the written program computes the eigenvalues, eigenvectors and corresponding frequencies and damping ratios. The speed at which the real part of eigenvalue for any mode changes sign from negative to positive, is considered the critical speed. The mode for the critical speed is then determined from the eigenvectors.

In this section, the validation of the developed EDCW models is first carried out by comparing their limiting cases with the known behaviour of conventional rigid wheelset system. The results of stability analysis with the EDCW are then presented under two headings. Under the first heading, the effects of Elasto-Damper coupling on the stability behaviour of the wheelset are presented. And under the second heading, the results of parametric study are presented, which

---

* IMSL International Mathematical and Statistical Libraries.

illustrates the effect of model parameters on the critical speed of EDCW.

The nominal parameters for the model used in this part of the study are listed in Table 3.1. These parameters are based on data available from literature, and are representative of conventional wheelset. The mass and moment of inertia values in the table are based on the laboratory test results from the AAR Research Center [46]. The wheel-rail geometry and primary suspension parameters are based on values commonly used in literature, for full-size wheelset model. As discussed earlier, the creep coefficients and suspension stiffnesses are load dependent parameters and are taken from Tables 2.1 and 2.2, respectively, as presented in Chapter 2. In all computations of critical speeds, the values are rounded off to nearest 1.5 m/s (5 ft/s), for computing efficiency.

3.4.1 Model Validation

Before considering any simulation results from the mathematical models developed for the EDCW, it is important to carry out possible validation of the models, so that some confidence can be placed on the results. The best validation would be a complete quantitative correlation of simulation and experimental results. However, for EDCW there are no existing experimental results. Even for conventional wheelset, there are only limited experimental results available. Furthermore, correlation between results from experiments with scale model on a roller rig and actual track is very difficult [101]. On the other hand, a lower level of validation can be carried out by a qualitative correlation between predicted trends in the simulation, and

Table 3.1 Nominal Parameters for EDCW Model

m_w	=	1117.9 kg (76.6 slugs)	I_{w_1}	=	608.0 kg.m^2 (448.0 slug.ft^2)
I_{w_2}	=	72.0 kg.m^2 (53.1 slug.ft^2)			
a	=	0.75 m (2.46 ft)	r_0	=	0.419 m (1.375 ft)
λ	=	0.05	δ_0	=	0.05
Γ	=	0.05	Δ	=	0.0
k_{y_p}	=	7.297 x 10^5 N/m (5.0 x 10^4 lb/ft)	k_{ψ_p}	=	1.695 x 10^6 N.m/rad (1.25 x 10^6 lb.ft/rad)
D_{y_p}	=	0.0 N.sec/m (0.0 lb.sec/ft)	D_{ψ_p}	=	0.0 N.m.sec/rad (0.0 lb.ft.sec/rad)
k_{AX}	=	variable N.m/rad (variable lb.ft/rad)	D_{AX}	=	variable N.m.sec/rad (variable lb.ft.sec/rad)
k'_{AX}	=	variable N.m/rad (variable lb.ft/rad)	W_{APP}	=	(5.60 x 10^4 N (1.26 x 10^4 lb)
f_{11}	=	2.563 x 10^6 N/wheel (5.763 x 10^5 lb/wheel)	f_{22}	=	2.212 x 10^6 N/wheel (4.973 x 10^5 lb/wheel)
f_{23}	=	3.12 x 10^4 N.m/wheel (2.3 x 10^3 lb.ft/wheel)	f_{33}	=	16.0 N.m^2/wheel (38.75 lb.ft^2/wheel)

experimentally observed behaviour. In this part of the study, the validation of the developed models in their limiting case is carried out in two stages.

"First Stage" Validation

In the first stage of validation, the EDCW models are considered in their limiting case to check against a two DOF conventional wheelset model of similar complexity available in the literature. The limiting case for the EDCW models are obtained by appropriately selecting large value of coupler torsional stiffness (1.356×10^{10} N.m/rad (1×10 lb. ft/rad)), which are referred to as "EDCW with rigid coupler". In the validation stages, the simulation results are obtained using the parameters in Table 3.1 with the exception for $k_{y_p} = 4.378 \times 10^5$ N/m (3×10^4 lb/ft) and $k_{\psi_p} = 1.356 \times 10^5$ N.m/rad (1×10^5 lb.ft/rad), so that the parameters are comparable to the studies considered for comparison.

The primary objective in this stage of validation is quantitative numerical comparison of EDCW models (Configurations 2 and 3) with rigid coupler, with those corresponding to conventional wheelset model taken from the literature as reference. For this purpose, the equations of motion of a two DOF conventional wheelset taken from [105] is used as a reference. Since no numerical results were presented in [105], solutions are obtained for the conventional model along with EDCW models for identical parameters. The eigenvalue solutions at each speed, corresponding to lateral and yaw modes are compared and found to be identical to 4th decimal places.

Detailed eigenvalue loci for conventional and EDCW (Configuration 2 are shown in Figures 3.1 and 3.2, respectively, for variation of speed from 3 to 58 m/s (10 to 190 ft/s). In these figures each mode and velocity lines are labeled. The loci for conventional model (Figure 3.1) shows the lateral and yaw modes of the wheelset, where the lateral mode becomes unstable at a forward velocity of 58 m/s (190 ft/s). The shape of the loci is identical to that shown in [105]. The eigenvalue loci for the EDCW is shown in Figure 3.2, which indicates three modes, i.e. lateral (y), yaw (ψ) and relative spin (β) between left and right wheels. This result (Figure 3.2) obtained for Configuration 2, with rigid coupler gives lateral, and yaw loci identical to the conventional model. The relative spin locus in this case, appears as rigid body mode with high natural frequency.

Figures 3.3 to 3.5 show the sensitivity of the eigenvalue loci to increase in speed for Configuration 3, with various coupling parameters simulating a rigid axle. The results show, that for any appropriate combination of coupling parameters simulating rigid axle, the eigenvalue loci for lateral (y), yaw (ψ), and relative spin (β) modes are identical to that of Configuration 2, where (y) and (ψ) modes are also identical to conventional model. The locus for the spin mode β_2 (relative spin between β_i and β_R) is however, affected by the combination of coupling parameters. When all coupling parameters (k_{AX}, k'_{AX}, and D_{AX}) are set to very large value, as shown in Figure 3.3, β_2 appears as rigid mode with high natural frequency. When the same parameters are used with D_{AX} equal to zero, the β_2 mode appears as lightly damped rigid body mode. Figure 3.5 shows that, when k'_{AX} is also set to zero, the β_2 mode gives zero eigenvalue, indicating neutrally stable situation for that mode.

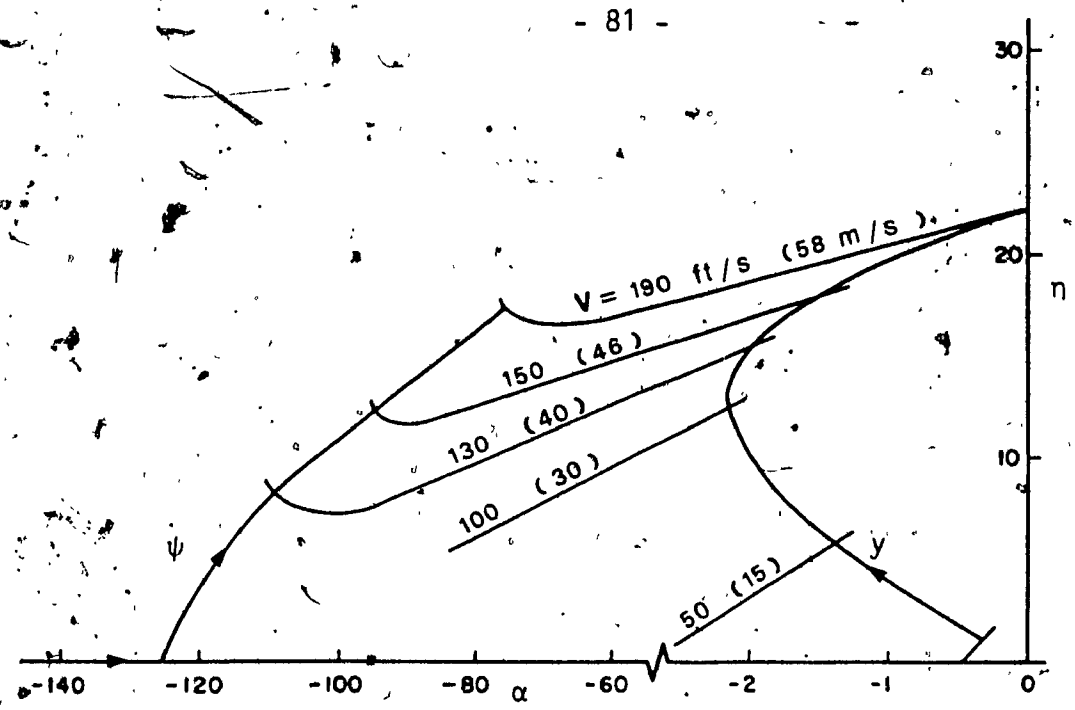

Figure 3.1 Eigenvalue loci with increasing speed for a two DOF conventional wheelset model.

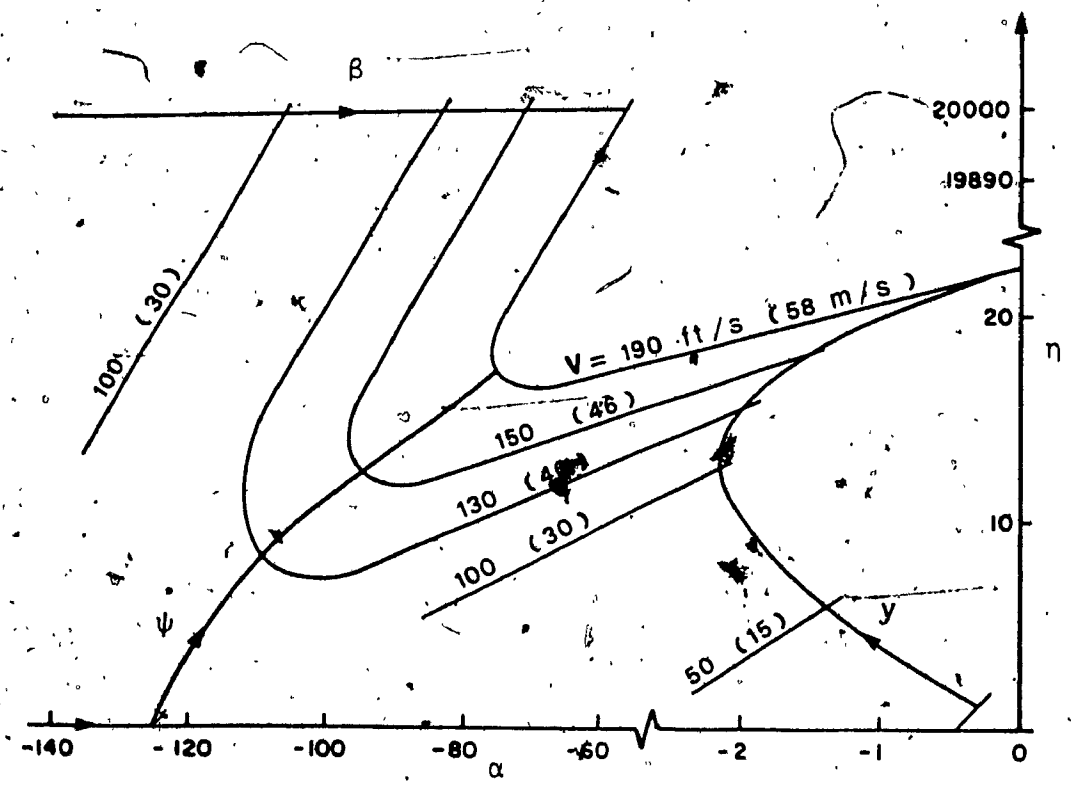

Figure 3.2 Eigenvalue loci with increasing speed for EDCW model (configuration 2) with k_{AX} = 1.356 x 10^{10} N.m/rad (10^{10} lb.ft/rad)

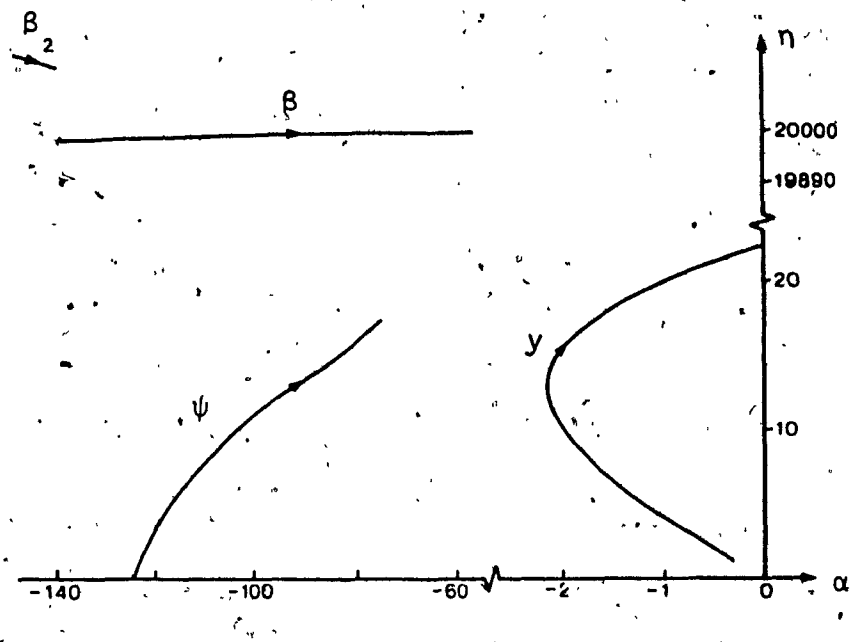

Figure 3.3 Eigenvalue loci for EDCW (configuration 3) with coupler parameters $k_{AX} = k'_{AX} = 1.356 \times 10^{10}$ N.m/rad (10^{10} lb.ft/rad), $D_{AX} = 1.356 \times 10^{10}$ N.m/rad (10^{10} lb.ft/rad).

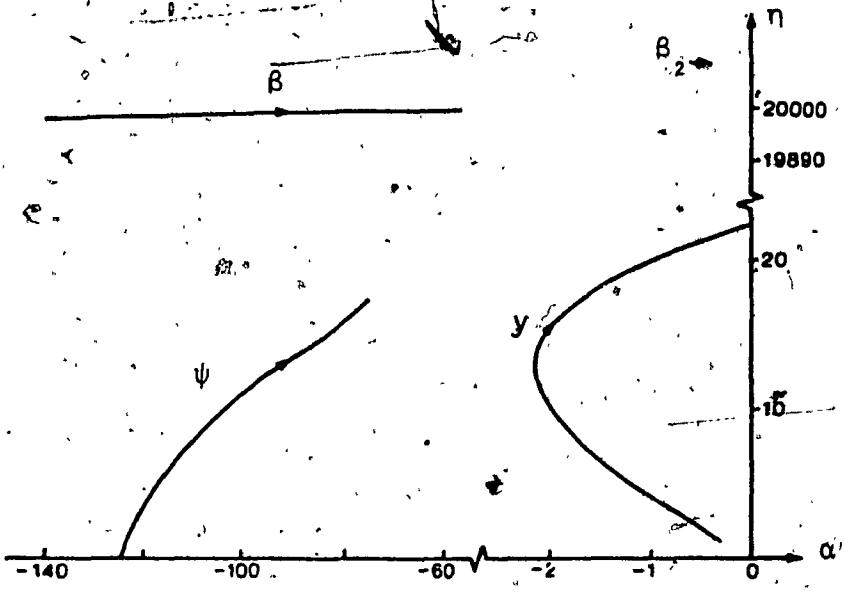

Figure 3.4 Eigenvalue loci for EDCW (configuration 3) with coupler parameters $k_{AX} = k'_{AX} = 1.356 \times 10^{10}$ N.m/rad (10^{10} lb.ft/rad), $D_{AX} = 0$.

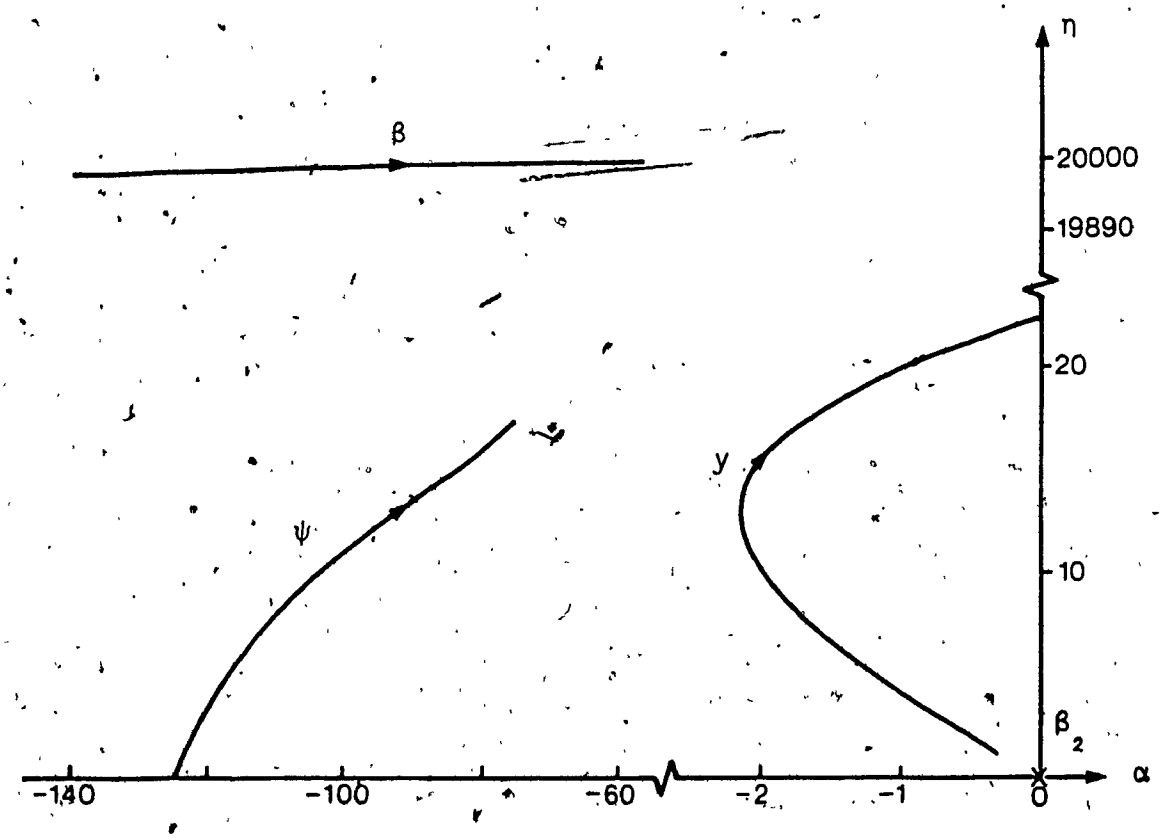

Figure 3.5 Eigenvalue loci for EDCW (configuration 3) with coupler parameters $k_{AX} = 1.356 \times 10^{10}$ N.m/rad (10^{10} lb.ft/rad), $k'_{AX} = D_{AX} = 0$.

For both Configurations 2 and 3, eigenvalue loci are also obtained for all coupling parameters set to zero, effectively simulating an IRW. As shown in Figures 3.6 and 3.7, both these configurations produce identical results where the lateral mode has zero eigenvalue, and the spin (β) is the critical mode that becomes unstable as the speed is increased. In case of Configuration 3 (Figure 3.7), β_2 also appears as neutrally stable mode.

The results obtained in this stage of validation show that by appropriately selecting large value of coupler parameters, the EDCW models can effectively simulate rigid axle wheelset. Also, when coupler parameters are selected to simulate an IRW, the prediction from the models are identical to those made in previous investigations as discussed in the literature review. The results further showed that due to specific coupler configuration, the stability behaviour of spin modes are obtained as one would expect from the physical nature of the problem.

"Second Stage" Validation

The primary objectives of the second stage of validation are to compare the simulated results of EDCW with rigid coupler, to those corresponding to wheelset stability behaviour and observed trends presented in literature from freight truck and car studies. For this, identical parameters to those used in the previous stage of validation are used. The results for the conventional wheelset model [105] and for EDCW models with rigid coupler are obtained in terms of damping ratio, frequency, as well as critical speed sensitivity to selected important wheelset parameters.

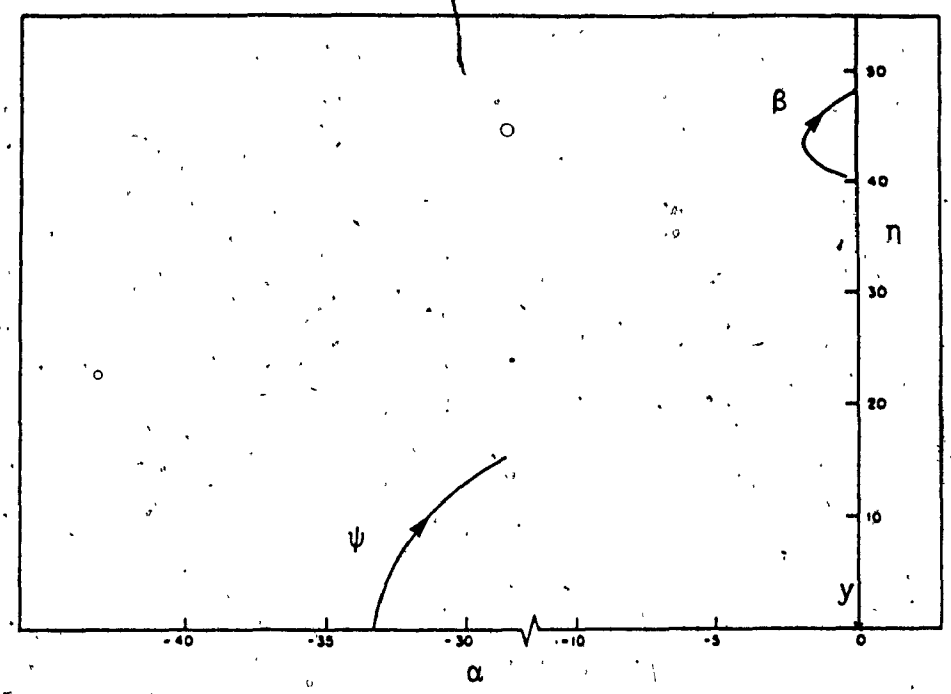

Figure 3.6 Eigenvalue loci for EDCW (configuration 2) simulating an IRW, ($k_{AX} = D_{AX} = 0$).

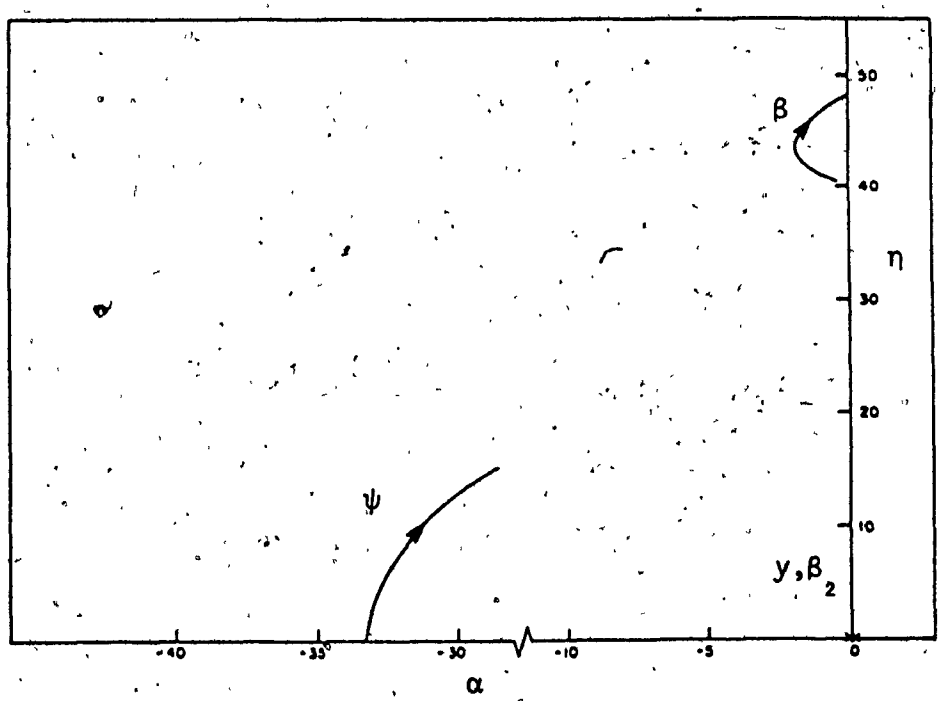

Figure 3.7 Eigenvalue loci for EDCW (configuration 3) simulating an IRW, ($k_{AX} = k'_{AX} = D_{AX} = 0$).

From the eigenvalue solutions, the modal damping ratios and modal frequencies of the critical wheelset lateral mode are plotted as a function of forward speed. These results are shown in Figures 3.8 and 3.9 and are identical for conventional and EDCW models with rigid coupler. Garg et al. [106] obtained similar results for a wheelset, from a study of four axled railway vehicle, and are shown in Figures 3.8 and 3.9. The results show good agreement with the simulation results. The finding here also show good qualitative correlation with experimental results [101] from a scaled model, presented earlier in Figure 2.5. The frequency-speed relation obtained in Figure 3.9 further shows close agreement with the kinematic relation for wheelset oscillation frequency given by [30]:

$$\omega = \frac{V}{(\lambda/ar_0)^{\frac{1}{2}}} \tag{3.9}$$

In order to determine the trend of stability behaviour the sensitivity of the critical speed for both conventional and EDCW models with rigid coupler to wheelset parameters are examined. The wheelset critical speeds for lateral mode as a function of wheel conicity, as well as primary lateral and yaw stiffnesses are shown in Figures 3.10 and 3.11, respectively. Once again, identical results are obtained for both conventional and EDCW models. As shown in Figure 3.10, it is a well known fact that rigid axle wheelset with high effective conicity will hunt at lower speed than those having low conicity. Figure 3.11 also agrees with the observed trend of conventional wheelset critical speed to variation in primary stiffness. As shown in Figure 3.11, the wheelset lateral critical speed increases significantly with increase in yaw stiffness and increases slightly with increase in lateral stiffness.

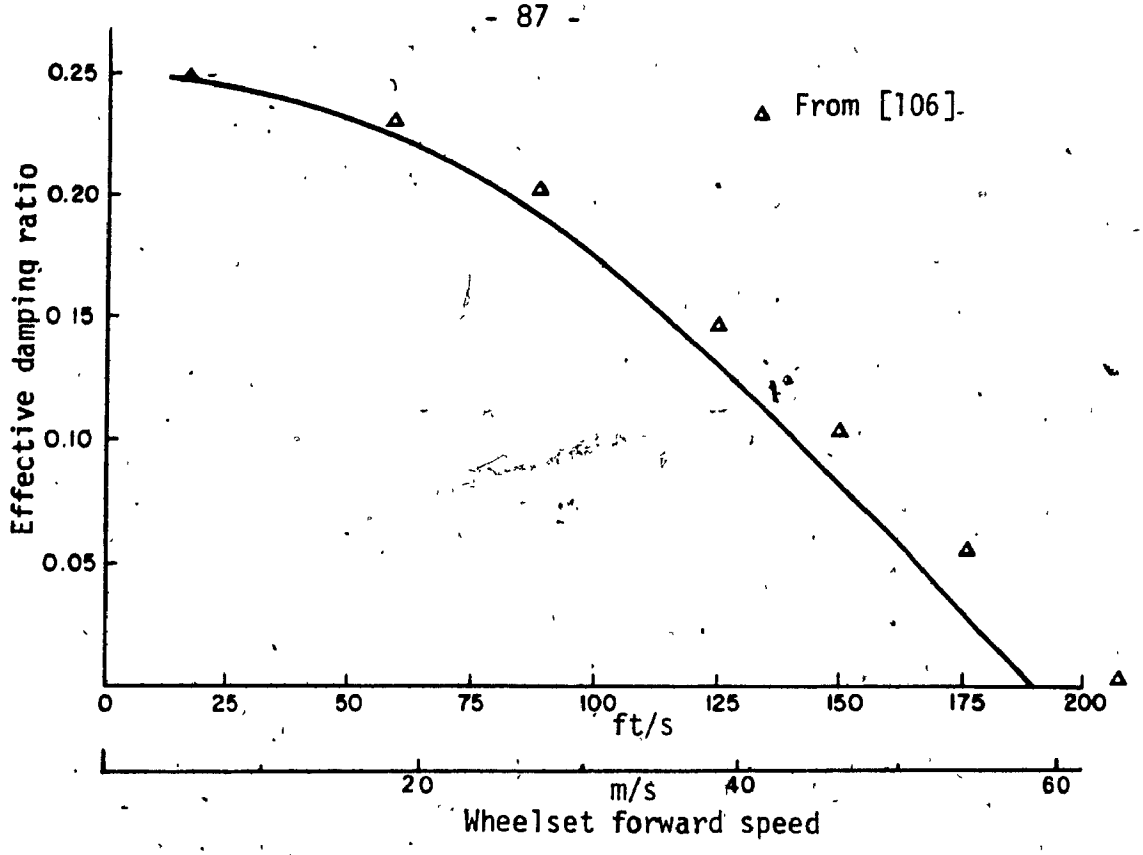

Figure 3.8 Effective lateral damping ratio versus forward speed for EDCW model with rigid coupler (Δ denotes result for conventional system [106]).

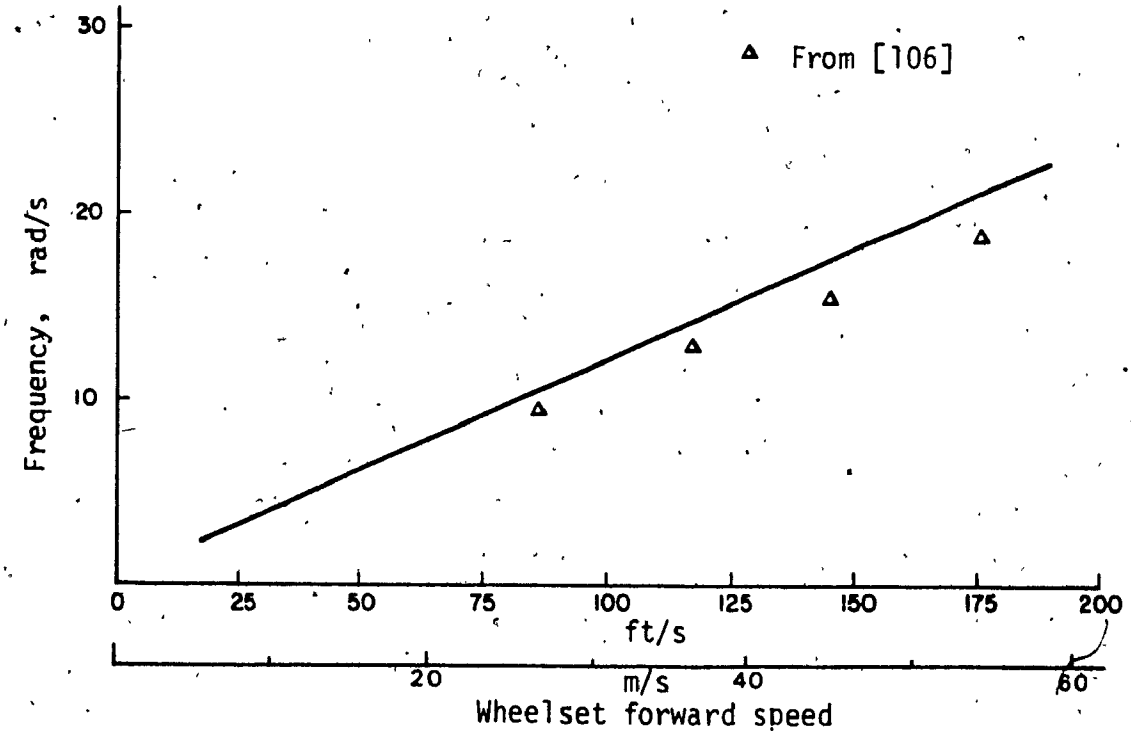

Figure 3.9 Lateral frequency versus forward speed for EDCW model with rigid coupler (Δ denotes result for conventional system [106]).

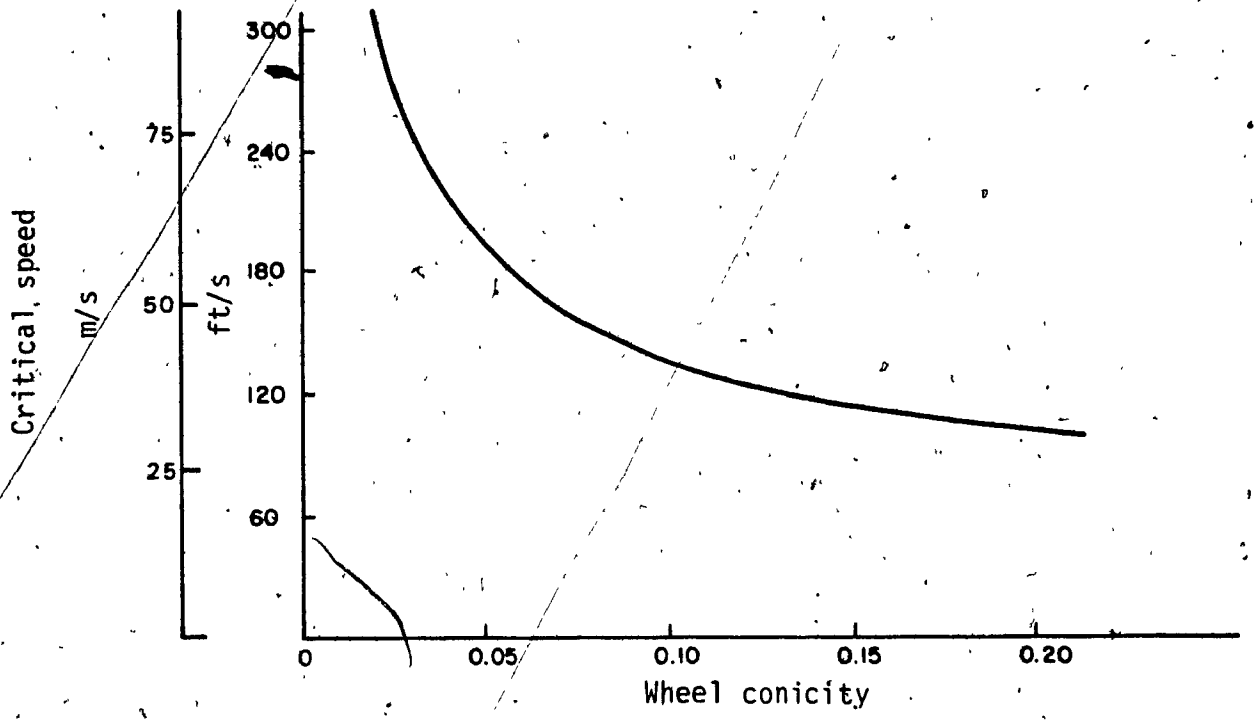

Figure 3.10 Critical speed versus effective wheel conicity for conventional wheelset and EDCW with rigid coupler.

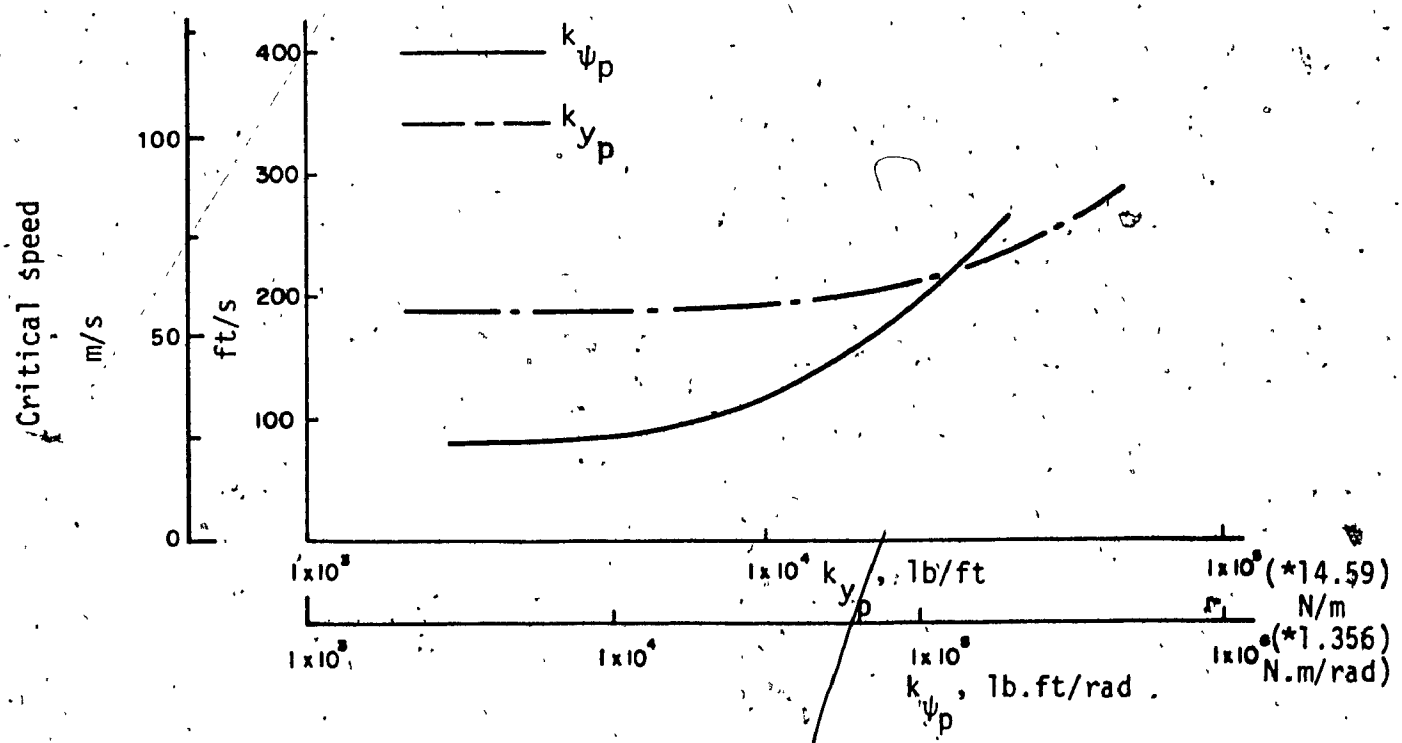

Figure 3.11 Critical speed versus primary stiffness for conventional wheelset and EDCW with rigid coupler.

Qualitative validations presented above are useful and important, since it gives confidence in the model and the trend of predicted results. Such models, even when does not represent the exact system, are invaluable in making design changes and in devising successful experiments, because they provide information about the sensitivity of system behaviour to parameter changes.

3.4.2 Elasto-Damper Coupled Wheelset Stability Behaviour

The objective of this part of the study is to examine the effect of wheelset coupling on its stability behaviour. For this, the coupler Configurations 1, 2, and 3 discussed earlier, are considered in sequence, to study the effect of each element and their combination in the coupling arrangements.

First, for Configuration 1, to study the influence of coupler damping D_{AX} alone, the EDCW model (Configuration 2) is considered with coupler stiffness, $k_{AX} = 0$, which is also identical to the four degrees-of-freedom model (Configuration 3) with k'_{AX} set to very large value, and $k_{AX} = 0$. Eigenvalue loci are obtained as the speed is increased for D_{AX} = 0, 678 and 1,356 N.m.s/rad (0, 500 and 1,000 lb.ft.s/rad) with the nominal parameters as given in Table 3.1. The results as shown in Figure 3.12 indicate, that when the torsional stiffness (k_{AX}) is zero, the mathematical model always has a consistent zero eigenvalue for lateral mode. This is expected from the physical point of view, which means, that when there is no torsional stiffness between the wheels, it will lose its self-centering or guidance capability, and may randomly wander from side to side in response to track irregularities. The results

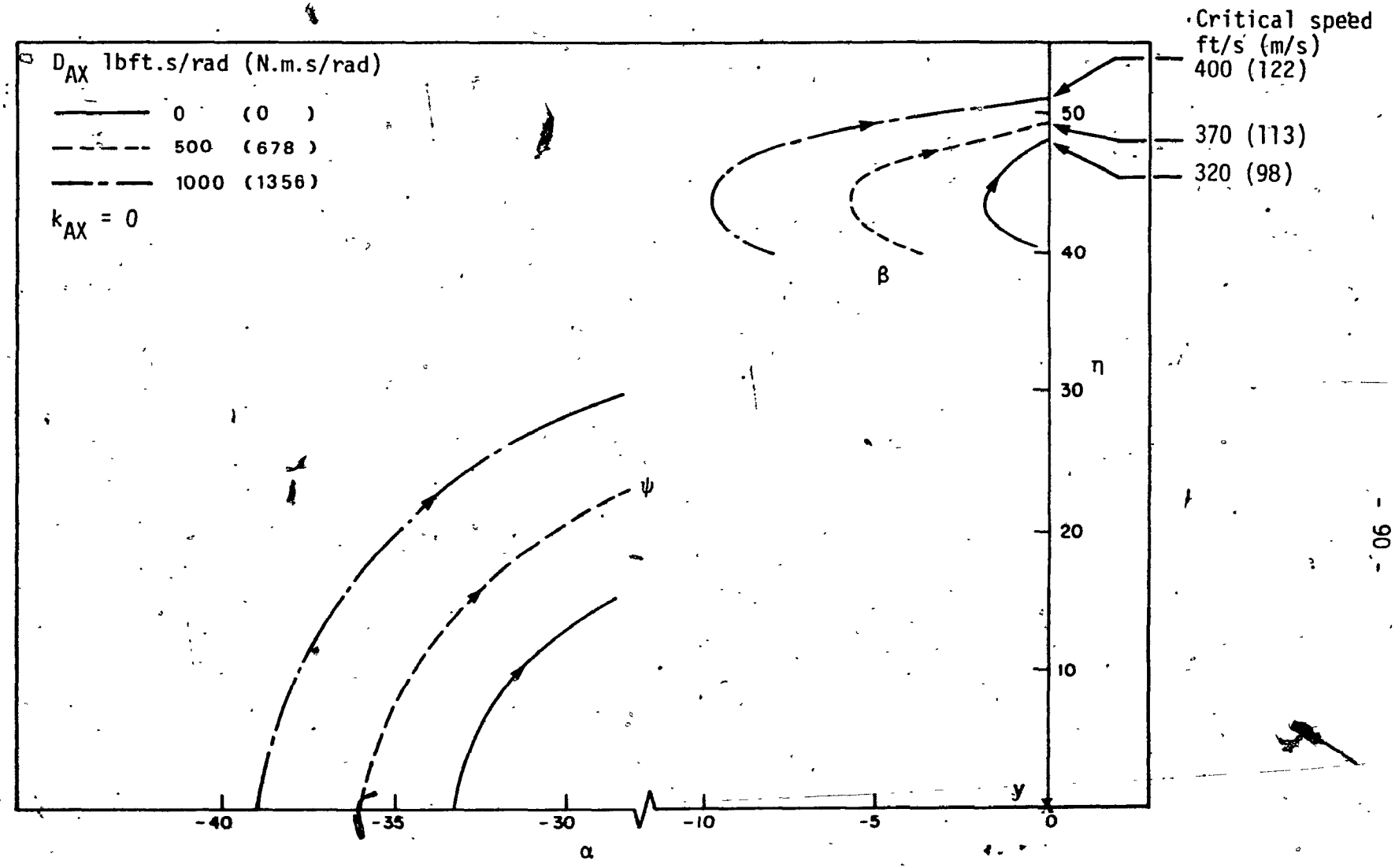

Figure 3.12 Eigenvalue loci of EDCW (configuration 1) as velocity is increased, for different values of coupler torsional damping (D_{AX}).

further indicate that when k_{AX} is zero, variation of D_{AX} has no influence on the lateral mode. However, variation of D_{AX} has direct effect on the spin mode. Besides neutrally stable situation for lateral mode, as the speed is increased, the spin mode becomes unstable at 98 m/s (320 ft/s) for $D_{AX} = 0$. As the value of D_{AX} is increased, the critical speed for the spin mode increases and approaches the critical speed of a conventional rigid axle model, which is 136 m/s (445 ft/s). Therefore, it is apparent that for the wheelset model considered, torsional damping alone can not improve the stability behaviour of the wheelset in terms of critical speed.

The EDCW of Configuration 2, is next considered to examine the effects of k_{AX}. For this, eigenvalue loci are obtained at various fixed speeds for different values of D_{AX} as k_{AX} is increased. The results of critical modes (i.e. lateral and spin), for forward velocities 30, 91, and 152 m/s (100, 300, and 500 ft/s) are shown in Figures 3.13 to 3.15, respectively. The results indicate, that for low velocities (Figure 3.13) the wheelset lateral mode is stable for all values of $k_{AX} > 0$, but for $D_{AX} = 0$, as k_{AX} is increased, the spin mode becomes unstable for a range of k_{AX}. As k_{AX} is increased further the spin mode becomes stable again. At this speed for $k_{AX} > 0$, lateral mode is always stable, and relative stability of this mode increases with increase in k_{AX}. From Figure 3.13, the effect of D_{AX} is also apparent, which improves the stability of spin mode and has very little influence on the lateral eigenvalue locus. The effect of k_{AX} on lateral mode is more apparent for higher speeds, as it can be seen in Figure 3.14. For velocity of 91 m/s (300 ft/s), when $D_{AX} = 0$, the range of k_{AX} for spin instability is greater. At this speed, as k_{AX} is increased, the relative stability of

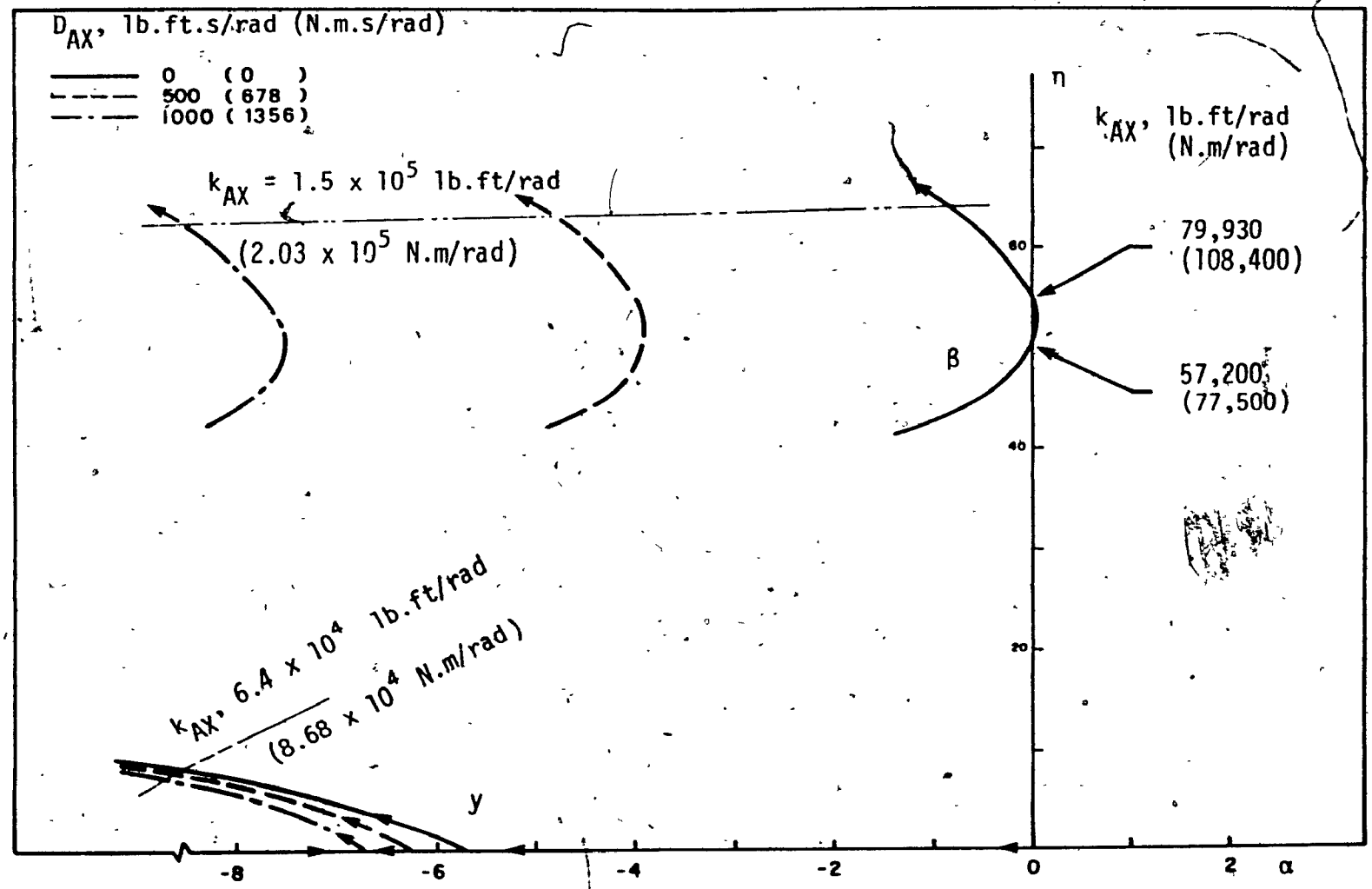

Figure 3.13 Eigenvalue loci of EDCW (configuration 2) as torsional stiffness (k_{AX}) is increased, for forward velocity, V = 30 m/s (100 ft/s).

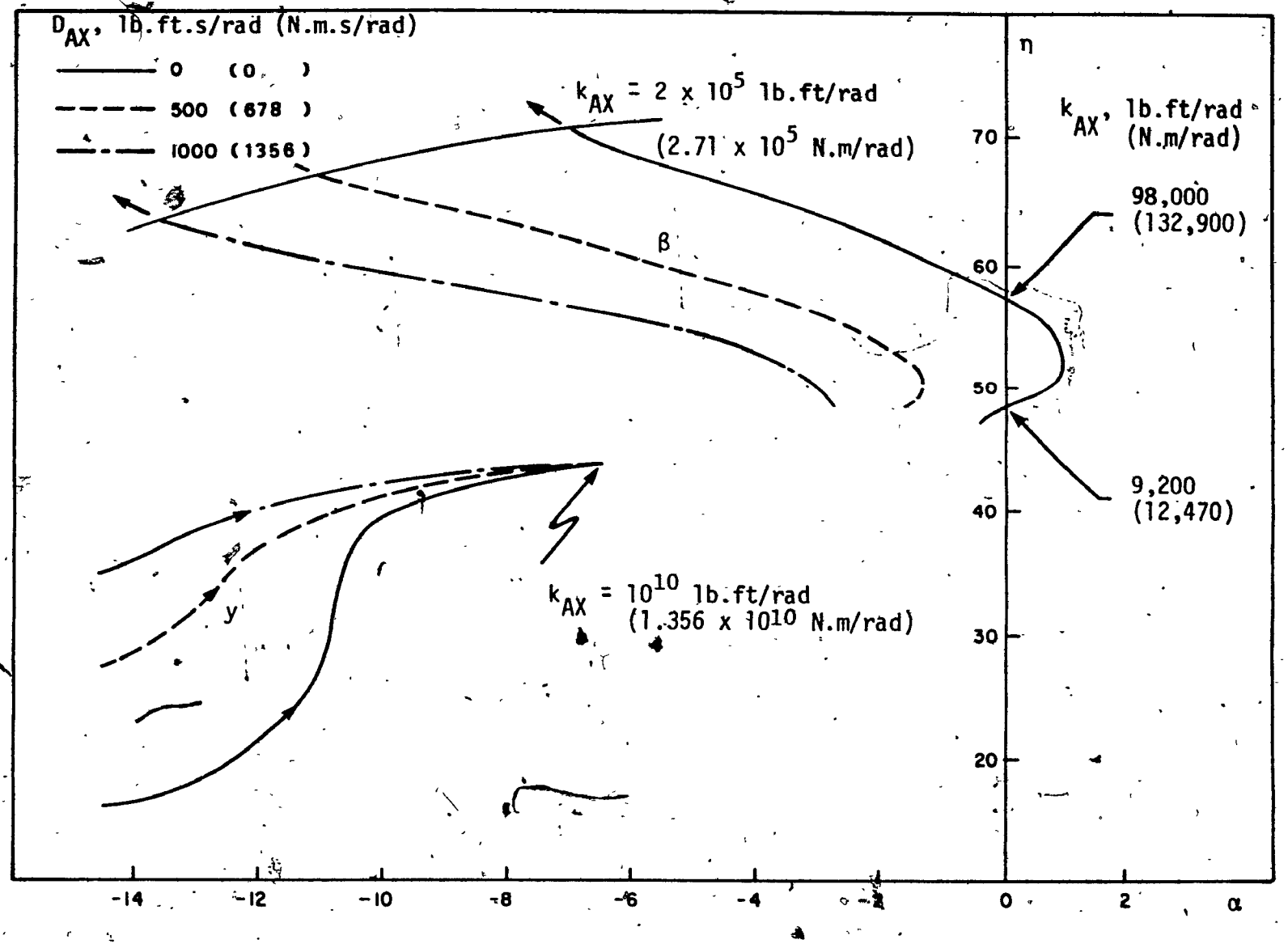

Figure 3.14 Eigenvalue loci of EDCW (configuration 2) as torsional stiffness (k_{AX}) is increased, for forward velocity, V = 91 m/s (300 ft/s).

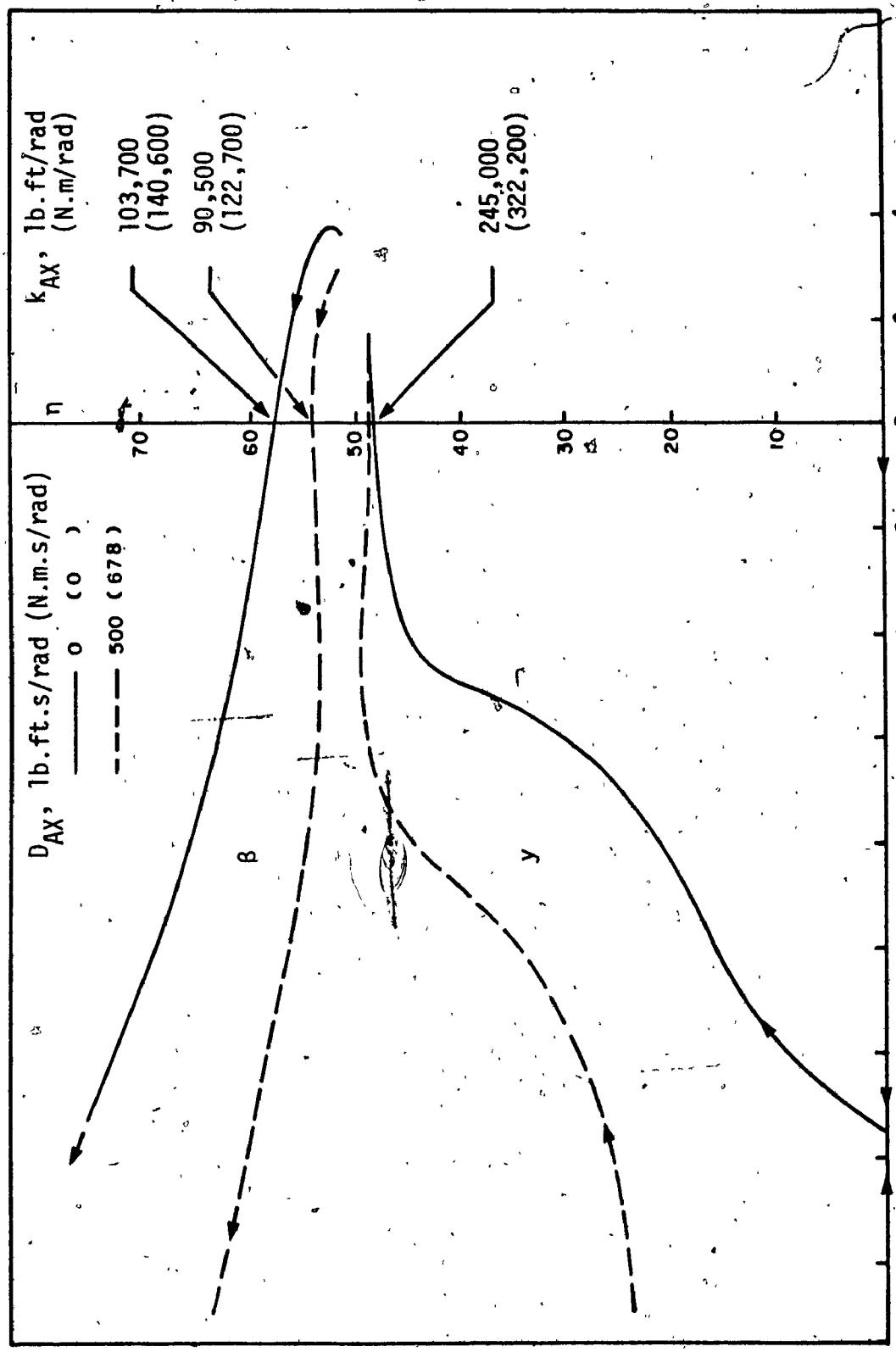

Figure 3.15 Eigenvalue loci of EDCW (configuration 2) as torsional stiffness ($k_{A\chi}$) is increased, for forward velocity, V = 152 m/s (500 ft/s).

the lateral mode decreases and that of spin mode increases. At velocity 152 m/s (500 ft/s), as shown in Figure 3.15, the sensitivity of k_{AX} on the root locus of lateral mode increases with increased speed. In this case, the spin mode is unstable for small values of k_{AX}, and becomes stable as k_{AX} is increased. At the same time, the lateral mode becomes unstable as k_{AX} is increased. As it can be seen in Figure 3.15, there is a range of k_{AX}, for which both the spin and lateral modes are stable. This range of k_{AX} reduces at higher speeds, until a speed is reached where spin mode becomes stable and lateral mode becomes unstable simultaneously at a value of k_{AX}. This optimal value of k_{AX} provides the maximum possible value for critical speed of the EDCW.

The effect of k_{AX} and D_{AX} on the wheelset critical speed can be visualized more clearly from the plots of critical speed versus these parameters, as shown in Figures 3.16 and 3.17. Figure 3.16 shows the critical speed boundaries of the EDCW (Configuration 2), as k_{AX} is varied for different values of D_{AX}. As the results indicate, there are two distinct regions of instability, for k_{AX} approximately less than and greater than 1.356×10^5 N.m/rad (1×10^5 lb.ft/rad). When k_{AX} is less than this value, the critical mode is the wheelset spin mode, that becomes unstable beyond certain forward speed, where lateral mode is always stable. For k_{AX} greater than the above value, the critical mode corresponds to that of wheelset lateral motion.

As shown in Figure 3.16, when the value of k_{AX} is increased from small value, the critical speed of spin mode reduces until it reaches a minimum value, and then it increases rapidly to become stable for all speeds. But at the same time with increase in k_{AX}, the critical speed of

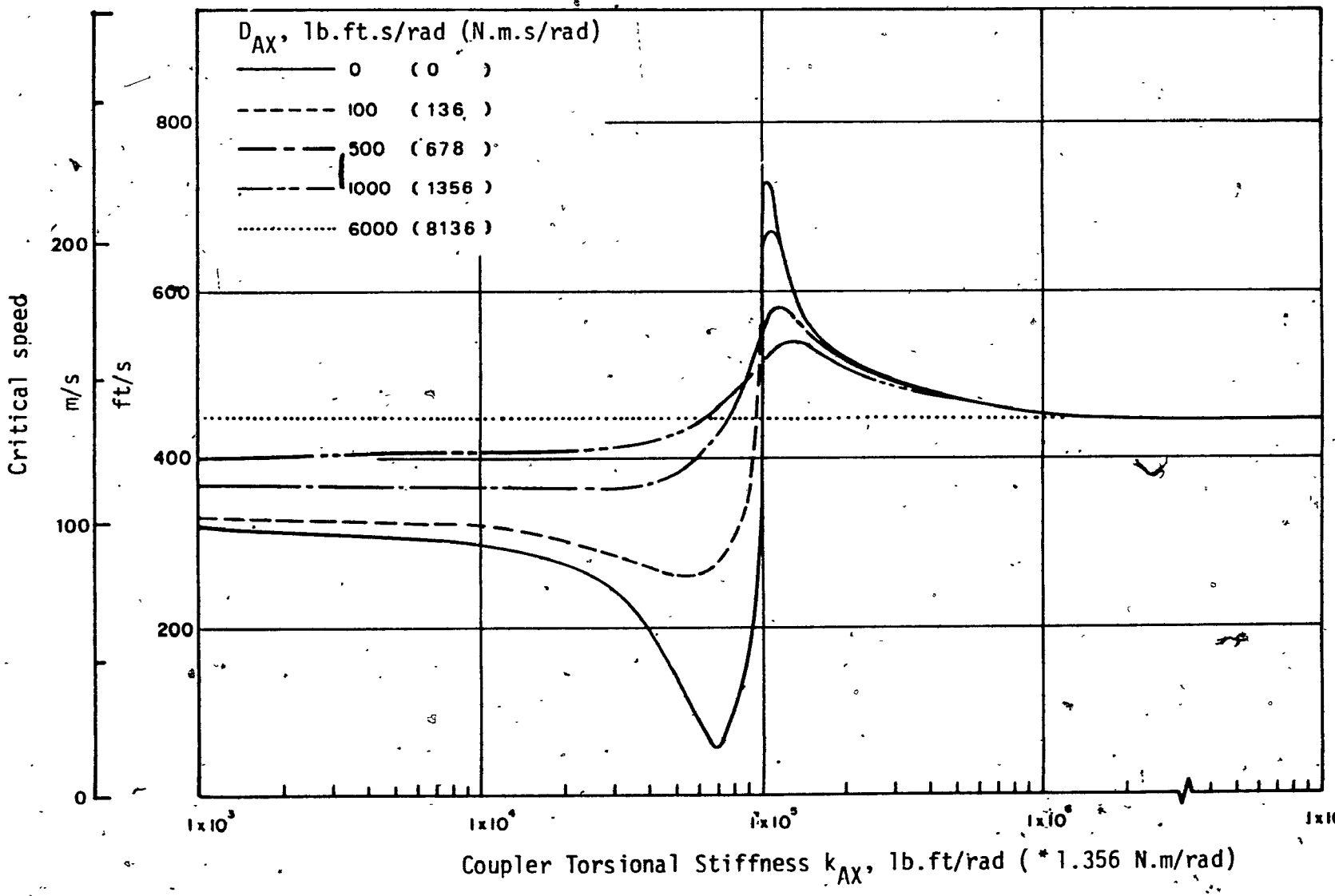

Figure 3.16 Critical speed boundaries of EDCW (configuration 2) as k_{AX} is increased, for various values of D_{AX}.

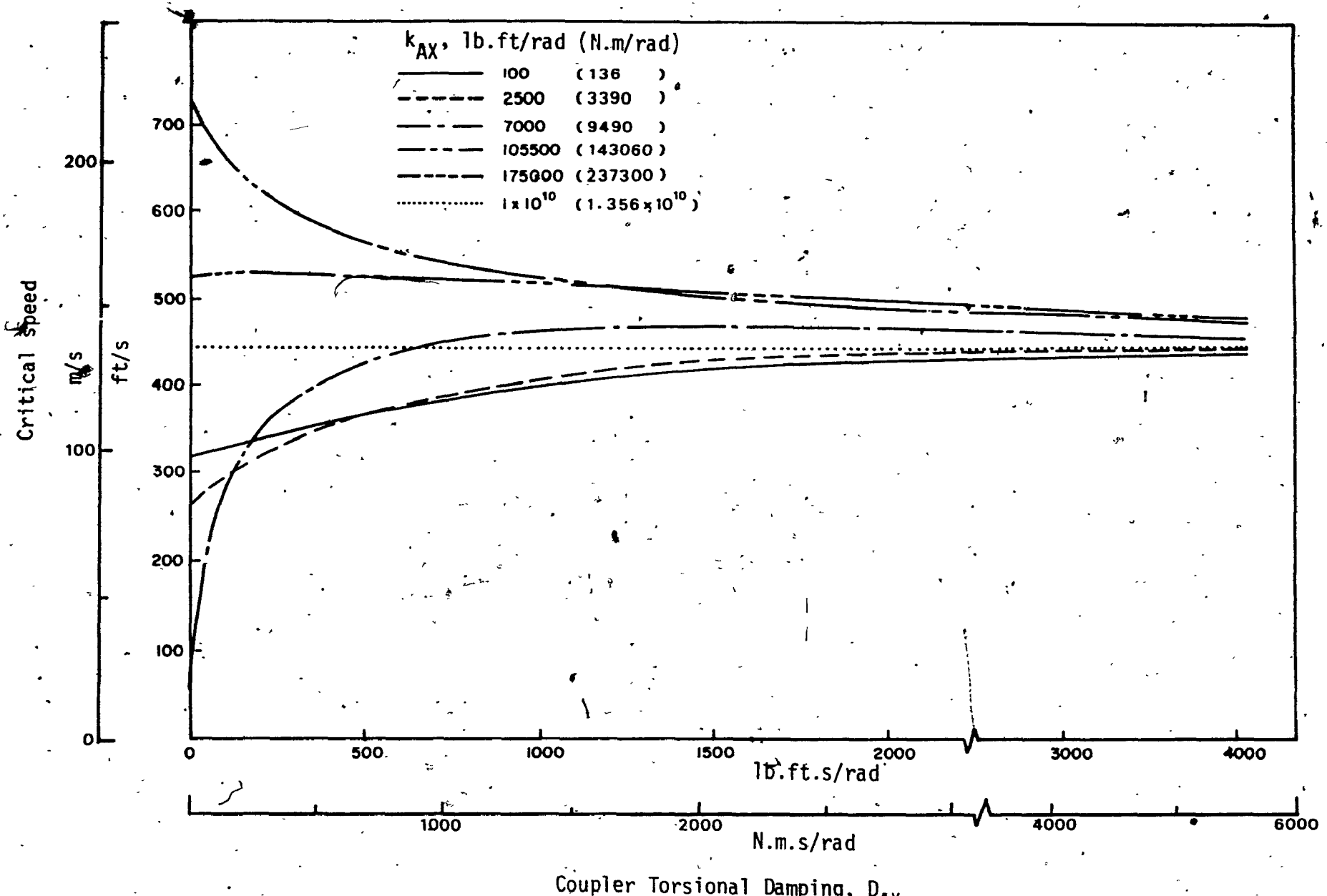

Figure 3.17. Critical speed boundaries of EDCW (configuration 2) as D_{AX} is increased, for various values of k_{AX}.

lateral mode decreases. For the baseline EDCW with D_{AX} = 0; the spin and lateral mode critical speed boundaries coincide, at the value of k_{AX} = 1.44 x 10^5 N.m/rad (1.06 x 10^5 lb.ft/rad). This is the optimal torsional stiffness of the coupler that provides maximum critical speed, when D_{AX} = 0. The coupler damping D_{AX} on the other hand has influence on the spin mode only. Increase in D_{AX} increases the critical speed of spin mode, and effectively reduces the peak critical speed of the EDCW. For very large values of either k_{AX} or D_{AX}, the EDCW effectively simulates conventional rigid axle wheelset system.

The effect of wheelset coupler parameters in Configuration 3 is finally considered, using the four degrees-of-freedom EDCW model. To obtain a combination of stiffness and damper in series, the parallel stiffness of the coupler, k_{AX} is set to zero, which leaves k'_{AX} and D_{AX} in series. For this, the critical speed boundaries are obtained as k'_{AX} is increased for various values of D_{AX}. The results are shown in Figure 3.18, which indicate that for the series arrangement, k'_{AX} has no influence on the critical speed when D_{AX} is small. This is due to the fact that when there is no resisting moment due to D_{AX}, k'_{AX} in series can not play any role, where the critical speed is due to the spin mode and is identical to the critical speed corresponding to Configuration 2 for small damping and stiffness in parallel. As the value of D_{AX} is increased, effectively making the damping element rigid, the effect of k'_{AX} is found to be same as that of Configuration 2 without any damping. This results in the maximum critical speed of 222 m/s (730 ft/s), when the torsional stiffness element of the coupler k'_{AX} = 1.44 x 10^5 N.m/rad (1.06 x 10^5 lb. ft/rad), and is identical to the results obtained for Configuration 2. Examining other stiffness-damper combinations in

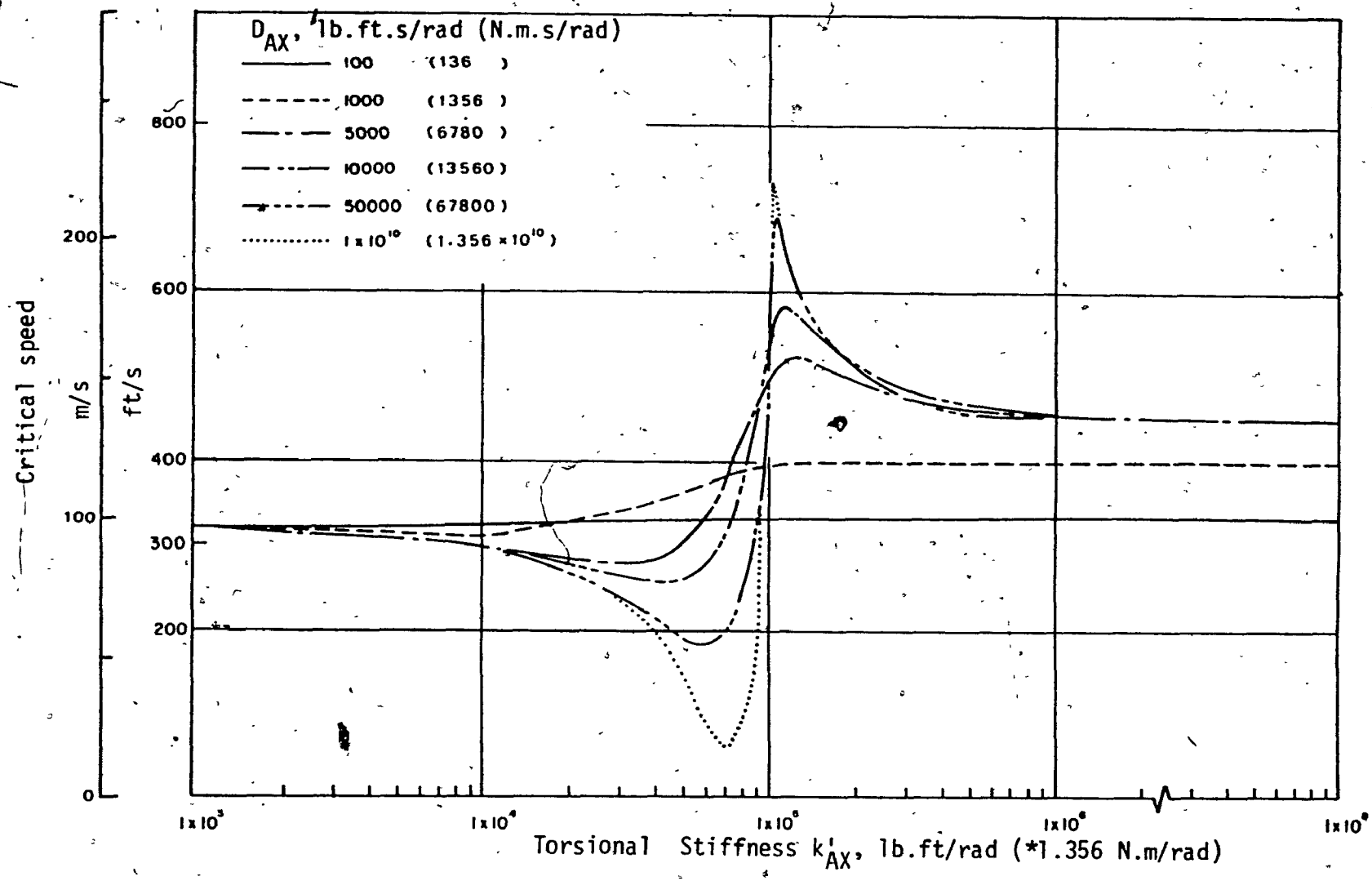

Figure 3.18 Critical speed boundaries of EDCW (configuration 3) as k'_{AX} is increased, for various values of D_{AX}, ($k_{AX} = 0$).

Configuration 3, similar results are obtained for various values of k_{AX}. A sample plot for k_{AX} = 13,560 N.m/rad (10^4 lb.ft/rad) is shown in Figure 3.19. The results are similar to Figure 3.18, except in this case addition of parallel stiffness k_{AX} causes a shift of the curves to the left by an amount of the value of k_{AX}. This indicates that regardless of coupling arrangement, the intersection of the stability boundaries and the peak critical speed is provided by total coupler stiffness of 1.44 x 10^5 N.m/rad (1.06 x 10^5 lb.ft/rad).

The results obtained in this section of the study showed that for a given set of wheelset parameters there exists an optimal torsional stiffness to maximize the critical speed. The influence of coupler in maximizing critical speed are summarized in Table 3.2. For the baseline EDCW, the maximum critical speed is 222 m/s (730 ft/s), for optimal coupler parameter with total torsional stiffness of 1.44 x 10^5 N.m/rad (1.06 x 10^5 lb.ft/rad). This is 64% greater than the critical speed of 136 m/s (445 ft/s) that corresponds to baseline model of conventional rigid axle wheelset.

In the following sub-sections, the influence of other wheelset parameters on the critical speed of EDCW model are examined, and compared with that corresponding to conventional wheelset.

3.4.3 Influence of Wheelset Parameters

A comprehensive parametric study of the EDCW model is carried out to determine the influence of various model parameters on the stability of the wheelset. Various parameters considered include:

- effective wheel conicity;

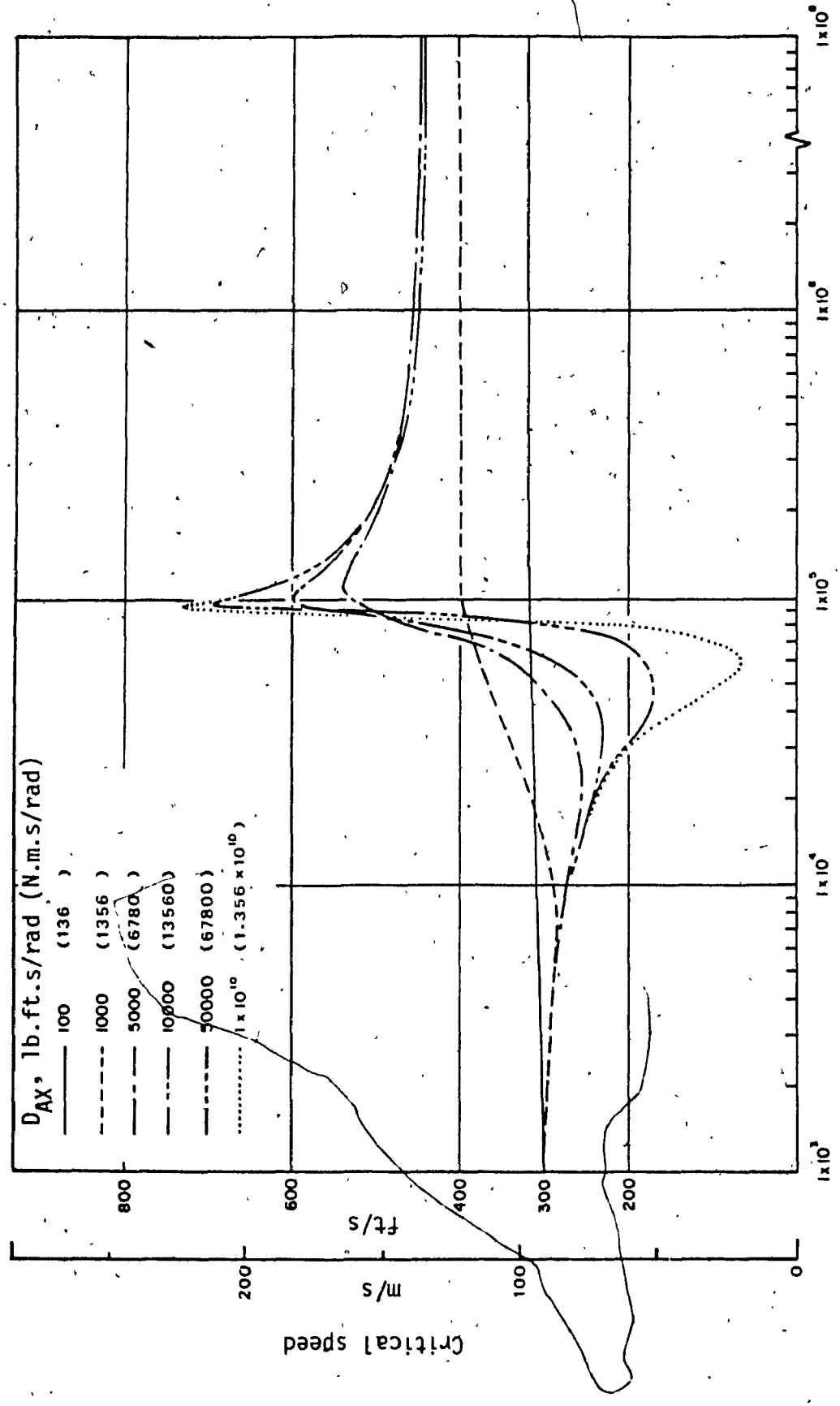

Figure 3.19 Critical speed boundaries of EDCW (configuration 3) as k'_{AX} is increased, for various values of D_{AX}, (k_{AX} = 1.356 x 10^4 N.m/rad (10^4 lb.ft/rad)).

Table 3.2 Summary of Coupler Influence in Maximizing Wheelset Critical Speed

Model	Coupler Parameter		Critical Speed m/s (ft/s)
	Damping, N.m.s/rad (lb.ft.s/rad)	Stiffness, N.m/rad (lb.ft/rad)	
Conventional	-	-	136 (445)
EDCW Configuration 1	$D_{AX} >$ 5,400 (4,000)	-	136 (445)
EDCW Configuration 2	0	$k_{AX} =$ 1.44×10^5 (1.06×10^5)	222 (730)
EDCW Configuration 3	$D_{AX} >$ 1.356×10^{10} (1×10^{10})	$k_{AX} + k'_{AX} =$ 1.44×10^5 (1.06×10^5)	222 (730)

- primary yaw stiffness;
- creep coefficients;
- axle loading.

The primary objective is to investigate the influence of these parameters on the optimal value of coupler torsional stiffness, and on the critical speeds corresponding to the optimal coupler stiffness. The EDCW with coupler arrangement in Configuration 2 is only considered in this part of the study. Effects of each parameter is examined one at a time while nominal values are maintained for the other parameters. For various values of each parameter, stability boundary curves are obtained as torsional stiffness (k_{AX}) is increased from 1.356×10^3 to 1.356×10^8 N. m/rad (10^3 to 10^8 lb.ft/rad) with $D_{AX} = 0$. The largest value of k_{AX} represents a conventional rigid axle wheelset. The critical speed sensitivity of EDCW with optimal coupler parameter to variation in each of the model parameters considered, are compared to that of conventional system. In the following sections, the EDCW of Configuration 2 is simply referred to as "EDCW system".

Effect of Conicity

The critical speed curves or stability boundaries for varying torsional stiffness k_{AX} are obtained for effective wheel conicity in the range of 0.02 to 0.2, as shown in Figure 3.20. For all values of effective wheel conicity, the general shape of the curves are similar, however, as the results indicate, the lateral mode critical speed is more sensitive to wheel conicity than that corresponding to spin mode. A general trend is that an increase in wheel conicity decreases the critical speed for all values of k_{AX}. This destabilizing effect of wheel

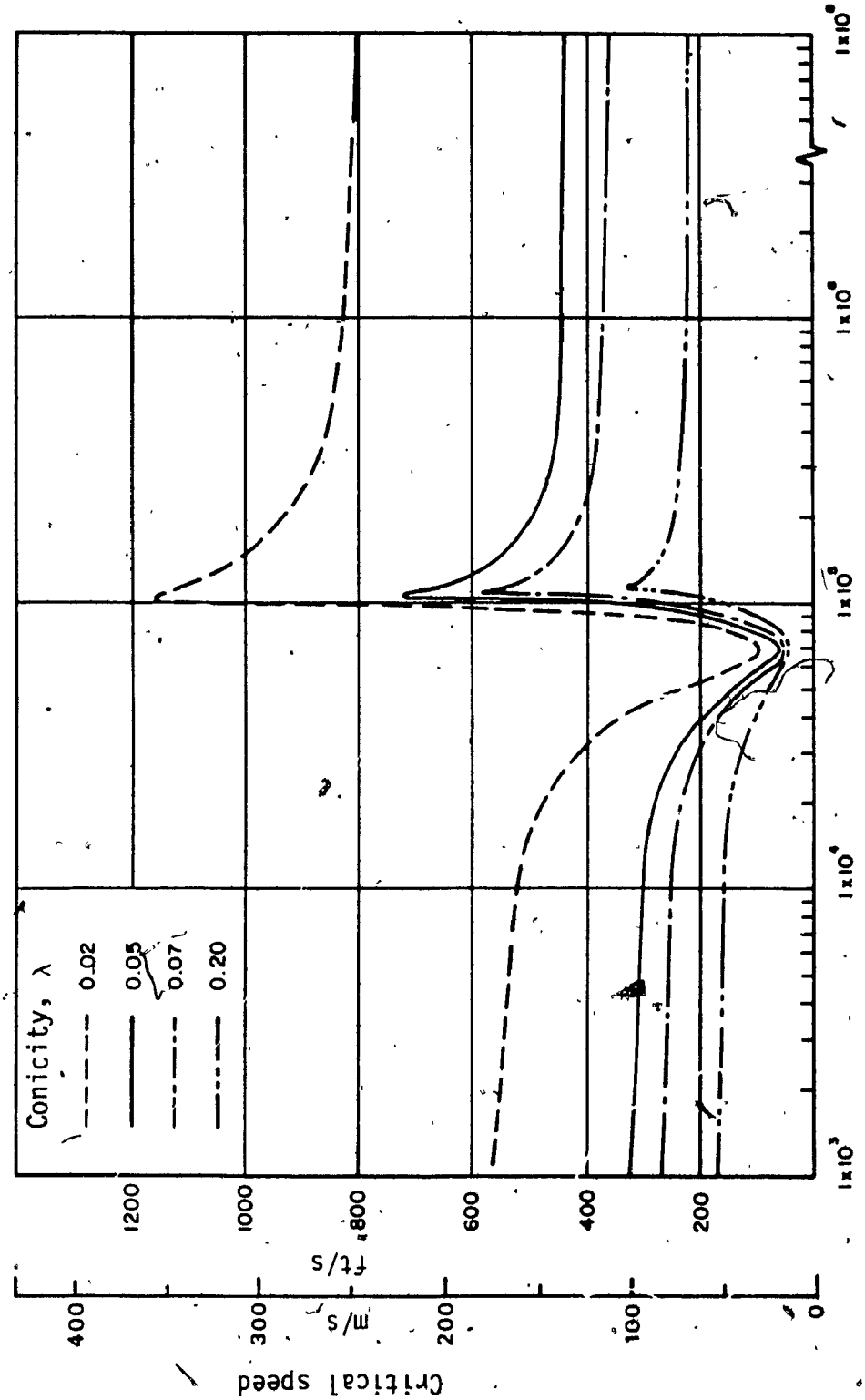

Figure 3.20 Effect of wheel conicity on the critical speed boundaries of EDCW as k_{AX} is increased, ($D_{AX} = 0$).

conicity is a well known fact in the dynamic behaviour of conical railway wheelsets.

For the EDCW with small values of k_{AX}, when wheel conicity (λ) is reduced from 0.2 to 0.02 rad., the critical speed corresponding to spin mode increased by 122 m/s (400 ft/s). For the same variation in λ, the critical speed corresponding to optimal k_{AX} increased by 256 m/s (840 ft/s), while for rigid axle wheelset, the critical speed increased by 181 m/s (595 ft/s) where critical mode is the wheelset lateral motion. The results in Figure 3.20 further indicate that, as the wheel conicity is reduced, the optimal value of k_{AX} for the EDCW also reduces slightly.

The critical speed sensitivity to effective wheel conicity for EDCW with optimal coupler, as well as for rigid axle are shown in Figure 3.21. From the results, the superiority of EDCW over the conventional system is evident in the entire conicity range.

Effect of Yaw Stiffness

To study the effect of primary yaw stiffness ($k_{\psi p}$) on the critical speed of EDCW, critical speed versus torsional stiffness (k_{AX}) are obtained for various values of $k_{\psi p}$. The results, as plots of stability boundary curves are shown in Figure 3.22 for four different values of $k_{\psi p}$. The results indicate that, as $k_{\psi p}$ is increased, the critical speed increases for all values of k_{AX} except for the value of k_{AX} where the critical speed corresponding to spin mode is minimum. It can be seen that the critical speed boundaries are of similar shape and move to the right as $k_{\psi p}$ is increased. This indicates that, optimal coupler stiffness increases significantly as the yaw stiffness is increased.

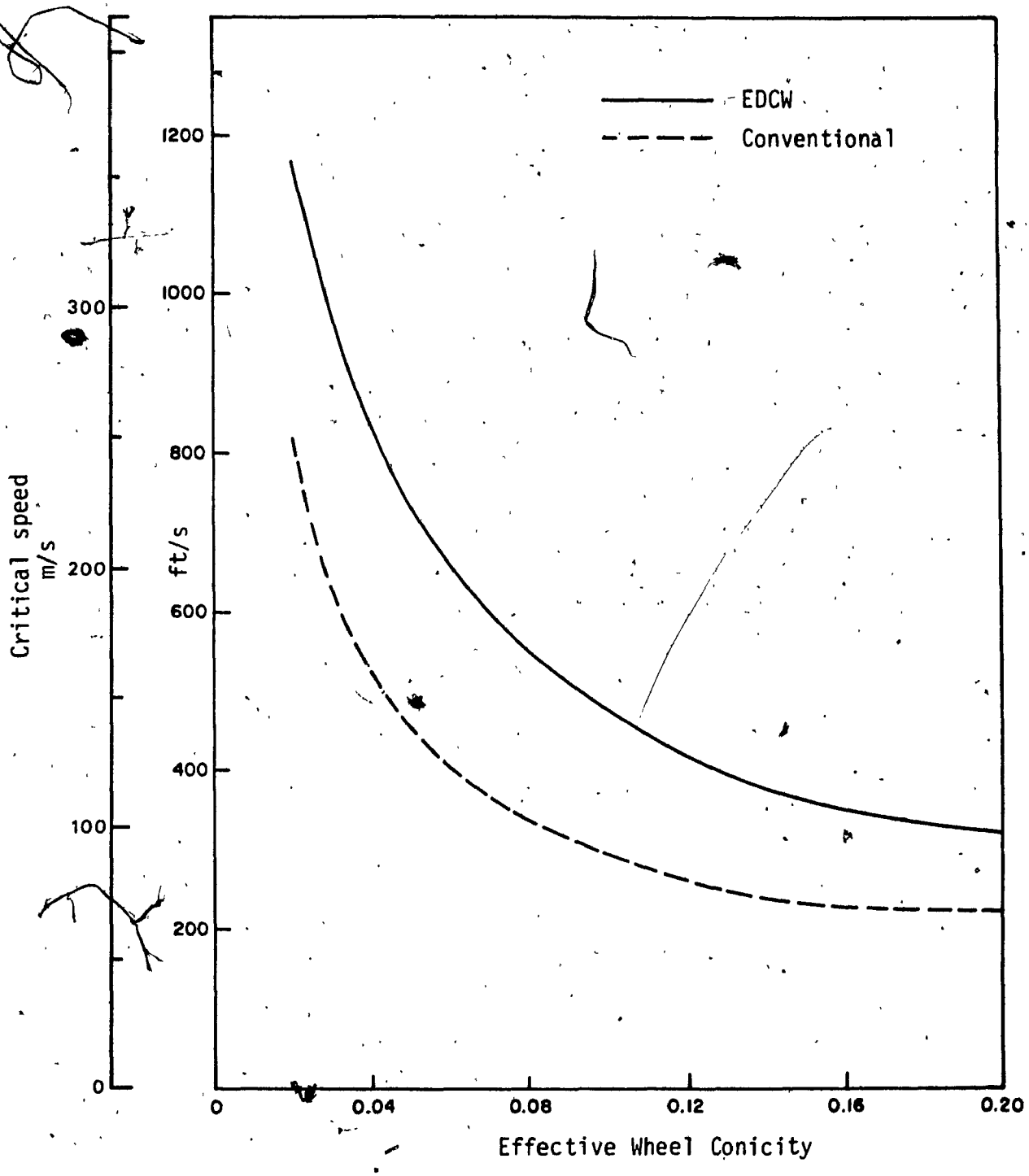

Figure 3.21 Critical speed versus effective wheel conicity for conventional and EDCW system with optimal coupler.

Further, it can be seen from Figure 3.22, that when k_{AX} is small, the spin critical speed sensitivity increases significantly with increase in $k_{\psi p}$. Similar behaviour is also observed for a rigid coupler simulating a conventional wheelset. The sensitivity of the critical speed for optimal k_{AX}, however varies uniformly throughout the range of $k_{\psi p}$ considered. The results in Figure 3.22 further show that when large restraints in the yaw is provided, the influence of coupler stiffness on the wheelset lateral mode decreases considerably.

The critical speed sensitivity to primary yaw stiffness for both EDCW with optimal coupler and rigid axle wheelset are shown in Figure 3.23. In the practical range of $k_{\psi p}$, the EDCW provides significantly superior performance over the conventional system.

Effect of Creep Coefficients

As discussed earlier, the nominal creep coefficients for the wheelset model considered in this study are based on Kalker's linear theory. In this section, the influence of variation in creep coefficients on the critical speed of EDCW is examined, as the torsional stiffness is varied. The results as critical speed boundaries are shown in Figure 3.24, for creep coefficients in the range of 50 to 200% of their nominal values. In general, for all values of k_{AX}, increase in creep coefficients reduces the critical speed. The results also show that for either small or large values of k_{AX}, the critical speed boundary has negligible change for variation in creep coefficients in the range of 100 to 200% of nominal values. For the same range of creep coefficients, the effect is maximum near the optimal value of k_{AX}. On the other hand,

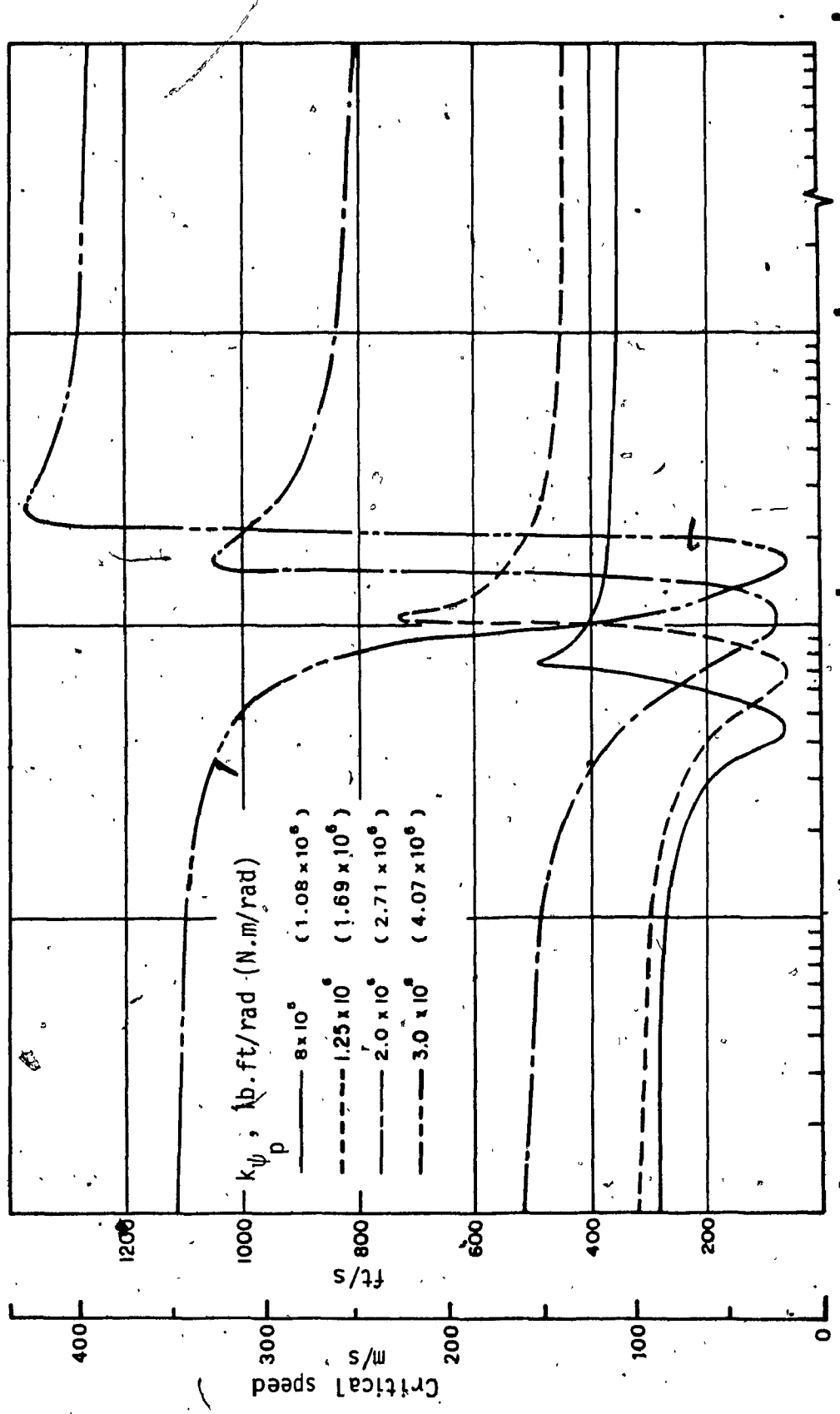

Figure 3.22 Effect of axle load on the critical speed boundaries of EDCW system as k_{AX} is increased, (D_{AX} = 0).

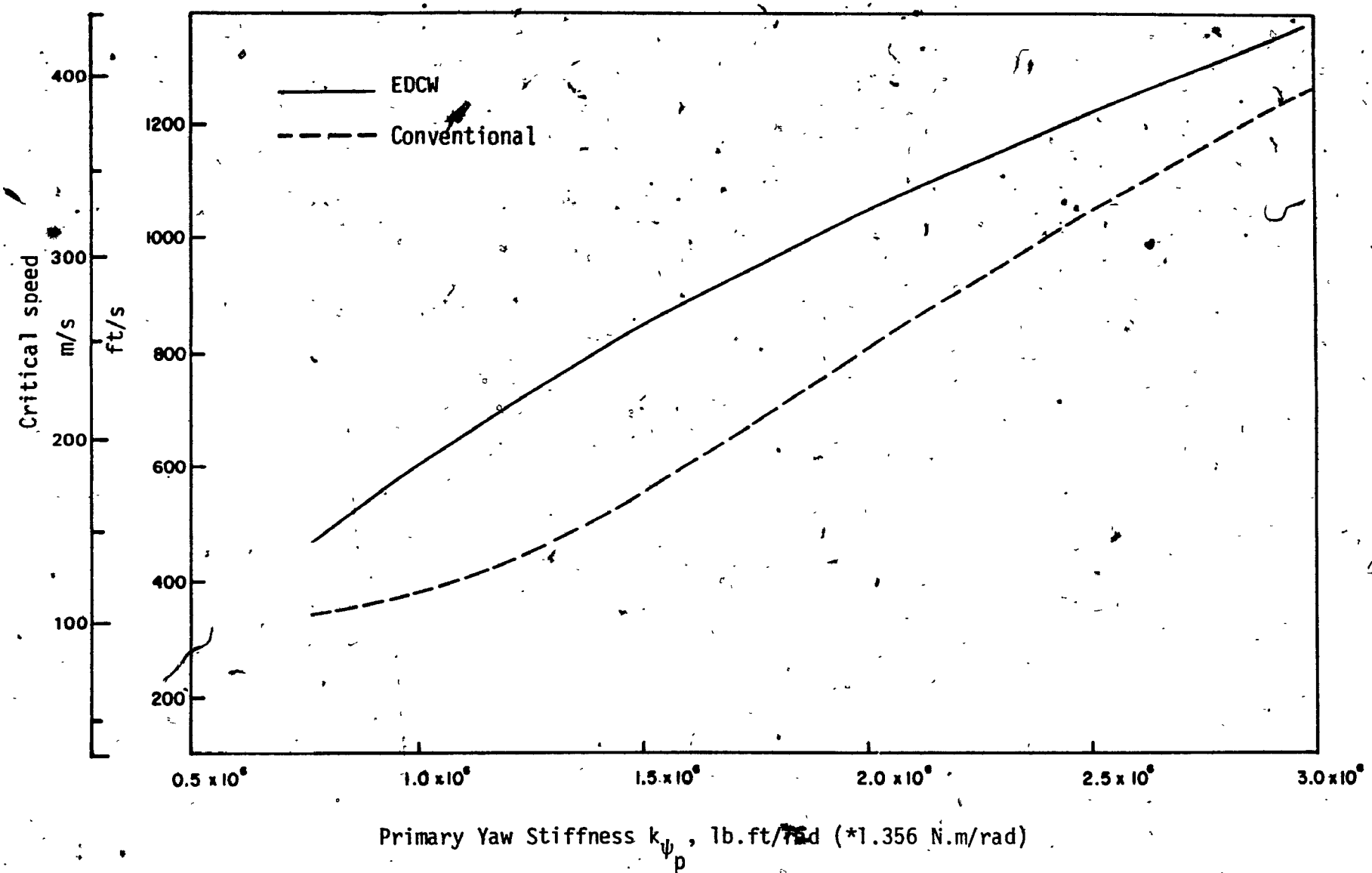

Figure 3.23 Critical speed versus primary yaw stiffness for conventional and EDCW system with optimal coupler.

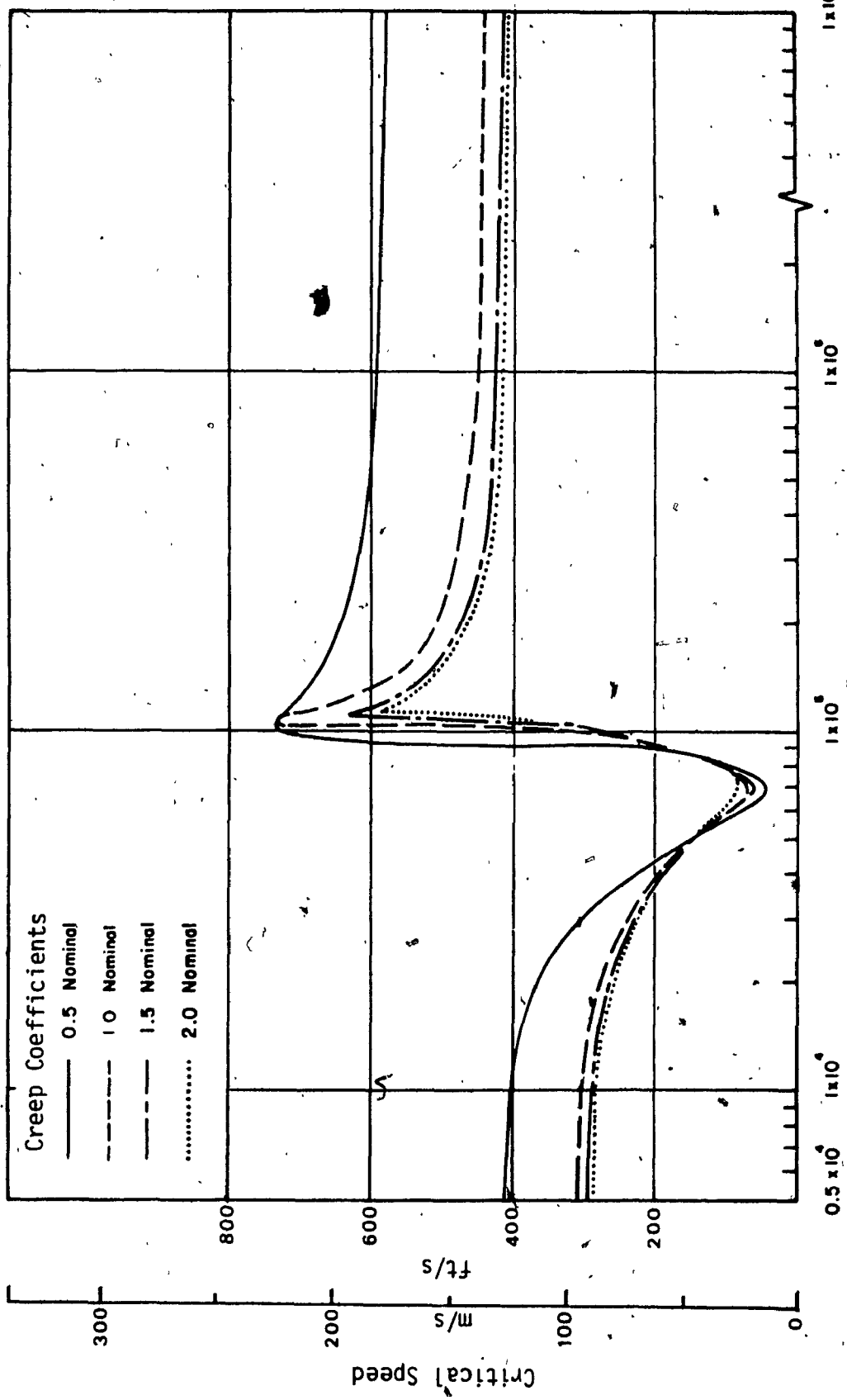

Figure 3.24 , Effect of creep coefficients on the critical speed boundaries of EDCW system as k_{AX} is increased, ($D_{AX} = 0$).

when creep coefficients are reduced to 50% of the nominal value, there is a considerable improvement of critical speed when k_{AX} is either small or very large. For reduced creep coefficient, however, the effect is negligible for optimal k_{AX}.

Effect of Axle Load

To examine the effect of axle loads on the critical speed of EDCW, stability boundary curves are obtained or three different axle loads. These loadings correspond to axle load due to empty, symmetric half-load and full-load of a 70 ton freight car [40]. As discussed in Sections 2.3.1, 2.3.2, and 2.3.3. the creep coefficients, gravitational stiffness, and primary suspension stiffnesses are functions of axle load. The gravitational stiffness force is however, expressed in the equations of motion in terms of axle load. In this part of the study, nominal wheelset parameters are used except for creep coefficients, and for primary suspension constants. The value of these parameters are taken from Tables 2.1 and 2.2 corresponding to each axle loading.

Figure 3.25 shows the stability boundaries of the EDCW as the coupler stiffness (k_{AX}) is varied. For each axle loading (W_{APP}), the general shape of the curve remains similar, where the curve effectively shifts at the right as W_{APP} is increased. This indicates that optimal k_{AX} value is larger for larger axle load. With the increase in W_{APP}, there is a small increase in critical speed for both small and large values of k_{AX}, indicating better stability in both spin and lateral modes. However, the axle load shows hardly any effect on the maximum critical speed at the optimal value of k_{AX}. Although critical speed of

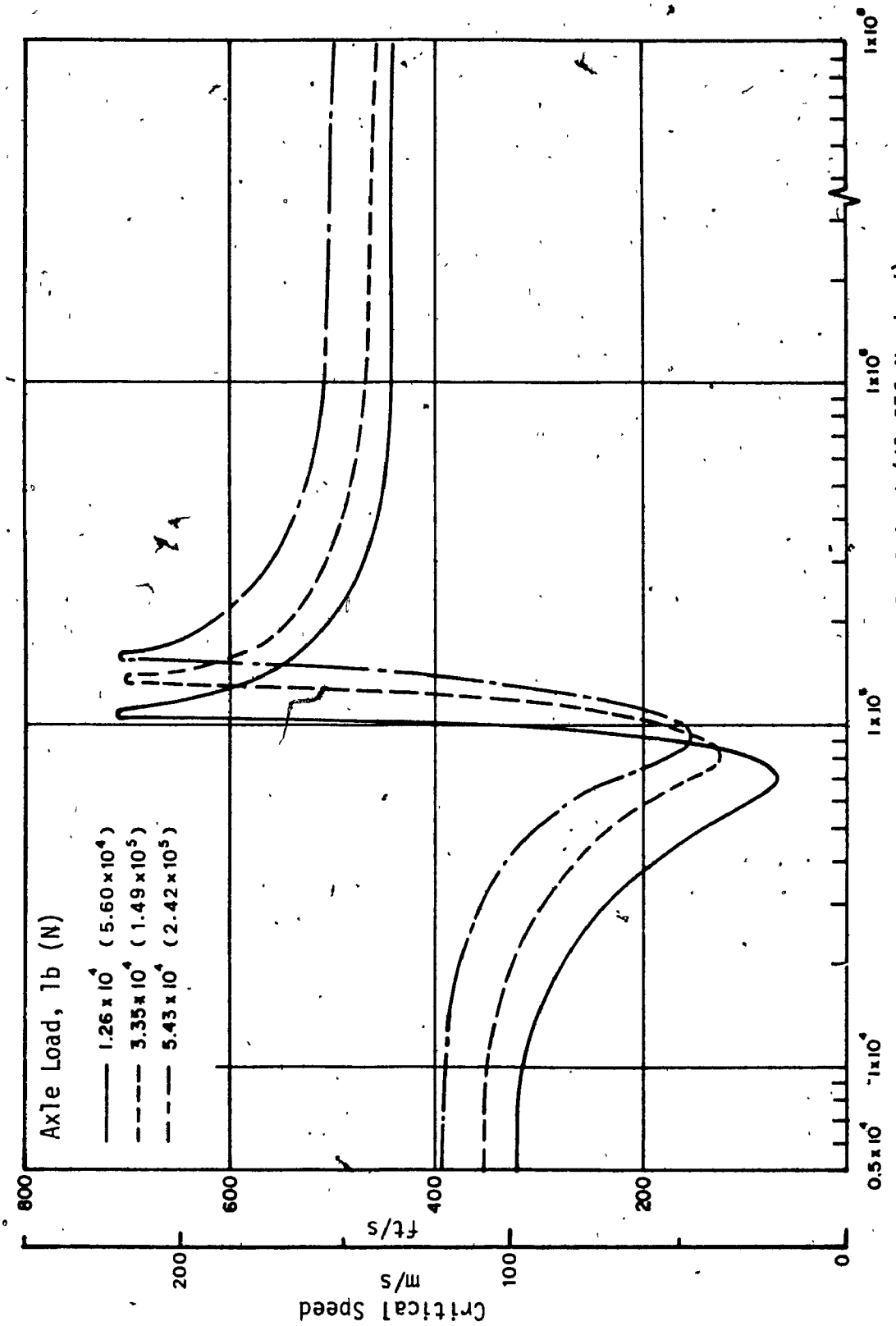

Figure 3.25 Effect of axle load on the critical speed boundaries of EDCW as k_{AX} is increased, ($D_{AX} = 0$).

rigid axle wheelset improves with W_{APP}, the critical speed corresponding to optimal EDCW is significantly greater than that of conventional wheelset over the entire range of axle load.

3.5 Summary and Conclusion

In this section of the study, detailed stability analysis of a single EDCW is presented and the results are discussed. The stability boundary or the critical speed of the wheelset is determined in terms of forward speed where one of the mode becomes unstable. The results are obtained through eigenvalue solutions, from which damping ratios and frequencies of each modes are computed.

The mathematical models of EDCW developed have been validated by quantitative comparison with published mathematical model of conventional wheelset as well as qualitative comparison with experimental and observed trends. The results showed that by setting the wheelset coupling parameters to rigid, the EDCW model can effectively simulate conventional rigid axle system. Also when coupling parameters are appropriately set to zero, the model simulates IRW.

The stability analysis of the EDCW is carried out by examining the effect of coupler parameters on the eigenvalue solutions. When coupling between wheels consists of a damper alone (EDCW - Configuration 1), the mathematical models consistently have a zero eigenvalue for lateral mode indicating loss of guidance. Besides neutrally stable lateral mode, in this case. the critical mode of the wheelset is the spin mode, that becomes unstable as forward speed is increased. As the coupler damping is increased, the spin mode critical speed increases, and for very large

damping the model simulates conventional wheelset.

When the coupler consists of parallel stiffness and damper, (EDCW-Configuration 2), the results showed that for small torsional stiffness the lateral mode is always stable, whereas the spin mode becomes unstable with increased speed. As the stiffness is increased, the critical speed of the spin mode first decreases and then increases rapidly to become stable for all speeds, where the lateral mode becomes unstable with increased speed. For this configuration, torsional damping showed significant influence only where spin mode is unstable.

Finally, when coupler consists of series stiffness and damper as well as parallel stiffness (EDCW - Configuration 3), the results showed that regardless of coupler arrangement, the lateral stability behaviour of the wheelset depends on the total stiffness of the coupler. Specific highlights of the results for the baseline EDCW can be summarized in terms of coupler stiffness (k_{AX}) range as follows:

Range 1:

$0 \leq k_{AX} < 9.5 \times 10^4$ N.m/rad ($0 \leq k_{AX} < 7.0 \times 10^4$ lb.ft/rad)

When k_{AX} is zero, there is always an eigenvalue at zero for lateral mode, indicating that, the guidance provided by conventional di-cone arrangement is lost. As k_{AX} is increased, the natural frequency of the wheelset spin mode reduces, making the wheelset unstable in that mode at a lower velocity, where lateral mode is stable up to very high forward velocity. In this range of k_{AX}, when torsional damping (D_{AX}) is introduced and increased, the relative spin motion reduces, increasing the critical speed. However, damping alone can not increase the critical

speed of the wheelset beyond the critical speed of conventional rigid axle wheelset.

Range 2:

$9.5 \times 10^4 < k_{AX} < 1.5 \times 10^5$ N.m/rad ($7.0 \times 10^4 < k_{AX} < 1.1 \times 10^5$ lb.ft/rad)

For values of k_{AX} beyond 9.5×10^4 N.m/rad, the relative spin mode stability improves rapidly, and is always stable for $k_{AX} > 1.44 \times 10^5$ N.m/rad. At this point, wheelset lateral mode becomes unstable, and the critical speed of the lateral mode decreases as k_{AX} is increased further. Therefore, there exists a maximum value of critical speed at the intersection of the stability boundary curves corresponding to wheelset lateral and relative spin modes. In this range of k_{AX}, similar to previous range, increase in D_{AX} improves the critical speed where instability is in the spin mode. However, for large values of D_{AX}, the critical speed boundaries become less sensitive to the variation in k_{AX}. Thus, the peak critical speed at the intersection of spin and lateral stability boundaries is reduced by increasing the value of D_{AX}. For the baseline EDCW, the optimal coupler parameters to maximize critical speed are found to be $k_{AX} = 1.44 \times 10^5$ N.m/rad (1.06×10^5 lb.ft/rad) and $D_{AX} = 0$. The critical speed of the baseline EDCW with optimal coupler parameters is found to be 222 m/s (730 ft/s).

Range 3:

$k_{AX} > 1.5 \times 10^5$ N.m/rad ($k_{AX} > 1.1 \times 10^5$ lb.ft/rad)

As the value of k_{AX} is increased further, the lateral amplitude increases making the wheelset unstable at a lower velocity. And as the value of k_{AX} approaches very large, representing rigid axle, the critical

speed approaches the critical speed for conventional model. In this range of k_{AX}, there is almost no effect of variation in D_{AX}. For the baseline wheelset, the critical speed corresponding to a rigid coupler simulating conventional wheelset in found to be 136 m/s (445 ft/s).

The results of parametric study showed that the sensitivity of wheelset critical speed to effective wheel conicity and primary yaw stiffness is similar for both optimally coupled wheelset and rigid axle wheelset, where optimally coupled wheelset provides significantly higher critical speed in comparison to conventional model. When creep coefficients are varied, the optimally coupled wheelset is found to be more sensitive to increase in creep coefficients, than conventional model. Whereas the effect of axle load is noticeable for conventional model, and almost negligible for optimally coupled wheelset. These results further showed that the value of optimal coupler parameter is also sensitive to the model parameters. The effect is however, very small, except for primary yaw stiffness and axle load. Increase in these two parameters require increased value of k_{AX} for maximizing the critical speed of EDCW.

Although this part of the study provided basic understanding of the EDCW stability behaviour, the obvious limitations of this model are that it considered only one wheelset, and there is no influence of truck dynamics. In this study, the truck is assumed to be a fixed reference that moves along the track, and primary suspension provides the major restoring force. In reality, the freight car critical mode is the truck hunting mode and not the wheelset hunting mode. Therefore, more useful and practical results for freight car stability behaviour should be

obtained from a model that includes a truck as well as the effect of car body. In the following chapters, a freight truck model with two EDCW and a pseudo-car body is developed and used for stability analysis.

CHAPTER 4

FREIGHT TRUCK MODELING CONSIDERATIONS AND APPROACH

4.1 Introduction

The problem of interest in this section of the study is the lateral stability of a freight car system on tangent track. In practice, rail vehicles exhibit two distinct modes of lateral oscillations or instability referred to as hunting. They are commonly classified as car body or primary hunting, and truck or secondary hunting. The primary hunting generally occurs at relatively low speeds, and with effective secondary suspension, the vehicle can pass through this condition to operate successfully above this hunting speed. On the other hand, truck hunting occurs at higher speeds and once started, the amplitude of oscillation grows. Consequently, secondary hunting is of direct importance in evaluating stability and operating speeds.

Freight truck hunting is a phenomenon mainly associated with wheel-rail interaction, and the stability behaviour of the wheelsets. In the previous sections, detailed linear stability analysis of a single wheelset with elasto-damper coupling are presented. The results showed that there exists an optimal coupler parameter that can provide considerably improved stability performance of an EDCW over the conventional rigid wheelset model. However, for freight car system, the critical problem is that of truck hunting, and to study the effect of EDCW, a complete freight car or a truck model with EDCW has to be developed.

The complexity of the model depends upon the requirements of the dynamic simulation. The basic goal is to develop a simple model which yields the results to meet the study goals. Most investigations of conventional system to study truck hunting behaviour considers a simplified truck model consisting of truck frames and wheelsets, where car body is a reference that moves along the track [36]. To develop dynamic simulation of a truck, that faithfully reproduces truck performance of a freight vehicle, it is necessary to include realistic bolster and truck connections, as well as car body and bolster connection.

To study the influence of EDCW on the stability behaviour of freight car system, a freight truck model with two EDCW and a pseudo car-body is developed. The truck model, capable of showing both primary and secondary hunting behaviour, can be considered as a representative of freight car system. The wheelset model developed in Chapter 2 is reconsidered here with extension to incorporate truck motions, where the truck also has lateral, yaw and warp degrees-of-freedom (DOF). The pseudo car-body, further has lateral and roll degrees-of-freedom. Therefore, with three DOF for each EDCW, a 11-DOF truck model can demonstrate completely the lateral dynamic behaviour of a freight car system.

In the following sections, the truck model is presented, various modeling considerations are discussed, the assumptions are listed, and the equations of motion are derived for lateral stability analysis on tangent track.

4.2 Model Description

The railway freight truck consists of two complete wheel-axle sets, truck frames and suspension elements connecting wheelsets and car body to the truck frame. The primary components of conventional freight truck are wheelsets, primary suspension elements, truck frame, secondary suspension elements and bolster, as shown in Figure 4.1.

The wheelset is the fundamental common component of all rail vehicles. Conventional wheels are conical and are rigidly connected to the axle. In this study, EDCW are considered, where each wheelset are connected to the truck frame through primary suspension elements. The only coupler arrangement considered in this part of the study in that of Configuration 2, which includes torsional stiffness and damper in parallel. The model for the wheelset was discussed in details in Chapter 2.

As shown schematically in Figure 4.2, the main parts of the freight truck frame are the two side frames and a bolster. The bolster is connected to the side frames through a set of springs which are a part of secondary suspension elements. Other elements that provide secondary suspension effect are centre plate connection between bolster and car body, as well as effective resistance to truck warp motion. Similar to primary suspension, the secondary suspension elements of freight cars exhibits non-linear characteristics that fall into the categories of:

- non-linear springs;
- coulomb friction;
- clearances and stops.

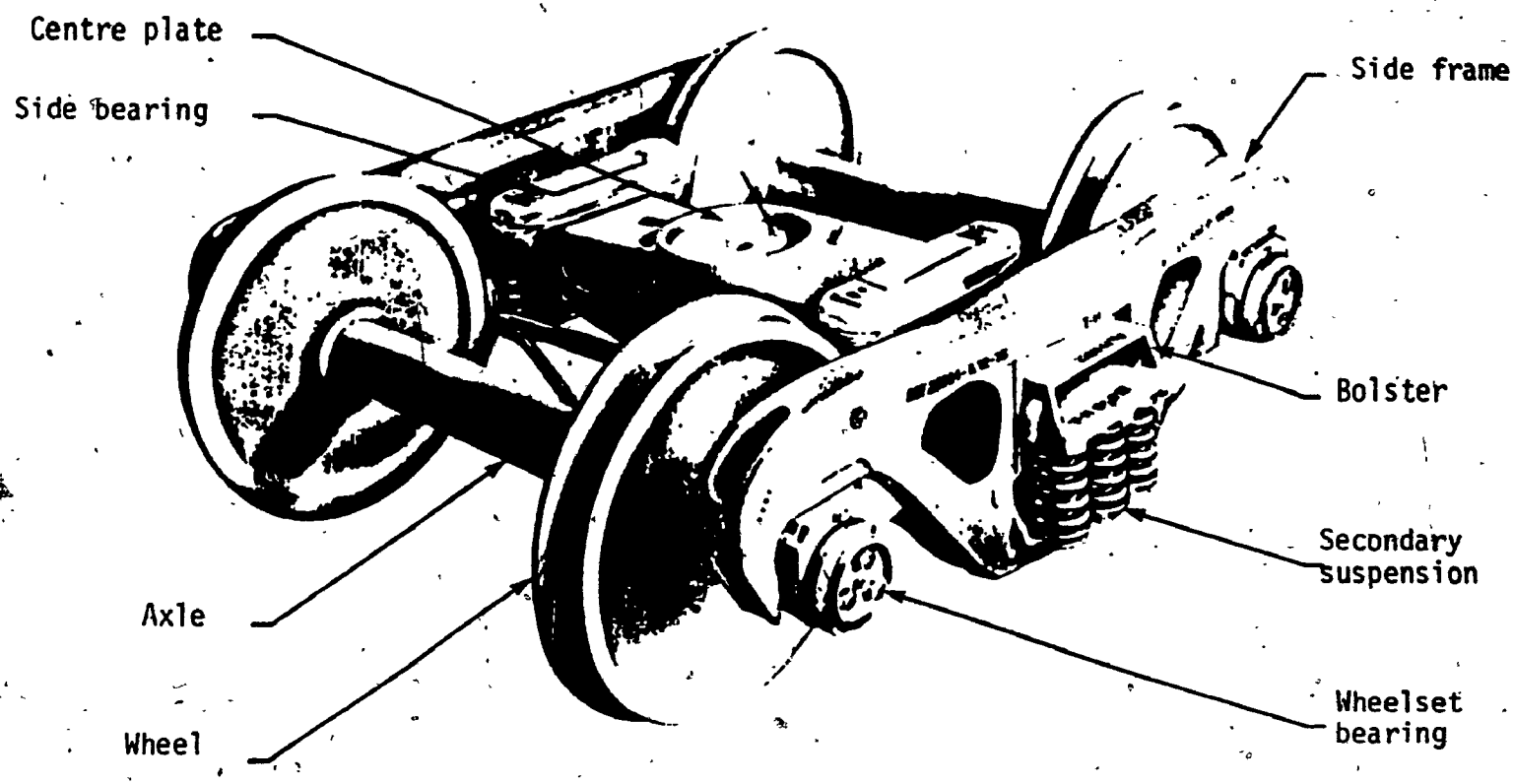

Figure 4.1 Typical North American three-piece freight truck

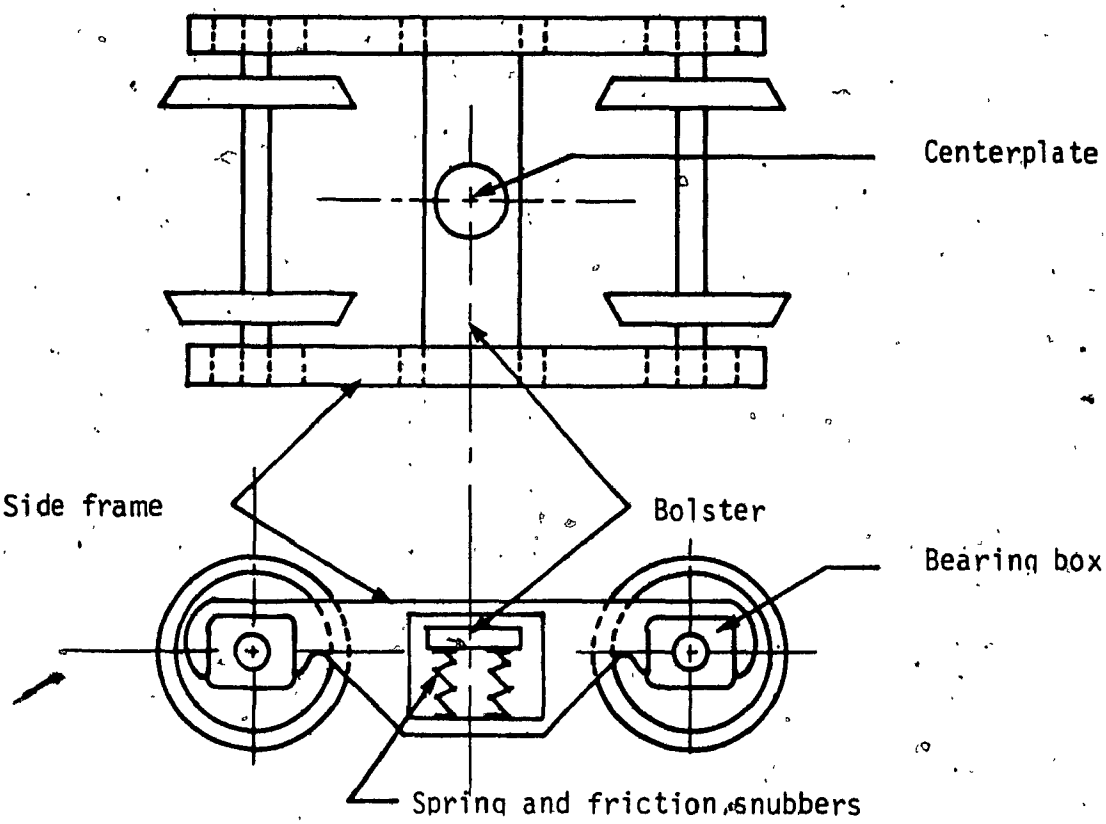

Figure 4.2 Schematic of typical freight truck.

For linear study, they can however, be linearized with varying degree of accuracy, by linear springs and equivalent viscous damping.

In the truck model, there are two EDCW, each having three DOF i.e., lateral, yaw and spin. The lateral and yaw displacements are with respect to side frame, resisted by primary suspension. The spin DOF is between left and right wheels, resisted by wheelset coupler. The truck frame can move in lateral and yaw directions resisted by primary suspension with respect to the wheelsets, as well as secondary suspension with respect to the bolster-car body assembly. The third DOF for the truck frame is the "warping" motion, where the three-piece frame (two side frames and bolster) can deform, so that the wheelset and side frame assume a sort of parallelogram shape. Finally, for the pseudo-car body, there are two DOF i.e., lateral and roll motions. In modeling the pseudo-car body, the bolster is assumed to be a part of car body, hence the motions of car body is only resisted by secondary suspension elements with respect to the truck side frames.

The schematic diagrams of the 11-DOF truck model with pseudo-car body, both in equilibrium and disturbed configurations are shown in Figures 4.3 to 4.5. This freight truck model can be considered as a simplified representation of freight car system, from which stability behaviour of wheelset, truck and the car body can be determined. In this investigation only linearized model of truck with pseudo-car body and EDCW is considered for stability analysis. The various DOF of the model as illustrated in Figures 4.4 and 4.5, are listed with their symbols as follows:

y_{w_1} : leading wheelset lateral

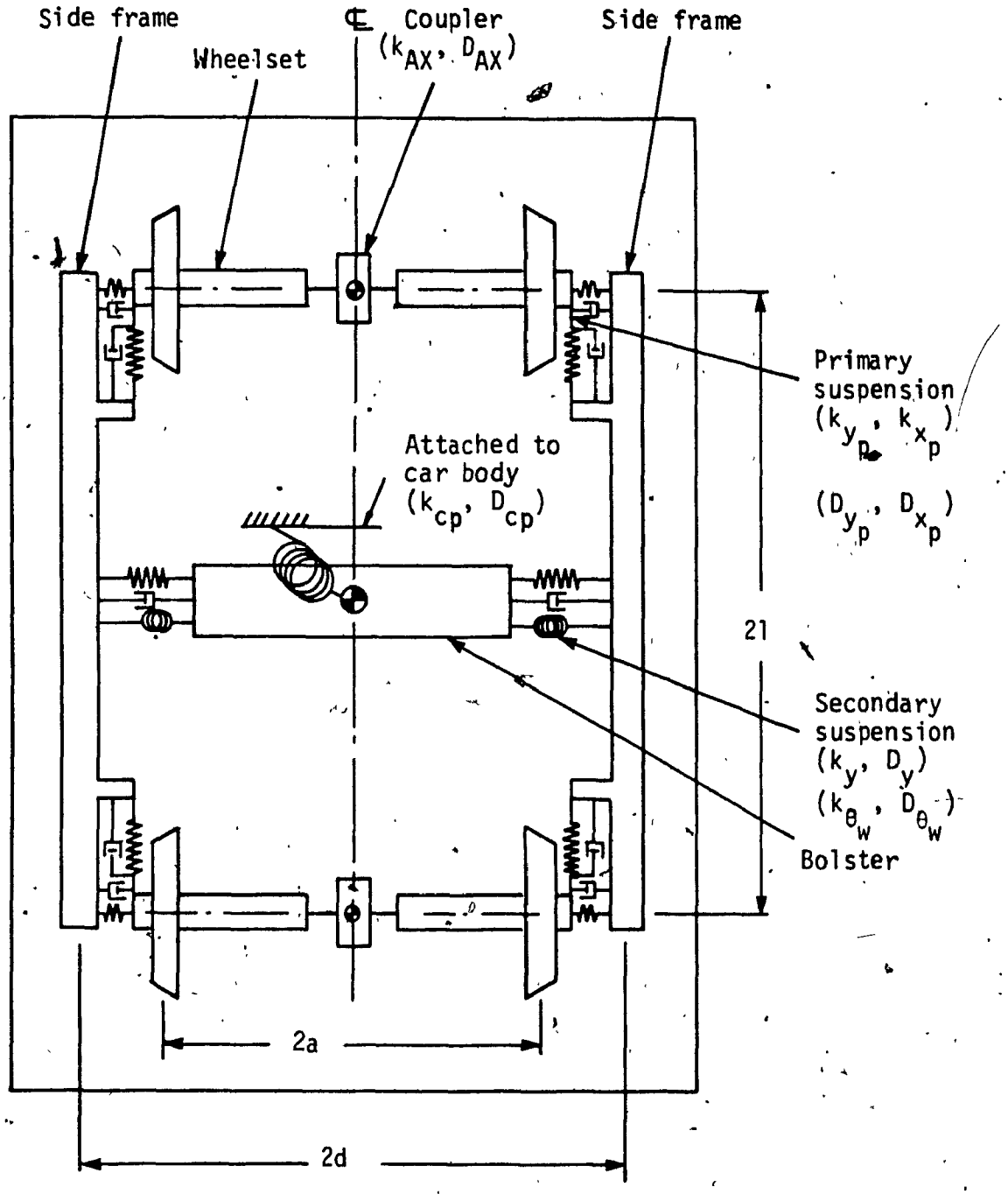

Figure 4.3 Schematic diagram of freight truck model with Elasto-Damper Coupled Wheelset (EDCW), in equilibrium.

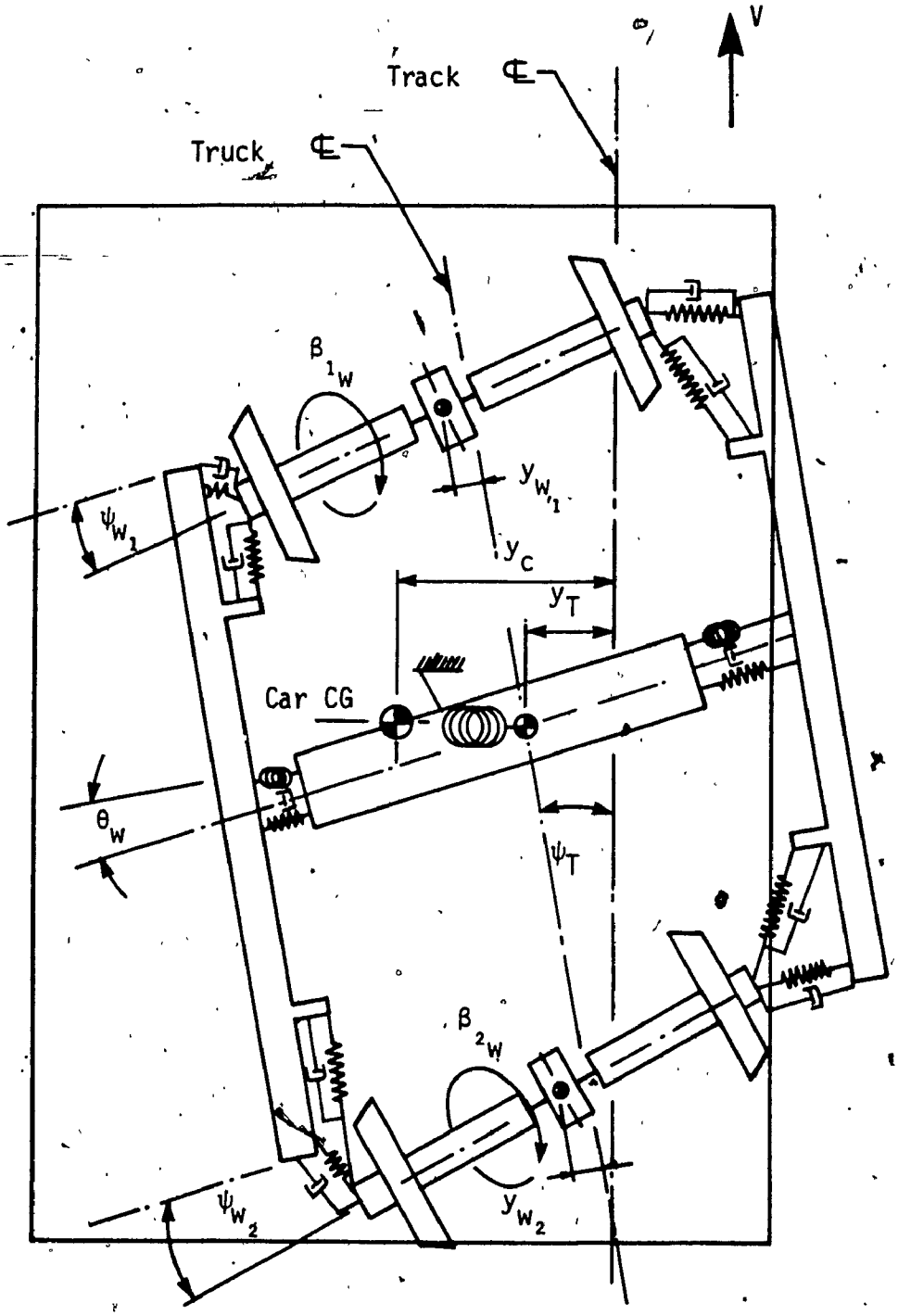

Figure 4.4 Schematic diagram of 11-DOF freight truck model with pseudo-car body and EDCW (disturbed plan view).

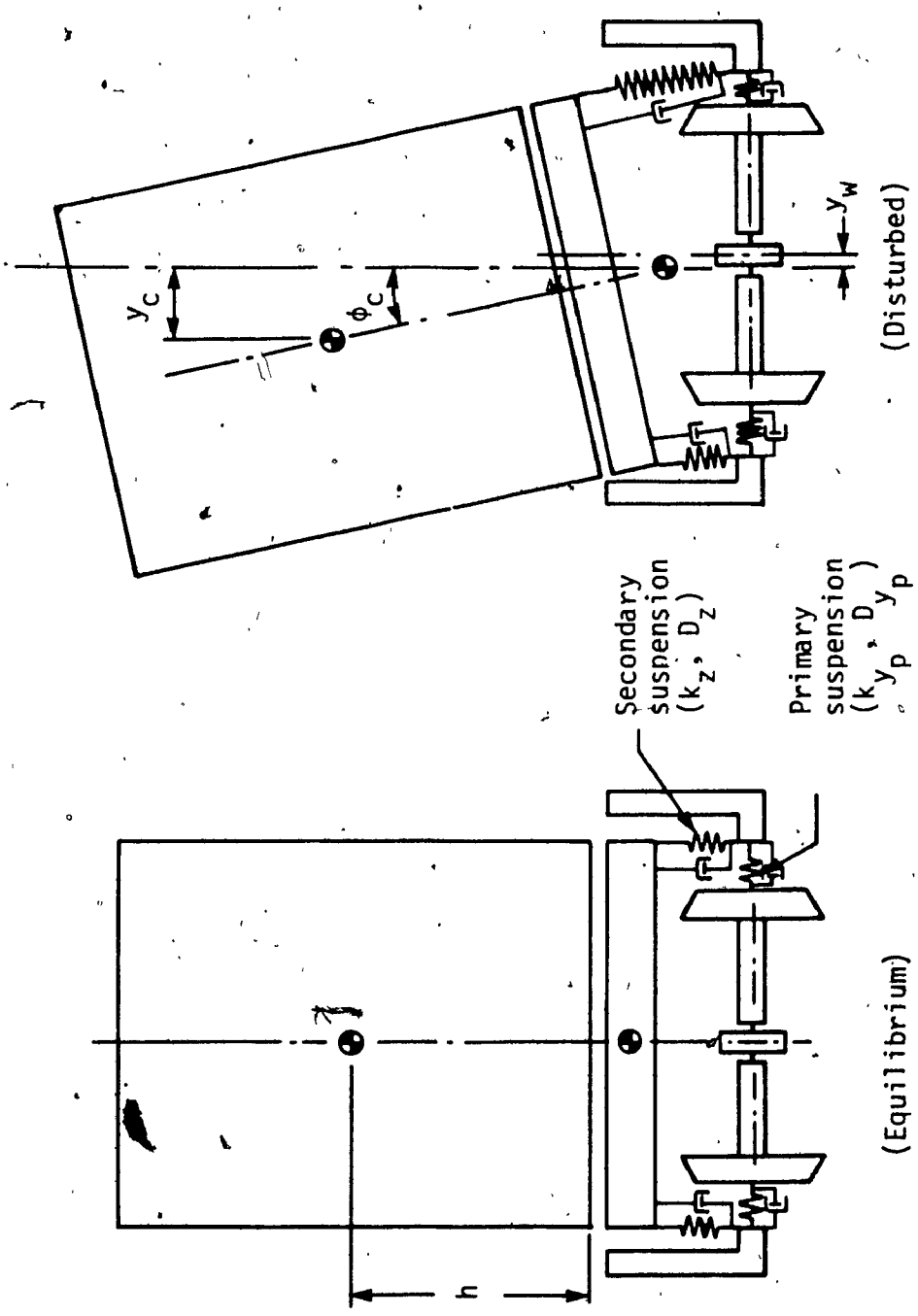

Figure 4.5 Schematic diagram of a 11-DOF truck model with pseudo-car body and EDCW (front view).

ψ_{w_1} : leading wheelset yaw

β_1 : leading wheelset relative spin

y_{w_2} : trailing wheelset lateral

ψ_{w_2} : trailing wheelset yaw

β_2 : trailing wheelset relative spin

y_T : truck frame lateral

ψ_T : truck frame yaw

θ_w : truck frame warp

y_c : car body lateral

ϕ_c : car body roll

4.3 Modeling Consideration

In the modeling approach to obtain a mathematical model for a freight truck with pseudo-car body, various considerations are outlined here. The various elements of the model are identified and analytical expressions for forces and moments due to each element are developed. The modeling approach used here is similar to that used in [44].

4.3.1 Wheelset

The contact forces between wheel and rail, namely the creep and normal forces are essentially the same as those derived earlier for single wheelset study. The same is also valid for primary suspension and wheelset coupler. The EDCW model developed in Chapter 2, can easily be adopted for a truck model by redefining the lateral and yaw displacement variables to include the lateral, yaw and warp motions of the truck frame. The total displacements for the leading and trailing wheelsets

are redefined as:

For leading wheelset:

$$y = y_{w_1} + y_T + l\psi_T \tag{4.1}$$

$$\psi = \psi_{w_1} + \psi_T + \theta_w \tag{4.2}$$

For trailing wheelset:

$$y = y_{w_2} + y_T - l\psi_T \tag{4.3}$$

$$\psi = \psi_{w_2} + \psi_T + \theta_w \tag{4.4}$$

where, y and ψ are total displacements of the wheelsets, and y_{w_1}, ψ_{w_1} and y_{w_2}, ψ_{w_2} are the lateral and yaw displacements of leading and trailing wheelsets respectively, relative to the truck frame. y_T, ψ_T and θ_w are the lateral, yaw, and warp displacements of the truck frame, respectively.

4.3.2 The Truck Frame

The truck frames are supported by the wheelsets through primary suspension. The car body-bolster is supported by the truck frame through the secondary suspension. Therefore, the truck side frame motion is subjected to resistive forces from both the suspension systems. The warp motion of the truck frame is subjected to resistive force from total warp stiffness and damping present in the truck side frame-bolster assembly.

The various forces and moments acting on the side frame and bolster assembly is shown in a free body diagram (Figure 4.6), where direction of

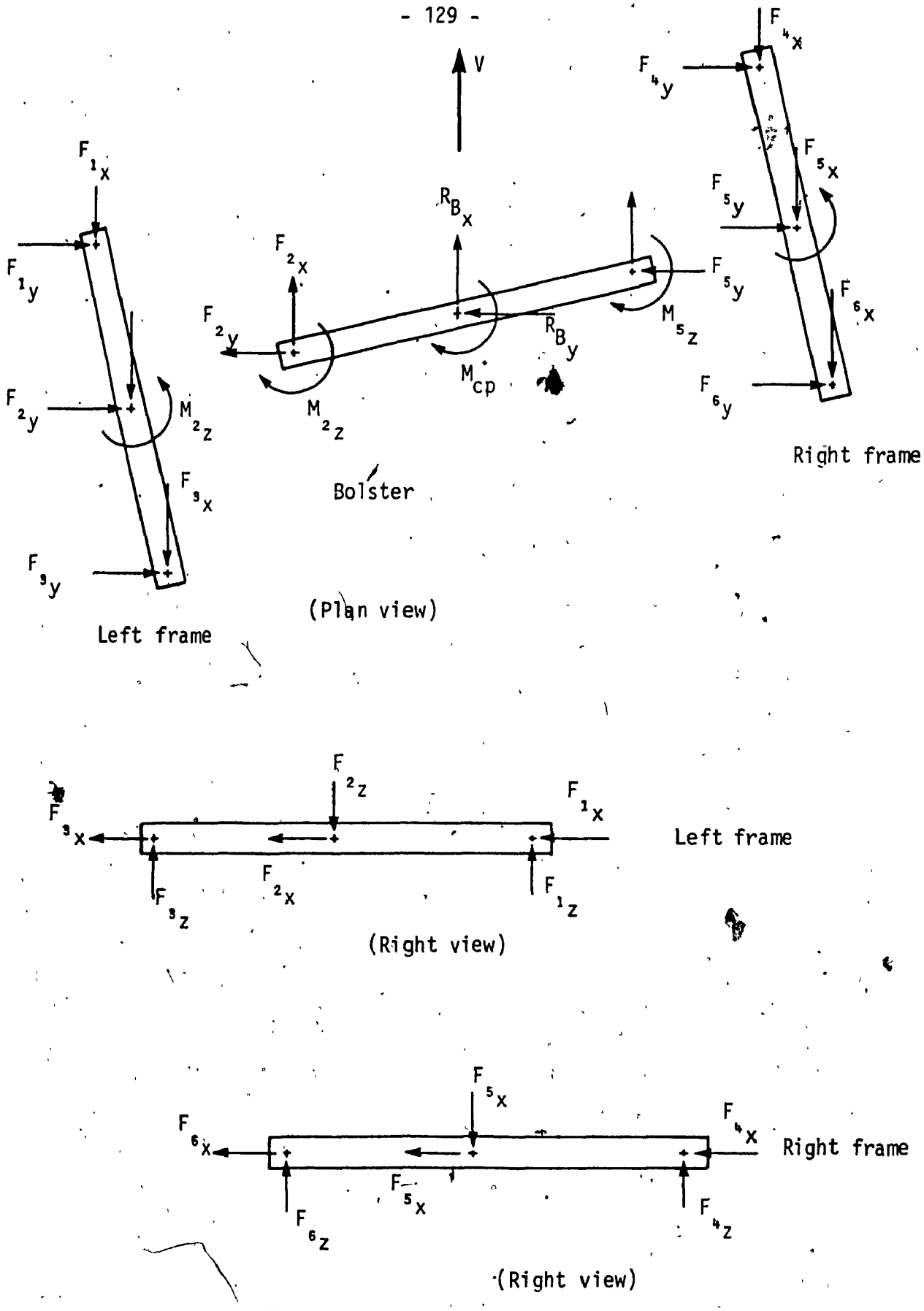

Figure 4.6 Free body diagram showing forces and moments acting on the truck components.

forces oppose positive lateral, yaw and warp motions. The expressions for the suspension forces and moments on the truck frame are obtained as follows:

Primary Suspension:

Similar to the single wheelset model, for linear study, the primary suspension between wheelset and side frame is taken as linear spring and viscous damper in parallel, in the longitudinal and lateral directions. With reference to Figure 4.6, the lateral force exerted on the left and right side frames due to relative displacement between leading wheelset and frame are:

$$F_{1_y} = F_{4_y} = -(D_{y_p}\dot{y}_{w_1} + k_{y_p}y_{w_1}) \tag{4.5}$$

and due to relative motion between trailing wheelset and frame, the forces on the left and right side frames are:

$$F_{3_y} = F_{6_y} = -(D_{y_p}\dot{y}_{w_2} + k_{y_p}y_{w_2}) \tag{4.6}$$

The longitudinal forces exerted on left and right side frames due to relative yaw motion between leading wheelset and side frames are:

$$F_{1_x} = -F_{4_x} = d(D_{x_p}\dot{\psi}_{w_1} + k_{x_p}\psi_{w_1}) \tag{4.7}$$

Similarly, for the trailing wheelset:

$$F_{3_x} = -F_{6_x} = d(D_{x_p}\dot{\psi}_{w_2} + k_{x_p}\psi_{w_2}) \tag{4.8}$$

where, y_{w_1}, ψ_{w_1}, and y_{w_2}, ψ_{w_2} are defined earlier as lateral and yaw

displacements of leading and trailing wheelsets respectively, with respect to the truck frame.

Secondary Suspension:

As mentioned earlier, in reality secondary suspension system of conventional freight cars exhibit non-linear characteristics. These non-linearities may be described by combinations of three non-linear elements as shown in Figure 4.7. The secondary spring groups may have hardening/softening springs, where vertical spring group have typically "hard" characteristics. Coulomb friction is present at every joint of freight truck configuration [46]. The yaw motion of the truck frame-bolster assembly is resisted by centre plate connection with respect to car body which imparts Coulomb friction and dead band spring. The warp motion of the truck frame is resisted by the wheelset and side frame joints as well as bolster and side frame joints, effectively producing Coulomb friction and dead band spring effect.

For linear study, with small displacement assumptions, all suspension elements are taken as linear spring in parallel with equivalent viscous damper. The warp stiffness of the truck is represented by torsional stiffness $k_{\theta w}$ as shown in Figure 4.3. Therefore resisting moments to warp applied by side frames to the bolster are:

$$M_{2_z} = M_{5_z} = \frac{1}{2}(D_{\theta_w}\dot{\theta}_w + k_{\theta_w}\theta_w) \qquad (4.9)$$

1. Deadband spring or damper:

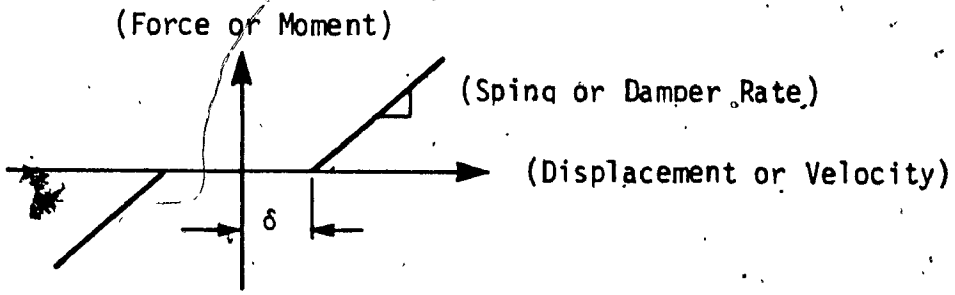

2. Hardening/softening spring or damper:

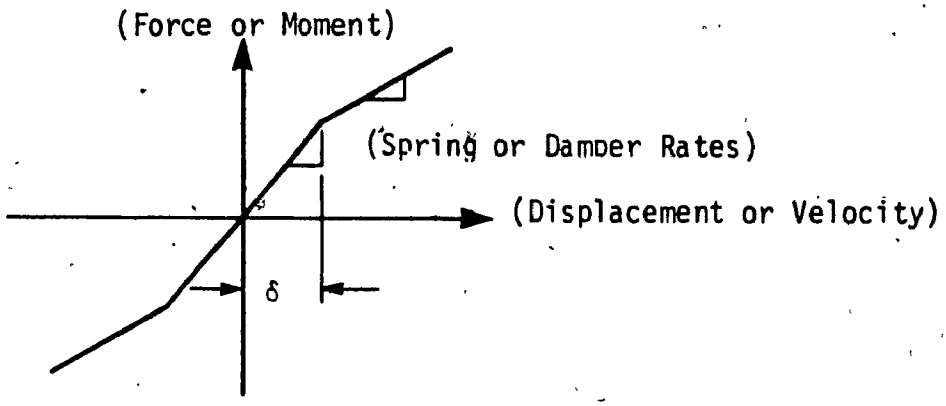

3. Coulomb friction:

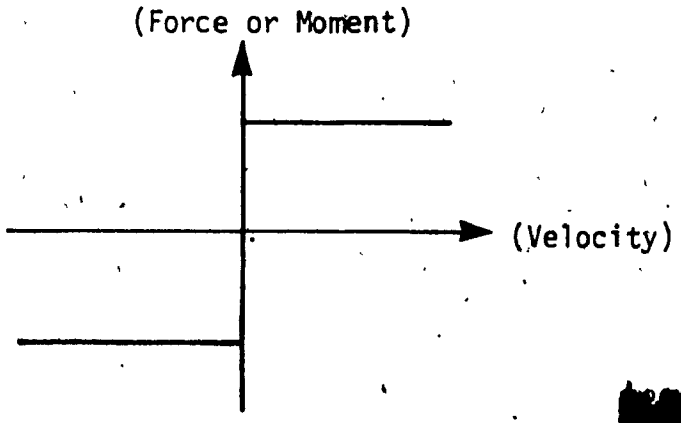

Figure 4.7 Freight truck system non-linear elements.

4.3.3 Pseudo-Car Body

The truck model considered in this study includes a single truck with half car body represented as a pseudo-car body. Here, the bolster of the truck does not have independent DOF, instead it is assumed that the bolster and car body move together in lateral and roll directions. An extension of the free body diagram of the truck frame shown in Figure 4.6, is given in Figure 4.8 to include bolster and pseudo-car body assembly. Since bolster and pseudo-car body move together, the lateral forces due to secondary suspension are:

$$F_{2_y} = F_{5_y} = D_y(\dot{y}_T - \dot{y}_C - h\dot{\phi}_C) + k_y(y_T - y_C - h\phi_C) \tag{4.10}$$

The vertical forces due to secondary suspension depend on relative roll motion between the truck frame and bolster with pseudo-car body, and can be expressed as:

$$F_{2_z} = -F_{5_z} = D_z d(\dot{\phi}_T - \dot{\phi}_C) + k_z d(\phi_T - \phi_C) \tag{4.11}$$

where, truck frame roll (ϕ_T) is not considered as a dynamic DOF, and is assumed to roll with the wheelsets. Therefore, the roll angle of the truck frame may be substituted as the instantaneous average of the roll angles of the two wheelsets under it. Further, since wheelset roll angles are expressed as linear function of wheelsets lateral displacement ($\phi = \Gamma y/a$), substituting for y from Equations (4.1) and (4.3) gives:

$$\phi_T = \frac{\Gamma}{2a}(y_{w_1} + y_{w_2} + 2y_T) \tag{4.12}$$

substituting Equation (4.12) into Equation (4.11) leads to vertical

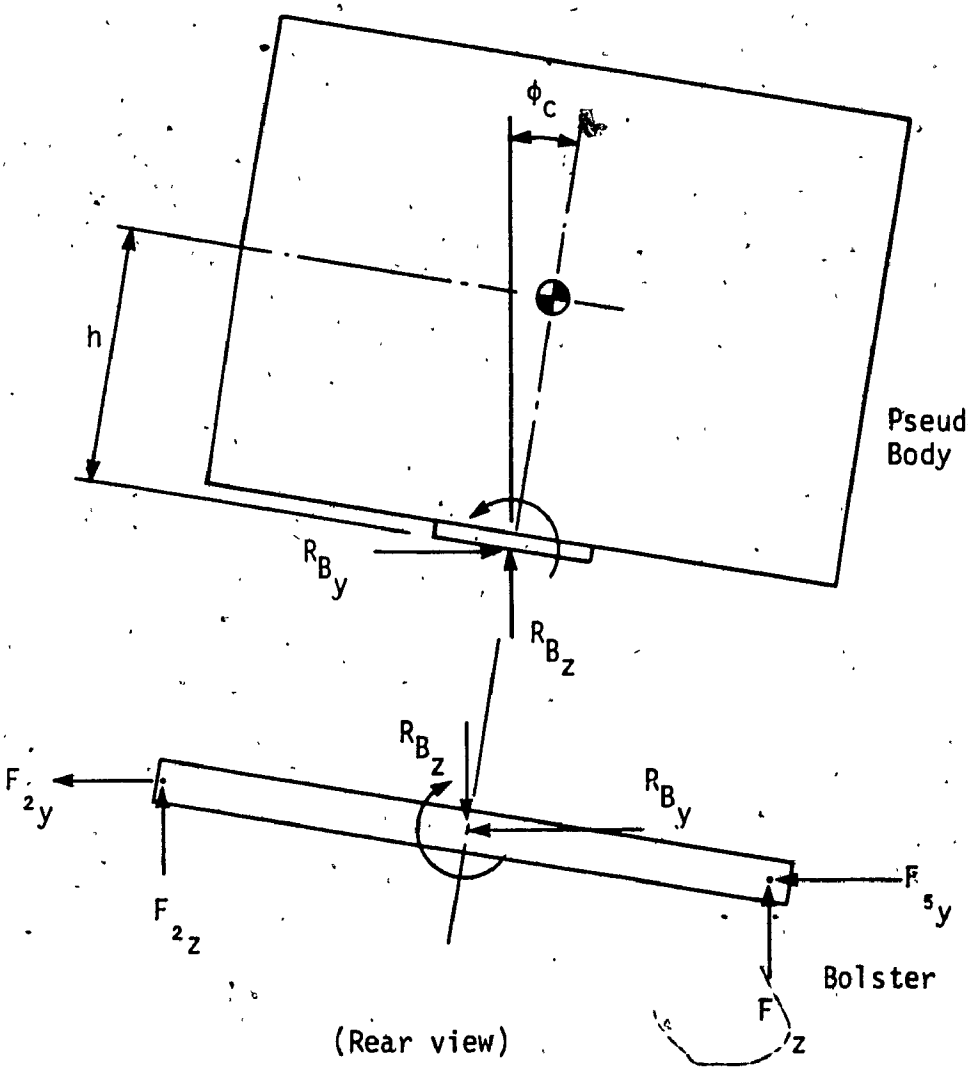

Figure 4.8 Free body diagram showing forces and moments acting on the truck frame and car body components.

suspension forces as:

$$F_{2_z} = -F_{5_z} = D_z d\left[\frac{\Gamma}{2a}(\dot{y}_{w_1} + \dot{y}_{w_2} + 2\dot{y}_T) - \dot{\phi}_c\right]$$

$$+ k_z d\left[\frac{\Gamma}{2a}(y_{w_1} + y_{w_2} + 2y_T) - \phi_c\right] \qquad (4.13)$$

Finally, the centre plate connection between bolster and car body provides resistance to bolster yaw motion. Since the bolster is assumed part of truck frame for the yaw and warp motions, the centre plate moment between car body and bolster is:

$$M_{cp} = D_{cp}(\dot{\phi}_T + \dot{\theta}_w) + k_{cp}(\phi_T + \theta_w) \qquad (4.14)$$

4.4 Assumptions and Limitations

The assumptions made in the modeling of a single EDCW are outlined in Section 2.4, and are also valid for this part of the study. In this case, however, the wheelsets motion are with respect to truck frame, where truck frame also has lateral, yaw and warp DOF. The freight truck model considered here also includes a simplified representation of car body, where the car body is assumed to have only lateral and roll motions. Since this study is aimed at truck stability, the model should be adequate, which can also exhibit primary hunting mode.

The truck and pseudo-car body are modeled as rigid masses, with the assumption that internal bending is negligible. In modeling the car body, the lateral and torsional flexibilities of the body are not included, although they are present in reality. This assumption can be

justified based on Hadden's study [44], which showed that these flexibilities for conventional model, have negligible effect for Hopper car, and only limited influence on some flat car configurations.

The freight truck model developed is for stability analysis and hence does not include effects of track irregularities, forces due to car to car coupling, and aerodynamics. For simplicity and convenience, the bolster is not assigned a separate DOF. Here, the bolster is assumed to yaw with truck frame resisted by centre plate connection. But for car body lateral and roll motions, the bolster is assumed to move with car body resisted by secondary suspension. The idealization of bolster and car body is acceptable at most operating speeds and condition, however, this assumption may not be true when severe rock and roll motions take place. In this situation, the car body may even lift completely off the bolster and roll with respect to the bolster until it contacts the side bearings at each end of bolster. This, on the other hand, occurs only at certain low forward speeds due to half-staggered rail joints [23].

To reduce complexity, the truck frame roll is not considered as a dynamic DOF. In the formulation of the model, the roll angle of the truck is calculated as the instantaneous average of the roll angles of the two wheelsets under it. Identical to wheelset modeling, the roll angles of each wheelset are analytically described in terms of their lateral displacements. All displacements are assumed small, and product of perturbation quantities are neglected in the equations. All suspension and wheelset coupler elements are assumed linear.

4.5 Equations of Motion

Based on the modeling considerations and assumptions discussed in the previous section, the equations of motion for the 11-DOF freight truck with two EDCW and pseudo-car body are formulated. The equations of motion are derived for the wheelsets, truck frame, and pseudo-car body in the following three sub-sections.

4.5.1 Wheelsets

The EDCW for the truck model is identical to that considered in Chapter 2, where the coupler consists of parallel stiffness and damper elements. Three equations of motion for the wheelset (lateral, yaw and relative spin) essentially remain the same as those derived previously for the initial wheelset study. Here, substitutions are only made to include the motion of truck frame at the leading end for leading wheelset, and at the trailing end for the trailing wheelset. The equations for leading wheelset are obtained by substituting Equations (4.1) and (4.2) for lateral and yaw terms into the initial EDCW equations formulated in Chapter 2. Similarly, for the trailing wheelset, Equations (4.3) and (4.4) are substituted for lateral and yaw terms in the initial EDCW equations. These substitutions are carried out for all y and ψ terms in the wheelset equations except for terms with primary suspension force and moment, where y_w is substituted for y and ψ_w is substituted for ψ, since y_w and ψ_w are defined as relative displacements between wheelset and truck frame. In doing so, final set of equations for the wheelsets of the truck model can be summarized as:

Leading wheelset lateral:

$$m_w \ddot{y}_{w_1} + [2D_{y_p} + \frac{2f_{22}}{V}(1+\frac{r_0\Gamma}{a})]\dot{y}_{w_1} + [2k_{y_p} + \frac{W_{APP}}{2}(\Gamma+\Delta) - \frac{2f_{23}\Delta}{r_0 a}]y_{w_1}$$

$$+[\frac{f_{23}}{V} - \frac{I_{w_2}V\delta_0}{r_0 a}]\dot{\phi}_{w_1} - 2f_{22}\phi_{w_1} + m_w\ddot{y}_T + \frac{2f_{22}}{V}(1+\frac{r_0\Gamma}{a})\dot{y}_T$$

$$+[\frac{W_{APP}}{a}(\Gamma+\Delta) - \frac{f_{23}\Delta}{r_0 a}]y_T + [\frac{2f_{23}}{V} - \frac{I_{w_2}V\delta_0}{r_0 a}]\dot{\phi}_T - 2f_{22}\phi_T$$

$$+m_w l\ddot{\phi}_T + \frac{f_{22}}{V}(1+\frac{r_0\Gamma}{a})l\dot{\phi}_T + [\frac{W_{APP}}{a}(\Gamma+\Delta) - \frac{2f_{23}}{r_0}\Delta]l\phi_T$$

$$+[2\frac{f_{23}}{V} - \frac{I_{w_2}V\delta_0}{r_0 a}]\theta_w - 2f_{22}\theta_w = 0 \qquad (4.15)$$

Leading wheelset yaw:

$$I_{w_1}\ddot{\phi}_{w_1} + [D_{\phi_p} + \frac{2f_{33}}{V} + \frac{2f_{11}a^2}{V}]\dot{\phi}_{w_1} + [k_{\phi_p} + 2f_{23} - W_{APP}a\delta_0]\phi_{w_1}$$

$$+[\frac{I_{w_2}V\Gamma}{r_0 a} - \frac{2f_{23}}{V} + \frac{2f_{23}r_0\Gamma}{Va}]\dot{y}_{w_1} + [\frac{2f_{11}a\lambda}{r_0} - \frac{2f_{33}\Delta}{r_0 a}]y_{w_1} + \frac{2f_{11}ar_0\dot{\beta}_1}{V}w$$

$$+I_{w_1}\ddot{\phi}_T + [\frac{2f_{33}}{V} + \frac{2f_{11}a^2}{V}]\dot{\phi}_T + [2f_{23} - W_{APP}a\delta_0]\phi_T + [\frac{I_{w_2}V\Gamma}{r_0 a} -$$

$$\frac{2f_{23}}{V} - \frac{2f_{23}r_0\Gamma}{Va}]\dot{y}_T + [\frac{2f_{11}a\lambda}{r_0} - \frac{2f_{33}\Delta}{r_0 a}]y_T + [\frac{I_{w_2}V\Gamma}{ar_0} - \frac{2f_{23}}{V} -$$

$$\frac{2f_{23}r_0\Gamma}{Va}]\,l\dot{\phi}_T + [\frac{2f_{11}a\lambda}{r_0} - \frac{2f_{33}\Delta}{r_0 a}]\,l\phi_T + I_{w_1}\ddot{\theta}_w +$$

$$[\frac{2f_{33}}{V} + \frac{2f_{11}a^2}{V}]\,\dot{\theta}_w + [2f_{23} - W_{APP}a\delta_0]\,\theta_w = 0 \qquad (4.16)$$

Leading wheelset spin:

$$I_{w_2}\ddot{\beta}_{1_w} + [4D_{AX} + \frac{2f_{11}r_0^2}{V}]\,\dot{\beta}_{1_w} + 4k_{AX}\beta_{1_w} + \frac{2r_0f_{11}a}{V}\,\dot{\psi}_{w_1} + 2f_{11}\lambda y_{w_1}$$

$$+ \frac{2r_0f_{11}a}{V}\,\dot{\psi}_T + 2f_{11}\lambda y_T + 2f_{11}\lambda l\psi_T + \frac{2r_0f_{11}a}{V}\,\dot{\theta}_w = 0 \qquad (4.17)$$

Trailing wheelset lateral:

$$m_w\ddot{y}_{w_2} + [2D_{y_p} + \frac{2f_{22}}{V}(1 + \frac{r_0\Gamma}{a})]\,\dot{y}_{w_2} + [2k_{y_p} + \frac{W_{APP}}{a}(\Gamma + \Delta)$$

$$- \frac{2f_{23}\Delta}{r_0 a}]\,y_{w_2} + [\frac{2f_{23}}{V} - \frac{I_{w_2}V\delta_0}{ar_0}]\,\dot{\psi}_{w_2} - 2f_{22}\psi_{w_2} + m_w\ddot{y}_T +$$

$$[2\frac{f_{22}}{V}(1 + \frac{r_0\Gamma}{a})]\,\dot{y}_T + [\frac{W_{APP}}{a}(\Gamma + \Delta) - \frac{2f_{23}\Delta}{r_0 a}]\,y_T + [\frac{2f_{23}}{V} - \frac{I_{w_2}V\delta_0}{r_0 a}]\,\dot{\psi}_T$$

$$- 2f_{22}\psi_T - m_w l\ddot{\psi}_T - \frac{2f_{22}}{V}(1 + \frac{r_0\Gamma}{a})\,l\dot{\psi}_T - [\frac{W_{APP}}{a}(\Gamma + \Delta) - \frac{2f_{23}}{r_0 a}\Delta]l\psi_T$$

$$+ [\frac{2f_{23}}{V} - \frac{I_{w_2}V\delta_0}{r_0 a}]\,\theta_w - 2f_{22}\theta_w = 0 \qquad (4.18)$$

Trailing wheelset yaw:

$$I_{w_1}\ddot{\psi}_{w_2} + \left[D_{\psi_p} + \frac{2f_{33}}{V} + \frac{2f_{11}a^2}{V}\right]\dot{\psi}_{w_2} + \left[k_{\psi_p} + 2f_{23} - W_{App}a\delta_0\right]\psi_{w_2}$$

$$+\left[\frac{I_{w_2}V\Gamma}{ar_0} - \frac{2f_{23}}{V} - \frac{2f_{23}r_0\Gamma}{Va}\right]\dot{y}_{w_2} + \left[\frac{2f_{11}a\lambda}{r_0} - \frac{2f_{33}\Delta}{r_0 a}\right]y_{w_2} + \frac{2f_{11}ar_0\dot{\beta}_{2_w}}{V}$$

$$+I_{w_1}\ddot{\psi}_T + \left[\frac{2f_{33}}{V} + \frac{2f_{11}a^2}{V}\right]\dot{\psi}_T - \left[\frac{I_{w_2}V\Gamma}{ar_0} - \frac{2f_{23}}{V} - \frac{2f_{23}r_0\Gamma}{Va}\right]l\dot{\psi}_T$$

$$+\left[2f_{23} - W_{App}a\delta_0\right]\psi_T - \left[\frac{2f_{11}a\lambda}{r_0} - \frac{2f_{33}\Delta}{r_0 a}\right]l\psi_T + \left[\frac{I_{w_2}V\Gamma}{r_0 a} - \frac{2f_{23}}{V} - \frac{2f_{23}r_0\Gamma}{Va}\right]\dot{y}_T + \left[\frac{2f_{11}a\lambda}{r_0} - \frac{2f_{33}\Delta}{r_0 a}\right]y_T + I_{w_1}\ddot{\theta}_w$$

$$+\left[\frac{2f_{33}}{V} + \frac{2f_{11}a^2}{V}\right]\dot{\theta}_w + \left[2f_{23} - W_{App}a\delta_0\right]\theta_w = 0 \qquad (4.19)$$

Trailing wheelset spin:

$$I_{w_2}\ddot{\beta}_{2_w} + \left[4D_{AX} + \frac{2f_{11}r_0^2}{V}\right]\dot{\beta}_{2_w} + 4K_{AX}\beta_{2_w} + 2f_{11}\lambda y_{w_2} + \frac{2r_0f_{11}a}{V}\dot{\psi}_{w_2}$$

$$+2f_{11}\lambda y_T + \frac{2r_0f_{11}a}{V}\dot{\psi}_T - 2f_{11}\lambda l\psi_T + \frac{2f_{11}r_0a}{V}\dot{\theta}_w = 0 \qquad (4.20)$$

where,

$$\beta_{1_w} = \frac{\beta_{L_1} - \beta_{R_1}}{2} \quad \text{and} \quad \beta_{2_w} = \frac{\beta_{L_2} - \beta_{R_2}}{2}$$

4.5.2 Truck Frame

As discussed earlier, the truck frame is assigned three DOF, i.e. lateral, yaw and warp. In obtaining the equations for truck frame, equations of motion for each component shown in the free body diagram (Figure 4.6) are first obtained. With reference to Figure 4.6, the side frame equations of motion are:

Left frame lateral:

$$-(F_{1_y} + F_{2_y} + F_{3_y}) = m_s \ddot{y}_T \tag{4.21}$$

Right frame lateral:

$$-(F_{4_y} + F_{5_y} + F_{6_y}) = m_s \ddot{y}_T \tag{4.22}$$

Substituting the expressions for the force terms, from Equations (4.5), (4.6), and (4.10) into each of the above equations lead to identical expressions for truck frame lateral motion as:

Left and right frames lateral:

$$m_s \ddot{y}_T + D_y \dot{y}_T + k_y y_T - D_{y_p} \dot{y}_{w_1} - D_{y_p} \dot{y}_{w_2} - k_{y_p} y_{w_1} - k_{y_p} y_{w_2}$$

$$-D_y \dot{y}_c - k_y y_c - D_y h \dot{\phi}_c - k_y h \phi_c = 0 \tag{4.23}$$

Similarly, the longitudinal equations of motion for the left and right frames, respectively, are:

$$-(F_{1_x} + F_{2_x} + F_{3_x}) = -m_s d(\ddot{\psi}_T + \ddot{\theta}_w) \tag{4.24}$$

$$-(F_{4_x} + F_{5_x} + F_{6_x}) = -m_s d(\ddot{\psi}_T + \ddot{\theta}_w) \tag{4.25}$$

where the longitudinal motions of right and left frames ($^{x}r_s$, $^{x}l_s$) are expressed as:

$$x_{r_s} = -x_{l_s} = d(\psi_T + \theta_w) \tag{4.26}$$

Substituting for the force terms in Equations (4.24) and (4.25) form (4.7) and (4.8) lead to the expressions:

Left frame longitudinal:

$$m_s d(\ddot{\psi}_T + \ddot{\theta}_w) - D_{x_p} d\dot{\psi}_{w_1} - k_{x_p} d\psi_{w_1} - D_{x_p} d\dot{\psi}_{w_2} - k_{x_p} d\psi_{w_2} - F_{2_x} = 0 \tag{4.27}$$

Right frame longitudinal:

$$m_s d(\ddot{\psi}_T + \ddot{\theta}_w) - D_{x_p} d\dot{\psi}_{w_1} - k_{x_p} d\psi_{w_1} - D_{x_p} d\dot{\psi}_{w_2} - k_{x_p} d\psi_{w_2} + F_{5_x} = 0 \tag{4.28}$$

The yaw equations for the left and right frames, respectively can be expressed as:

$$M_{2_z} + (F_{1_x} - F_{3_x})l\psi_T + (-F_{1_y} + F_{3_y})l = I_{s_3}\ddot{\psi}_T \tag{4.29}$$

$$M_{5_z} + (F_{4_x} - F_{6_x})l\psi_T + (-F_{4_y} + F_{6_y})l = I_{s_3}\ddot{\psi}_T \tag{4.30}$$

Substituting for force and moment expressions from Equations (4.5) to (4.8), and neglecting the products of perturbation quantities, the above equations yield identical expressions for the yaw motion of left

and right frames as:

$$I_{s_3}\ddot{\phi}_T - \frac{1}{2}D_{\theta_w}\dot{\theta}_w - \frac{1}{2}k_{\theta_w}\theta_w - D_{y_p}l\dot{y}_{w_1} - k_{y_p}ly_{w_1} + D_{y_p}l\dot{y}_{w_2} + k_{y_p}ly_{w_2} = 0 \quad (4.31)$$

The equations of motion for the bolster are obtained by force and moment balance. With reference to the free body diagrams (Figures 4.6 and 4.8), force and moment balance lead to bolster equations as:

Bolster lateral:

$$F_{2_y} + F_{5_y} + R_{B_y} = m_B(\ddot{y}_c + h\ddot{\phi}_c) \quad (4.32)$$

Bolster roll:

$$(-F_{2_y} + F_{5_y})d\phi_c + (F_{2_z} - F_{5_z})d + M_x = I_{B_1}\ddot{\phi}_c \quad (4.33)$$

Bolster yaw:

$$-M_{z_2} - M_{5_z} - M_{cp} + (-F_{2_y} + F_{5_y})d(\phi_T + \theta_w) + (-F_{2_x} + F_{5_x})d$$

$$= I_{B_3}(\ddot{\phi}_T + \ddot{\theta}_w) \quad (4.34)$$

Substituting for the forces and moments in the above equations from the expressions defined in Section 4.3, leads to three bolster equations as:

Bolster lateral:

$$m_B(\ddot{y}_c + h\ddot{\phi}_c) + 2D_y(\dot{y}_c + h\dot{\phi}_c - \dot{y}_T) + 2k_y(y_c + h\phi_c - y_T) = R_{B_y} \quad (4.35)$$

Bolster roll:

$$I_{B_1}\ddot{\phi}_c + 2D_z d^2\dot{\phi}_c + 2k_z d^2\phi_c - D_z d^2\frac{\Gamma}{a}(\dot{y}_{w_1} + \dot{y}_{w_2} + 2\dot{y}_T)$$

$$- k_z d^2\frac{\Gamma}{a}(y_{w_1} + y_{w_2} + 2y_T) - M_x = 0 \qquad (4.36)$$

Bolster yaw:

$$I_{B_3}(\ddot{\psi}_T + \ddot{\theta}_w) + D_{\theta_w}\dot{\theta}_w + k_{\theta_w}\theta_w + D_{cp}(\dot{\psi}_T + \dot{\theta}_w) + k_{cp}(\psi_T + \theta_w)$$

$$+ (F_{2_x} - F_{5_x})d = 0 \qquad (4.37)$$

From the equations of motion for each component in the free body diagram, the three equations for the truck motion can now be obtained in the following manner:

Truck lateral:

In describing the lateral motion of the truck, the bolster is lumped with the car body. Therefore, the lateral equation of the truck can be obtained by simply adding the lateral equations of left and right frames given by Equation (4.23) to yield:

$$2(m_s\ddot{y}_T + D_y\dot{y}_T + k_y y_T - D_{y_p}\dot{y}_{w_1} - D_{y_p}\dot{y}_{w_2} - k_{y_p}y_{w_1} - k_{y_p}y_{w_2}$$

$$-D_y\dot{y}_c - k_y y_c - D_y h\dot{\phi}_c - k_y h\phi_c) = 0 \qquad (4.38)$$

Truck yaw:

In describing the yaw of the truck, the bolster is lumped with the two side frames, and the yaw equation is derived by adding yaw equation of each side frame (Equations 4.31) with yaw equation of bolster (Equations 4.37), and longitudinal equation of each side frame (Equations 4.27 and 4.28) times half the distance between side frames (d). In doing so, the expression for truck yaw equation is:

$$\left[2I_{s_3} + I_{B_3} + 2m_s d^2\right] \ddot{\psi}_T + D_{cp}\dot{\psi}_T + k_{cp}\psi_T + \left[I_{B_3} + 2m_s d^2\right] \ddot{\theta}_w + D_{cp}\dot{\theta}_w$$

$$+k_{cp}\theta_w - 2D_{y_p} l\dot{y}_{w_1} - 2k_{y_p} l y_{w_1} + 2D_{y_p} l\dot{y}_{w_2} - 2D_{x_p} d^2\dot{\psi}_{w_1} + 2k_{y_p} l y_{w_2}$$

$$-2K_{x_p} d^2\psi_{w_1} - 2D_{x_p} d^2\dot{\psi}_{w_2} - 2k_{x_p} d^2\psi_{w_2} = 0 \qquad (4.39)$$

Truck warp:

Similarly, the truck warp equation is obtained by adding bolster yaw Equation (4.37) with longitudinal equations of each side frame (Equations 4.27 and 4.28) times half the distance between side frames, which results in:

$$\left[I_{B_3} + 2m_s d^2\right] \ddot{\theta}_w + D_{\theta_w}\dot{\theta}_w + D_{cp}\dot{\theta}_w + k_{\theta_w}\theta_w + k_{cp}\theta_w + \left[I_{B_3} + 2m_s d^2\right]\ddot{\psi}_T +$$

$$D_{cp}\dot{\psi}_T + k_{cp}\psi_T - 2D_{x_p} d^2\dot{\psi}_{w_1} - 2k_{x_p} d^2\psi_{w_1} - 2D_{x_p} d^2\dot{\psi}_{w_2} - 2k_{x_p} d^2\psi_{w_2} = 0 \quad (4.40)$$

4.5.3 Pseudo-Car Body

The car body and bolster are considered as one unit in deriving the equations of motion of pseudo-car body in the lateral and roll directions.

Pseudo-car lateral:

With reference to Figure 4.8, the lateral equation of motion for the car body is simply given by:

$$- R_{B_y} = m_c \ddot{y}_c \tag{4.41}$$

Substituting for R_{B_y} from bolster lateral Equation (4.35), the above expression expands to:

$$[m_c + m_B] \ddot{y}_c + 2D_y \dot{y}_c + 2K_y y_c - 2D_y \dot{y}_T - 2k_y y_T + m_B h \ddot{\phi}_c$$

$$+ 2D_y h \dot{\phi}_c + 2k_y h \phi_c = 0 \tag{4.42}$$

Pseudo-car roll:

Similarly, by taking moment about car body CG, with reference to Figure 4.8, the roll equation is:

$$- R_{B_y} h - M_x + m_c g h \phi_c = I_{c_1} \ddot{\phi}_c \tag{4.43}$$

substituting for R_{B_y} and M_x from Equations (4.35) and (4.36),

respectively, the pseudo-car body roll equation can be expressed as:

$$[I_{c_1} + I_{B_1} + m_B h^2] \ddot{\phi}_c + [2D_y h^2 + 2D_z d^2] \dot{\phi}_c + [2k_y h^2 + 2k_z d^2 - m_c g h] \phi_c + m_B h \ddot{y}_c + 2D_y h \dot{y}_c + 2k_y h y_c - 2D_y h \dot{y}_T - 2D_z d^2 \frac{\Gamma}{a} \dot{y}_T - 2k_y h y_T - 2k_z d^2 \frac{\Gamma}{a} y_T - D_z d^2 \frac{\Gamma}{a} \dot{y}_{w_1} - k_z d^2 \frac{\Gamma}{a} y_{w_1} - D_z d^2 \frac{\Gamma}{a} \dot{y}_{w_2} - k_z d^2 \frac{\Gamma}{a} y_{w_2} = 0 \qquad (4.44)$$

4.6 Summary

In this chapter, a freight truck model with EDCW and pseudo-car body is developed for stability analysis on tangent track. First the model is presented, which is primarily a conventional three-piece freight truck, except each wheelset of the truck is an EDCW. The EDCW are identical to that considered in Chapter 2, where the coupler consists of parallel stiffness and damper elements. In this chapter, various components of the truck model and component connections are identified, and expressions for forces and moments at each joint are developed. Various assumptions made in the modeling approach are also discussed and outlined. This is subsequently followed by derivation of the equations of motion for the truck model. Equations are first obtained for each component of the truck model and then by combining them, the final 11 equations of motions are obtained to describe the motion of the wheelsets, truck frame, and pseudo-car body of the truck model. The formulated truck model can be considered as a simplified representation of a freight car system, which can be studied pertaining to wheelset, truck as well as car body stability behaviour. In the following chapter, the equations derived in this section are used to carry out detailed

lateral stability analysis of the freight truck model on tangent track.

CHAPTER 5

LATERAL STABILITY ANALYSIS OF FREIGHT TRUCK SYSTEM WITH EDCW ON TANGENT TRACK

5.1 Introduction

In conventional railway freight car, the lateral instability of truck or the truck hunting is the critical mode. Consequently, the primary concern in this part of the study is to evaluate the effect of EDCW on the stability performance of railway freight truck system.

The motion of railway vehicle can be defined in terms of a sum of its independent modes of motion, i.e. wheelset, truck and car body modes. The characteristics of each mode change with forward speed. The critical speed of the model can be defined as the speed at which one of these mode has zero damping, which indicate a sustained (oscillation) motion.

The performance criterion and method of solution used for the truck model is the same as that used for the wheelset model, as discussed in Sections 3.2 and 3.3, respectively. The equations of motion for an 11-DOF truck model developed in Chapter 4, are used in this chapter to carry out stability analysis. The primary objectives of this chapter are to obtain and discuss results pertaining to lateral stability behaviour of truck model with EDCW. First, the model is validated by comparing its limiting case with other conventional railway truck and car model results. Secondly, a detailed study is carried out to investigate the influence of EDCW coupler parameters on the stability behaviour of the model. Finally, a parametric study is carried out to determine the effect of selected model parameters on the critical speed of truck model with

EDCW. Similar to single wheelset study, the results of this part are compared with that of truck model with conventional rigid axle wheelsets.

5.2 Method of Solution

In Section 4.5, the equations of motion for the 11 DOF truck model are obtained as a set of homogeneous, second-order linear differential equations. These Equations (4.15 to 4.20, 4.38 to 4.40, 4.42 and 4.44) can be represented in a matrix form as:

$$[M]\{\ddot{X}\} + [D]\{\dot{X}\} + [K]\{X\} = 0 \qquad (5.1)$$

where $\{X\}^T$ is a vector of variables $\{y_{w_1}, \psi_{w_1}, \beta 1_w, y_{w_2}, \psi_{w_2}, \beta 2_w, y_T, \psi_T, \theta_w, y_c, \phi_c\}$, representing each DOF. $\{\dot{X}\}$ and $\{\ddot{X}\}$ are vectors representing velocities and accelerations, respectively. [M], [D], and [K] are (11 x 11) inertia, damping, and stiffness matrices, respectively.

The truck stability problem is associated with the determination of critical velocity, at which a perturbation on the system will cause divergent mode of oscillations. The critical speeds and corresponding modes are determined via eigenvalue solutions, similar to the wheelset study discussed in Section 3.3. The nominal (baseline) model parameters used in this part of the study are listed in Tables 5.1 and 5.2. These parameters are from various sources and laboratory experiments for a 80 ton conventional hopper car and as reported in [40, 46]. However, there may be variations from truck to truck and some parameters do change with use and environmental conditions. Some of the parameters are also dependent on axle loading. The nominal parameters in Table 5.1 corresponds to an empty car. In Table 5.2 the load dependent parameters

Table 5.1 Nominal Parameters for the Truck Model

Wheel/Rail Parameters

$\lambda = 0.05$ $\delta_0 = 0.05$ $\Gamma = 0.05$ $\Delta = 0.0$

$f_{11} =$ 2.563×10^6 N/wheel (5.763×10^5 lb/wheel)

$f_{22} =$ 2.212×10^6 N/wheel (4.973×10^5 lb/wheel)

$f_{23} =$ 3.12×10^3 N.m/wheel (2.3×10^3 lb-ft/wheel)

$f_{33} =$ 16.01 N.m^2/wheel (38.75 lb-ft^2/wheel)

Geometry

$a = 0.75$ m (2.46 ft) $d = 0.99$ m (3.25 ft)

$l = 0.853$ m (2.8 ft) $r_0 = 0.419$ m (1.375 ft)

$h = 0.912$ m (2.994 ft)

Mass and Inertia

$m_w = 1117.9$ kg (76.6 slugs) $m_s = 350.26$ kg (24.0 slugs)

$m_B = 526.8$ kg (36.1 slugs) $m_c = 8041.3$ kg (551 slugs)

$I_{w_1} = I_{w_3} = 608.1$ kg.m^2 (448.5 slug.ft^2) $I_{w_2} = 72.0$ kg.m^2 (53.1 slug ft^2)

$I_{s_3} = 105.2$ kg.m^2 (77.6 slug.ft^2) $I_{B_1} = I_{B_3} = 262.21$ kg.m^2 (178.6 slug.ft^2)

$I_{c_1} = 881.3$ kg.m^2 (6500 slug.ft^2) $W_{APP} = 5.60 \times 10^4$ N (1.26×10^4 lb)

where, $W_{APP} = \frac{1}{2}[m_c + 2m_w + 2m_s + m_B]g$

Table 5.1 Nominal Parameters for the Truck Model (Cont'd)

Suspension and Coupler Elements

m_{y_p} = 7.297 x 10^5 N/m (5 x 10^4 lb/ft)

$k_{\psi_p} = 2k_{x_p}d^2$ = 1.695 x 10^6 N.m/rad (1.25 x 10^6 lb.ft/rad)

D_{y_p} = 0.0 N.s/m (lb.s/ft)

D_{ψ_p} = 0.0 N.m.s/rad (lb.ft.s/rad)

k_y = 3.503 x 10^5 N/m (2.4 x 10^4 lb/ft)

k_z = 3.794 x 10^6 N/m (2.6 x 10^5 lb/ft)

D_y = 2.917 x 10^4 N.sec/m (2 x 10^3 lb.sec/ft)

D_z = 4.375 x 10^4 N.s/m (3 x 10^3 lb.sec/ft)

k_{θ_w} = 5.166 x 10^6 N.m/rad (3.81 x 10^6 lb.ft/rad)

D_{θ_w} = 1.792 x 10^4 N.m.s/rad (1.322 x 10^4 lb.ft.s/rad)

k_{cp} = 67.79 N.m/rad (50.0 lb.ft/rad)

D_{cp} = 3.01 x 10^3 N.m.s/rad (2.22 x 10^3 lb.ft.sec/rad)

k_{AX} = variable N.m/rad (lb.ft/rad)

D_{AX} = variable N.m.s/rad (lb.ft.s/rad)

For Moderately Worn Wheels

λ = 0.14 $\quad$ r = 0.07 $\quad$ δ_0 = 0.07 $\quad$ Δ = 10.35

Table 5.2 Load Dependent Parameters

Parameters	W_{APP} N (lb)	
	Half Load 1.49×10^5 (3.35×10^4)	Full Load 2.41×10^5 (5.43×10^4)
k_y N/m (lb/ft)	9.88×10^5 (6.77×10^4)	1.61×10^6 (1.10×10^5)
k_{y_p} N/m (lb/ft)	1.02×10^6 (7.00×10^4)	1.36×10^6 (9.30×10^5)
k_{ψ_p} N.m/rad (lb.ft/rad)	2.03×10^6 (1.50×10^6)	2.31×10^6 (1.70×10^6)
k_{θ_w} N.m/rad (lb.ft/rad)	5.71×10^6 (4.21×10^6)	6.25×10^6 (4.61×10^6)
D_{cp} N.m.s/rad (lb.ft.s/rad)	1.12×10^4 (8.23×10^3)	1.86×10^5 (1.37×10^5)
D_{θ_w} N.m.s/rad (lb.ft.s/rad)	3.69×10^4 (2.72×10^4)	6.05×10^4 (4.46×10^4)
f_{11} N/wheel (lb/wheel)	5.92×10^6 (1.33×10^6)	7.72×10^6 (1.74×10^6)
f_{22} N/wheel (lb/wheel)	5.69×10^6 (1.28×10^6)	7.12×10^6 (1.60×10^6)
f_{23} N.m/wheel (lb.ft/wheel)	1.42×10^4 (1.05×10^4)	2.11×10^4 (1.56×10^4)
f_{33} N.m^2/wheel (lb.ft^2/wheel)	4.08×10^1 (9.87×10^1)	6.94×10^1 (1.68×10^2)
m_c kg (Slug)	2.69×10^4 (1.85×10^3)	4.58×10^4 (3.14×10^3)
I_{c_1} kg.m^2 (Slug.ft^2)	3.41×10^5 (2.52×10^5)	5.95×10^5 (4.39×10^5)
h m (ft)	0.798 (2.62)	1.408 (4.62)

for half and full loading condition are listed, which will be considered in this study. In the following sub-sections, the results of the study are presented and discussed.

5.3 Stability Analysis Results

The results of truck stability analysis are presented and discussed in this section. As mentioned earlier, the results in this section are obtained in three phases, and are presented in the following three sub-sections. First, attention is directed towards validating the developed model by comparing its results with existing model results. Once the validation is complete, the results are then obtained to analyze the effect of wheelset coupler parameters on the stability behaviour of the truck model. Finally, parametric study results are obtained to examine the effects of selected model parameters on the critical speed of truck with EDCW, in comparison to that of conventional system.

5.3.1 Model Validation

The approach taken here for model validation is identical to that considered for single wheelset study, and discussed in Section 3.4.1. The validation of the 11-DOF truck model with EDCW and pseudo-car body is carried out by comparing its stability behaviour in a limiting case, against results of existing freight truck system. Similar to the wheelset study, the limiting case is obtained by selecting a very large value for wheelset torsional stiffness (1.356×10^{10} N.m/rad (1×10^{10} lb.ft/rad), effectively simulating conventional model with rigid axle. Comparisons are made in terms of root loci, frequency, and damping ratio

as the forward velocity is increased.

The eigenvalue solutions of the truck model with nominal parameters and rigid torsional stiffness are obtained as the forward velocity is increased. From eigenvectors corresponding to each eigenvalue the various modes of the system are identified. Figure 5.1 shows the root loci of four modes which are critical (i.e. near the imaginary axis), for velocity in the range of 6 to 73 m/s (20 to 240 ft/s). An examination of the eigenvalue clearly show, that the unstable mode leading to critical speed is a predominantly lateral mode. The root loci obtained in Figure 5.1, can be readily compared with that from a 17-DOF freight car model developed by Law et al. [50]. This model was used by Ramachandran et al. [49] as one of the most sophisticated linear model of conventional freight car lateral stability, in an attempt at validating the model through experiments. It was concluded in their study, that the model is best suited for qualitative comparison. The result of this study (Figure 5.1) also shows good qualitative agreement with the 17-DOF model results [49], in terms of eigenvalue trend as shown in Figure 5.2. No attempt on quantitative comparison of the results is made because the vehicle parameters used in [49] are not known.

Corresponding to root loci shown in Figure 5.1, the effective damping ratio of various modes as the speed is increased are shown in Figure 5.3. These damping ratio trends, which pertain to railway vehicle truck and car body lateral modes, are identical to those given in Ref. [81]. Similar trend for truck lateral mode was also reported by Fries et al. [46], based on experimental investigation of freight car lateral dynamics, which is also shown on Figure 5.3.

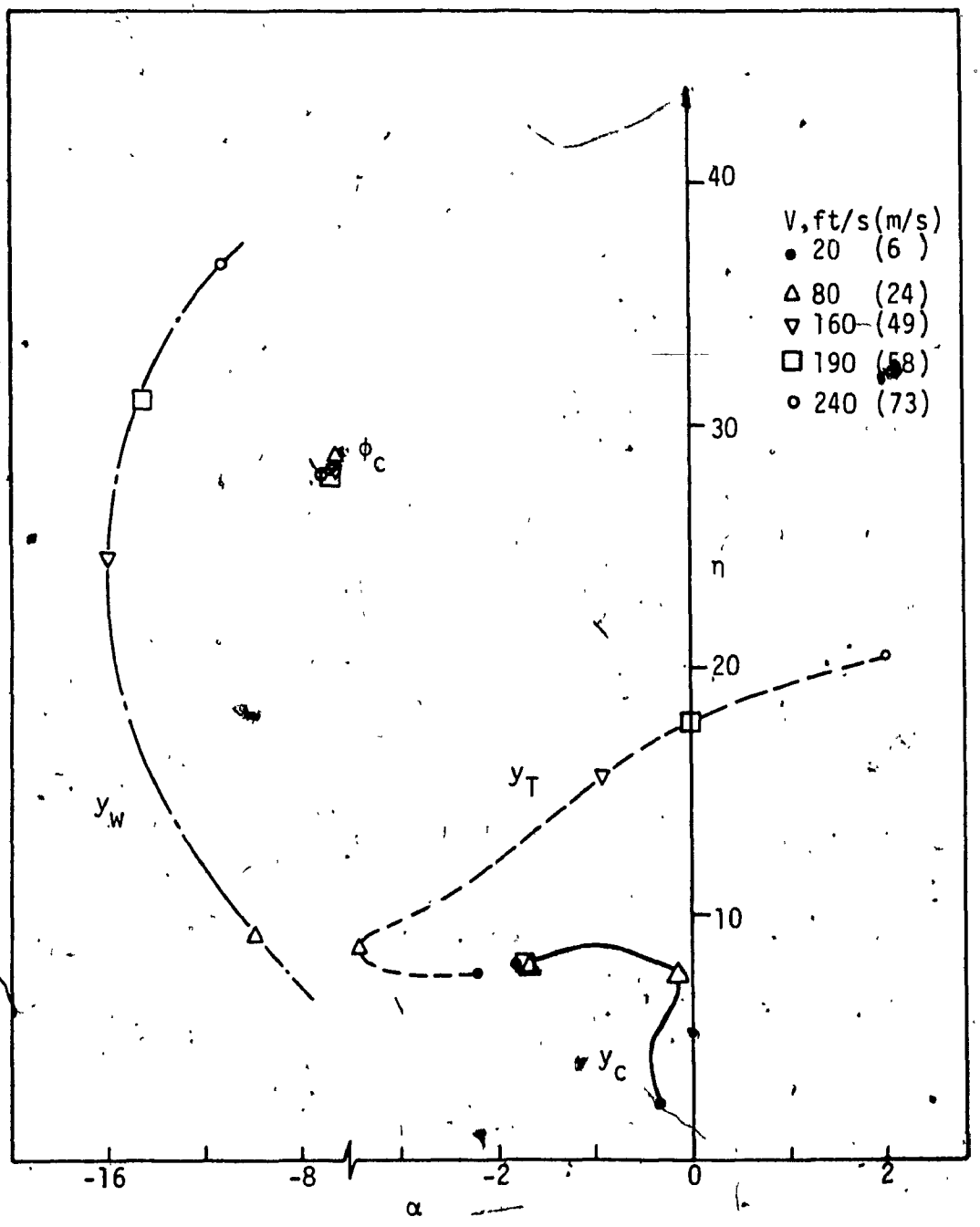

Figure 5.1 Root-loci of principal motions for truck model with rigid wheelset coupler, as velocity is increased.

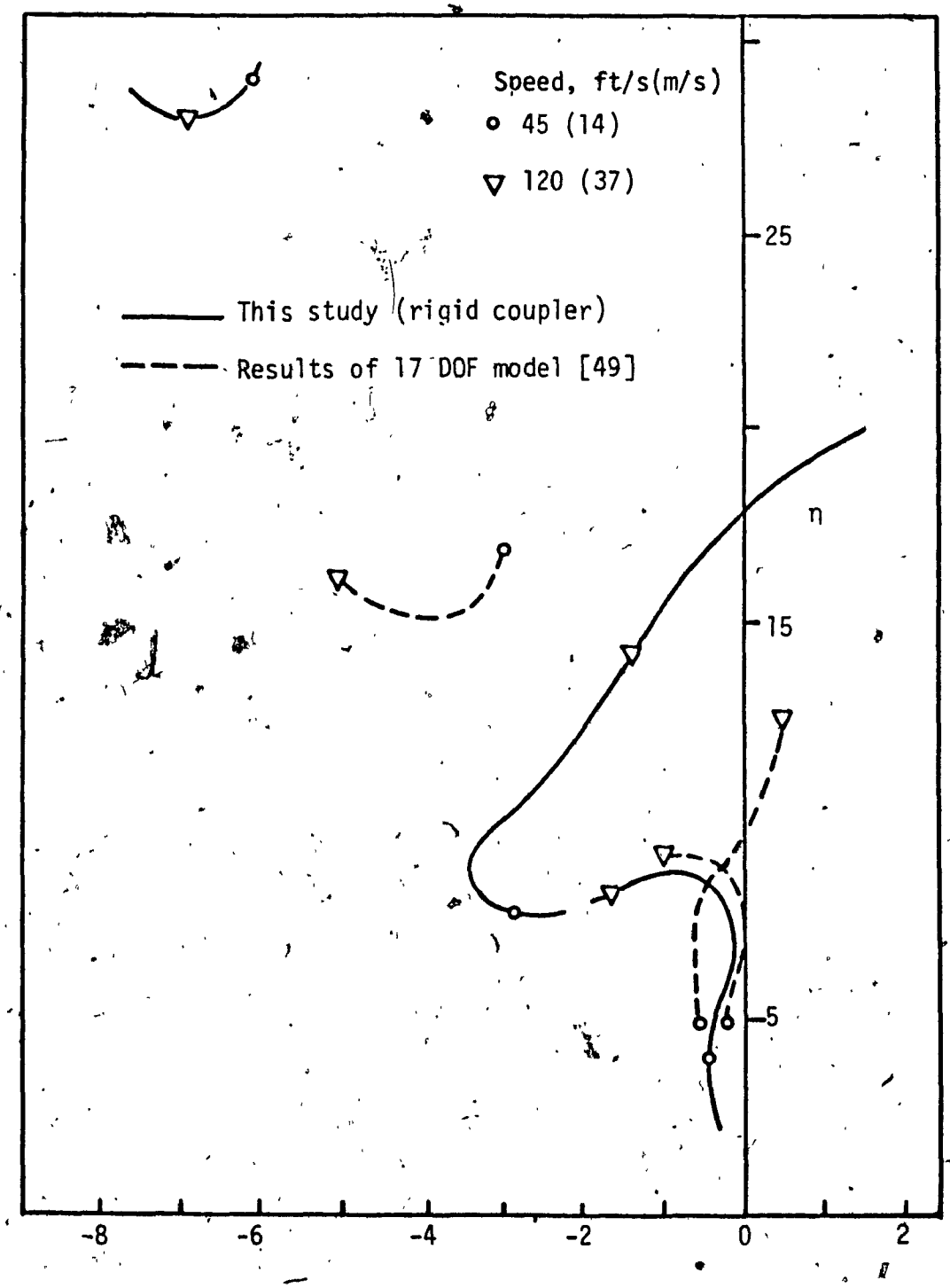

Figure 5.2 Comparison of root-loci from this study (rigid coupler) with that of a 17-DOF conventional freight car model [49].

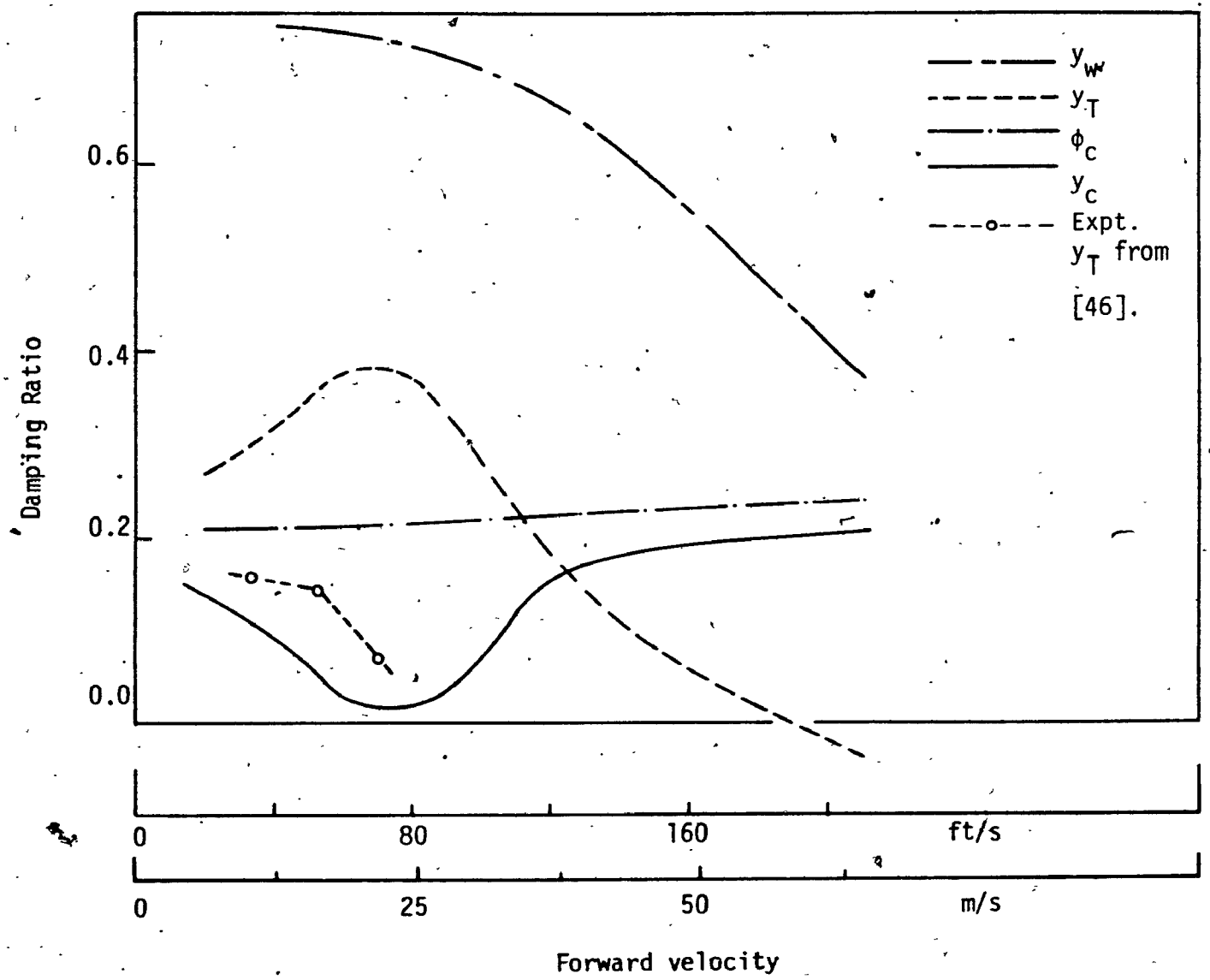

Figure 5.3 Variation of damping ratios for principal modes with velocity for rigid wheelset coupler, (-O- represents experimental result for conventional system [46]).

The results in terms of modal frequencies as a function of forward speed are shown in Figure 5.4. Once again, the trends are identical to those presented in Ref. [81]. The experimental result of the critical truck lateral mode from Ref. [46], is also shown in Figure 5.4, which indicates good correlation with the results of this investigation. The experimental results shown in Figures 5.3 and 5.4, are from a complete freight car study, for which the primary suspension parameters and system dimensions were not reported. Hence, the comparison of results are only based on qualitative trends and not on quantitative basis.

From the results obtained in this part of the study, it is evident that truck lateral mode is the least damped mode that becomes unstable before the wheelset lateral mode. As it can be seen from Figures 5.3 and 5.4, the frequencies and damping ratios associated with car body modes are essentially invariant for high speeds. In the vicinity of velocity, V = 24 m/s (80 ft/s), a decrease in the effective damping ratio of the least damped car body mode (y_c) occurs, where the frequencies associated with the truck motion are in close proximity to car body natural frequency. This situation leads to an increase in car body oscillations referred to as primary hunting. Once this speed region is passed, car body oscillations decrease and the damping ratio reaches a comparable value to that of low speed condition.

On the other hand, the frequencies associated with the wheelset and truck lateral oscillations increase approximately linearly with speed. They are often referred to as kinematic modes of wheelset and truck motion. As Figure 5.3 indicates, when the speed is increased, the damping ratio of these two modes start to decrease rapidly, resulting in

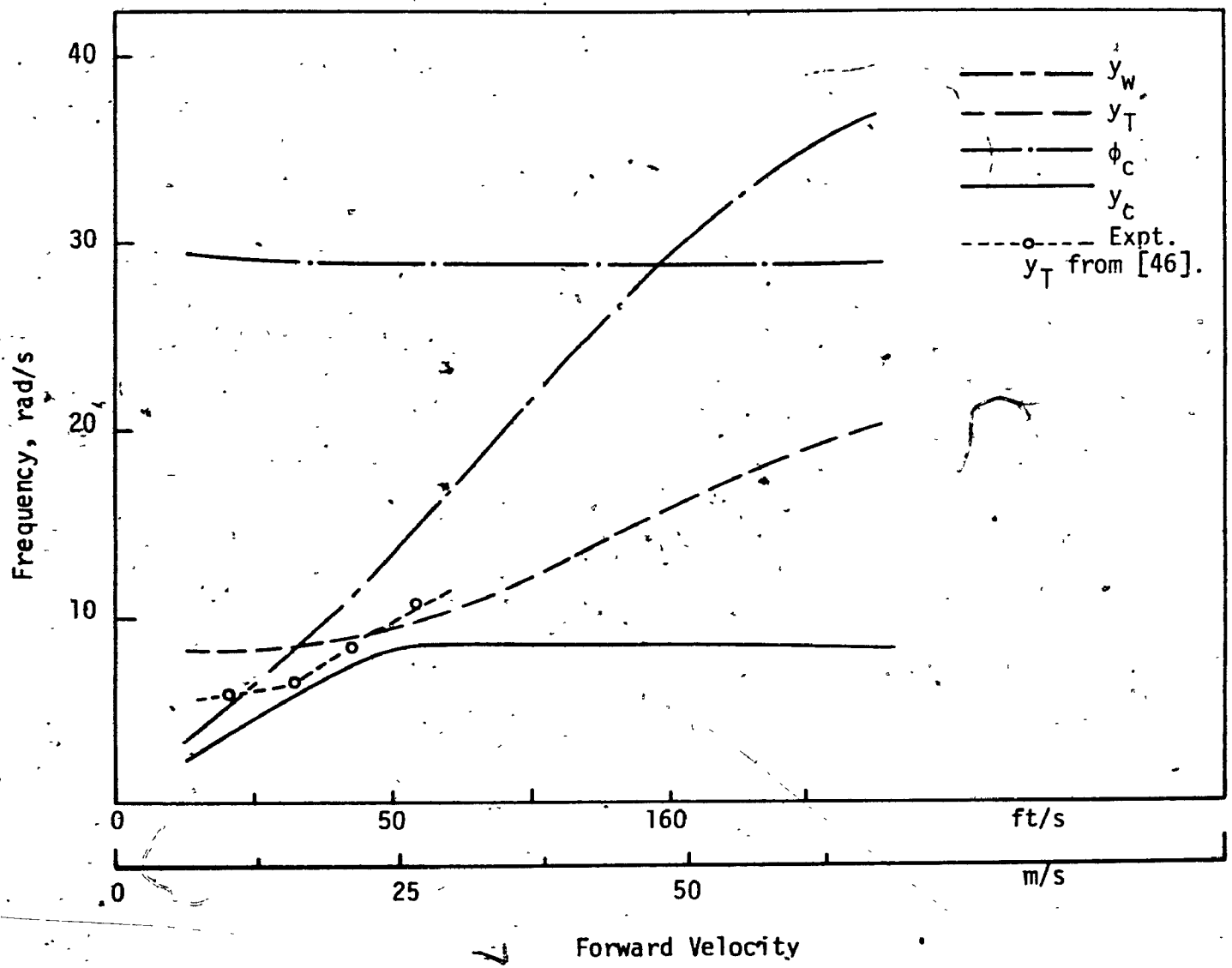

Figure 5.4 Variation of principal modal frequencies with velocity for rigid wheelset coupler, (-O- represents experimental result for conventional system [46]).

increased truck lateral oscillations referred to as secondary hunting, which eventually becomes unstable. For the baseline model used, the critical speed at which this occurs is 58 m/s (190 ft/s), for the conventional system with rigid wheelset coupler.

On the basis of validation carried out in this section, certain confidence can be placed on the truck model with EDCW to give useful results in terms of stability behaviour. In the following sub-sections, the results of study into the effects of EDCW on the truck stability are presented.

5.3.2 Stability Behaviour of Truck Model with EDCW

The objective in this section of the study is to examine the influence of wheelset coupler on the stability behaviour of the truck model. For this, the 11-DOF truck model with EDCW and pseudo-car body is used with nominal set of parameters. Critical speeds are computed for various values of wheelset coupler stiffness (k_{AX}), and damper (D_{AX}), through eigenvalue solution.

The results are presented as stability boundary curves for a fixed value of D_{AX} with variation in k_{AX}. By examining the eigenvalues and corresponding eigenvectors, the critical modes are identified as car body lateral, truck lateral, wheelset lateral, and wheelset relative spin. For various values of D_{AX}, the critical speed boundaries for each of these modes are plotted as shown in Figures 5.5 to 5.10. All values of critical speeds are rounded-off to nearest 1.5 m/s (5 ft/s) for computing efficiency.

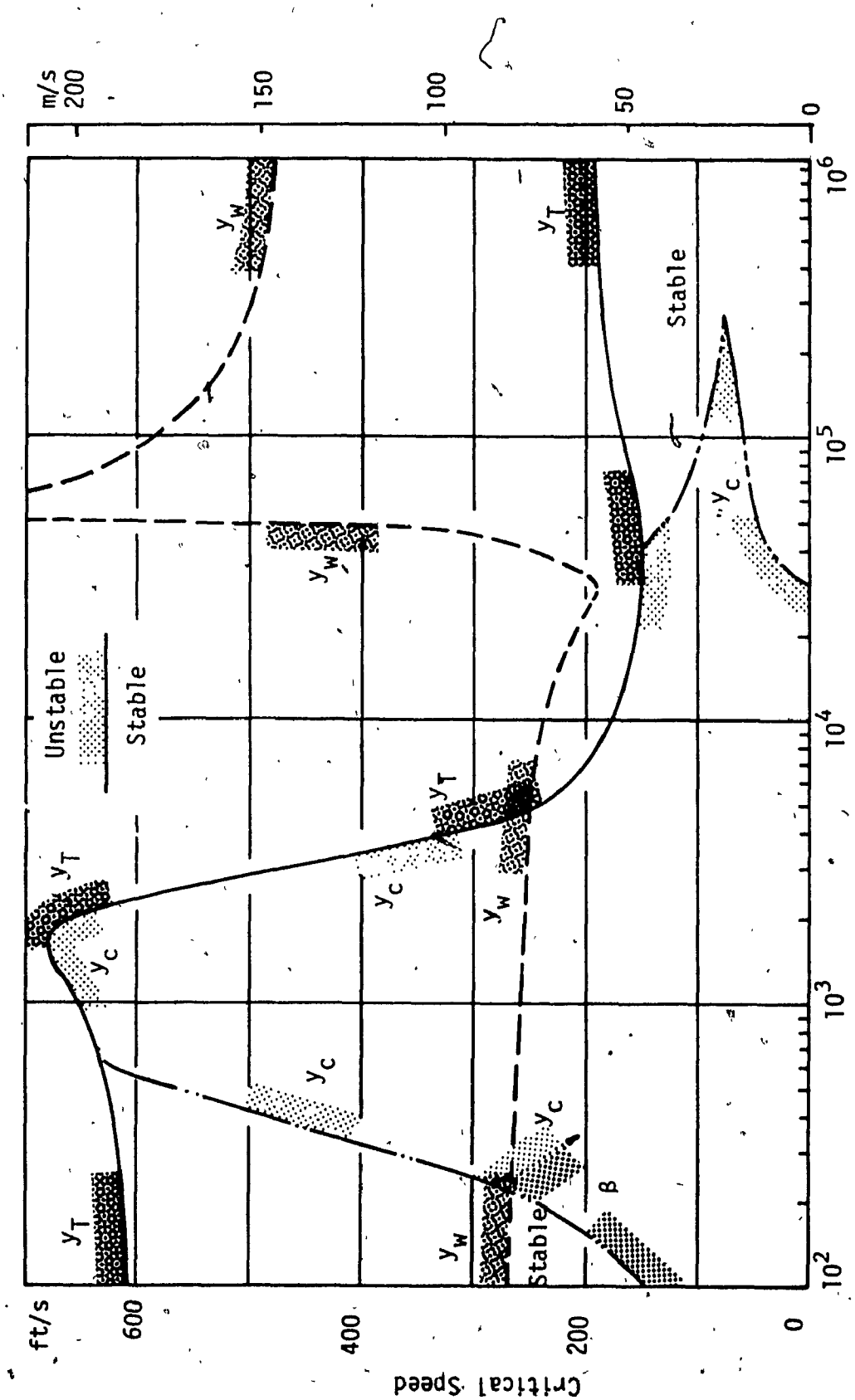

Figure 5.5 Critical speed boundaries of truck model with EDCW as k_{AX} is varied, for D_{AX} = 27 N.m.s/rad (20 lb.ft.s/rad).

In Figure 5.5, for small values of wheelset torsional damping (D_{AX} = 27 N.m.s/rad (20 lb ft s/rad)), when k_{AX} is very small, the wheelset spin mode (β) is unstable for a velocity range of zero to 48 m/s (150 ft/s). At this stiffness, for velocity range 46 to 82 m/s (150 to 270 ft/s), all the modes are stable. As the speed is increased further, the wheelset lateral mode (y_w) is unstable for velocity (V) greater than 82 m/s (270 ft/s), and the truck lateral mode (y_T) becomes unstable at V = 186 m/s (610 ft/s). However, for practical purposes, as soon as one of the modes become unstable, the truck system is declared unstable. For the same value of D_{AX} (Figure 5.5) as the value of k_{AX} is increased, one or more of the modes are always unstable (except for the small triangular region labeled "stable" in the left-hand side of Figure 5.5), until k_{AX} = 4.07×10^4 N.m/rad (3×10^4 lb.ft/rad) is reached. For values of k_{AX} beyond this, the car body lateral mode is unstable for certain ranges of velocity, where the range decreases as k_{AX} is increased. This primary hunting (car lateral instability) phenomenon becomes stable at higher speeds. As the forward speed is increased further, the truck lateral (y_T) mode becomes unstable. When k_{AX} is very large (right-hand side of Figure 5.5), the critical mode is y_T, that becomes unstable at V = 58 m/s (190 ft/s), this critical speed corresponds to the truck system with conventional wheelsets.

As the results further show, for conventional system, critical speed corresponding to y_w mode is significantly greater than the one corresponding to y_T mode. In the absence of wheelset coupler damping (or small damping), the only major stable region is due to large value of k_{AX}. This stable region is very similar to the results obtained by Hadden and Law [86], and Doyle et al. [94] with the exception of the

small unstable region due to car lateral mode. This small primary hunting zone (car lateral instability) in Figure 5.5, is due to relatively smaller value of secondary lateral damping (D_y) used in this study. As shown later in the parametric study, for comparable value of D_y as reported in [86] and [94], this unstable region completely disappeared and followed the results in [86] and [94].

The most interesting aspect of the result in Figure 5.5, is the small triangular stable region that exists for small values of k_{AX}. For small values of k_{AX} the results further show that contrary to rigid axle, in this case critical speed corresponding to y_T is significantly greater than that of (y_w) mode.

The influence of D_{AX} is next explored by obtaining similar plots for larger values of D_{AX}. Figures 5.6 to 5.10 show these results for D_{AX} in the range of 339 to 6,780 N.m.s/rad (250 to 5,000 lb.ft.s/rad). As these results indicate, when the value of D_{AX} is increased, the instability range corresponding to β mode reduces drastically, while the critical speed boundary corresponding to y_w mode increases, which results in a rapid increase of the stable region for small values of k_{AX}. At the same time, as the left-hand end of the figures indicate, the critical speed boundary corresponding to y_T mode reduces as D_{AX} is increased. On the other hand, in the right-hand end of the plots, for large values of k_{AX}, variation in D_{AX} has little effect on the stability boundaries.

Since for small values of k_{AX}, increase in D_{AX} increases the critical speed of wheelset lateral mode and reduces critical speed of truck lateral mode, there exists an optimal value of D_{AX}, for which the critical speed boundaries of these two modes coincide as indicated in

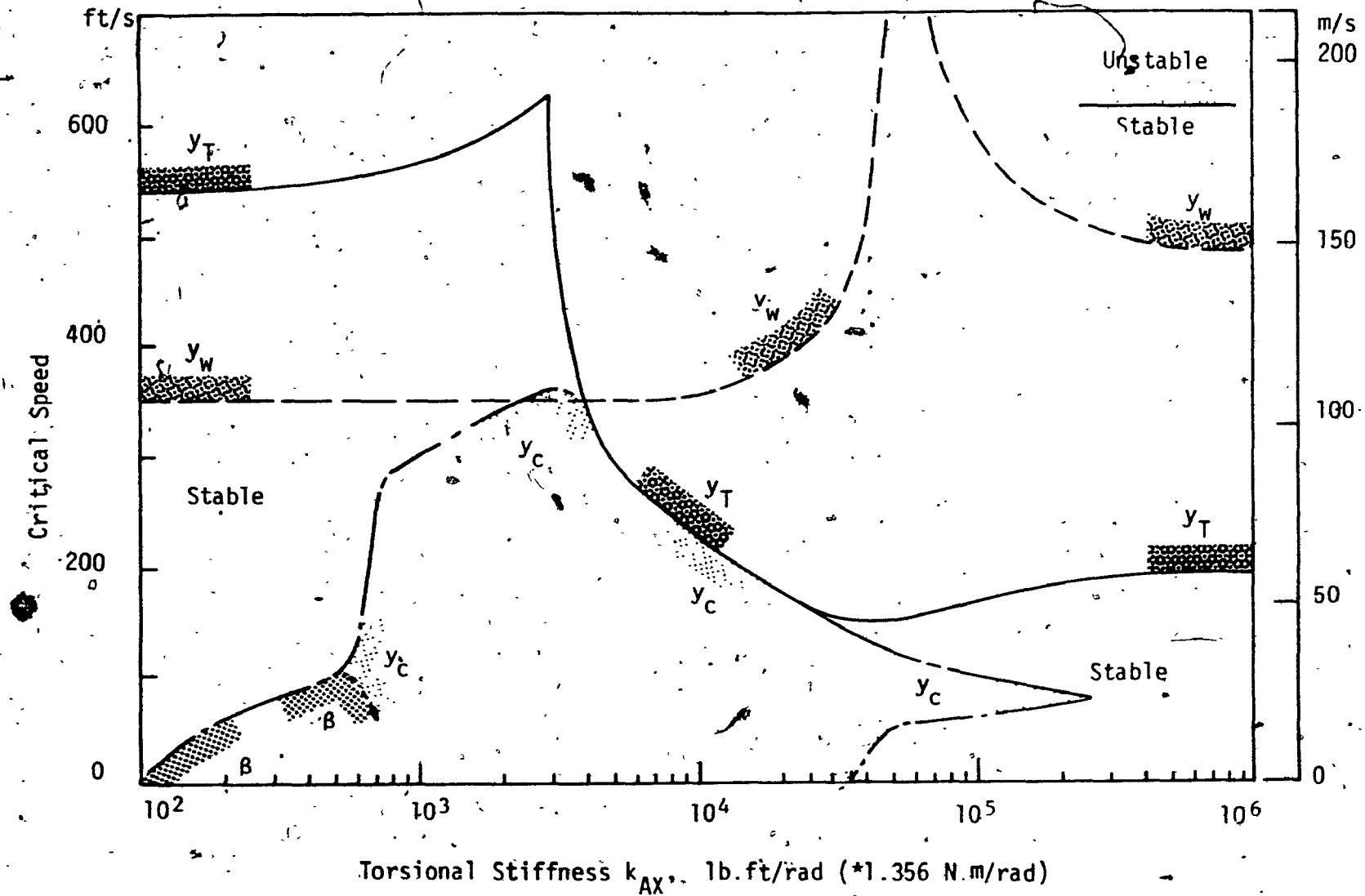

Figure 5.6 Critical speed boundaries of truck model with EDCW as k_{AX} is varied, for D_{AX} = 339 N.m.s/rad (250 lb.ft.s/rad).

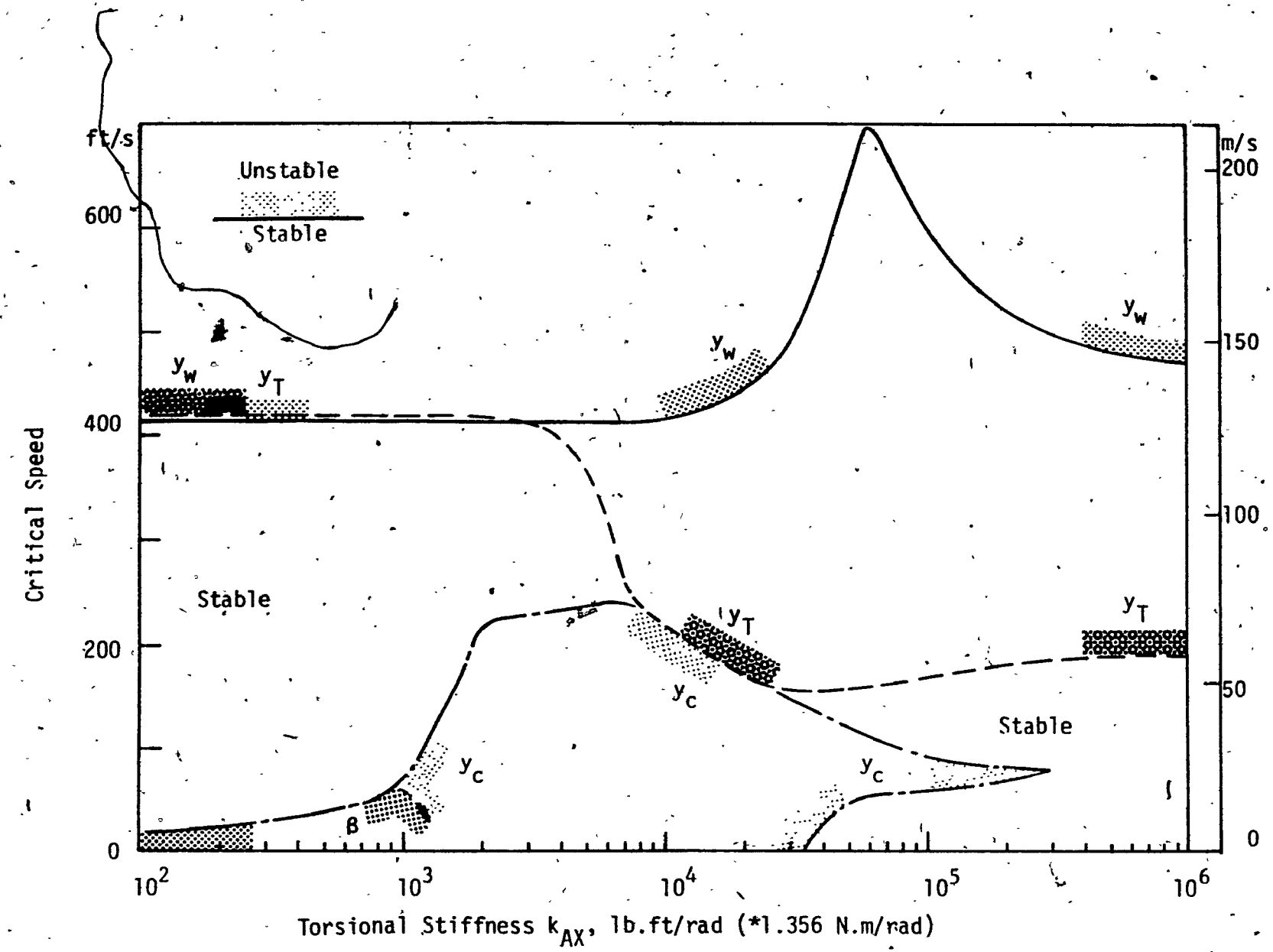

Figure 5.7 Critical speed boundaries of truck model with EDCW as k_{AX} is varied, for D_{AX} = 678 N.m.s/rad (500 lb.ft.s/rad).

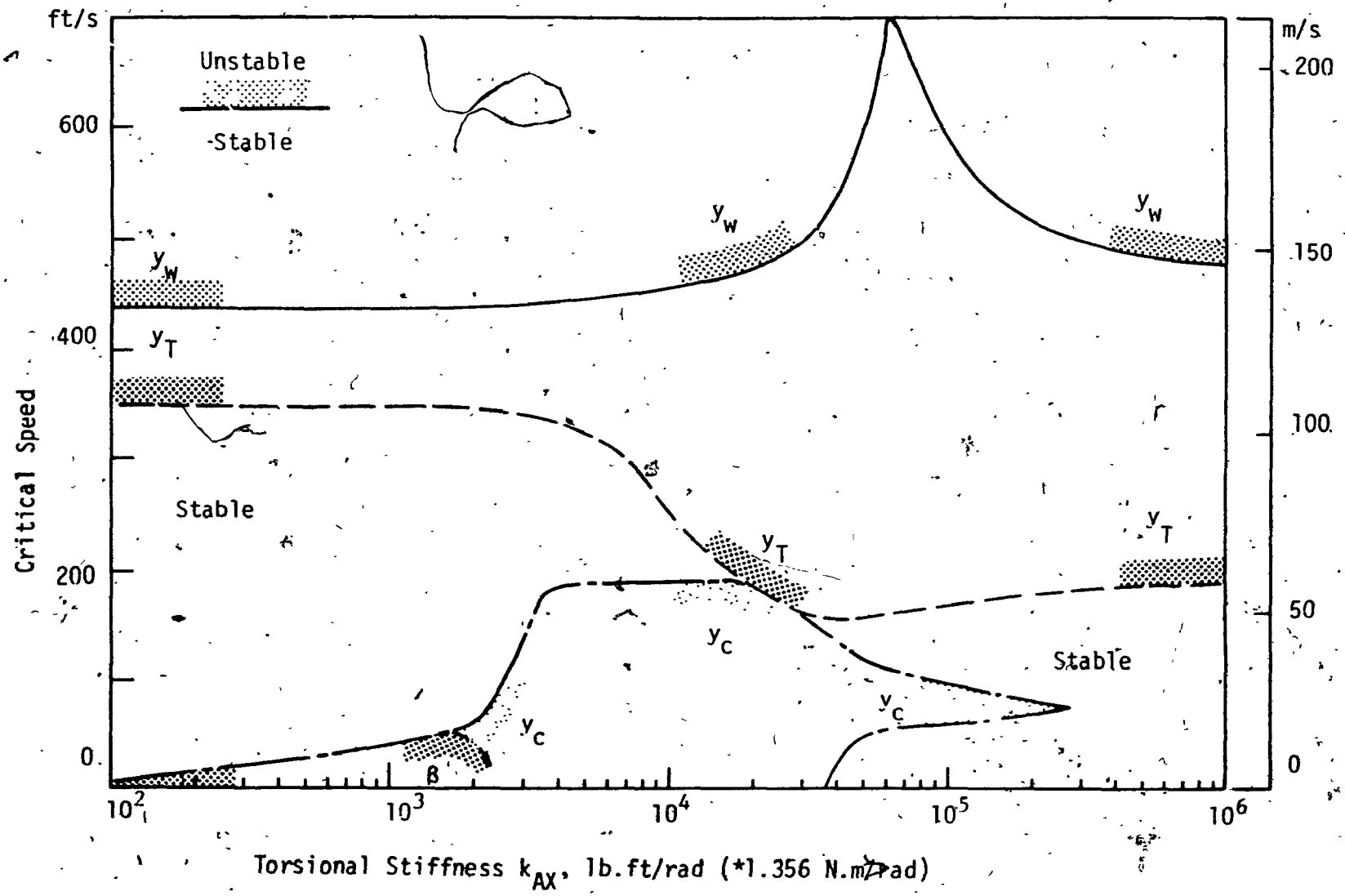

Figure 5.8 Critical speed boundaries of truck model with EDCW as k_{AX} is varied, for D_{AX} = 1017 N.m.s/rad (750 lb.ft.s/rad)

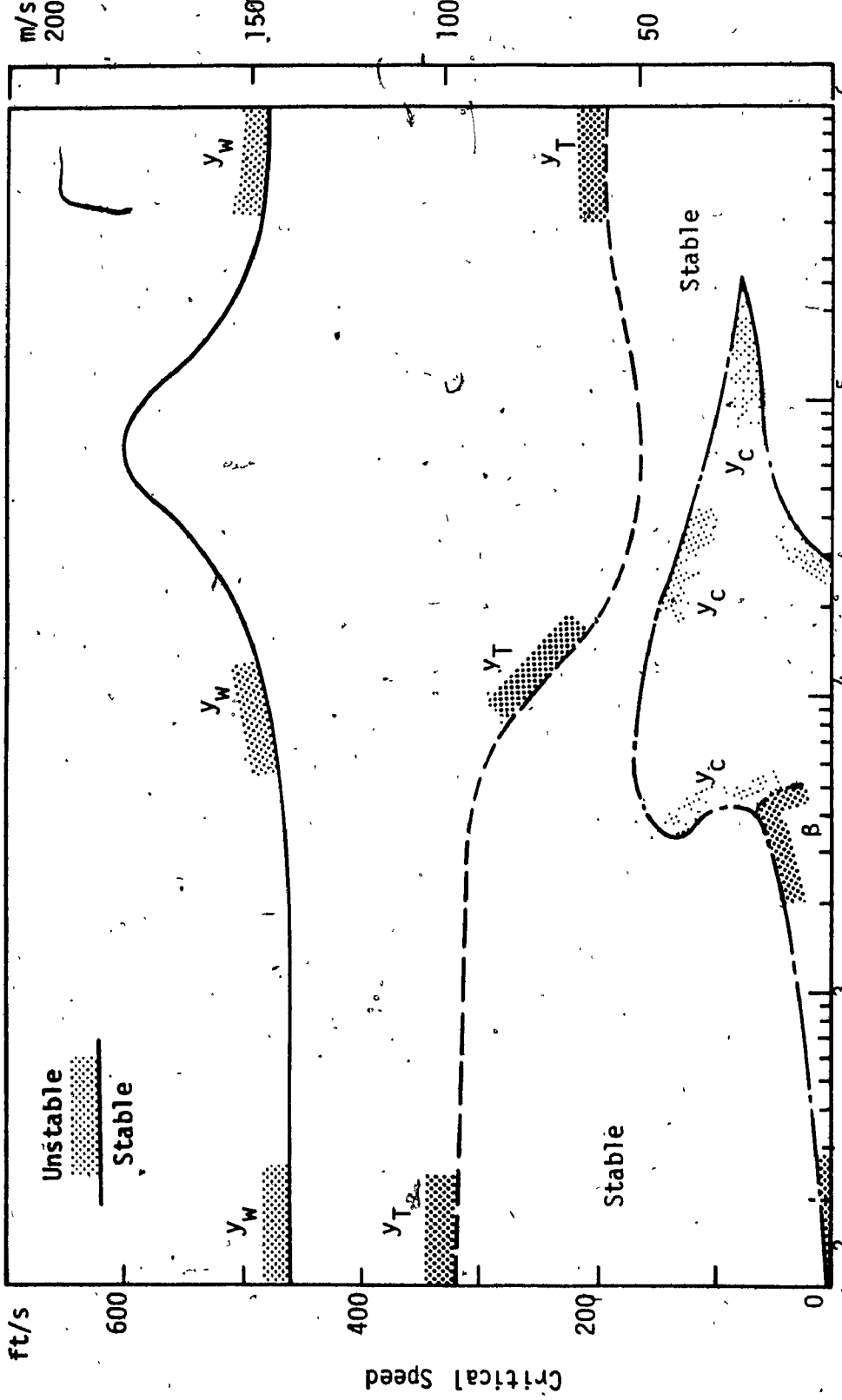

Figure 5.9 Critical speed boundaries of truck model with EDCW as k_{AX} is varied, for D_{AX} = 1,356 N.m.s/rad (1,000 lb.ft.s/rad).

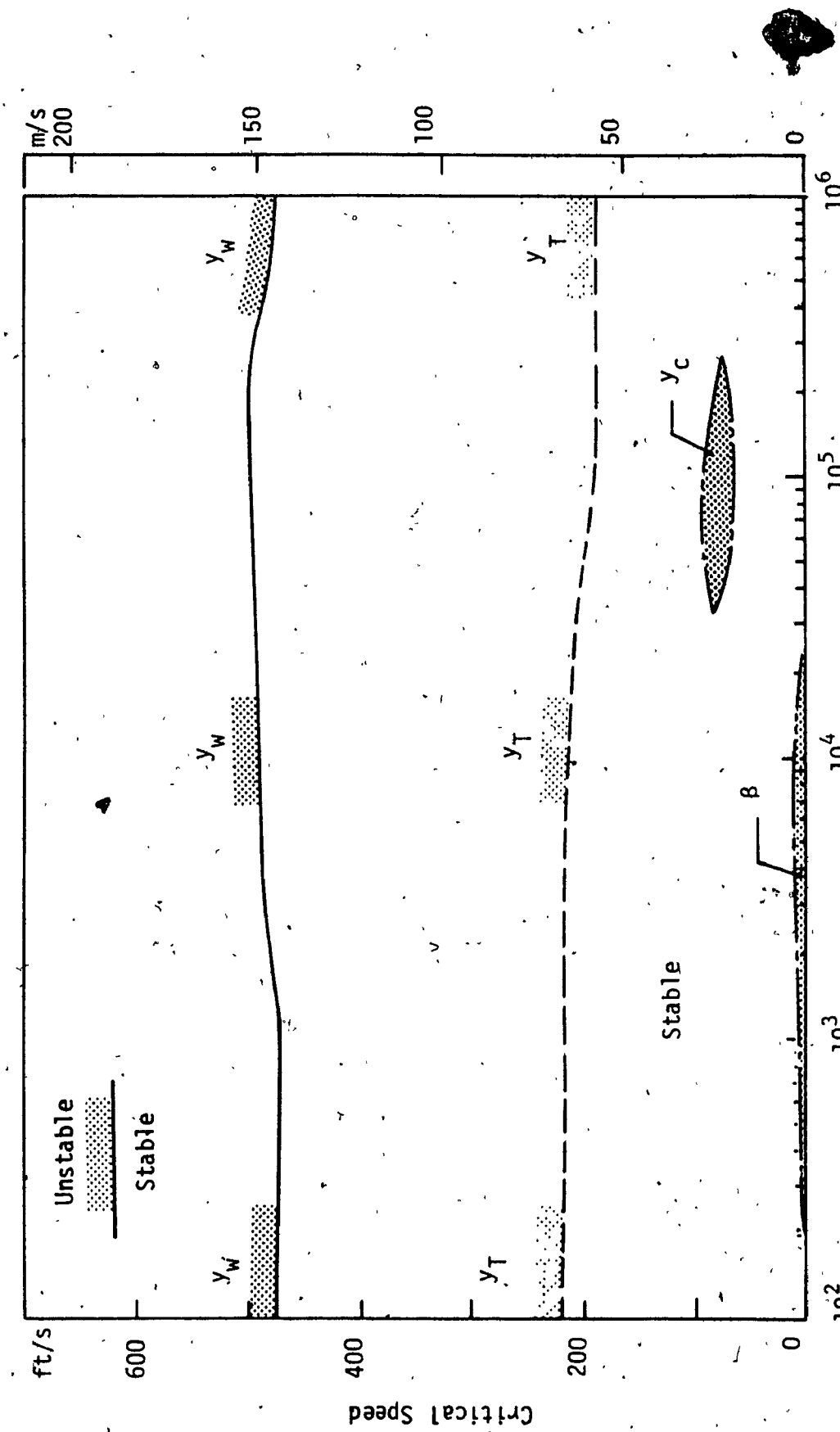

Figure 5.10 Critical speed boundaries of truck model with EDCU as k_{AX} is varied, for D_{AX} = 6,780 N.m.s/rad (5,000 lb.ft.s/rad).

Figure 5.7. Beyond this optimal damping value of D_{AX}, as shown in Figures 5.8 to 5.10, the critical speed boundaries for wheelset and truck lateral modes crossover, and the critical speed corresponding to truck lateral mode continues to decrease. For the baseline truck model, the value of optimal D_{AX} is found to be 678 N.m.s/rad (500 lb.ft.s/rad), for which stability boundaries are shown in Figure 5.7. As the Figure 5.7 indicates, for small values of k_{AX} and optimal D_{AX}, ignoring the spin mode, a critical speed of 125 m/s (410 ft/s) can be obtained, compared to 58 m/s (190 ft/s) for conventional system. However, for this value of D_{AX}, the spin mode remains unstable for a range of initial velocities, which can be eliminated by increasing D_{AX} as indicated in Figure 5.10. But as Figures 5.8 to 5.10 show, further increase in D_{AX} reduces the critical speed boundary of truck lateral mode. This conflicting requirement can be overcome by utilizing a variable torsional damper of the coupler, that provides large damping at low speed and small damping at high speeds, while k_{AX} is maintained to be a constant small value. This requirement of variation in D_{AX} with velocity is expected since the improvement is to be obtained by counteracting the longitudinal creep force, which is proportional to 1/V.

The results obtained in this part of the study show, that in order to achieve the maximum possible critical speed of 125 m/s (410 ft/s), for the baseline truck model, the variation in D_{AX} is required in such a way, that D_{AX} is greater than 13,560 N.m.s/rad (10^4 lb.ft.s/rad) for V less than 6 m/s (20 ft/s) and D_{AX} in equal to 678 N.m.s/rad (500 lb.ft.s/rad) when V is 125 m/s (410 ft/s). This trend of D_{AX} can be obtained by expressing D_{AX} as:

$$D_{AX} = C_{D_{AX}} (1XV) \qquad (5.2)$$

where $C_{D_{AX}}$ is a constant and equal to 8.47 x 10^4 N.m^2/rad (2.05 x 10^5 lb.ft^2/rad) for the baseline model. From practical point of view, design of a wheelset coupler to give the required variation with speed should be physically possible. However, this is not included within the scope of the present investigation. A coupler, that provides a value of D_{AX} according to Equation (5.2) and k_{AX} = 200 N.m/rad (150 lb.ft/rad), is referred to as an optimal coupler for the truck model with EDCW. A small value for k_{AX} is selected so that the initial spin instability is not present (Figure 5.10). The value of D_{AX} at the critical speed, V = $V_{critical}$ is referred as D_{AX} and it is the optimal damping value at the critical speed.

For the baseline model with nominal parameters and optimal coupler, the root loci of eigenvalues are obtained, as the speed is increased. The root loci corresponding to wheelset, truck and car lateral modes are shown in Figure 5.11. The corresponding damping ratios as function of speed are shown in Figure 5.12. These Figures 5.11 and 5.12, can be readily compared with the results of conventional system presented earlier in Figures 5.1 and 5.3. As the comparison indicate, an optimal EDCW can provide significant improvement in both primary and secondary hunting modes over the entire speed range. This improvement on the other hand is obtained at the expense of wheelset lateral mode damping ratio, which shows significant decrease in comparison to the conventional system. However, the damping ratio corresponding to wheelset lateral mode remains positive for all velocities until the truck critical speed is reached.

Therefore, the results obtained so far indicate that through EDCW,

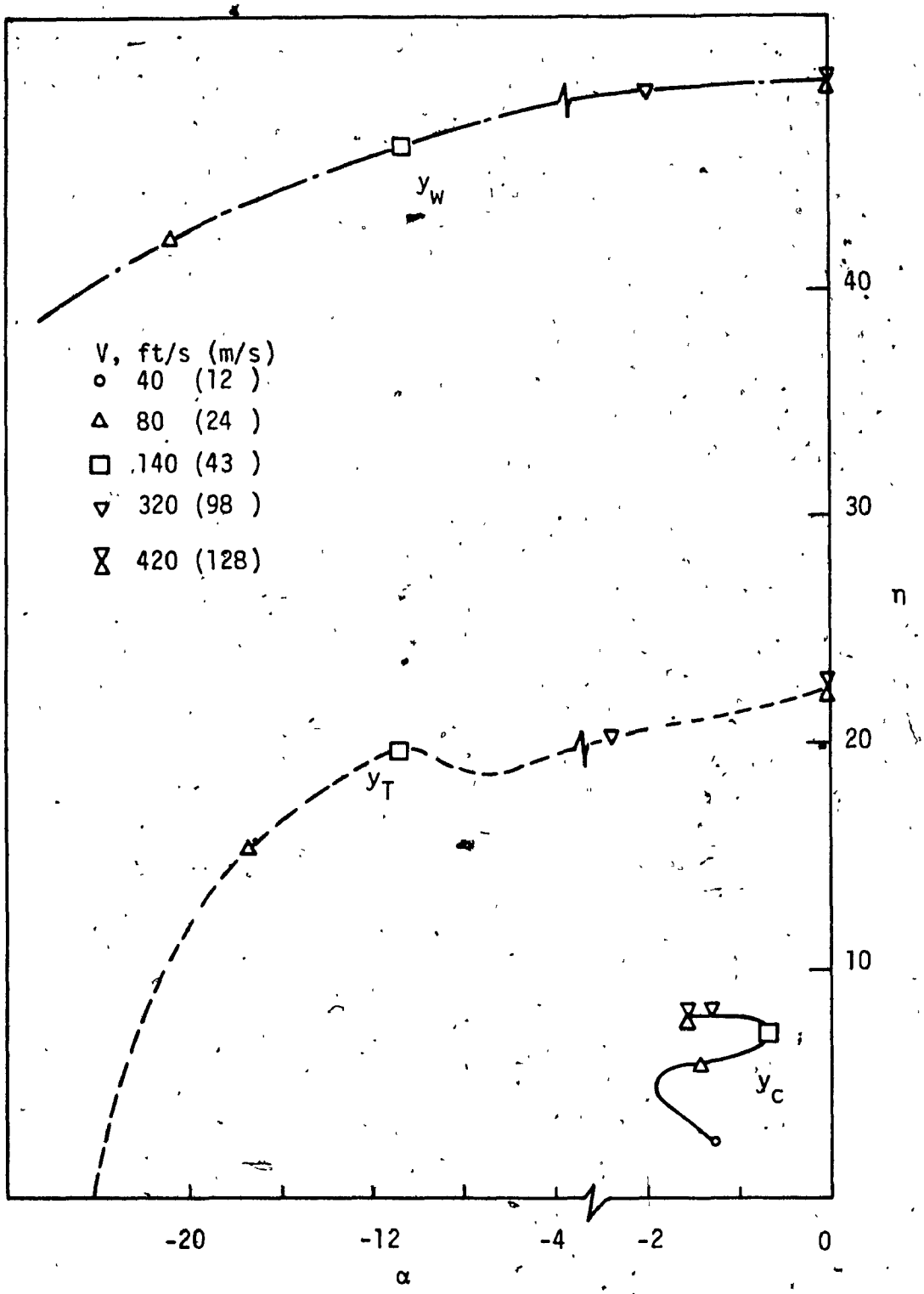

Figure 5.11 Root-loci of prinicpal motions for the model with optimal wheelset coupler, as velocity is increased.

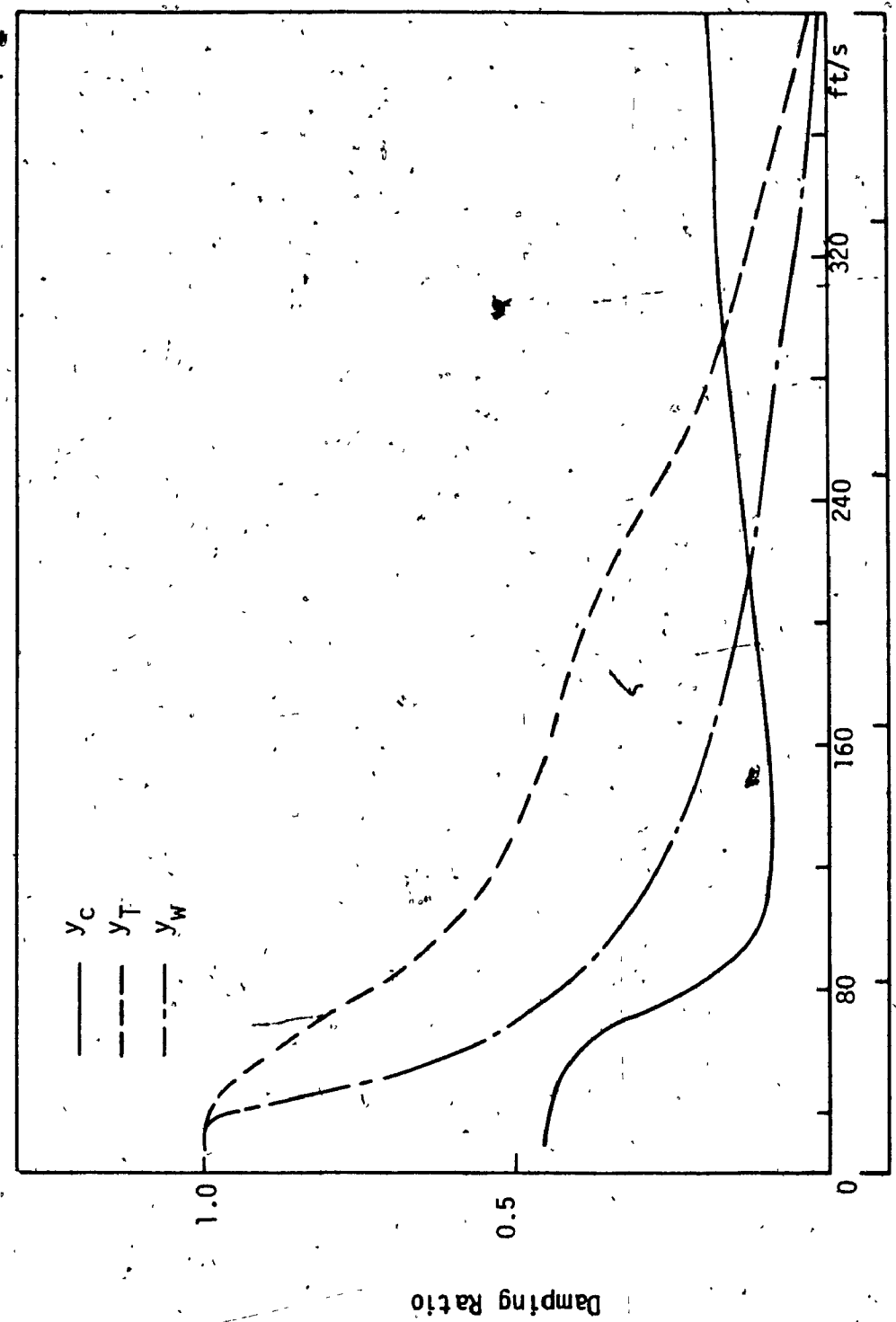

Figure 5.12 Variation of principal mode damping ratios with velocity for the model with optimal wheelset coupler.

the lateral stability behaviour of both wheelset and truck can be controlled, such that both the modes have identical critical speeds. In doing so, the critical speed of the freight car system can be maximized. For the nominal parameters, the critical speed corresponding to truck model with optimal wheelset coupler is 115% greater than that of conventional system with rigid axle wheelsets. In the following sub-section, parametric study is carried out with the truck model to examine the influences of model parameters on the stability behaviour of the truck model with EDCW, as well as on the optimal value of wheelset coupler are evaluated.

5.3.3 Influence of System Parameters

The railway freight truck model employed in this investigation include a very large number of parameters. To study the influence of each parameter on the stability behaviour is a tedious task. In this section of the investigation, a limited set of parametric study is carried out to determine the influence of variation in selected parameters, on the critical speed of the truck model. Important parameters pertaining to conventional system, such as wheel conicity and primary suspension stiffnesses are considered. In addition to these, this study includes the influence of axle loading. Further, the effect of variation in secondary lateral damping is also examined, since the results for baseline model showed dominance of car body lateral mode for certain range of coupler parameters.

In all cases, the results for the truck model with EDCW are obtained for optimal coupler parameter. The "optimal coupler" is referred in this study as the speed dependant coupler damping D_{AX}, which

provides optimal coupler torsional damping value according to Equation (5.2), while coupler torsional stiffness k_{AX} is maintained to be 200 N.m/rad (150 lb.ft/rad). The results of the parametric study are discussed under the following sub-headings, where only one system parameter is varied at a time, while the others are kept constant and equal to their nominal values.

5.3.3.1 Influence of Wheel Conicity

Results are obtained as stability boundary curves for effective wheel conicity in the range of 0.02 to 0.2 rad. Corresponding to each value of wheel conicity considered, the value of optimal coupler damping D^*_{AX} is first determined, for which the y_W and y_T critical speed boundaries of the truck model with EDCW coincide.

For each value of conicity (λ), and optimal wheelset coupler (D^*_{AX}), results are obtained as plots of critical speed boundaries versus torsional stiffness (k_{AX}). Figures 5.13, 5.14, and 5.15 show these critical speed boundaries for λ = 0.07, 0.1, and 0.2, respectively. As these figures indicates, the general shape of the curves remain similar for all values of conicity. However, the critical speeds for truck and wheelset lateral modes decrease with increase in wheel conicity. Also, when the value of wheel conicity is increased, the region of car lateral instability reduces.

The results further indicate that, the optimal speed dependant wheelset coupler damping value D^*_{AX} is also sensitive to variation in effective wheel conicity. Table 5.3 shows the critical speed of the truck model for various values of wheel conicity, where the optimal

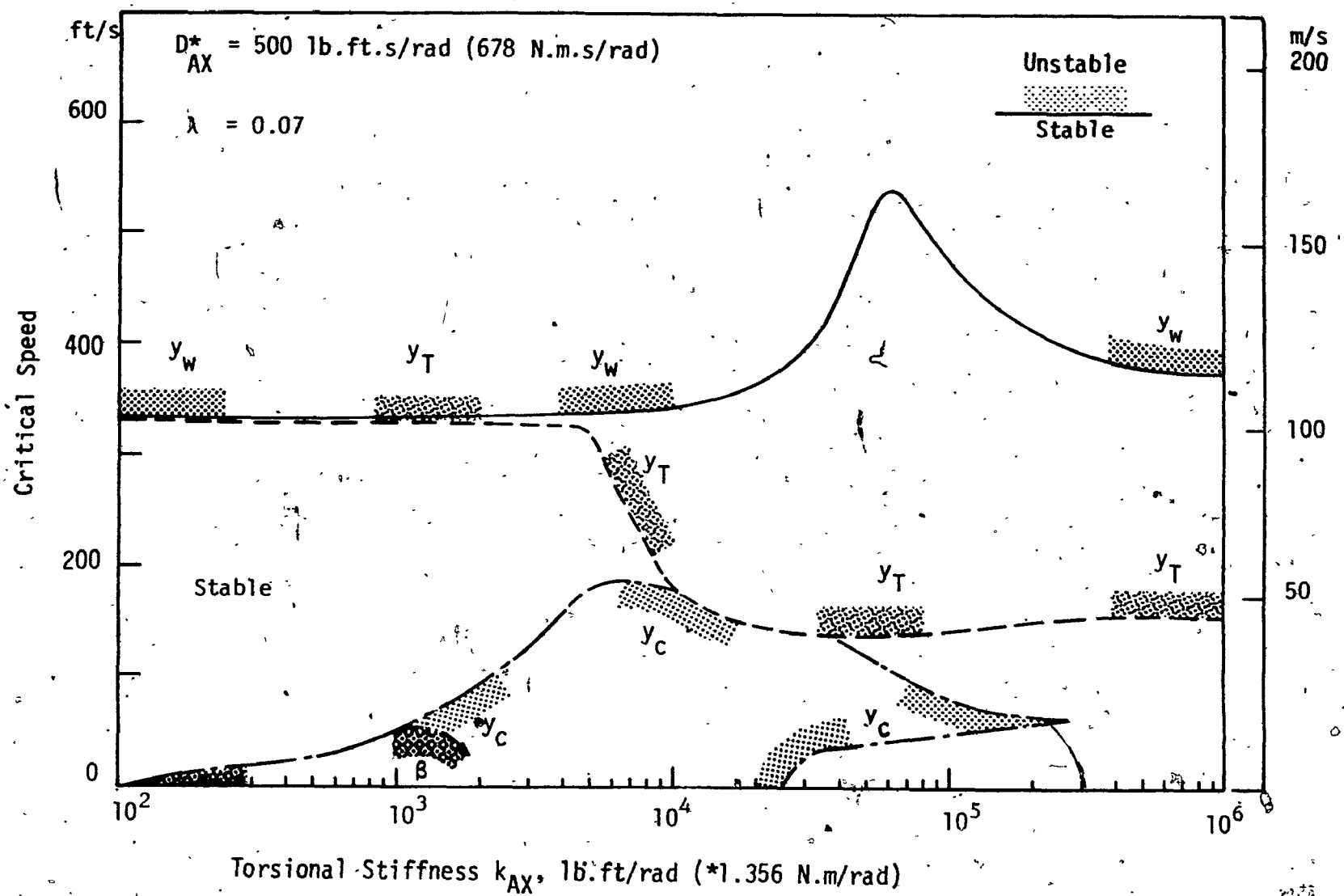

Figure 5.13 Critical speed boundaries of truck model with effective wheel conicity, λ = 0.07 and corresponding optimal value of D_{AX}, as k_{AX} is increased.

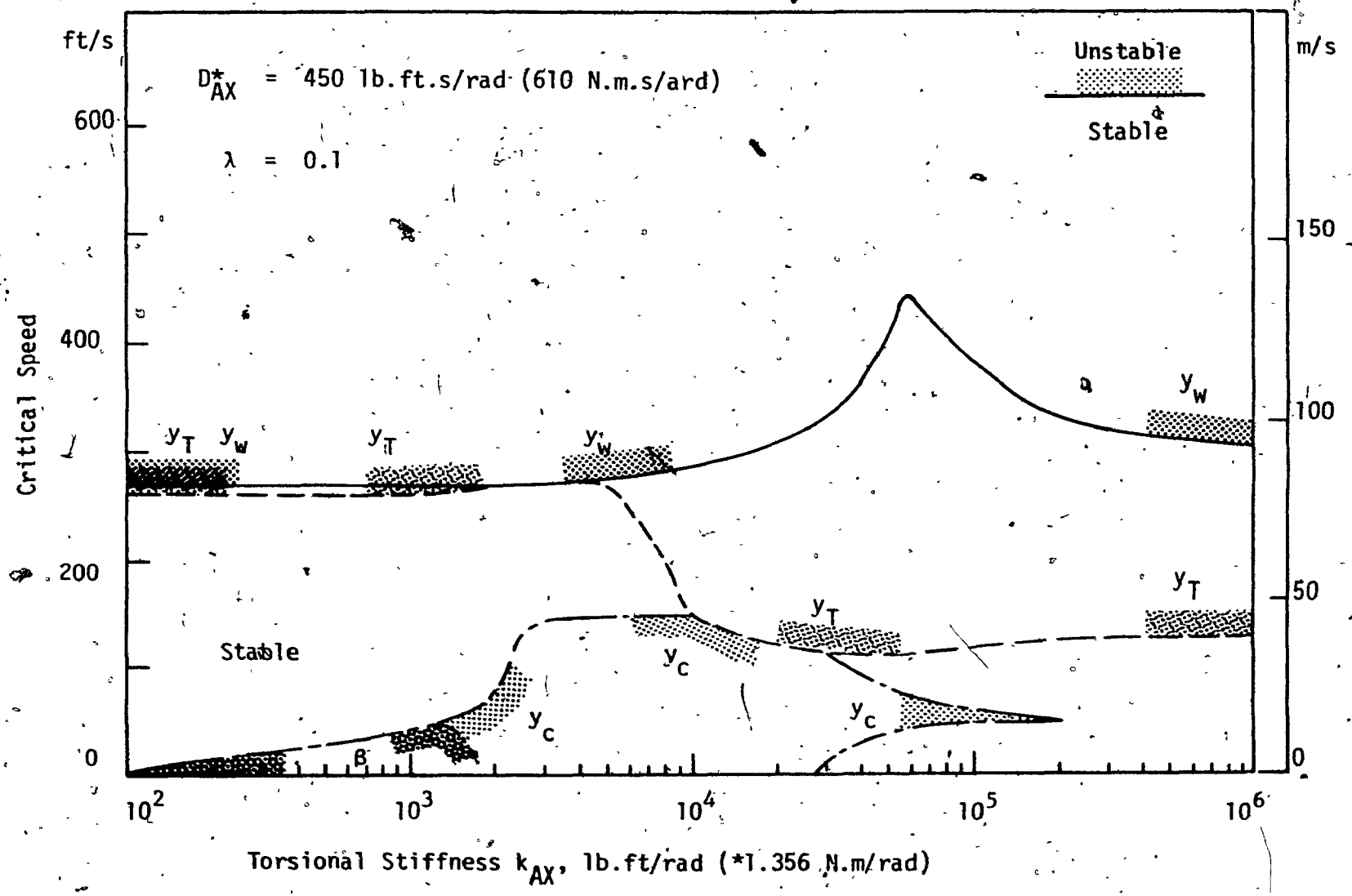

Figure 5.14 Critical speed boundaries of truck mdoel with effective wheel conicity, λ = 0.1 and corresponding optimal value of D_{AX}, as k_{AX} is increased.

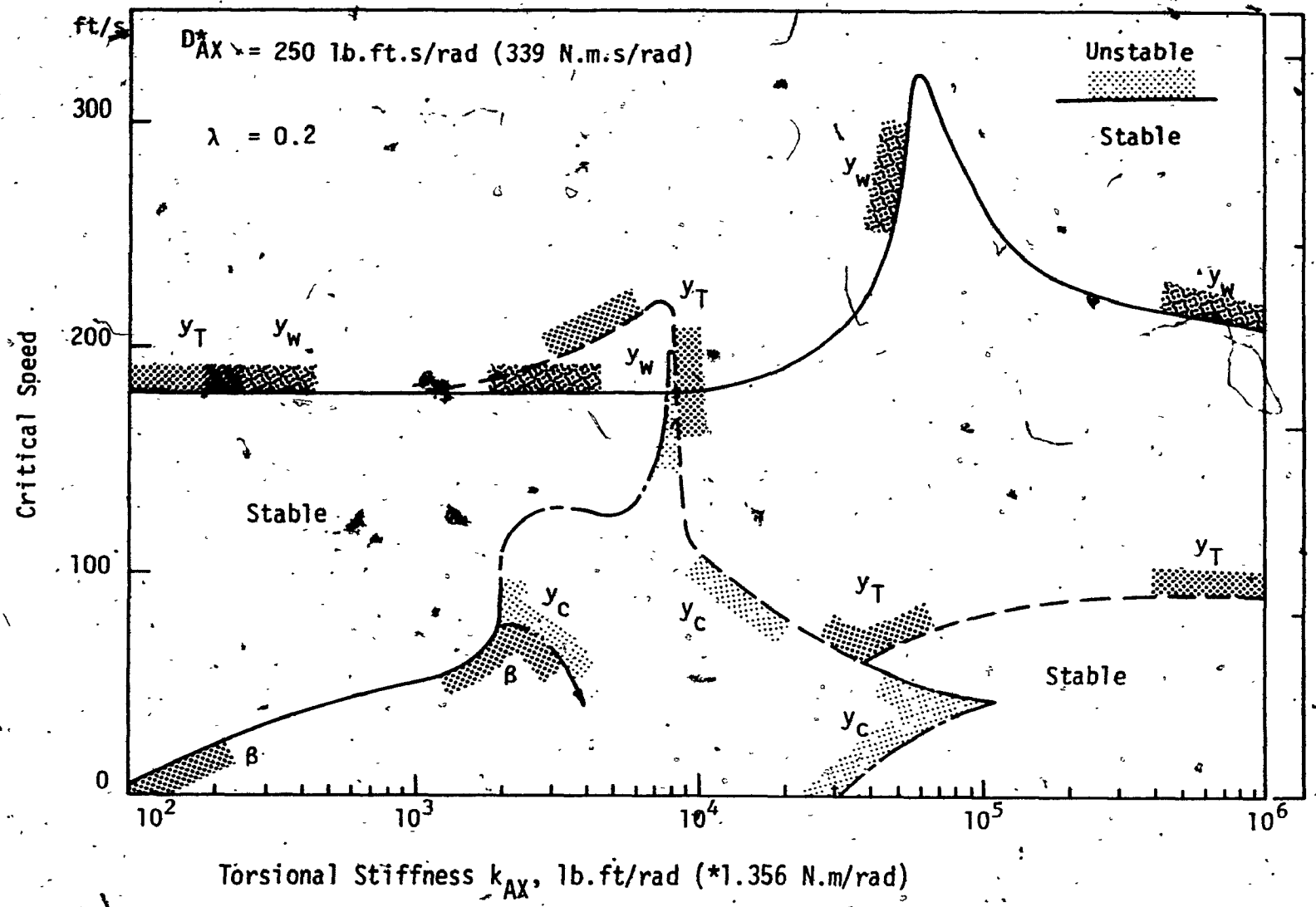

Figure 5.15 Critical speed boundaries of truck model with effective wheel conicity, λ = 0.2 and corresponding optimal value of D_{AX}, as k_{AX} is increased.

Table 5.3 Effect of Wheel Conicity on Critical Speed of the Truck Model

Wheel Conicity	Model with EDCW		Conventional Model
	D_{AX}^{*} N.m.s/rad (lb.ft.s/rad)	Critical Speed m/s (ft/s)	Critical Speed m/s (ft/s)
0.02	583 (430)	244 (800)	101 (330)
0.05 (nominal)	678 (500)	125 (410)	58 (190)
0.07	678 (500)	101 (330)	49 (160)
0.10	610 (450)	79 (260)	40 (130)
0.14	475 (350)	67 (220)	34 (110)
0.20	339 (250)	55 (180)	27 (90)

coupler damping D^*_{AX}, and the corresponding critical speed of the truck model with EDCW are shown. The table also shows the critical speed of a truck with conventional rigid axle wheelset system. These results are plotted as critical speed versus wheel conicity in Figure 5.16, which shows that the critical speed corresponding to truck model with EDCW is significantly superior to that of conventional system over the entire conicity range. Figure 5.16 also shows the effect of using one fixed value of D^*_{AX} on the critical speed for variation in conicity value, and is referred to as "Baseline Optimal Coupler". For this, the value of D^*_{AX} obtained for $\lambda = 0.05$ is used.

In order to determine the effect of profiled wheels, a moderately worn profile with wheel/rail geometric parameters given in Table 5.1 is considered. The critical speed boundaries are shown in Figure 5.17. For the profiled wheel, the effective wheel conicity is 0.14, which gives a critical speed of 69 m/s (225 ft/s) for the truck model with EDCW and for which the value of D^*_{AX} is 542 N.m.s/rad (400 lb.ft.s.rad). For the same condition, the critical speed for the conventional system is 40 m/s (130 ft/s). These critical speeds are slightly higher than those for conical wheels with $\lambda = 0.14$, shown in Table 5.3. This illustrates that the worned wheel profile has more influence on conventional model than the model with EDCW. The critical speed boundaries in Figure 5.17 show the influence of profiled wheel on the stability behaviour of truck system with EDCW. In comparison to EDCW with conical wheels of similar conicity (Figure 5.14 for $\lambda = 0.1$), the profiled wheels (Figure 5.17 for $\lambda = 0.14$) eliminate the unstable regions corresponding to spin and car lateral modes. Therefore, the latter case also eliminates the need for speed dependent damping.

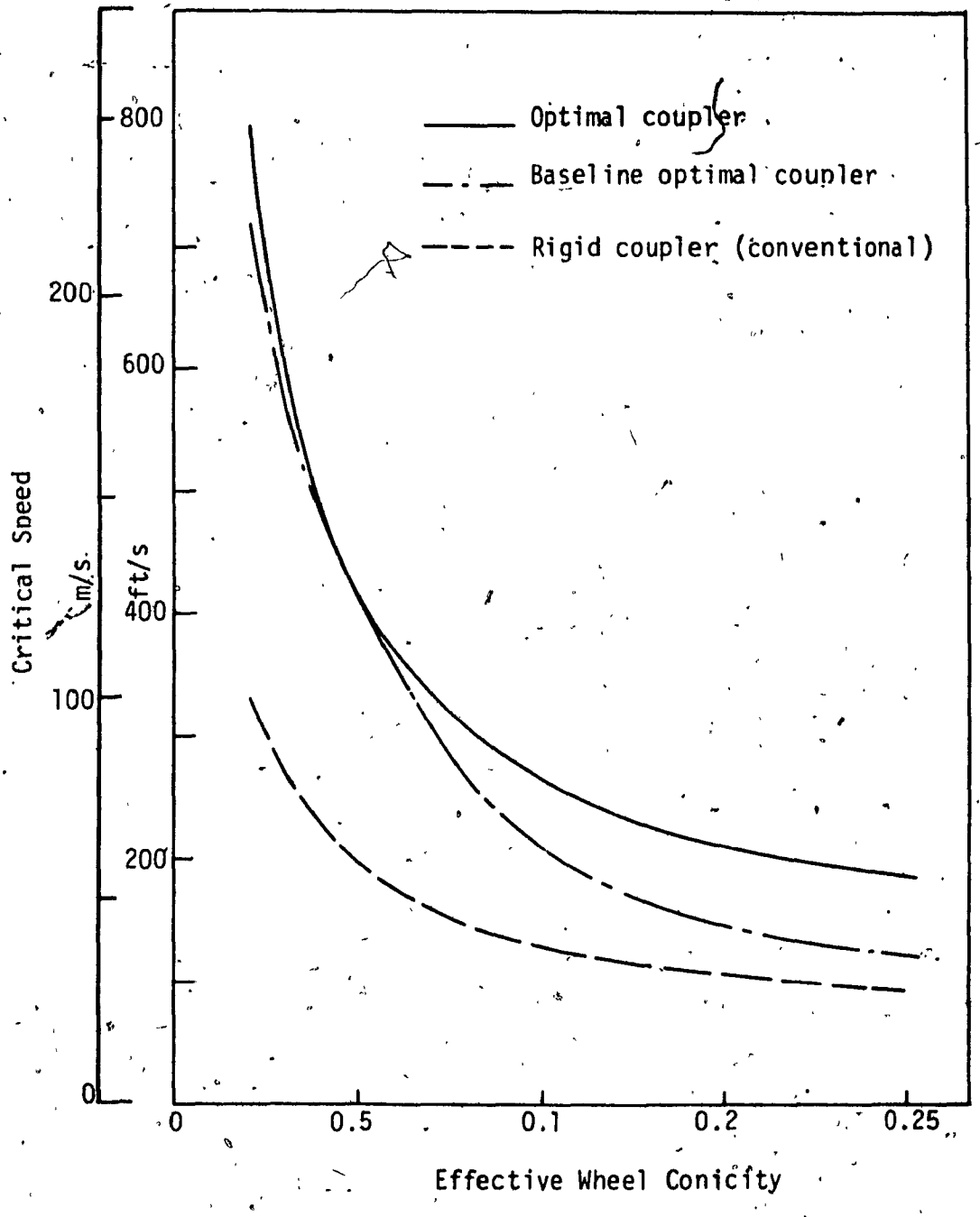

Figure 5.16 Effect of wheel conicity on the critical speed of freight truck system with EDCW and rigid axle wheelsets.

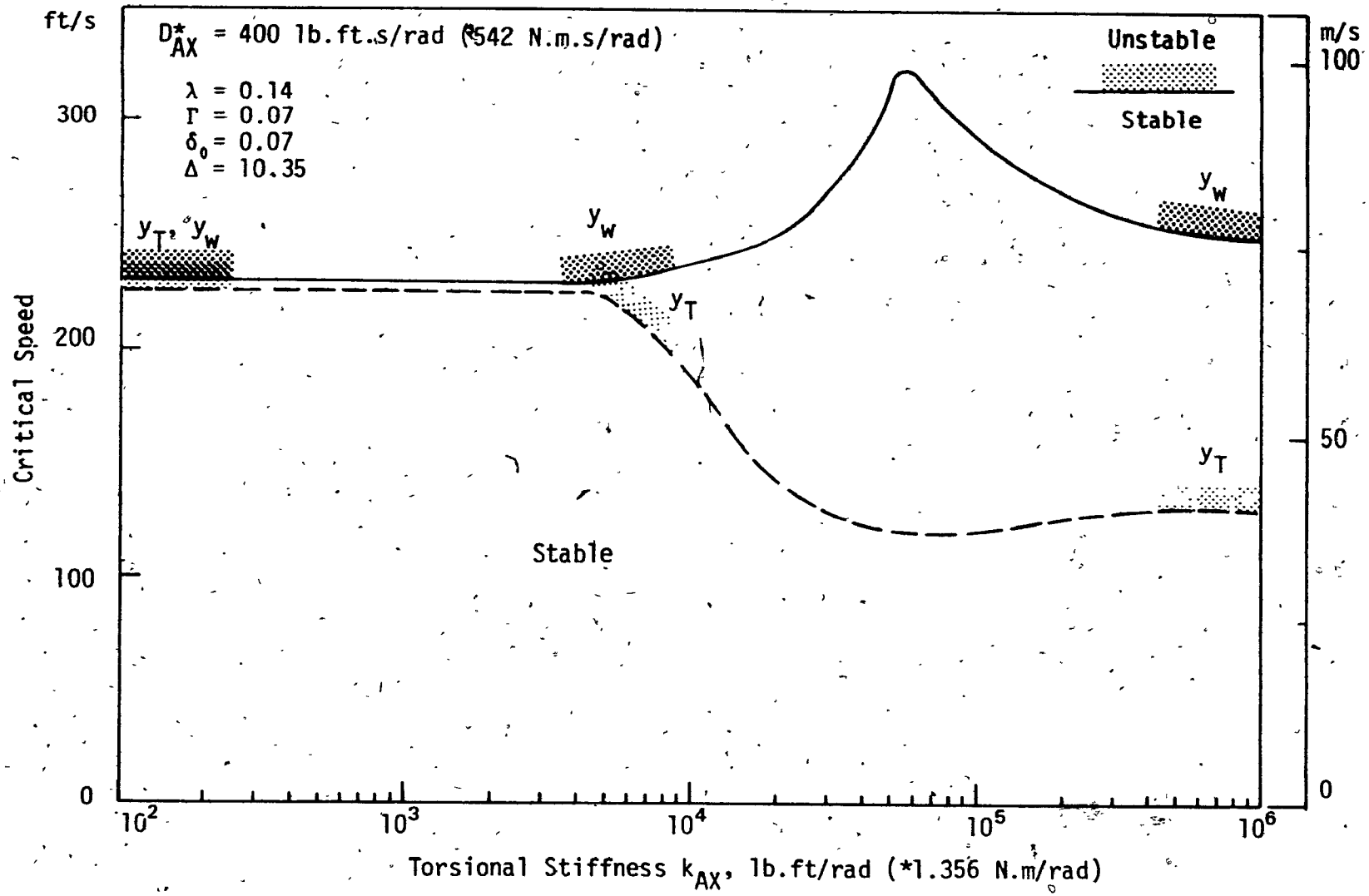

Figure 5.17 Critical speed boundaries of truck model with moderately worn wheel profile parameters, and corresponding optimal value of D_{AX}, as k_{AX} is increased.

5.3.3.2 Influence of Primary Suspension

Similar to wheel conicity, the effect of variation in primary lateral and yaw stiffnesses on the critical speed of truck model with EDCW is investigated. One parameter at a time is varied, and for each value of the parameter, optimal coupling parameter, D^*_{AX} is first obtained, which provides maximum critical speed. The critical speed corresponding to truck model with optimal coupler damping is then compared with that of truck system with conventional wheelsets. The results showing the influences of primary lateral and yaw stiffnesses are presented as follows:

Primary Lateral Stiffness (k_{y_p})

For different values of k_{y_p}, ranging from 25% to 400% of the nominal value, critical speeds of the truck model are computed for optimal wheelset coupler parameter, and rigid coupler condition. The results are shown in Table 5.4, which includes the optimal coupler damping at the critical speed for each value of k_{y_p}. Figure 5.18 shows these results as critical speed versus k_{y_p} for the truck model with both EDCW and rigid wheelset systems. It can be seen that the critical speed for both the systems increases with increase in k_{y_p}. However, the critical speed is not very sensitive to k_{y_p}, for k_{y_p} greater than its nominal value. The results further show, that for small values of k_{y_p} the critical speed of the model with EDCW is more sensitive to k_{y_p}, than that corresponding to conventional wheelset.

For each value of k_{y_p} and corresponding value of D^*_{AX}, examination of the critical speed boundaries show that as k_{AX} is varied, the general

Table 5.4 Influence of Primary Lateral Stiffness on Critical Speed of the Truck Model

Primary Lateral Stiffness (k_{y_p}) N.m (lb.ft)	Model with BDCW		Conventional Model
	D^*_{AX} N.m.s/rad (lb.ft.s/rad)	Critical Speed m/s (ft/s)	Critical Speed m/s (ft/s)
1.82×10^5 (1.25×10^4)	102 (75)	85 (280)	40 (130)
3.65×10^5 (2.50×10^4)	339 (250)	107 (350)	52 (170)
7.3×10^5 (nominal) (5.0×10^4)	678 (500)	125 (410)	58 (190)
1.46×10^6 (1.0×10^5)	873 (640)	133 (435)	61 (200)
2.92×10^6 (2.0×10^5)	876 (650)	139 (455)	64 (210)

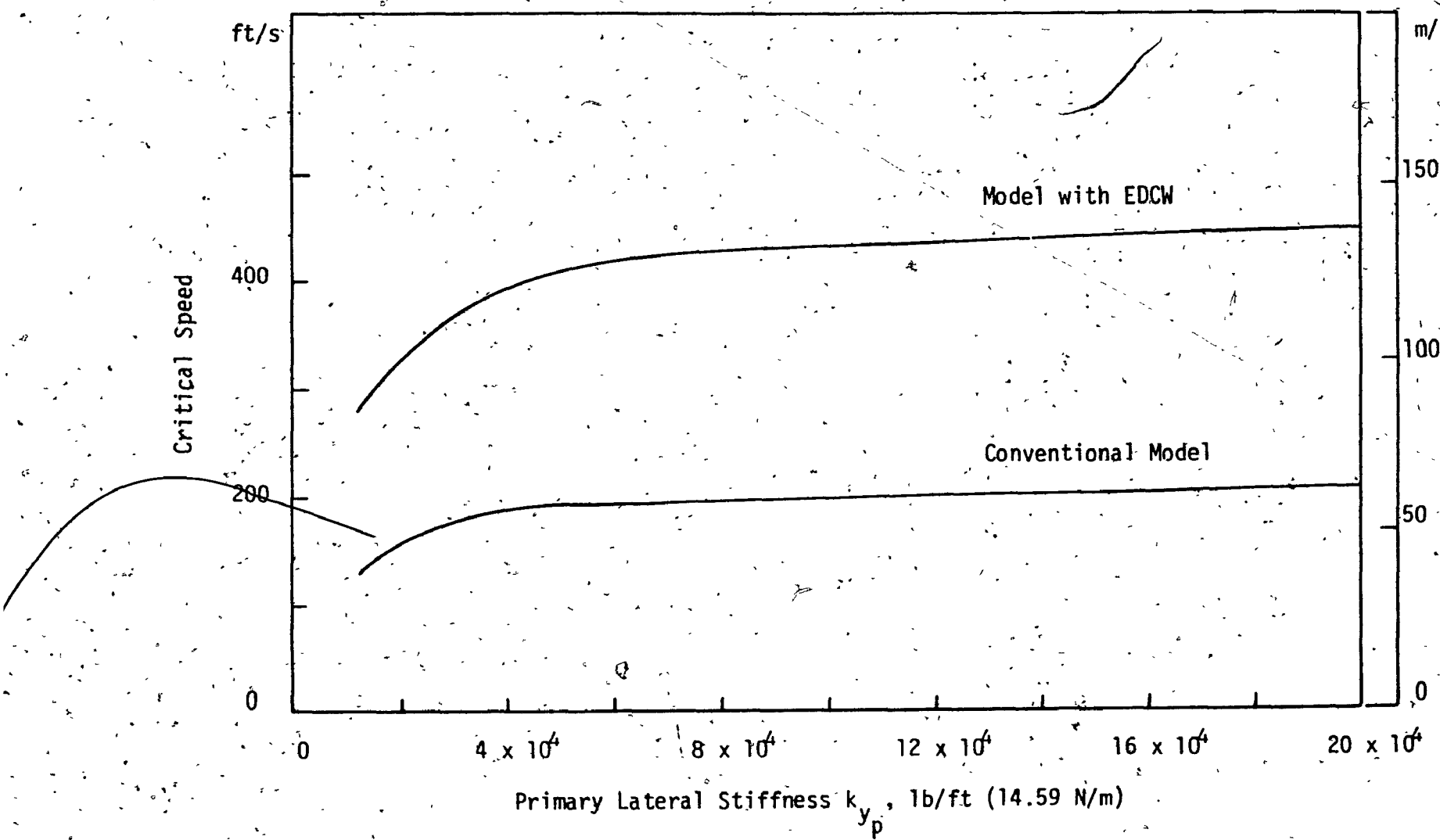

Figure 5.18 Effect of primary lateral stiffness on the critical speed of freight truck system with EDCW and rigid axle conventional wheelsets.

shape of the critical speed boundaries remain unchanged. However, for smaller values of k_{y_p} the optimal damping D^*_{AX}, that provides maximum critical speed is smaller, which results in the reduction of the relative stability corresponding to spin mode. As k_{y_p} is increased, the relative stability of both spin and primary hunting modes improve. Further, eigenvector analysis shows, that in order to minimize the lateral amplitude of wheelsets, it is necessary to adapt large k_{y_p} which also increases critical speed.

Primary Yaw Stiffness (k_{ψ_p})

Similar to primary lateral stiffness, in this section the influence of primary yaw stiffness (k_{ψ_p}) on the critical speed of the truck model is examined. The value of k_{ψ_p} is varied from 25% to 400% of its nominal value. Corresponding to each value of k_{ψ_p}, the optimal value of coupler damping is first determined. The critical speed sensitivity to k_{ψ_p} for the truck model with optimal coupler damping is compared to that corresponding to rigid coupler.

Table 5.5 lists the optimal values of D^*_{AX} and the corresponding critical speed for each value of k_{ψ_p} considered. The table also shows the critical speed for rigid coupler, representing the conventional system. The critical speed sensitivity to k_{ψ_p} for both truck systems with EDCW and conventional wheelset are shown in Figure 5.19. As the results indicate, the critical speed of both the systems is sensitive to k_{ψ_p}, and increases with increase in k_{ψ_p}. The sensitivity of the critical speed for truck with EDCW is, however, remarkably more significant than that corresponding to conventional system.

Table 5.5 Influence of Primary Yaw Stiffness on Critical Speed of the Truck Model

Primary Yaw Stiffness (k_{ψ_p}) N.m/rad (lb.ft/rad)	Model with EDCW		Conventional Model
	D^*_{AX} N.m.s/rad (lb.ft.s/rad)	Critical Speed m/s (ft/s)	Critical Speed m/s (ft/s)
4.24×10^5 (3.125×10^5)	339 (250)	70 (230)	43 (140)
8.47×10^5 (6.25×10^5)	746 (550)	91 (300)	49 (160)
1.69×10^6 (nominal) (1.25×10^6)	678 (500)	125 (410)	58 (190)
3.39×10^6 (2.5×10^6)	68 (50)	287 (940)	64 (210)
4.07×10^6 (3.0×10^6)	23 (17)	317 (1,040)	66 (215)
4.75×10^6 (3.5×10^6)	22 (16)	329 (1,080)	67 (220)
6.78×10^6 (5.0×10^6)	22 (16)	329 (1,080)	70 230

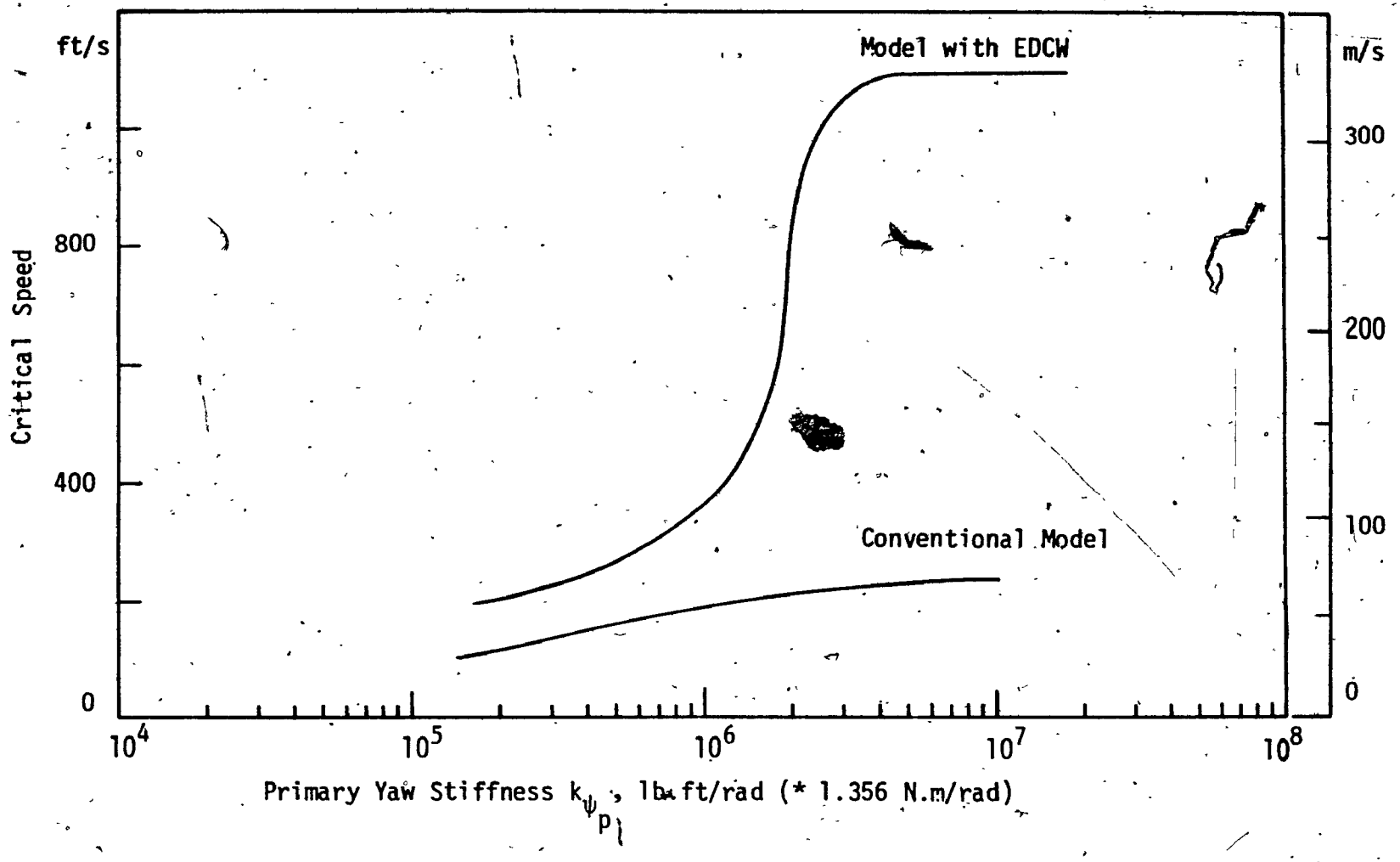

Figure 5.19 Effect of primary yaw stiffness on the critical speed of freight truck system with EDCW and rigid axle conventional wheelsets.

Analysis of the stability boundary results, further shows that when k_{ψ_p} is small (25% of nominal value), the conventional system exhibits primary hunting for a range of velocity between 15 and 24 m/s (50 and 80 ft/s). As the value of k_{ψ_p} is increased, this range of primary hunting (car lateral instability) decreases and becomes stable near the nominal value of k_{ψ_p}. For the truck system with EDCW, on the other hand, as k_{ψ_p} is increased the value of optimal coupler damping parameter (D^*_{AX}) to maximize critical speed reduces significantly. This in turn results in an increase in relative spin motion for very large values of k_{ψ_p} and corresponding values of D^*_{AX}. However, for the case of EDCW with optimal coupler according to Equation 5.2, in the range of k_{ψ_p} considered, all the modes remain stable until critical speeds of truck and wheelset lateral modes are reached simultaneously.

The results (Table 5.5 and Figure 5.19) further indicate that, for the baseline truck model with EDCW, nothing can be gained by increasing k_{ψ_p} over 4.75×10^6 N.m/rad (3.5×10^6 lb.ft/rad), since the critical speed over 329 m/s (1,080 ft/s) cannot be reached. As the results in Figure 5.19 show, there is a tremendous scope for EDCW to improve the critical speed of freight car system on tangent track, by selecting proper value of k_{ψ_p}.

5.3.3.3 Influence of Vehicle Loading

The results presented so far are for axle load corresponding to unloaded car. In this section, influence of car loading on the critical speed is examined for half and fully loaded cars. As discussed earlier, several freight car system parameters depend on axle loading. These load

dependent parameter values corresponding to half and full loading of a freight car are shown in Table 5.2. For both half and full loading conditions, the corresponding load sensitive parameter values from Table 5.2 and other nominal values from Table 5.1 are used to obtain the critical speeds. The critical speeds are computed for both rigid axled conventional system and the model with EDCW.

Similar to the other parametric studies, for each axle loading, optimal coupler damping is used to maximize critical speed of the model with EDCW. The results are shown in Table 5.6 which indicate, that the value of the optimal coupler damping increases significantly with increased axle load. This is due to the fact that creep forces vary with normal load, and with increased longitudinal creep force, larger value of torsional damping is required to counter act.

The critical speed versus axle load for optimal and rigid coupler of EDCW are shown in Figure 5.20, from which it can be seen, that for axle load corresponding to empty to half car load, there is a slight improvement of critical speed for both the systems. For axle load corresponding to half to full car load, however, there is a significant increase in critical speed for conventional model, and relatively less increase for the model with EDCW. However, for conventional system, increased axle load resulting from increased car body mass, introduces car body lateral instability region as shown in Figure 5.20. Whereas, for the model with EDCW with optimal coupler, all the modes remain stable until both truck and wheelset lateral modes become unstable at the critical speed shown.

Table 5.6 Influence of Axle Load on the Truck Hunting Critical Speed

Axle Load W_{APP} N (lb)	Model with EDCW		Conventional Model
	D^*_{AX} N.m.s/rad (lb.ft.s/rad)	Critical Speed m/s (ft/s)	Critical Speed m/s (ft/s)
Empty			
5.605×10^4	678	125	58
(1.26×10^4)	(500)	(410)	(190)
Half Load			
1.49×10^5	781	128	70
(3.35×10^4)	(576)	(420)	(230)
Fulf Load			
2.42×10^5	2,712	155	146
(5.43×10^4)	(2,000)	(510)	(480)

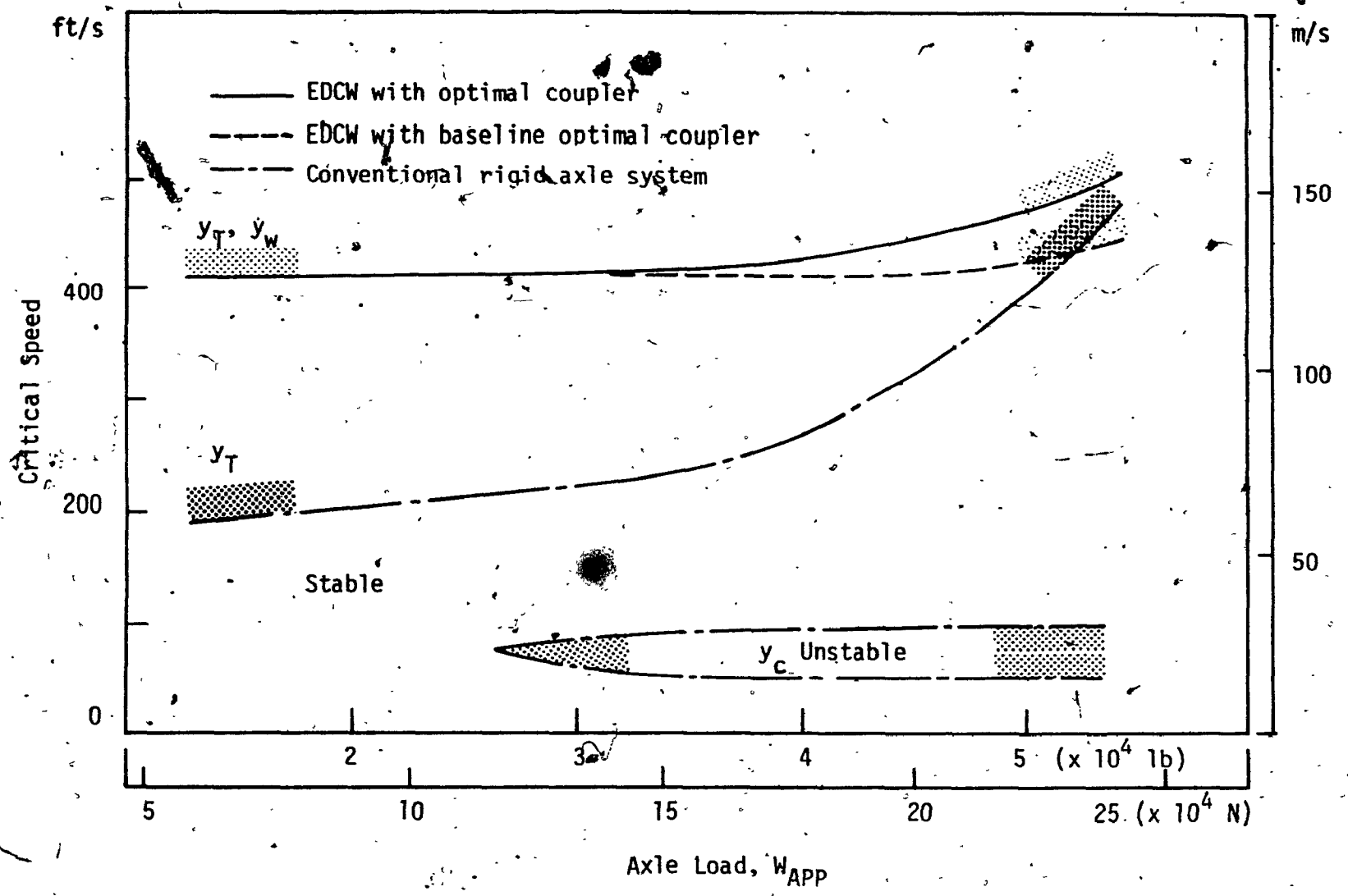

Figure 5.20 Effect of axle load on the critical speed of freight truck system with EDCW and rigid axle conventional wheelsets.

Similar to wheel conicity, which may change with wear, axle load for a truck may change during scheduled operating period. Figure 5.20, therefore, also shows the effect of having a fixed optimal coupler, corresponding to the nominal axle load. As the results show, a fixed coupler damping parameter (D_{AX}^*) will lead to reduced critical speed at other loads, in comparison to optimal D_{AX}^* at each load. The decreased sensitivity of freight car system critical speed to axle load for the system with EDCW is a desirable factor, since it allows identical operating speed for all loading conditions.

5.3.3.4 Influence of Secondary Lateral Damping (D_y)

Throughout the study of freight truck system with pseudo-car body, it is observed that car body lateral mode is a critical mode in the mid-range of torsional stiffness (k_{AX}) values. This is perhaps due to the relatively small value of secondary lateral damping (D_y) selected for the baseline model. In this section of the parametric study the influence of increase in the value of D_y on the critical speed boundaries is examined.

For this, the critical speed boundaries are obtained for D_y equal to 2.92×10^4, 8.76×10^4, and 1.46×10^5 N.s./rad (2×10^3, 6×10^3, and 1×10^4 lb.s/ft), and for optimal coupler damping D_{AX}^* corresponding to each value of D_y. The stability boundaries as a function k_{AX} are shown in Figures 5.21 to 5.23. The results indicate that as D_y is increased, the dynamic coupling between the truck and car body increases, resulting in larger car body lateral instability region. For large value of D_y as shown in Figure 5.23, the car body lateral mode is unstable for certain range of velocities, throughout the range of k_{AX}. These results further

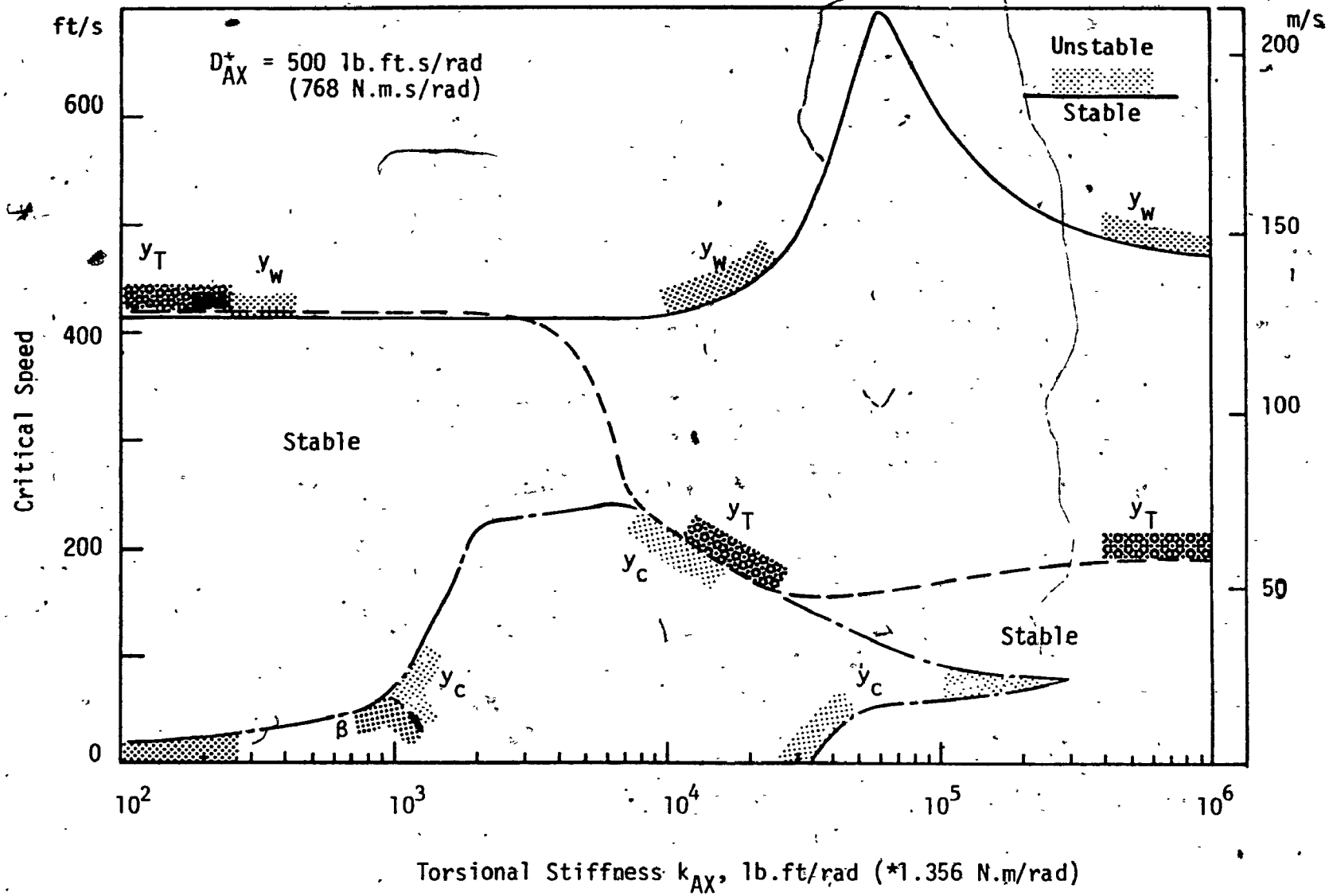

Figure 5.21 Critical speed boundaries of truck model with secondary lateral damping D_y = 2.918 x 10^4 N.s/m (2,000 lb.s/ft), and corresponding optimal value of D_{AX}, as k_{AX} is increased.

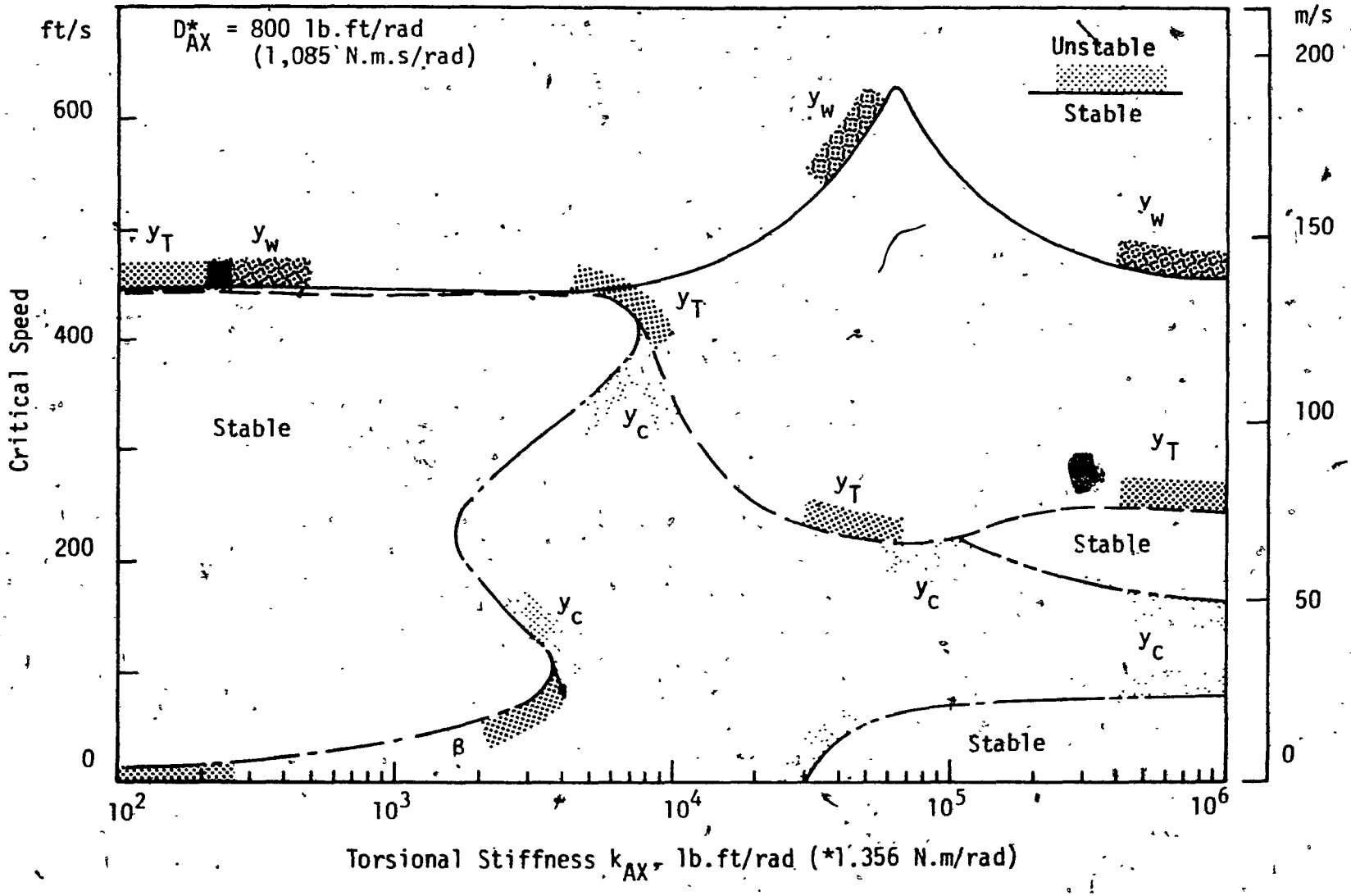

Figure 5.22 Critical speed boundaries of truck model with secondary lateral damping D_y = 8.754 x 10^4 N.s/m (6,000 lb.s/ft) and corresponding optiaml value of D_{AX}, as k_{AX} is increased.

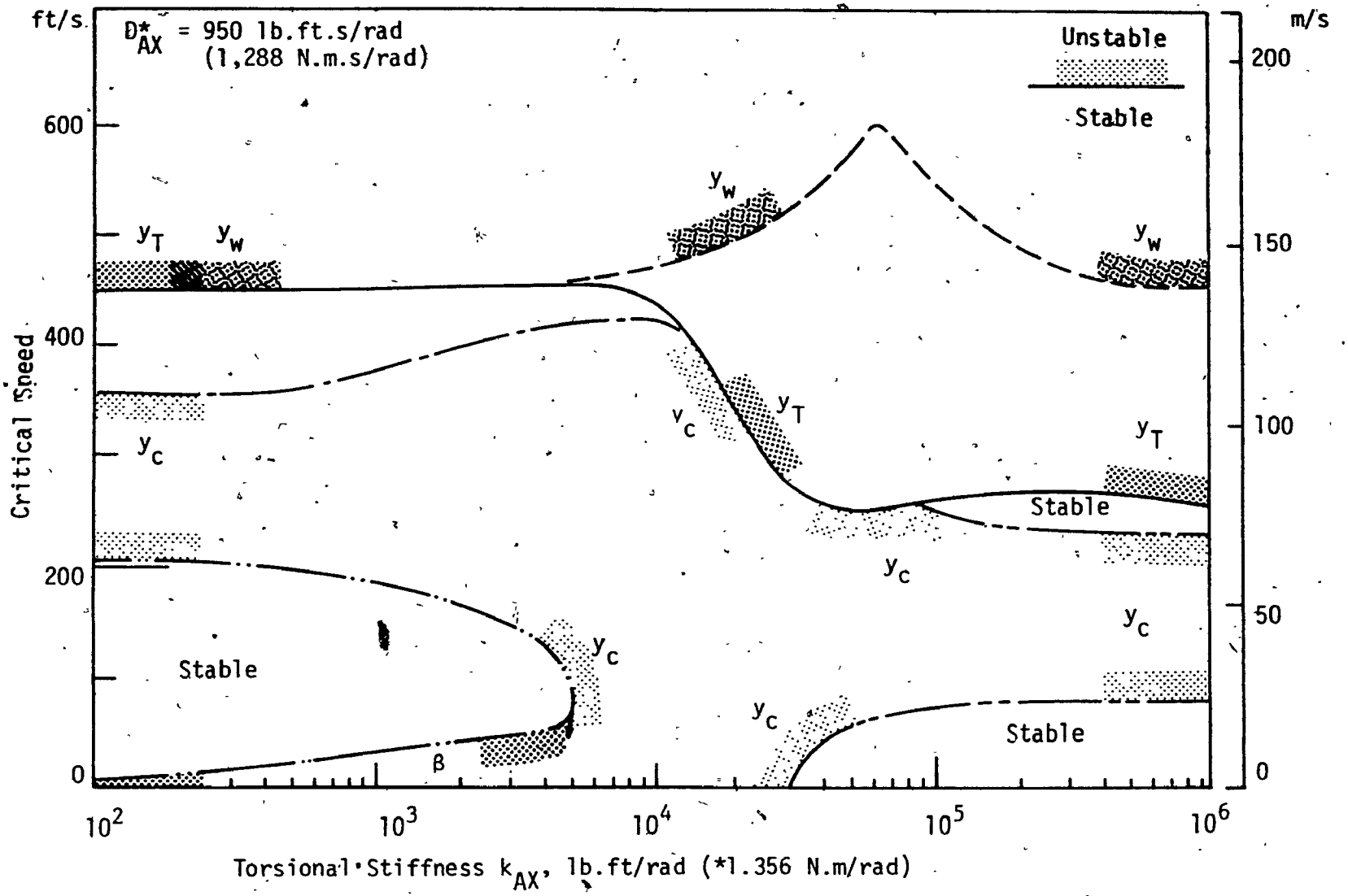

Figure 5.23 Critical speed boundaries of truck model with secondary lateral damping D_y = 1.459 x 10^5 N.s/m (10^4 lb.s/ft) and corresponding optimal value of D^y_{AX}, as k_{AX} is increased.

show, that as D_y is increased the stable region on the right-hand end of the plots, between car body and truck lateral instability boundaries reduces, and eventually both boundaries coincide. This trend with increase in D_y, for large values of k_{AX} leading to rigid coupler, results in reduction in the effective stable region in comparison to those corresponding to smaller values of D_y.

As discussed earlier, previous studies [86, 94], that considered only torsional stiffness (k_{AX}) between wheels with large value of D_y showed, that the critical speed of freight car system is zero for small values of k_{AX}, and that the critical speed increases with increase in k_{AX} beyond certain value. The trend of the result obtained by Hadden and Law [86] is discussed in the literature review and presented as Figure 1.8 in Chapter 1. In the absence of coupler damping, identical trend is observed for the model considered in this study as shown in Figure 5.24, which corresponds to baseline model with identical value of D_y used in [86].

For the range of D_y considered in this study, the critical speeds are computed similar to other parametric studies presented earlier. Table 5.7 presents the values of optimal coupler parameter (D^*_{AX}) and resulting critical speeds corresponding to truck lateral mode, for various values of D_y. The table also shows the truck lateral critical speeds for rigid coupler or conventional system. Figure 5.25 shows these critical speeds as well as the range of speeds, where car lateral mode is unstable. As these results show, the freight car system with EDCW is not only superior in terms of critical speed, but it can also utilize larger value of D_y to maximize critical speed of the system without introducing primary hunting.

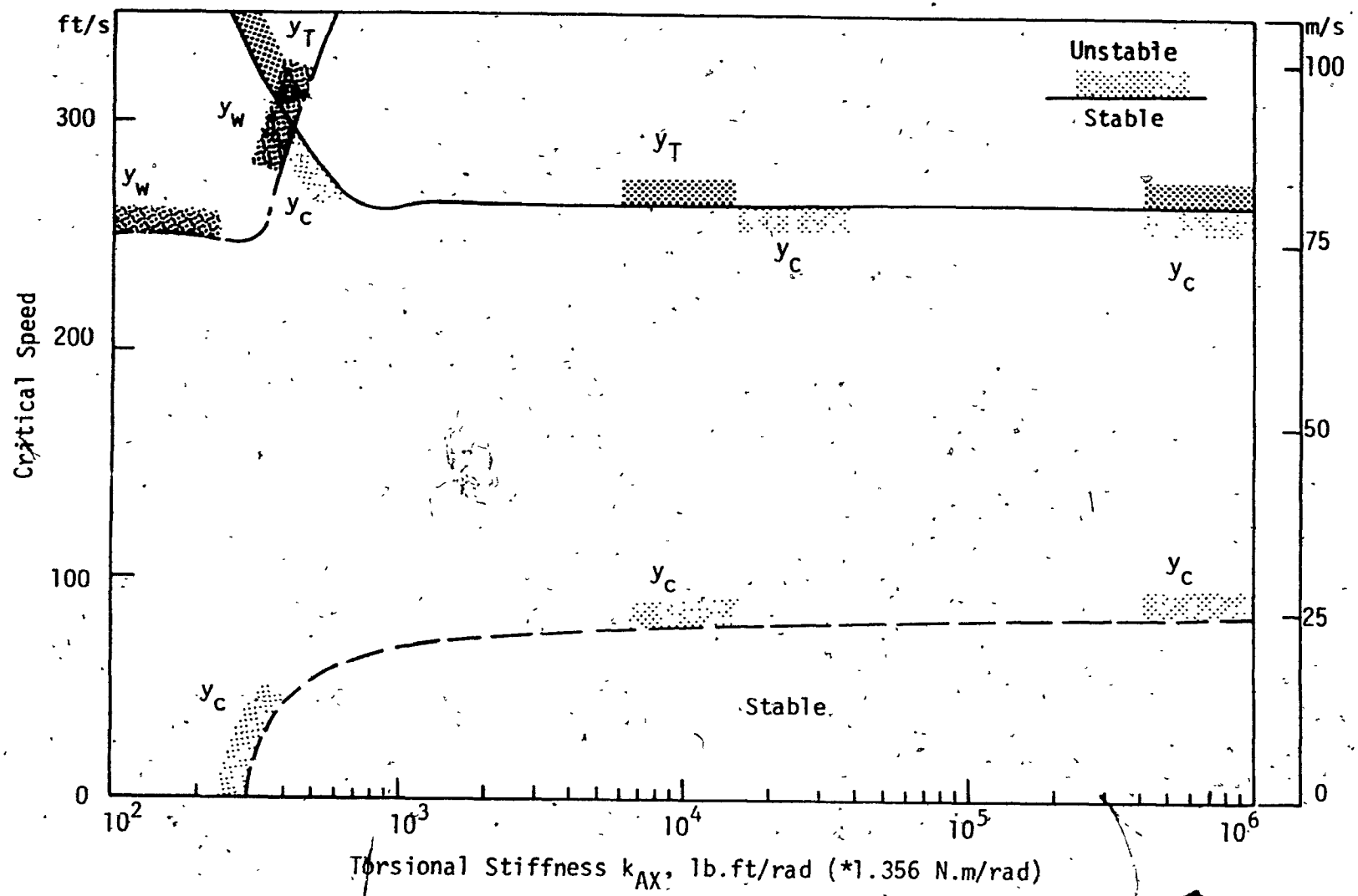

Figure 5.24 Critical speed boundaries of truck model with secondary lateral damping D_y = 1.8436 x 10^5 N.s/m (1.2645 x 10^4 lb.s/ft), as k_{AX} is increased, in the absence of D_{AX}.

Table 5.7 Influence of Secondary Lateral Damping on the Truck Hunting Critical Speed

Secondary Lateral Damping D_y N.s/ft (lb.s/ft)	Model with EDCW		Conventional Model
	D_{AX}^* N.m.s/rad (lb.ft.s/rad)	Critical Speed m/s (ft/s)	Critical Speed m/s (ft/s)
1.46×10^4 (1.0×10^3)	577 (425)	120 (395)	53 (175)
2.92×10^4 (nominal) (2.0×10^3)	678 (500)	125 (410)	58 (190)
5.84×10^4 (4.0×10^3)	949 (700)	131 (430)	67 (220)
8.76×10^4 (6.0×10^3)	1,085 (800)	136 (445)	75 (245)
1.17×10^5 (8.0×10^3)	1,187 (875)	137 (450)	79 (260)
1.46×10^5 (1.0×10^4)	1,289 (950)	137 (450)	79 (260)

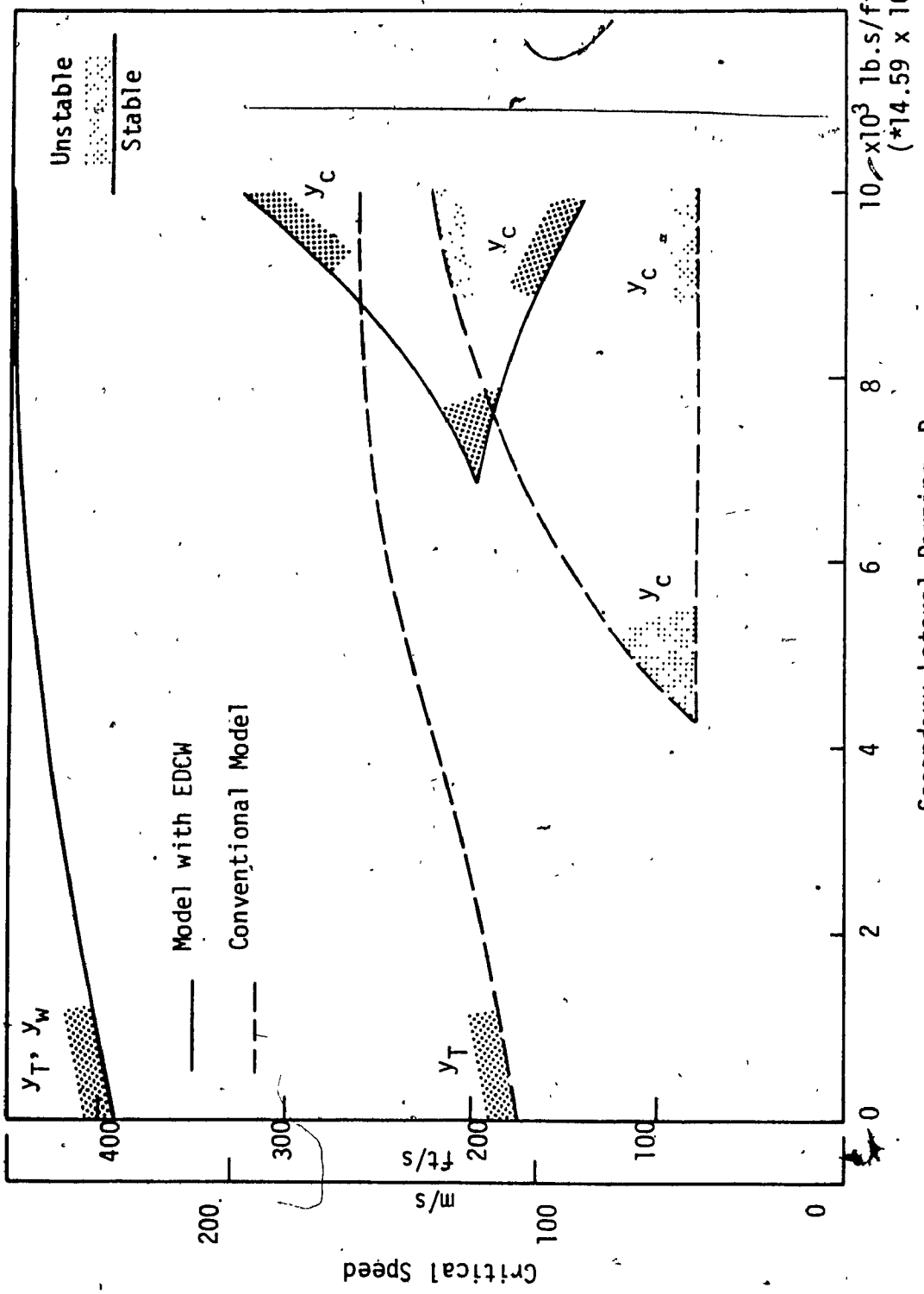

Figure 5.25 Effect of secondary lateral damping on the primary and secondary hunting critical speeds of freight truck system with EDCW and rigid axle conventional wheelsets.

5.4 Summary and Conclusion

This chapter primarily deals with stability analysis of a 11-DOF truck model with EDCW, on a tangent track. The truck model developed in Chapter 4, has been verified by comparing its stability behaviour with other conventional model, in the limiting case of rigid coupling between wheels. The result showed that the truck model can simulate rigid axle conventional model, as well as it can exhibit complete freight car stability behaviour, in terms of both primary and secondary hunting phenomena.

Stability analysis of the truck model with EDCW is first carried out by examining the effects of wheelset coupler parameters on the stability behaviour of various modes of the system. The results showed that for small or no coupler damping, torsional stiffness (k_{AX}) alone cannot improve the critical speed beyond the critical speed of conventional model with rigid axle. It is also found that for very small values of torsional stiffness (k_{AX}), there is a stable region. In this range of k_{AX}, the relative spin mode is unstable for a range of initial velocities, where the critical speed corresponding to truck lateral mode is significantly greater than that of wheelset lateral mode. Further, the results show that the spin instability region can be reduced to zero by making D_{AX} very large. In addition to this, as D_{AX} is increased, the critical speed corresponding to wheelset lateral mode is found to increase, while that of truck lateral mode decreases. Consequently, an optimal value of D_{AX} is found, for which these two modes become unstable at the same velocity giving maximum obtainable critical speed. However, this optimal value of D_{AX} is not large enough to totally eliminate the

unstable region of spin mode at the initial velocities. This problem of initial instability for optimal value of D_{AX} is overcome by introducing a speed dependent damper in the coupler. Utilizing such a coupler. the critical speed of freight truck model with EDCW is improved by over 100% in comparison to a conventional system.

The results of limited parametric study carried out, showed overall superiority of the model with EDCW, over the conventional model. When the effect of moderately worn wheel profile is compared with that of conical wheel of same conicity, the conventional model showed 18% improvement of critical speed due to increase in gravitational stiffness. Whereas, the model with EDCW showed less than 3% improvement. This result indicates that the model with EDCW is less sensitive to gravitational stiffness. Similar conclusion can also be drawn from the study of sensitivity to axle loading, for which conventional system also showed greater sensitivity. From a practical point of view, wheel profile changes with use and axle loads vary in a specified schedule or operation. Hence, the reduction in the sensitivity of stability performance to profiled wheel and axle load is a positive aspect of freight car system with EDCW. This should aid in maintaining consistent operating speed in all operating conditions.

The section of the study into the influence of secondary lateral damping (D_y), showed that increased value of D_y improves the truck hunting critical speed slightly. But at the same time, as D_y reaches certain value, primary hunting is initiated for a range of velocities. This is due to an increased dynamic coupling between car body and truck modes, in the presence of large D_y. Consequently, this imposes

limitation on the increase of D_y. The result, here, showed significant superiority of the model with EDCW over the conventional model.

The results showing influence of primary yaw stiffness (k_{ψ_p}) on the critical speed indicate, that drastic improvement of the critical speed of truck model with EDCW can be obtained by increasing k_{ψ_p} to certain extent. Whereas, the critical speed of conventional model although increases with k_{ψ_p}, the sensitivity is significantly less.

Any design requirement for a freight car system cannot be based on stability analysis alone, since the conventional system is well known for its conflicting requirement between stability and curving performance. In the forthcoming Chapters 6 and 7, steady-state curving model of a freight truck is developed and analyzed to evaluate curving performance of freight truck system with EDCW.

CHAPTER 6

FREIGHT TRUCK MODELING CONSIDERATIONS ON CURVED TRACK

6.1 Introduction

Considerable proportion of the total length of track on a railway system is composed of curved track. When a railway vehicle negotiates a curve, a number of new phenomena such as centrifugal force, wheel load shift etc. occur, as compared to tangent track operation. In general during curving, conical wheelsets move laterally and yaw in an attempt to align themselves radially with the track, to provide pure rolling. But due to constraints, depending on radius of curve, there are tracking errors and consequent generation of large wheel/rail forces. As a result, there is an increase in wheel/rail wear, generation of noise, and potential danger of derailment due to wheel climb, rail rollover, and lateral track shift. Further, there is a raise in power consumption due to increased rolling resistance on curve.

For conventional rigid axle freight car system, it is well known that there is conflicting requirement between stability behaviour on tangent track and better curving ability. The results of truck model with EDCW on tangent track showed excellent potential for improving the stability behaviour. But the model should also be able to negotiate a curved track. In this, and the following chapter, freight truck model with EDCW is considered to determine its performance on curved track.

Previous work related to rail vehicle curving analysis are discussed in detail in the literature review. The primary objectives of this chapter are to discuss various considerations in developing the

truck model on curved track, and formulate the curving equations. As pointed out in literature review, steady-state curving analysis of rail vehicle system is very efficient in providing vast information regarding the effects of model parameters, track curvature, cant deficiency (lateral unbalance) etc., on the curving performance. The curving performance indices used in this study are discussed in the forthcoming chapter.

In this chapter, steady-state curving model of conventional and EDCW trucks of same complexity are developed. It is necessary to develop the conventional model to aid in model validation, as well as to carry out direct quantitative comparison of the EDCW system with that of conventional system. In contrast to tangent track modeling, the curved track also includes radius of curvature, super-elevation, and the presence of centrifugal force. In the following sections, various modeling considerations are discussed, the steady-state curving equations for the truck models are developed, and the assumptions are outlined.

6.2 Model Description

The basic 11-DOF truck model with pseudo-car body and EDCW considered earlier for stability analysis is reconsidered here to determine its steady-state curving performance. For the steady-state curving analysis, the track is considered to be rigid and of constant centerline radius (R), with uniform angle of super-elevation (ϕ_{se}). The truck model, and model components are the same as those considered and discussed in Chapter 4, and are shown on a curved track in Figures 6.1 and 6.2. The various forces and moments acting on the model include

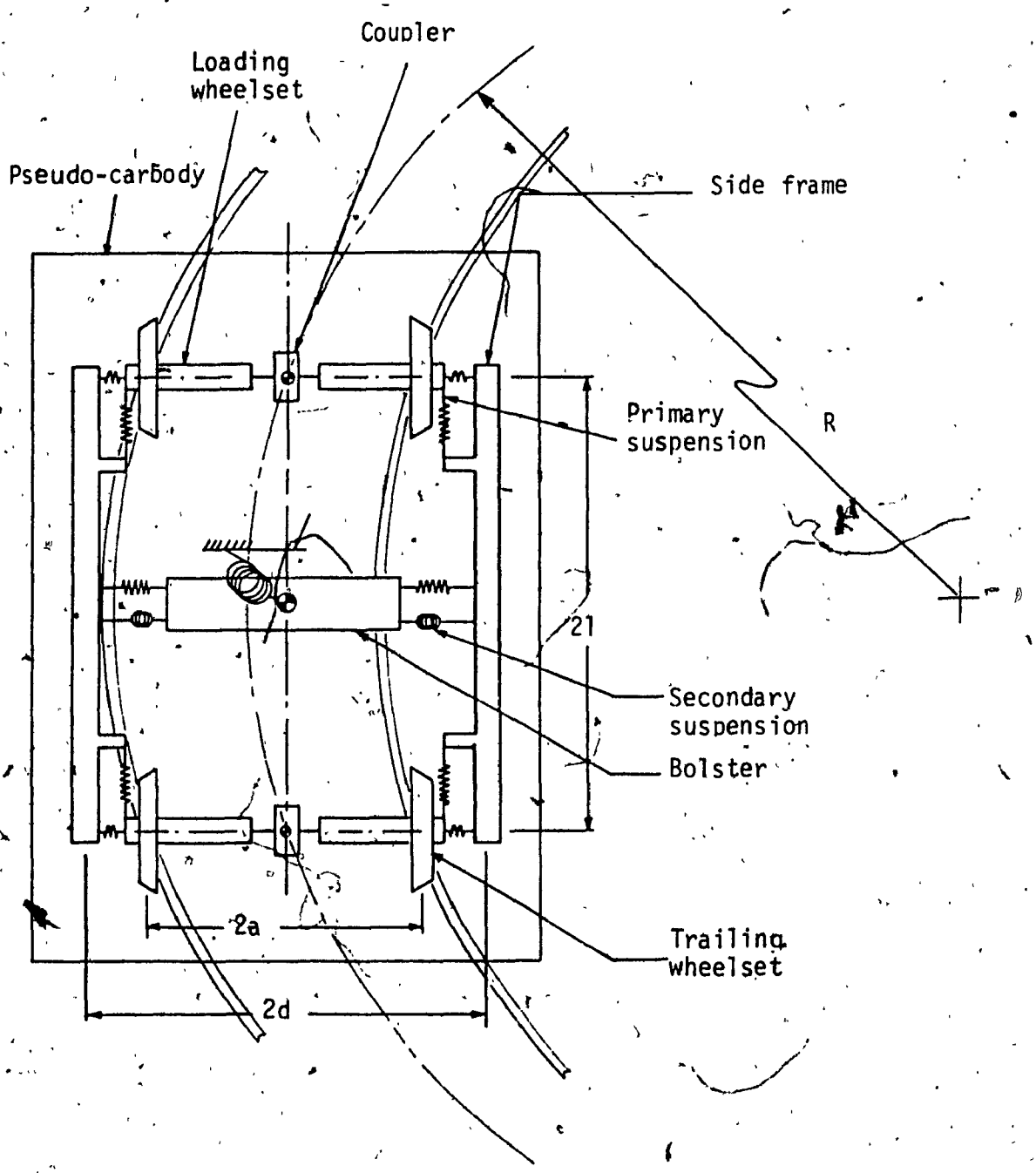

Figure 6.1 Components of freight truck model on curved track (plan view).

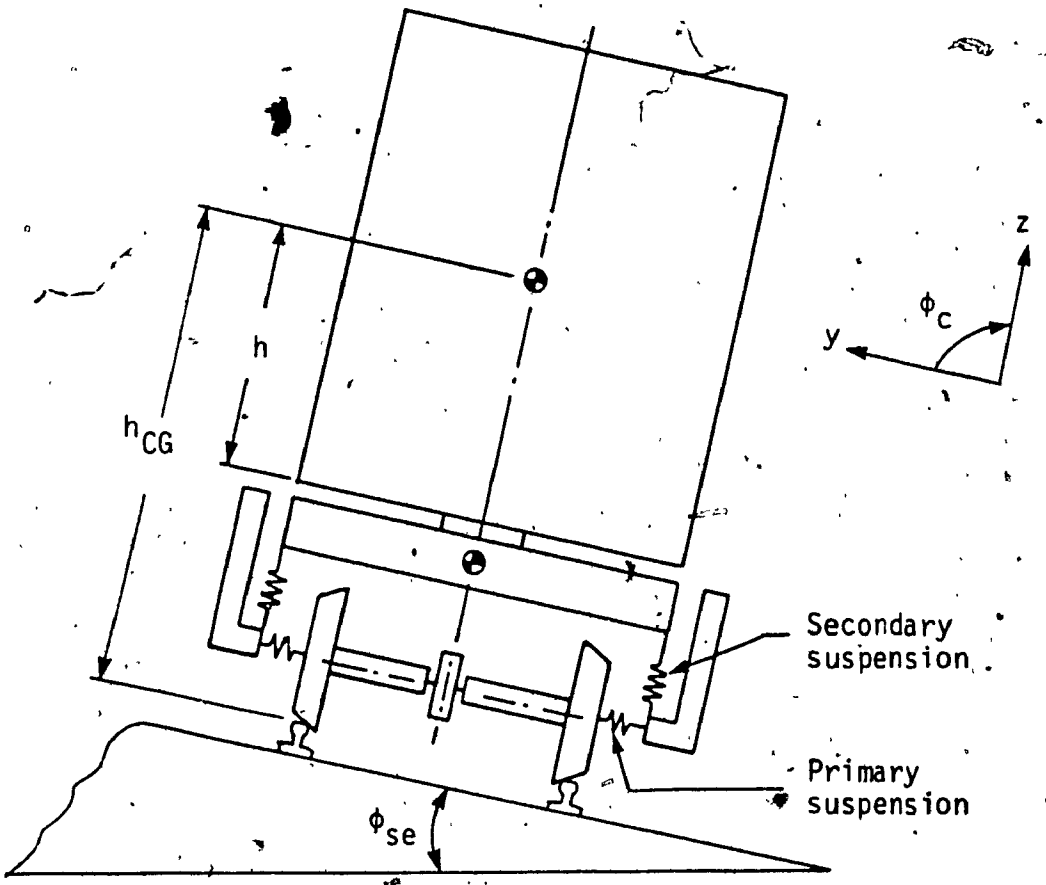

Figure 6.2 Components of freight truck model on curved track (rear view).

wheel/rail interaction forces and moments, wheelset coupler moment, primary and secondary suspension forces and moments, gravitational stiffness force, as well as centrifugal or lateral unbalance force.

If the sum of the forces and moments are taken in the plane of the rails, all the expressions for forces and moments due to suspensions and geometry remain identical to those derived earlier in Chapter 4. For tangent track stability analysis, the wheelset coupler is modeled as parallel stiffness and damper elements. The results of stability analysis in Chapter 5, showed that optimal wheelset coupler is a velocity dependent torsional damper with small value of torsional stiffness (k_{AX}). In the steady-state curving analysis, to simplify the problem, it is assumed that k_{AX} is small and hence, the product of k_{AX} and differential spin (β) is negligible.

In curved track modeling, due to radius of curved track, the velocity expressions for the wheelset are different from that of tangent track, and consequently additional terms are introduced in the expressions for creep forces and moments. Further, due to track super-elevation (ϕ_{se}) and velocity dependent centrifugal force, a net lateral unbalance force acts on the system. This factor introduces wheel load shift, which in turn affects the gravitational stiffness force. These aspects of curved track modeling are discussed and developed in the following section.

6.3 Modeling Considerations

Curved track model is essentially obtained by extending the tangent track model to include the radius of curved track and super-elevation.

In the curved track there is an additional precession velocity affecting the expressions for creepage. Also there is centrifugal force that acts on each component of the model. And due to super-elevation, depending on centrifugal force there is a lateral unbalance force. Further, due to lateral unbalance, there is a shift of wheel load which affects the gravitational stiffness force.

For steady-state analysis, the track is considered to be of constant centerline radius (R), with uniform angle of super-elevation (ϕ_{se}). The track curvature can be defined as radius R in meter (ft) or degree curve defined as angle subtended by 30.48 m. (100 ft) chord. This relationship is illustrated in Figure 6.3. Figure 6.4 shows the definition of super-elevation. The relationship between radius of curvature and degree curve is shown as a plot in Figure 6.5. In the following sub-sections, the effect of R, and ϕ_{se} on cant deficiency force, wheel load shift, gravitational stiffness, and creep forces and moments are discussed.

6.3.1 Cant Deficiency Force

On curved sections of the track, super-elevation is provided to aid in negotiating a curve of a given radius at a given speed. The objective of the super-elevation is to counter balance the centrifugal force by gravitational cant force. In curving analysis of railway vehicles, the lateral force unbalance is usually expressed in terms of cant deficiency ϕ_d. The cant deficiency is defined as the angle between the resultant of centrifugal force (mV^2/R) and the weight (mg), and the normal into the rail plane as illustrated in Figure 6.6.

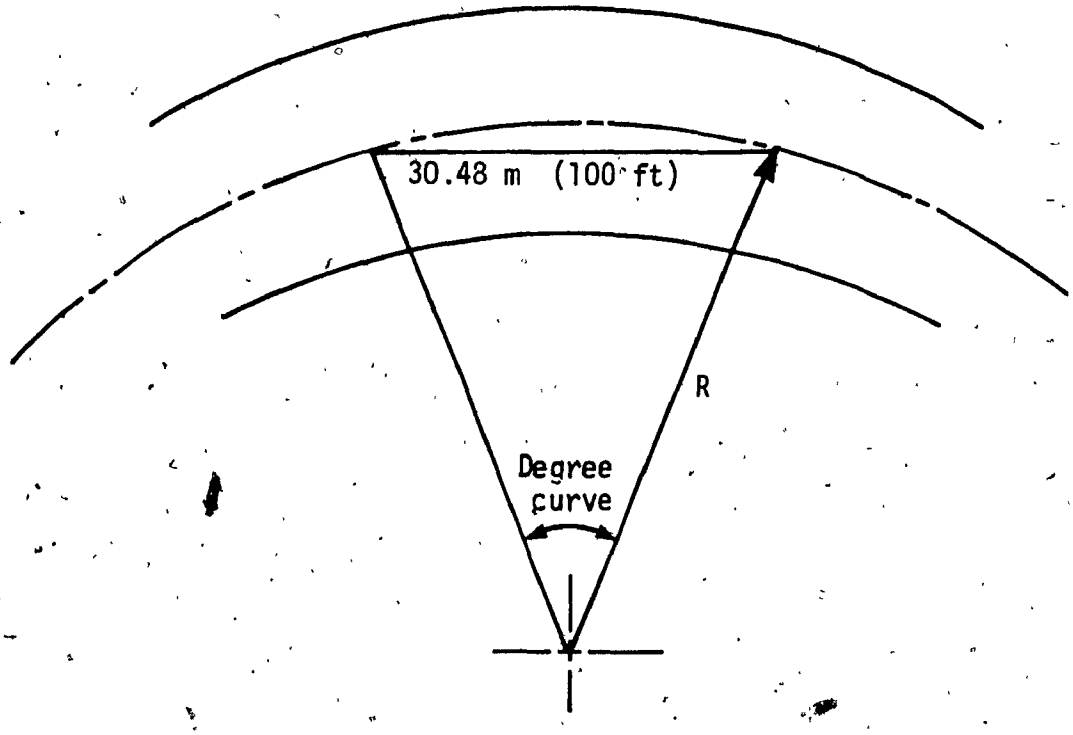

Figure 6.3 Definition of degree curve.

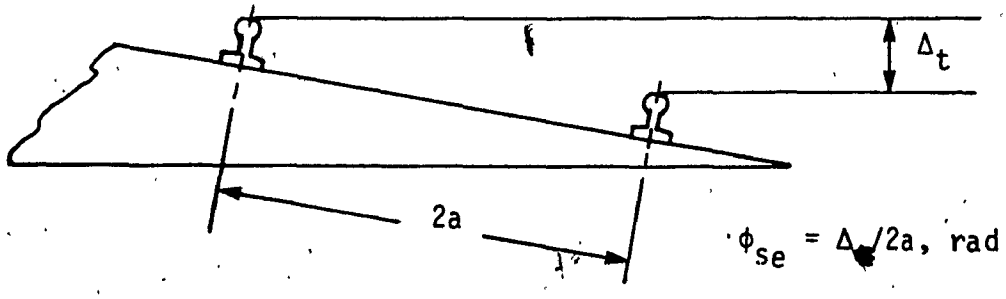

Figure 6.4 Definition of track super-elevation.

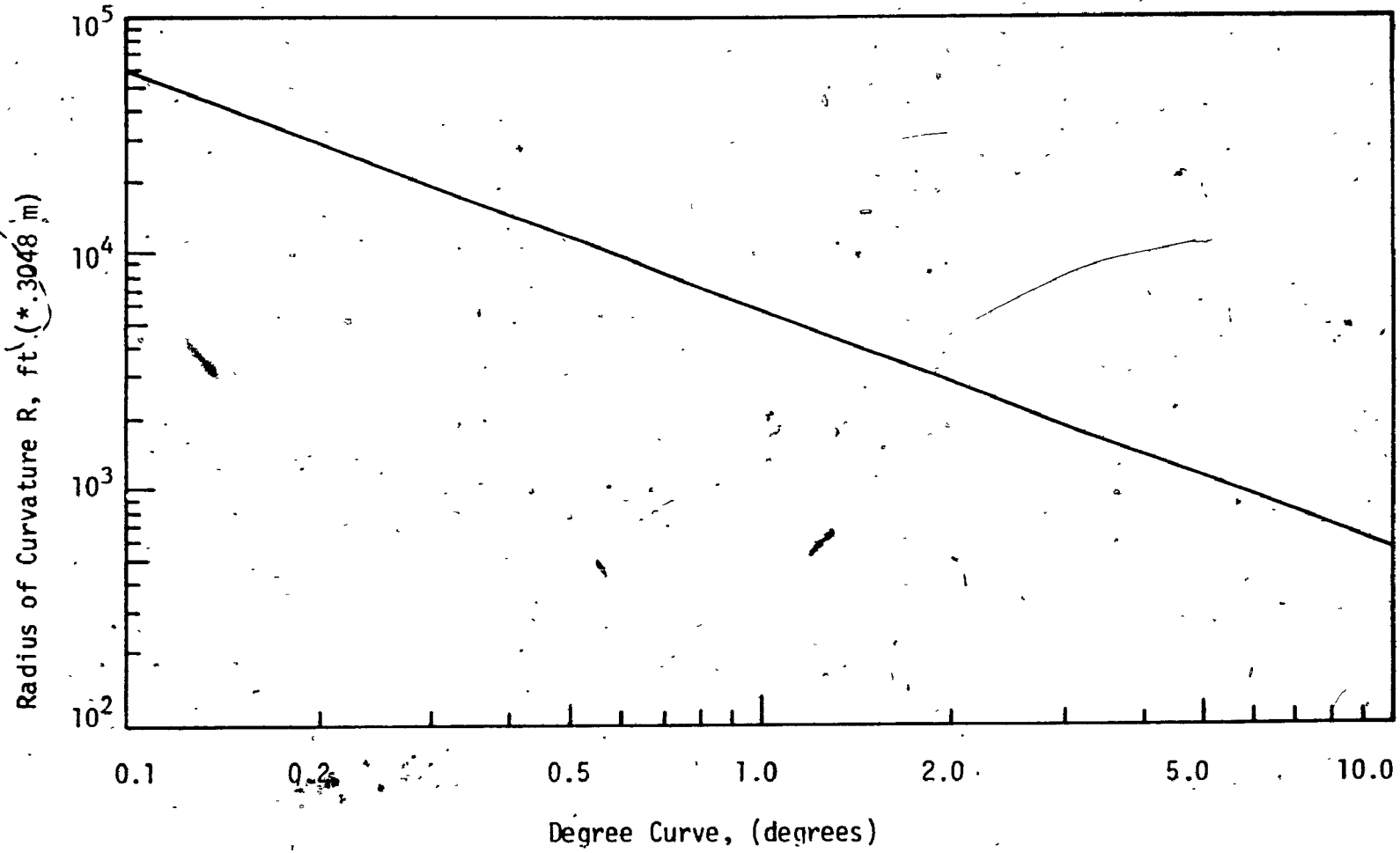

Figure 6.5 Relationship between radius of track curvature and degree curve.

For each component of the model with mass, the resultant of the centrifugal force and weight acts as shown in Figure 6.6, where m is the mass and F is the resultant of gravitational and centrifugal forces. The magnitude of F can be expressed as:

$$| F | = \frac{mg}{\cos(\phi_d + \phi_{se})} = \frac{mV^2/R}{\sin(\phi_d + \phi_{se})} \tag{6.1}$$

Making small angle approximation and solving for ϕ_d, yields the definition of cant deficiency in radians as:

$$\phi_d = \frac{V^2}{Rg} - \phi_{se} \tag{6.2}$$

With reference to Figure 6.6, again assuming small angles, the cant deficiency force on each mass in the direction of rail plane is:

$$F_{\phi_d} = \frac{mV^2}{R} - mg\phi_{se} = mg\phi_d \tag{6.3}$$

When ϕ_d is zero, a condition of "balanced running" is achieved, for which the components of centrifugal force and weight, parallel to the rail cancel each other.

In practice, the cant deficiency loads are limited to low levels [27, 64], which enter into the equations as input force. From Equation (6.3), the expressions for cant deficiency force on wheelset, truck, and car body are:

$$\begin{aligned} \bar{F}_{\phi_d,w} &= m_w g\phi_d \\ \bar{F}_{\phi_d,T} &= m_T g\phi_d \\ \bar{F}_{\phi_d,c} &= m_c g\phi_d \end{aligned} \tag{6.4}$$

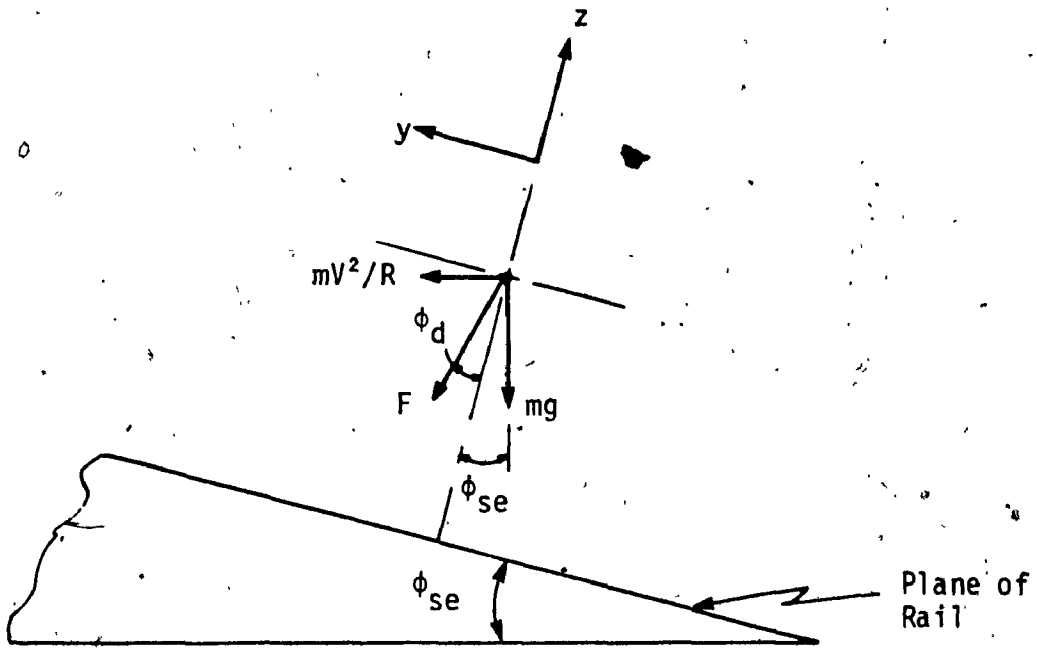

Figure 6.6 Force diagram showing centrifugal, gravity and resultant unbalance force acting on the model.

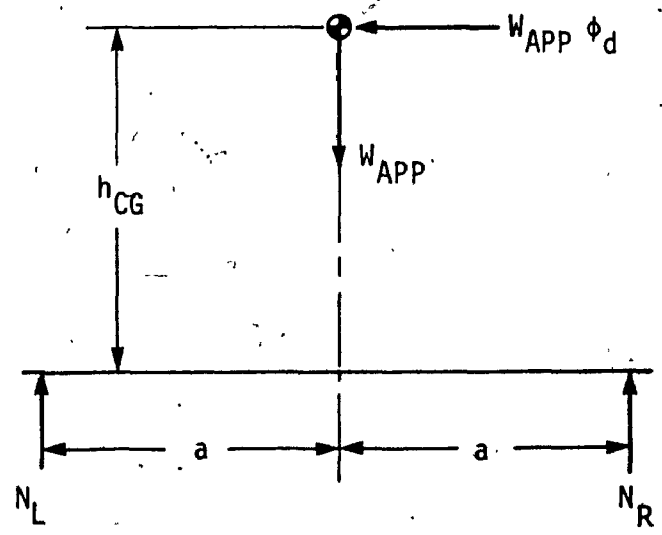

Figure 6.7 Force diagram showing effect of unbalance force on the wheel load shift.

where m_w, m_T, and m_c are masses of the wheelset, truck, and pseudo-car body respectively.

6.3.2 Wheel Load Shift

In the presence of cant deficiency, there is an unbalance force in the plane of the track, which introduces transfer of load between left and right wheels within an axle. This redistribution of load, under the influence of cant deficiency can be estimated by summing moments about a wheel-rail contact point. Figure 6.7 considers a single wheelset, for which axle load is W_{APP}, and the unbalance cant lateral force $W_{APP}\,\phi_d$ is acting through the CG of the vehicle at a height h_{CG} from the rail plane. Summing moments about right-hand wheel contact point leads to:

$$\left(N_L - \frac{W_{APP}}{2}\right) = \frac{W_{APP}\phi_d h_{CG}}{2a} \tag{6.5}$$

Therefore, the fractional load change on the left wheel is:

$$\frac{\left(N_L - \frac{W_{APP}}{2}\right)}{\frac{W_{APP}}{2}} = \frac{h_{CG}}{a}\,\phi_d \tag{6.6}$$

(6.6)

Similarly, taking moment about left wheel contact point, the resulting expression for normal load at the left and right wheels are:

$$N_L \cong \frac{W_{APP}}{2}(1 + h\phi_d)$$
$$N_R \cong \frac{W_{APP}}{2}(1 - h\phi_d) \qquad (6.7)$$

where h is substituted as an approximate value of h_{CG}/a.

6.3.3 Gravitational Stiffness Force

The expression for gravitational stiffness force (GSF) for a wheelset on tangent track is derived in Section 2.3.2, and is given by Equation (2.18), where it was assumed that half the axle load is shared by each wheel. This assumption, however, is not true for curved track with cant deficiency, as shown by Equation (6.7).

The lateral component of the normal force at the wheel-rail contact point, for the left and right wheels are shown in Chapter 2, by Equations (2.16) and (2.17). Summing the forces in the lateral direction results in:

$$GSF = -N_L(\delta_L + \phi) + N_R(\delta_R - \phi) = -N_L\delta_L + N_R\delta_R - (N_L + N_R)\phi \qquad (6.8)$$

Substituting for N_L and N_R from Equation (6.7) leads to:

$$GSF = -W_{APP}\left[\left(\frac{\delta_L - \delta_R}{2}\right) + h\phi_d\delta_0 + \phi\right] \qquad (6.9)$$

6.3.4 Creep Forces and Moments

The creep forces and moments associated with wheel-rail interaction

are discussed in Section 2.3.2. The general expressions for creepages, and creep forces and moments for an EDCW on curved track are derived in Appendix B. As mentioned earlier, the creep forces are defined as the product of creepage and creep coefficient, where the creep coefficients are function of normal load. For the curving model, under the influence of cant deficiency, the normal load (N) is not same for the left and right wheels. It is therefore, necessary to modify the creep coefficients for the left and right wheels. According to Kalker's theory of creep, the following expressions [27] are used to approximately correct the creep coefficients due to differential loads on left and right wheels:

$$\begin{aligned} &\text{Longitudinal} && f_{11} \sim N^{2/3} \\ &\text{Lateral} && f_{22} \sim N^{2/3} \\ &\text{Lat./Spin} && f_{23} \sim N \\ &\text{Spin} && f_{33} \sim N^{4/3} \end{aligned} \tag{6.10}$$

Using the proportionalities given by Equation (6.10), the creep coefficients for left and right wheels can be expressed as:

$$\begin{aligned} f_{11_L}, f_{11_R} &= f_{11}\left(1 \pm \tfrac{2}{3} h\phi_d\right) \\ f_{22_L}, f_{22_R} &= f_{22}\left(1 \pm \tfrac{2}{3} h\phi_d\right) \\ f_{23_L}, f_{23_R} &= f_{23}\left(1 \pm h\phi_d\right) \\ f_{33_L}, f_{33_R} &= f_{33}\left(1 \pm \tfrac{4}{3} h\phi_d\right) \end{aligned} \tag{6.11}$$

where subscripts L and R denote left and right wheels, respectively.

Substituting the expressions for creep coefficients for left and right wheels as shown in Equation (6.11), into expressions of creep forces and moments obtained in Appendix B, the final expressions are obtained. For the curving model, since only steady-state motions are considered, the derivative terms in the creep force and moment expressions are dropped, except for $\dot{\beta}$ terms, which gives:

$$\bar{F}_L = \left[f_{11}\left(1 + \frac{2}{3}h\phi_d\right)\left(\frac{r_L}{r_0} - 1 - \frac{a}{R} + \frac{r_L}{V}\dot{\beta}_L\right)\right]i''' +$$

$$\left[f_{22}\left(1 + \frac{2}{3}h\phi_d\right)\left(\psi + \frac{1^*}{R}\right) + f_{23}\left(1 + h\phi_d\right)\left(\frac{1}{R} + \frac{\delta_L}{r_0}\right)\right]j''' \qquad (6.12)$$

$$\bar{M}_L = \left[f_{33}\left(1 + \frac{4}{3}h\phi_d\right)\left(\frac{1}{R} + \frac{\delta_L}{r_0}\right) - f_{23}\left(1 + h\phi_d\right)\left(\psi + \frac{1^*}{R}\right)\right]k''' \qquad (6.13)$$

$$\bar{F}_R = \left[f_{11}\left(1 - \frac{2}{3}h\phi_d\right)\left(\frac{r_R}{r_0} - 1 + \frac{a}{R} + \frac{r_R}{V}\dot{\beta}_R\right)\right]i''' +$$

$$\left[f_{22}\left(1 - \frac{2}{3}h\phi_d\right)\left(\psi + \frac{1^*}{R}\right) + f_{23}\left(1 - h\phi_d\right)\left(\frac{1}{R} - \frac{\delta_R}{r_0}\right)\right]j''' \qquad (6.14)$$

$$\bar{M}_R = \left[f_{33}\left(1 - \frac{4}{3}h\phi_d\right)\left(\frac{1}{R} - \frac{\delta_R}{r_0}\right) - f_{23}\left(1 - h\phi_d\right)\left(\psi + \frac{1^*}{R}\right)\right]k''' \qquad (6.15)$$

where $1^*/R$ is $+1/R$ for leading wheelset, and $-1/R$ for trailing wheelset.

The $1^*/R$ term appears due to the chosen coordinate system as discussed in Appendix A.2. When $(\psi + 1^*/R)$ is zero, the wheelset is radially aligned with the track. In other words, with respect to reference axis, the leading and trailing wheelsets have to yaw by $+1/R$

and - 1/R, respectively, to be radially aligned with the curved track.

6.4 Assumptions and Limitations

The freight truck model with pseudo-car body and EDCW considered for tangent track stability analysis is reconsidered here for steady-state curving analysis. Various assumptions made in the development of that model are also valid here. Once again, the wheel/rail geometry is assumed to be linear with all angles small. Single point and continuous wheel/rail contact is assumed, where flange contact does not take place. This assumption introduces limitation on the model, however, it is reasonable since the curve negotiation is to be achieved through creep guidance and not flange guidance as discussed earlier.

The curved track is assumed to be smooth and of constant track center radius R , and also has a constant super-elevation, ϕ_{se}. The rails are assumed to be rigid, and they maintain a constant gage length. In reality, however, rails are flexible and can experience lateral and roll motions. Inclusion of rail flexibility in steady-state curving study effectively increases the rail gage. As indicated by Nagurka et al. [64], the flexure of rails results in greater lateral excursion of wheelset by up to 30 to 40%, but the angle of attack of the wheelset is relatively unaffected. Also the steady-state wheel/rail forces are not sensitive to flexure of the rail. For simplicity, therefore, in this study the rails are assumed rigid.

Further, the curve is assumed sufficiently long for initial transients to have died away and steady-state curving to be established, such that wheelsets are in force and moment static equilibrium. With the

steady-state assumption, all the derivative terms from the equations are dropped except for the spin velocity of each wheel ($\dot{\beta}$). This term is retained so that effects of coupler damping can be studied. Even for conventional model, the spin perturbation term should not be assumed equal to zero [27], when the effects of wheel load shift are included in the model.

The truck stability analysis showed, that the coupler torsional damping with negligible stiffness will provide maximum critical speed. Hence, the major objective in this part of the study is to examine the influence of wheelset torsional damping on the steady-state curving behaviour of the truck model. Therefore, to simplify the problem inclusion of both β and $\dot{\beta}$ terms in the equations is avoided. For this it is assumed that k_{AX} parameter of the EDCW is small, and $k_{AX\dot{\beta}}$ is negligible. Similar to tangent track model, the coupler is assumed to allow only differential spin motion between the left and right wheels.

6.5 Steady-State Curving Equations

For steady-state curving analysis of the truck model with pseudo-car body and EDCW, equations of equilibrium are derived in this section. The equations are obtained following the same steps as in Chapter 4. First, steady-state curving equation for a single EDCW is obtained, which is then extended to include truck motions. Since, only steady-state curving is considered, throughout the derivations it is assumed that each displacement has reached a fixed value, and the rate of change of all the displacement variables are zero. The fundamental equations therefore, can be obtained from the equilibrium condition of the external forces.

The expressions for external forces acting on the wheelset, truck, and car body are derived in Section 4.3. Among those, the ones influenced by R and ϕ_{se} are derived in the previous section.

Single EDCW

The wheelset model of the EDCW is identical to that considered for lateral stability analysis, where the relative spin terms (β and $\dot{\beta}$) appear in the equations. In the steady-state analysis, both β and $\dot{\beta}$ terms cannot be retained in the equations. Therefore, to simplify the problem, it is assumed that the wheelset coupler only consists of damper (D_{AX}), and stiffness (k_{AX}) is negligible. As discussed earlier, this decision is based on the conclusion made from stability analysis of the truck model, where optimal wheelset coupler parameters are found to be speed dependent D_{AX} and small value of k_{AX}. Therefore, assuming that the product $k_{AX}\beta$ to be negligible, the wheelset coupler moment becomes only a function of D_{AX} and $\dot{\beta}$.

The EDCW lateral, yaw, and spin equations are obtained by summation of external forces and moments in respective directions. Substitution of expressions for forces and moments due to creep, primary suspension, gravitational stiffness, and cant deficiency lead to the following set of equations:

Wheelset lateral:

$$2f_{22}\phi + \left[\frac{2f_{22}\Delta}{r_0 a} - W_{APP}\left(\frac{\Delta+\Gamma}{a}\right) - 2k_{y_p}\right]y$$

$$= -2f_{22}\frac{l^*}{R} - 2f_{23}\left(\frac{1}{R} + \frac{\delta_0}{r_0}h\phi_d\right) + W_{APP}h\phi_d\delta_0 - m_w g\phi_d \qquad (6.16)$$

Wheelset yaw:

$$\left(\frac{-2f_{11}a\lambda}{r_0} + \frac{2f_{33}\Delta}{r_0 a}\right)y + \left(W_{APP}a\delta_0 - 2f_{23} - k_{\psi_p} - 2f_{23}\frac{\delta_0 a}{r_0}\right)\psi -$$

$$\frac{f_{11}r_0 a}{V}\left(1 + \tfrac{2}{3}h\phi_d\right)\dot{\beta}_L + \frac{f_{11}ar_0}{V}\left(1 - \tfrac{2}{3}h\phi_d\right)\dot{\beta}_R =$$

$$-2f_{11}\frac{a^2}{R} - 2f_{33}\frac{1}{R} - \frac{8f_{33}\delta_0 h\phi_d}{3r_0} + 2f_{23}\frac{l^*}{R} - W_{APP}a\delta_0\frac{l^*}{R} + 2f_{23}\frac{a\delta_0 l^*}{r_0 R} \qquad (6.17)$$

Left wheel spin:

$$f_{11}\left(1 + \tfrac{2}{3}h\phi_d\right)\lambda y + \delta_0\left(1 + h\phi_d\right)\left(f_{23} - \frac{W_{APP}r_0}{2}\right)\psi$$

$$+ \left[f_{11}\left(1 + \tfrac{2}{3}h\phi_d\right)\frac{r_0^2}{V} + D_{AX}\right]\dot{\beta}_L - D_{AX}\dot{\beta}_R =$$

$$f_{11}\left(1 + \tfrac{2}{3}h\phi_d\right)\frac{ar_0}{R} - \delta_0\left(1 + h\phi_d\right)\left(f_{23} - \frac{W_{APP}r_0}{2}\right)\frac{l^*}{R} \qquad (6.18)$$

Right wheel spin:

$$-f_{11}\left(1 - \tfrac{2}{3}h\phi_d\right)\lambda y - \delta_0\left(1 - h\phi_d\right)\left(f_{23} - \frac{W_{APP}r_0}{2}\right)\psi$$

$$+ \left[f_{11}\left(1 - \tfrac{2}{3}h\phi_d\right)\frac{r_0^2}{V} + D_{AX}\right]\dot{\beta}_R - D_{AX}\dot{\beta}_L =$$

$$-f_{11}\left(1 - \tfrac{2}{3}h\phi_d\right)\frac{ar_0}{R} + \delta_0\left(1 - h\phi_d\right)\left(f_{23} - \frac{W_{APP}r_0}{2}\right)\frac{l^*}{R} \qquad (6.19)$$

Subtracting equation (6.19) from (6.18) and rearranging leads to the equation for differential spin between left and right wheels as:

$$2f_{11}\frac{r_0^2}{V}\dot{\beta} + 2f_{11}\lambda y + 2\delta_0\left(f_{23} - \frac{W_{APP}r_0}{2}\right)\psi + 4D_{AX}\dot{\beta} =$$

$$2f_{11}\frac{ar_0}{R} - \frac{2\delta_0 l^*}{R}\left(f_{23} - \frac{W_{APP}r_0}{2}\right) \qquad (6.20)$$

where,

$$\dot{\beta} = \frac{\dot{\beta}_L - \dot{\beta}_R}{2} \qquad (6.21)$$

Using the relation (6.21), and substituting for $\dot{\beta}$ from Equation (6.20) into wheelset yaw Equation (6.17), eliminates the spin equation and leads to the yaw equation as:

$$\left(-\frac{2f_{11}a\lambda}{r_0} + \frac{4f_{11}^2 r_0 a\lambda}{AV} + \frac{2f_{33}\Delta}{r_0 a}\right)y + \left(W_{APP}a\delta_0 - \frac{2\delta_0 f_{11}r_0^2 a W_{APP}}{AV}\right.$$

$$\left. - 2f_{23} + \frac{4\delta_0 f_{11}f_{23}ar_0}{AV} - \frac{2f_{23}a\delta_0}{r_0} - k_{\psi_p}\right)\psi =$$

$$\left(-2f_{11}a^2 + \frac{4f_{11}^2 a^2 r_0^2}{AV} - 2f_{33}\right)\frac{l}{R} + \left(2f_{23} - W_{APP}a\delta_0 + \frac{2f_{23}a\delta_0}{r_0}\right.$$

$$\left. - \frac{4f_{11}f_{23}\delta_0 r_0 a}{AV} + \frac{2f_{11}\delta_0 r_0^2 W_{APP}a}{AV}\right)\frac{l^*}{R} - \frac{8f_{33}h\phi_d\delta_0}{3r_0} \qquad (6.22)$$

Therefore, each EDCW now has two degrees-of-freedom, i.e. lateral and yaw motion represented by Equations (6.16) and (6.22), respectively. In the yaw Equation (6.22), the term AV is defined as:

$$AV = 2f_{11}r_0^2 + 4D_{AX}V \qquad (6.23)$$

Further, it is determined in Chapter 5, that only coupler parameter affecting stability of truck model, is velocity dependent damping

expressed as $C_{D_{AX}}/V$, where $C_{D_{AX}}$ (N.m^2/rad (lb.ft^2/rad)) represents the coefficient of velocity dependent damping. Therefore, substituting this for D_{AX} in the above expression (6.23):

$$AV = 2f_{11}r_0^2 + 4C_{D_{AX}} \tag{6.24}$$

Substitution of which in Equation (6.22) eliminates the velocity terms from the steady-state curving equations of the wheelset.

On the other hand, in order to obtain an independent equation of motion for yaw mode of a conventional rigid axle wheelset, longitudinal equation is used to obtain the expression for β', where β' is the perturbation of wheelset spin velocity above the nominal rotational velocity. Since the wheelset is assumed to travel at constant velocity, without any longitudinal perturbation.

$$x = 0 \ , \quad \text{and } F_{s_{p_x}} = 0$$

Therefore, the longitudinal equation is obtained by summation of external forces in the x-direction, which leads to wheelset longitudinal equation as:

$$\frac{f_{11}r_0}{V}\dot{\beta}_L + \frac{f_{11}r_0}{V}\dot{\beta}_R + \frac{2}{3}h\phi_d f_{11}\left(\frac{2\lambda y}{r_0} - \frac{2a}{R} + \frac{r_0}{V}\dot{\beta}_L - \frac{r_0}{V}\dot{\beta}_R\right) = 0 \tag{6.25}$$

For the conventional rigid axle wheelset:

$$\dot{\beta}_L = \dot{\beta}_R = \dot{\beta}' \tag{6.26}$$

Therefore, Equation (6.25) can be simplified to:

$$\dot{\beta}' = -\frac{2}{3}h\phi_d V\left(\frac{\lambda y}{r_0^2} - \frac{a}{r_0 R}\right) \tag{6.27}$$

Substituting the above relations (6.26) and (6.27) into the yaw equation (6.17), leads to the yaw equation for conventional rigid axle wheelset as:

$$\left[\frac{-2f_{11}a\lambda}{r_0}\left(1 - \frac{4}{9}h^2\phi_d^2\right) + \frac{2f_{33}\Delta}{r_0 a}\right]y + \left[W_{APP}a\delta_0 - 2f_{23} - k_{\psi_p} - 2f_{23}\frac{\delta_0 a}{r_0}\right]\phi$$

$$= -\frac{2f_{11}a^2}{R}\left(1 - \frac{4}{9}h^2\phi_d^2\right) - \frac{2f_{33}}{R} - \frac{8f_{33}h\phi_d\delta_0}{3r_0}$$

$$+ \left(2f_{23} - W_{APP}a\delta_0 + \frac{2f_{23}\delta_0 a}{r_0}\right)\frac{1^*}{R} \tag{6.28}$$

The lateral equation for the conventional wheelset is same as the one for EDCW model as given by Equation (6.15)

Truck with pseudo-car body and EDCW

Same approach as in Chapter 4 is used to obtain the steady-state curving equations for the truck model. The various DOF of the model include:

- lateral and yaw for leading wheelset;
- lateral and yaw for trailing wheelset;
- lateral, yaw and warp for truck frame;
- lateral and roll for pseudo-car body.

Leading and trailing wheelset equations are obtained by redefining the wheelset lateral and yaw variables to include the lateral, yaw and

warp motions of the truck frame. The wheelset equations are obtained, using the relationships defined in Section 4.3.1 by Equations (4.1) to (4.4), which are:

For the leading wheelset:

$$y = y_{w_1} + y_T + l\psi_T$$

$$\psi = \psi_{w_1} + \psi_T + \theta_w \qquad (6.29)$$

For the trailing wheelset:

$$y = y_{w_2} + y_T + l\psi_T$$

$$\psi = \psi_{w_2} + \psi_T + \theta_w \qquad (6.30)$$

Further, substituting for l^*/R by $+l/R$ for the leading wheelset, and by $-l/R$ for the trailing wheelset into the initial single wheelset Equations (6.16), (6.22) and (6.28), the final expressions for the wheelsets of the truck model are:

Leading wheelset lateral:

$$\left[\frac{2f_{23}\Delta}{r_0 a} - W_{APP}\left(\frac{\Delta + \Gamma}{a}\right) - 2k_{y_p}\right]y_{w_1} + 2f_{22}\psi_{w_1} + \left[\frac{2f_{23}\Delta}{r_0 a} - W_{APP}\left(\frac{\Delta + \Gamma}{a}\right)\right]y_T$$

$$+\left[2f_{22} + \frac{2f_{23}\Delta l}{r_0 a} - W_{APP}\left(\frac{\Delta + \Gamma}{a}\right)l\right]\psi_T + 2f_{22}\theta_w =$$

$$-\frac{2f_{22}l}{R} - \frac{2f_{23}}{R} - \frac{2f_{23}h\phi_d\delta_0}{r_0} + W_{APP}h\phi_d\delta_0 - m_w g\phi_d \qquad (6.31)$$

Trailing wheelset lateral:

$$\left[\frac{2f_{23}\Delta}{r_0 a} - W_{APP}\left(\frac{\Delta + \Gamma}{a}\right) - 2k_{y_p}\right]y_{w_2} + 2f_{22}\psi_{w_2} + \left[\frac{2f_{23}\Delta}{r_0 a} - W_{APP}\left(\frac{\Delta + \Gamma}{a}\right)\right]y_T$$

$$+\left[2f_{22} - \frac{2f_{23}\Delta l}{r_0 a} + W_{APP}\left(\frac{\Delta + \Gamma}{a}\right)l\right]\phi_T + 2f_{22}\theta_w =$$

$$\frac{2f_{22}l}{R} - \frac{2f_{23}}{R} - \frac{2f_{23}h\phi_d\delta_0}{r_0} + W_{APP}h\phi_d\delta_0 - m_w g\phi_d \qquad (6.32)$$

Leading wheelset yaw:

EDCW:

$$\left(-\frac{2f_{11}a\lambda}{r_0} + \frac{4f_{11}^2 r_0 a\lambda}{2f_{11}r_0^2 + 4C_{D_{AX}}} + \frac{2f_{33}\Delta}{r_0 a}\right)y_{w_1} + \left[W_{APP}a\delta_0 - \frac{2f_{11}r_0^2 a\delta_0 W_{APP}}{2f_{11}r_0^2 + 4C_{D_{AX}}}\right.$$

$$\left. - 2f_{23} + \frac{4f_{11}f_{23}r_0 a\delta_0}{2f_{11}r_0^2 + 4C_{D_{AX}}} - \frac{2f_{23}\delta_0 a}{r_0} - k_{\phi_p}\right]\psi_{w_1} + \left[-\frac{2f_{11}a\lambda}{r_0} + \right.$$

$$\left.\frac{4f_{11}^2 r_0 a\lambda}{2f_{11}r_0^2 + 4C_{D_{AX}}} + \frac{2f_{33}\Delta}{r_0 a}\right]y_T + \left[W_{APP}a\delta_0 - \frac{2f_{11}r_0^2 a\delta_0 W_{APP}}{2f_{11}r_0^2 + 4C_{D_{AX}}} - 2f_{23} + \right.$$

$$\left.\frac{4f_{11}f_{23}r_0 a\delta_0}{2f_{11}r_0^2 + 4C_{D_{AX}}} - \frac{2f_{23}\delta_0 a}{r_0} + \left(-\frac{2f_{11}a\lambda}{r_0} + \frac{4f_{11}^2 r_0 a\lambda}{2f_{11}r_0^2 + 4C_{D_{AX}}} + \frac{2f_{33}\Delta}{r_0 a}\right)l\right]\phi_T$$

$$+ \left(W_{APP}a\delta_0 - \frac{2f_{11}r_0^2 a\delta_0 W_{APP}}{2f_{11}r_0^2 + 4C_{D_{AX}}} - 2f_{23} + \frac{4f_{11}f_{23}r_0 a\delta_0}{2f_{11}r_0^2 + 4C_{D_{AX}}} - \frac{2f_{23}\delta_0 a}{r_0}\right]\theta_w$$

$$= \frac{-2f_{11}a^2}{R} + \left(\frac{4f_{11}^2 r_0^2 a^2}{2f_{11}r_0^2 + 4C_{D_{AX}}}\right)\frac{1}{R} - \frac{2f_{33}}{R} - \frac{8f_{33}h\phi_d\delta_0}{3r_0} + \left(2f_{23} + \right.$$

$$\left.\frac{2f_{23}\delta_0 a}{r_0} - \frac{4f_{11}f_{23}r_0 a\delta_0}{2f_{11}r_0^2 + 4C_{D_{AX}}} - W_{APP}a\delta_0 + \frac{2f_{11}ar_0^2\delta_0 W_{APP}}{2f_{11}r_0^2 + 4C_{D_{AX}}}\right]\frac{1}{R} \qquad (6.33)$$

Conventional wheelset:

$$\left[-\frac{2f_{11}a\lambda}{r_0}\left(1-\frac{4}{9}h^2\phi_d^2\right)+\frac{2f_{33}\Delta}{r_0 a}\right]y_{w_1}+\left(W_{APP}a\delta_0-2f_{23}-\frac{2f_{23}\delta_0 a}{r_0}\right.$$

$$\left.-k_{\psi_p}\right)\psi_{w_1}+\left[-\frac{2f_{11}a\lambda}{r_0}\left(1-\frac{4}{9}h^2\phi_d^2\right)+\frac{2f_{33}\Delta}{r_0 a}\right]y_T+\left\{W_{APP}a\delta_0-2f_{23}\right.$$

$$\left.-\frac{2f_{23}\delta_0 a}{r_0}+\left[-\frac{2f_{11}a\lambda}{r_0}\left(1-\frac{4}{9}h^2\phi_d^2\right)+\frac{2f_{33}\Delta}{r_0 a}\right]1\right\}\psi_T+\left(W_{APP}a\delta_0-2f_{23}\right.$$

$$\left.-\frac{2f_{23}\delta_0 a}{r_0}\right]\theta_w=-\frac{2f_{11}a^2}{R}\left(1-\frac{4}{9}h^2\phi_d^2\right)-\frac{2f_{33}}{R}-\frac{8f_{33}h\phi_d\delta_0}{3r_0}+\frac{2f_{23}1}{R}$$

$$-\frac{W_{APP}a\delta_0 1}{R}+\frac{2f_{23}a\delta_0 1}{r_0 R} \qquad (6.34)$$

Trailing wheelset yaw:

EDCW:

$$\left(-\frac{2f_{11}a\lambda}{r_0}+\frac{4f_{11}^2 r_0 a\lambda}{2f_{11}r_0^2+4C_{D_{AX}}}+\frac{2f_{33}\Delta}{r_0 a}\right)y_{w_2}+\left[W_{APP}a\delta_0-\frac{2f_{11}r_0^2 a\delta_0 W_{APP}}{2f_{11}r_0^2+4C_{D_{AX}}}\right.$$

$$\left.-2f_{23}+\frac{4f_{11}f_{23}r_0 a\delta_0}{2f_{11}r_0^2+4C_{D_{AX}}}-\frac{2f_{23}\delta_0 a}{r_0}-k_{\psi_p}\right]\psi_{w_2}+\left[-\frac{2f_{11}a\lambda}{r_0}+\right.$$

$$\left.\frac{4f_{11}^2 r_0 a\lambda}{2f_{11}r_0^2+4C_{D_{AX}}}+\frac{2f_{33}\Delta}{r_0 a}\right]y_T+\left[W_{APP}a\delta_0-\frac{2f_{11}r_0^2 a\delta_0 W_{APP}}{2f_{11}r_0^2+4C_{D_{AX}}}-2f_{23}+\right.$$

$$\left.\frac{4f_{11}f_{23}r_0 a\delta_0}{2f_{11}r_0^2+4C_{D_{AX}}}-\frac{2f_{23}\delta_0 a}{r_0}-\left(-\frac{2f_{11}a\lambda}{r_0}+\frac{4f_{11}^2 r_0 a\lambda}{2f_{11}r_0^2+4C_{D_{AX}}}+\frac{2f_{33}\Delta}{r_0 a}\right)1\right]\psi_T$$

$$+\left(W_{APP}a\delta_0-\frac{2f_{11}r_0^2 a\delta_0 W_{APP}}{2f_{11}r_0^2+4C_{D_{AX}}}-2f_{23}+\frac{4f_{11}f_{23}r_0 a\delta_0}{2f_{11}r_0^2+4C_{D_{AX}}}-\frac{2f_{23}\delta_0 a}{r_0}\right]\theta_w$$

$$= \frac{-2f_{11}a^2}{R} + \left(\frac{4f_{11}^2 r_0^2 a^2}{2f_{11}r_0^2 + 4C_{D_{AX}}}\right)\frac{1}{R} - \frac{2f_{33}}{R} - \frac{8f_{33}h\phi_d\delta_0}{3r_0} - \left(2f_{23} + \right.$$

$$\left. \frac{2f_{23}\delta_0 a}{r_0} - \frac{4f_{11}f_{23}r_0 a\delta_0}{2f_{11}r_0^2 + 4C_{D_{AX}}} - W_{APP}a\delta_0 + \frac{2f_{11}ar_0^2\delta_0 W_{APP}}{2f_{11}r_0^2 + 4C_{D_{AX}}}\right]\frac{1}{R} \qquad (6.35)$$

Conventional wheelset:

$$\left[-\frac{2f_{11}a\lambda}{r_0}\left(1 - \frac{4}{9}h^2\phi_d^2\right) + \frac{2f_{33}\Delta}{r_0 a}\right]y_{w_2} + \left(W_{APP}a\delta_0 - 2f_{23} - \frac{2f_{23}\delta_0 a}{r_0}\right.$$

$$\left. - k_{\psi_p}\right)\psi_{w_2} + \left[-\frac{2f_{11}a\lambda}{r_0}\left(1 - \frac{4}{9}h^2\phi_d^2\right) + \frac{2f_{33}\Delta}{r_0 a}\right]y_T + \left\{W_{APP}a\delta_0 - 2f_{23}\right.$$

$$\left. - \frac{2f_{23}\delta_0 a}{r_0} - \left[-\frac{2f_{11}a\lambda}{r_0}\left(1 - \frac{4}{9}h^2\phi_d^2\right) + \frac{2f_{33}\Delta}{r_0 a}\right]1\right\}\psi_T + \left(W_{APP}a\delta_0 - 2f_{23}\right.$$

$$\left. - \frac{2f_{23}\delta_0 a}{r_0}\right]\theta_w = -\frac{2f_{11}a^2}{R}\left(1 - \frac{4}{9}h^2\phi_d^2\right) - \frac{2f_{33}}{R} - \frac{8f_{33}h\phi_d\delta_0}{3r_0} - \frac{2f_{23}1}{R}$$

$$+ \frac{W_{APP}a\delta_0 1}{R} - \frac{2f_{23}a\delta_0 1}{r_0 R} \qquad (6.36)$$

The steady-state curving equations for the truck frame and pseudo-car body are obtained following the same steps as in Chapter 4. The assumptions made regarding connections between side frame, bolster and car body are also valid in this section. By summing external forces and resulting moments, including the unbalance force due to cant deficiency, the truck equations are obtained as follows:

Truck lateral:

$$2k_y y_T - 2k_{y_p} y_{w_1} - 2k_{y_p} y_{w_2} - 2k_y y_c - 2k_y h\phi_c = 2m_s g\phi_d \qquad (6.37)$$

Truck yaw:

$$k_{cp}\psi_T + k_{cp}\theta_w - 2k_{y_p}l y_{w_1} + 2k_{y_p}l y_{w_2} - 2k_{x_p}d^2\psi_{w_1} - 2k_{x_p}d^2\psi_{w_2} = 0 \qquad (6.38)$$

Truck warp:

$$(k_{\theta_w} + k_{cp})\theta_w + k_{cp}\psi_T - 2k_{x_p}d^2\psi_{w_1} - 2k_{x_p}d^2\psi_{w_2} = 0 \qquad (6.39)$$

For the car body lateral and roll motions, the bolster is assumed to move with the car body. Summation of force and moment in lateral and roll directions lead to the following steady-state curving equations for the pseudo-car body:

Pseudo-car lateral:

$$2k_y y_c - 2k_y y_T + 2k_y h\phi_c = (m_c + m_B)g\phi_d \qquad (6.40)$$

Pseudo-car roll:

$$2k_y h y_c - 2k_y h y_T - 2k_z d\frac{2\Gamma}{a} y_T - k_z d\frac{2\Gamma}{a} y_{w_1} - k_z d\frac{2\Gamma}{a} y_{w_2} +$$
$$(2k_y h^2 + 2k_z d^2 - m_c gh)\phi_c = m_B gh\phi_d \qquad (6.41)$$

6.6 Summary

In this chapter, the freight truck model with EDCW developed in Chapter 4, is reconsidered for steady-state curving analysis. Various curved track modeling considerations in contrast to tangent track include radius of curvature and track super-elevation. Their effects on creepage, lateral unbalance and wheel load shift are discussed, and the

expressions for resulting forces and moments are derived in this section.

The steady-state curving equations for the truck model are also developed in this chapter, following the same steps as that used in Chapter 4. Except in this case, the wheelset relative spin equations are substituted into yaw equations, reducing the model to a nine DOF system.

For steady-state curving analysis of truck system with conventional wheelsets, independent yaw equations for the wheelsets are derived. The model for the conventional system is considered, so that the results of truck model with EDCW in its limiting case can be validated against the conventional system of same complexity, as well as performance can be compared quantitatively.

Various assumptions made in the modeling of freight truck on curved track are also outlined in this section. In the following chapter, the mathematical model developed here is used to carry out detailed steady-state curving analysis.

CHAPTER 7

STEADY-STATE CURVING ANALYSIS OF FREIGHT TRUCK

7.1 Introduction

Freight truck stability analysis on tangent track presented in Chapter 5, showed that significant improvement of critical speed can be obtained by utilizing an optimal coupler between the wheels. The optimal coupler parameter to maximize critical speed is found to be speed dependent torsional damping with negligible torsional stiffness. The objective of this section of the study is to investigate the effect of torsional damper (D_{AX}) on the steady-state curving performance of the truck model.

The critical speed of conventional rigid axle freight car system can be improved to certain extent by selecting small value for wheel conicity and large value for primary yaw stiffness. But as discussed in the literature review, these parameters have conflicting requirement for better curving performance. In this study, the sensitivity of selective parameters on the curving performance of the truck model are also examined. This parametric sensitivity is further compared with that of stability performance sensitivity to identical parameters.

In all cases, the results of truck model with EDCW are compared with that of truck model with conventional wheelsets. The steady-state curving equations for conventional and EDCW systems derived in Chapter 6, are used to determine the curving performance of the truck models. In the following sub-sections, the curving performance indices are discussed, the method of solution is outlined, and the results are

presented and summarized.

7.2 Curving Performance Indices

The basic element of the rail vehicle for curving is the wheelsets. The curving performance is therefore, generally evaluated in terms of wheelset perturbation and resulting forces at the wheel/rail contacts. Over the years, several performance indices have been developed and used to represent the ability of a rail vehicle or wheelset to negotiate a curve. A number of simultaneous objectives may be identified, such as perfect steering, prevention of derailment, minimum wheel/rail forces, and minimum wheel/rail wear.

The perfect steering situation or optimal curve negotiation is achieved, if the wheelset adopts a radial position and displaces laterally so that it rolls without slip around a curve. In this respect, the wheelset lateral excursion form the track centerline (tracking error), and the angle of yaw with respect to radial alignment (angle of attack) are the natural performance indices. An undesirable situation exists, when the value of these indices are large, effectively causing flange contact or producing large creep forces, resulting in slip.

The derailment tendencies of a vehicle are associated with the magnitude of the (L/V) ratio of wheel/rail forces. The L/V ratio may be viewed as a wheel climb derailment indicator. Although, very simplified analysis have been attempted in calculating L/V ratio as derailment indicator, this is a very complex phenomenon and not understood very well. The ratio as a measure of derailment depends on several factors, such as angle of attack, vertical wheel load, dynamic load, flange angle,

coefficient of adhesion, wheelset mass, track stiffness, etc. Furthermore, it is associated with time duration of lateral force pulse. The L/V ratio is also associated with rail roll-over which again depends on several factors. A short discussion on these can be found in [2].

As a measure of curving performance several wear indices have been proposed to predict wear rate at wheel/rail interface. Since modeling the phenomenon of wear is a very complex problem, these indices are designed to relate to wear in a relative manner, and used for performance comparison rather than to represent actual wear. The wear indices, such as flange wear index, tread wear index, contact parch work, wear volume, etc., are listed in [64] as well as some discussed in [2].

From the above discussion, it is evident that there has been a wide range of performance indices used in the analyses of curving behaviour. Various studies [27, 61, 63] carried out with conventional system models have showed, that depending on radius of track curvature, wheel flanging occurs, which creates noise, increases stress level and power consumption. Therefore, it would be desirable if curving under the guidance of flange can be avoided, at least for mainline curves (1^0 to 3^0) [27].

In order to achieve this, curving has to be performed under the guidance of creep [61]. Creep guidance on the other hand can be achieved if the friction force at the wheel tread is sufficient to counter act creep force to avoid slip. To evaluate the curving performance of the models under study, very similar approach proposed by Newland [61] and Boocock [63] is considered. The curving performance of the truck models are determined in terms of two conditions:

1. The range of track curvature, R in m (ft) or in degree curve, and cant deficiency, ϕ_d (lateral unbalance), for which the wheelsets will not slip.

2. The value of the above curved track parameters (R, ϕ_d), that causes wheelset lateral excursion resulting in flange contact.

Among the two conditions, slip is a critical factor. When slip takes place, the wheelset may accelerate laterally causing flange impact. On the other hand, if flanging takes place first, the curve can still be negotiated under the guidance of flange, provided excessive forces are not developed.

In this study, the main performance index is the slip boundary indicating minimum radius of curvature on maximum degree curve, that can be negotiated without any of the wheels resulting in slip. Similarly, as a secondary index, flange boundary is also computed, but the model's ability to negotiate a curve under the guidance of flange cannot be evaluated from this investigation, since in the modeling it is assumed that flange contact does not take place.

7.3 Method of Solution

In the previous chapter, equations of steady-state curving are listed for a 9 degrees-of-freedom freight truck model. Equations (6.31, 6.32, 6.34, 6.36 and 6.37 to 6.41) represent conventional rigid axled truck model and Equations (6.31 to 6.33, 6.35 and 6.37 to 6.41) represent the model with EDCW. Each of these two sets of equations for steady-state curving solution may be expressed in a matrix form as:

$$[A]\{X\} = \{B\} \tag{7.1}$$

where, (9 x 9) matrix [A] contains the terms related to stiffness, creep and geometry parameters, {X} is the (9 x 1) vector of the model displacement variables, and [B] is the (9 x 1) input vector which contains the model parameters and the two input terms, i.e. cant deficiency and radius of track curvature. The linear algebraic equations of the form given by Equation (7.1) can readily be solved using Gaussian elimination technique to obtain the output displacement vector {x}.

To obtain the curving performance, first the vector of displacements is obtained for a given value of curvature and cant deficiency. From these, the components of creep forces and their vector sum is computed for each wheel and equated to limiting friction force available at each wheel. For the left and right wheels, the limiting equations are:

Left:

$$(F_{L_x}^2 + F_{L_y}^2)^{\frac{1}{2}} = \mu \frac{W_{APP}}{2} (1 + h\phi_d) \tag{7.2}$$

Right:

$$(F_{R_x}^2 + F_{R_y}^2)^{\frac{1}{2}} = \mu \frac{W_{APP}}{2} (1 - h\phi_d) \tag{7.3}$$

The components of creep forces are computed for conventional and EDCW systems as follows:

Conventional system:

The lateral and longitudinal component of creep forces for the conventional model is obtained by substituting for spin perturbation term from the longitudinal Equation (6.27) into creep force expressions given by Equations (6.12) and (6.13). Further, substituting for $1^*/R$ by $+1/R$ and $-1/R$ for leading and trailing wheelsets, respectively, the following expressions are obtained for each wheel:

Leading left wheel:

$$\bar{F}_{L_L} = [f_{11}(1 - \tfrac{4}{9} h^2\phi_d^2)(\frac{\lambda y_1}{r_0} - \frac{a}{R})]\hat{i}''' +$$

$$[f_{22}(1 + \tfrac{2}{3}h\phi_d)(\phi_1 + \frac{1}{R}) + f_{23}(1 + h\phi_d)(\frac{1}{R} + \frac{\delta_0}{r_0} + \frac{\Delta y_1}{ar_0})]\hat{j}''' \quad (7.4)$$

Leading right wheel:

$$\bar{F}_{R_L} = [-f_{11}(1 - \tfrac{4}{9} h^2\phi_d^2)(\frac{\lambda y_1}{r_0} - \frac{a}{R})]\hat{i}''' +$$

$$[f_{22}(1 - \tfrac{2}{3}h\phi_d)(\phi_1 + \frac{1}{R}) + f_{23}(1 - h\phi_d)(\frac{1}{R} - \frac{\delta_0}{r_0} + \frac{\Delta y_1}{ar_0})]\hat{j}''' \quad (7.5)$$

Trailing left wheel:

$$\bar{F}_{L_T} = [f_{11}(1 - \tfrac{4}{9} h^2\phi_d^2)(\frac{\lambda y_2}{r_0} - \frac{a}{R})]\hat{i}''' +$$

$$[f_{22}(1 + \tfrac{2}{3} h\phi_d)(\phi_2 - \frac{1}{R}) + f_{23}(1 + h\phi_d)(\frac{1}{R} + \frac{\delta_0}{r_0} + \frac{\Delta y_2}{ar_0})]\hat{j}''' \quad (7.6)$$

Trailing right wheel:

$$\bar{F}_{R_T} = [-f_{11}(1 - \tfrac{4}{9}h^2\phi_d^2)(\frac{\lambda y_2}{r_0} - \frac{a}{R})]\hat{i}''' +$$

$$[f_{22}(1 - \tfrac{2}{3}h\phi_d)(\psi_2 - \frac{1}{R}) + f_{23}(1 - h\phi_d)(\frac{1}{R} - \frac{\delta_0}{r_0} + \frac{\Delta y_2}{ar_0})]\hat{j}''' \qquad (7.7)$$

EDCW system:

For the model with EDCW, since $\dot{\beta}_L \neq \dot{\beta}_R$, $\dot{\beta}_L$ and $\dot{\beta}_R$ are first computed for leading and trailing wheelsets by substituting the response variables into left and right wheel spin Equations (6.18 and 6.19). The spin equations are therefore, written in the form:

For leading wheels:

$$\begin{bmatrix} f_{11}(1 + \frac{2}{3}h\phi_d)r_0^2 + C_{D_{AX}} & -C_{D_{AX}} \\ C_{D_{AX}} & -f_{11}(1 - \frac{2}{3}h\phi_d)r_0^2 - C_{D_{AX}} \end{bmatrix} \begin{Bmatrix} \dot{\beta}_{L_1}/V \\ \dot{\beta}_{R_1}/V \end{Bmatrix} =$$

$$\begin{bmatrix} -f_{11}(1 + \frac{2}{3}h\phi_d)\lambda & -\delta_0(1 + h\phi_d)(f_{23} - \frac{W_{APP}r_0}{2}) \\ -f_{11}(1 - \frac{2}{3}h\phi_d)\lambda & -\delta_0(1 - h\phi_d)(f_{23} - \frac{W_{APP}r_0}{2}) \end{bmatrix} \begin{Bmatrix} y_1 \\ \phi_1 \end{Bmatrix} +$$

$$\begin{Bmatrix} f_{11}(1 + \frac{2}{3}h\phi_d)\frac{ar_0}{R} - \delta_0(1 + h\phi_d)(f_{23} - \frac{W_{APP}r_0}{2})\frac{1}{R} \\ f_{11}(1 - \frac{2}{3}h\phi_d)\frac{ar_0}{R} - \delta_0(1 - h\phi_d)(f_{23} - \frac{W_{APP}r_0}{2})\frac{1}{R} \end{Bmatrix} \qquad (7.8)$$

For trailing wheels:

$$\begin{bmatrix} f_{11}(1 + \frac{2}{3} h\phi_d)r_0^2 + C_{D_{AX}} & - C_{D_{AX}} \\ C_{D_{AX}} & -f_{11}(1 - \frac{2}{3} h\phi_d)r_0^2 - C_{D_{AX}} \end{bmatrix} \begin{Bmatrix} \dot{\beta}_{L_2}/V \\ \dot{\beta}_{R_2}/V \end{Bmatrix} =$$

$$\begin{bmatrix} -f_{11}(1 + \frac{2}{3} h\phi_d)\lambda & -\delta_0(1 + h\phi_d)(f_{23} - \frac{W_{APP}r_0}{2}) \\ -f_{11}(1 - \frac{2}{3} h\phi_d)\lambda & -\delta_0(1 - h\phi_d)(f_{23} - \frac{W_{APP}r_0}{2}) \end{bmatrix} \begin{Bmatrix} y_2 \\ \phi_2 \end{Bmatrix} +$$

$$\begin{Bmatrix} f_{11}(1 + \frac{2}{3} h\phi_d)\frac{ar_0}{R} + \delta_0(1 + h\phi_d)(f_{23} - \frac{W_{APP}r_0}{2})\frac{1}{R} \\ f_{11}(1 - \frac{2}{3} h\phi_d)\frac{ar_0}{R} + \delta_0(1 - h\phi_d)(f_{23} - \frac{W_{APP}r_0}{2})\frac{1}{R} \end{Bmatrix} \qquad (7.9)$$

where, $C_{D_{AX}}$ is equal to D_{AX} V as defined earlier in Equation (5.2). Once the lateral and yaw displacements of wheelsets are computed for given values of R and ϕ_d, they are substituted into Equations (7.8) and (7.9), and the values of $\dot{\beta}_{L_1}/V$, $\dot{\beta}_{R_1}/V$, $\dot{\beta}_{L_2}/V$ and $\dot{\beta}_{R_2}/V$ are computed. Which, are in turn substituted into creep force expressions for each wheel rewritten from Equations (6.11) and (6.12) as:

For leading left wheel:

$$F_{L_L} = [f_{11}(1 + \frac{2}{3} h\phi_d)(\frac{\lambda y_1}{r_0} - \frac{a}{R} + \frac{r_0\dot{\beta}_{L_1}}{V})]\hat{i}''' +$$

$$[f_{22}(1 + \frac{2}{3} h\phi_d)(\phi_1 + \frac{1}{R}) + f_{23}(1 + h\phi_d)(\frac{1}{R} + \frac{\delta_0}{r_0} + \frac{\Delta y_1}{ar_0})]\hat{j}''' \qquad (7.10)$$

For leading right wheel:

$$F_{R_L} = [f_{11}(1 - \tfrac{2}{3} h\phi_d)(-\frac{\lambda y_1}{r_0} + \frac{a}{R} + \frac{r_0 \dot{\beta} R_1}{V})]\hat{i}''' +$$

$$[f_{22}(1 - \tfrac{2}{3} h\phi_d)(\phi_1 + \frac{1}{R}) + f_{23}(1 - h\phi_d)(\frac{1}{R} - \frac{\delta_0}{r_0} + \frac{\Delta y_1}{a r_0})]\hat{j}''' \qquad (7.11)$$

For trailing left wheel:

$$F_{L_T} = [f_{11}(1 + \tfrac{2}{3} h\phi_d)(\frac{\lambda y_2}{r_0} - \frac{a}{R} + \frac{r_0 \dot{\beta} L_2}{V})]\hat{i}''' +$$

$$[f_{22}(1 + \tfrac{2}{3} h\phi_d)(\phi_2 - \frac{1}{R}) + f_{23}(1 + h\phi_d)(\frac{1}{R} + \frac{\delta_0}{r_0} + \frac{\Delta y_2}{a r_0})]\hat{j}''' \qquad (7.12)$$

For trailing right wheel:

$$F_{R_T} = [f_{11}(1 - \tfrac{2}{3} h\phi_d)(-\frac{\lambda y_2}{r_0} + \frac{a}{R} + \frac{r_0 \dot{\beta} R_2}{V})]\hat{i}''' +$$

$$[f_{22}(1 - \tfrac{2}{3} h\phi_d)(\phi_2 - \frac{1}{R}) + f_{23}(1 - h\phi_d)(\frac{1}{R} - \frac{\delta_0}{r_0} + \frac{\Delta y_2}{a r_0})]\hat{j}''' \qquad (7.13)$$

The total creep force at each wheel can then be obtained by substituting components of creep forces computed from Equations (7.10) to (7.13) into Equations (7.2) and (7.3). Therefore, once the output vector is calculated all the other variables of interest, such as resultant creep force, slip boundary and flange boundary can be computed from it.

For the baseline vehicle, the nominal model parameters used for curving analysis are identical to those used earlier and listed in Table 5.1. The results of the steady-state curving performance are obtained in two steps. First, the equations representing conventional model is used to study the curving behaviour and performance of rigid axle wheelset. Next, the equations representing the model with EDCW is used to study the effect of wheelset coupler damping on the curving performance.

7.4 Steady-state Curving Results

Results of steady-state curving analysis are presented in this section for both conventional and EDCW truck models. In all cases, results are first obtained in terms of wheelset displacements in lateral and yaw directions, which are defined in terms of model variables as:

$$y_{1,2} = y_{w_{1,2}} + y_T \pm l\psi_T \tag{7.14}$$

$$\psi_{1,2} = \psi_{w_{1,2}} + \psi_T + \theta_w \tag{7.15}$$

where subscripts 1, 2 represent leading and trailing wheelsets, respectively. In rail vehicle curving study [61, 63], wheelset lateral displacements are frequently defined as "tracking error", which is the displacement from pure rolling line. The distance (y^*_0) of pure rolling line from the track centerline, in terms of geometry can be shown to be [61, 63]:

$$y_0^* = \frac{ar_0}{\lambda R} \tag{7.16}$$

Equation (7.16) defines the lateral displacement of unrestrained wheelset on a curve of radius R . Therefore, for this study, the wheelset lateral displacements from pure rolling line are defined as:

$$y^*_{1,2} = y_{1,2} - y^*_0 \tag{7.17}$$

Similarly, when an unrestrained wheelset negotiates a curve, the wheelset yaws to become radially aligned with the track. From geometry, the wheelset yaw angle for radial alignment is simply given by:

$$\psi_{1,2} = \mp 1/R \tag{7.18}$$

where 1,2 represent leading and trailing wheelsets, respectively. Similar to tracking error, wheelset yaw angle from radial alignment is defined as "angle of attack". For this study, due to chosen coordinate system, the angle of attack is expressed as:

$$\psi^*_{1,2} = \psi_{1,2} \pm 1/R \tag{7.19}$$

In the following sub-sections, results are first obtained for truck model with conventional wheelset to obtain in depth understanding of rail vehicle curving behaviour and to aid in the validation of the model with EDCW. Next, the model with EDCW is considered to study the effects of wheelset coupler parameter on the curving behaviour and performance.

7.4.1 Truck Model with Conventional Wheelset

To aid in the validation of the models, results are obtained for both unrestrained and restrained wheelsets. For an unrestrained

wheelset, the fundamental effect of balanced steady-state curving mechanism is the lateral shift of pure rolling line towards the outer rail, and yaw of the wheelsets to assume radial alignment with the rails [61, 63]. This behaviour is easily verified by obtaining results for cant deficiency, $\phi_d = 0$, with very small values of primary suspension stiffnesses. Numerical results for various values of wheel conicity (λ) and curve radius (R) produced identical results as:

$$y^*_{1,2} = \psi^*_{1,2} = 0 \tag{7.20}$$

which totally agree with the results obtained by Newland [61], and Boocock [63].

In the presence of cant deficiency, for unrestrained wheelsets, results are obtained in terms of same variables. These results indicate that, for unrestrained wheelset cant deficiency has no influence on the lateral displacement. But the yaw angle or the angle of attack is a function of axle load, lateral creep coefficient and cant deficiency ϕ_d. The numerical results are found to satisfy:

$$\psi^*_{1,2} = - \frac{W_{APP}\phi_d}{2f_{22}} \tag{7.21}$$

which is a closed form expression obtained and reported in [61] and [63].

When wheelsets are constrained due to finite primary suspension, they are restricted in their ability to steer towards pure rolling line in response to creep force, which results in tracking error. Numerical results are obtained for conventional model with nominal parameters to

study the effects of primary stiffness, radius of curvature, and cant deficiency on the wheelset tracking errors and angle of attack. Figure 7.1 shows, how the leading and trailing wheelsets of conventional model displace laterally from pure rolling line in response to track curvature as primary suspension stiffnesses (k_{y_p} , k_{ψ_p}) are varied. As the results indicate, for small value of k_{y_p} , the leading and trailing wheelset responses are in anti-phase, and for very large values of k_{y_p} the responses are in-phase. For intermediate primary stiffness, k_{y_p} the leading wheelset is always displaced outward, but the trailing wheelset may be displaced outwards or inwards, depending on the interaction between the lateral and yaw suspensions. The results shown in Figure 7.1 are for balanced running ($\phi_d = 0$) condition. When cant deficiency or unbalance is introduced, the sensitivity of lateral response to ϕ_d is found to be very small for nominal parameters. The lateral response however, is relatively more sensitive to ϕ_d for $k_{y_p} > k_{y_p}$ (nominal). For values of k_{ψ_p} smaller than the nominal value, lateral displacement of both leading and trailing wheelsets increases with increase in ϕ_d. But for k_{ψ_p} larger than nominal, as ϕ_d is increased the response of leading wheelset decreases, while that of trailing wheelset increases.

The influence of ϕ_d on wheelset misalignment or angle of attack is much more significant as shown in Figure 7.2, for variations in k_{y_p} and k_{ψ_p}. When k_{ψ_p} is relatively flexible, the misalignment for both the wheelsets remain constant and are equal for all values of k_{ψ_p}. But as indicated in Figure 7.2, when k_{ψ_p} is increased the misalignment of leading wheelset decreases while that of trailing wheelset increases. Increase in k_{ψ_p} further, results in leading and trailing wheelset misalignments approaching a constant but different values, and is

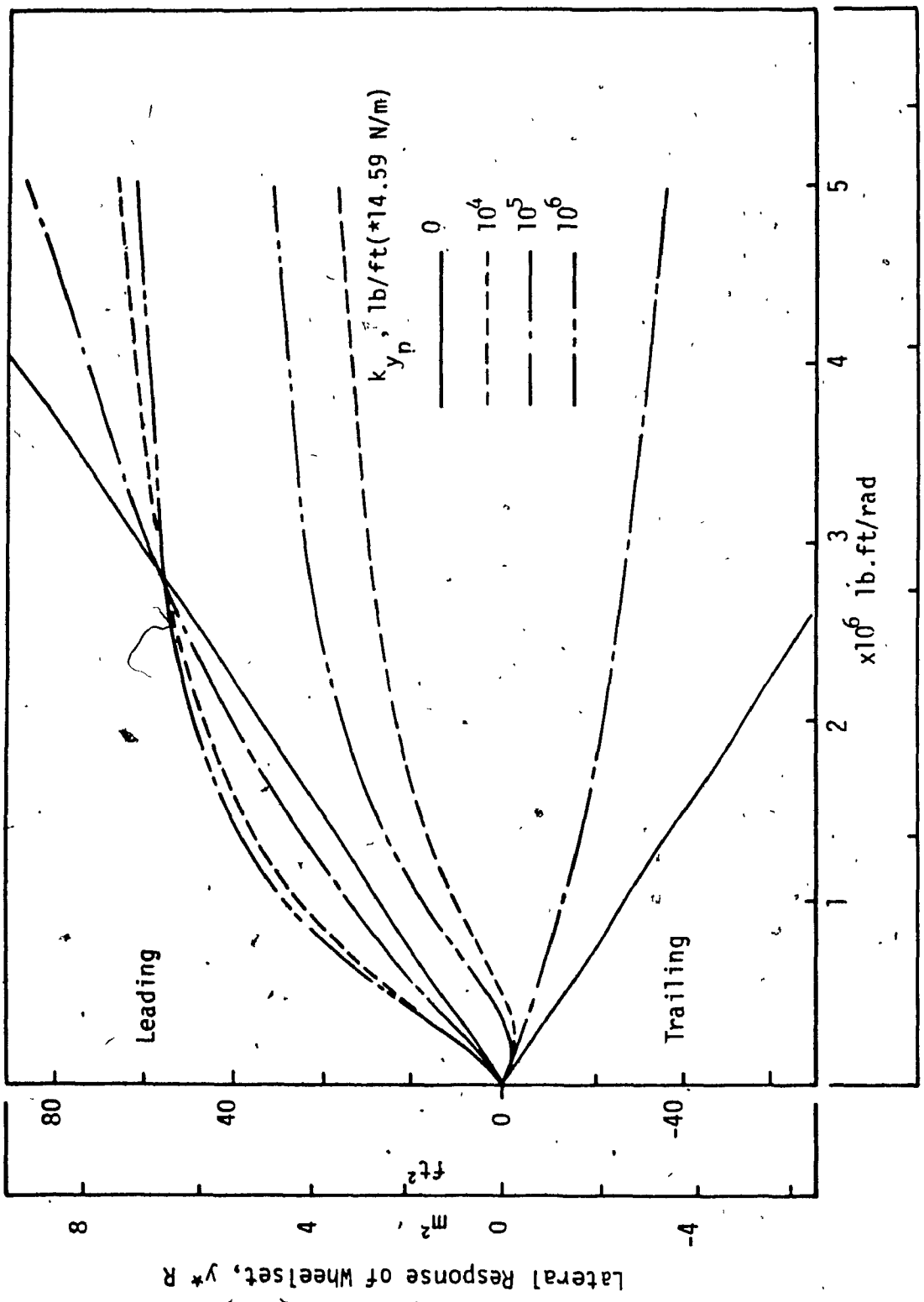

Figure 7.1 Effect of primary suspension stiffness on the lateral response of conventional wheelset to track curvature, for balanced running ($\phi_d = 0$).

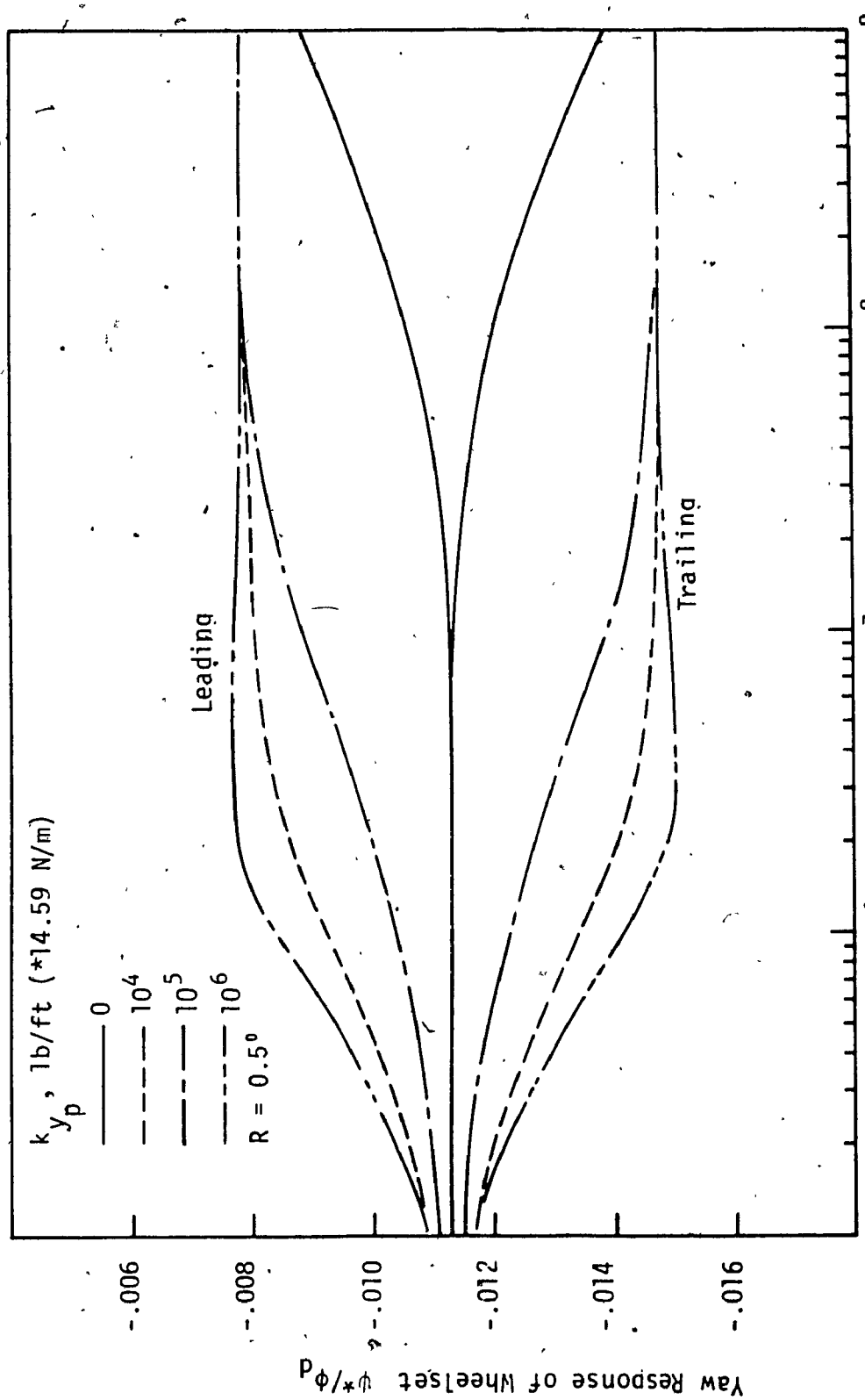

Figure 7.2 Effect of primary suspension stiffness on yaw response of conventional wheelset to cant deficiency, for R = 0.5°.

independent of the value of k_{y_p}. Boocock [63] obtained a simplified closed form misalignment expression for restrained wheelset with rigid primary suspension as:

$$\psi^*_{1,2} = \pm \frac{1}{R} - \frac{W_{APP}\,\Phi_d}{2f_{22}} \tag{7.22}$$

The numerical results obtained in Figure 7.2, follow the expression (7.22) for large value of k_{ψ_p} and cant deficiency in the range $(-4^o < \phi_d < 4^o)$. For larger cant deficiency, there is slight deviation from this simplified expression.

For the conventional system, steady-state curving performance of the model is next evaluated in terms of slip and flange boundaries. The slip boundary represents the conditions of cant deficiency and degree curve for which the largest resultant creep magnitude is equal to friction force at any wheel. The flange contact boundary represents the condition of cant deficiency and degree curve for which the largest lateral displacement of any wheelset in either direction is equal to the flange clearance.

For slip boundary, in general, a different curve is obtained for each wheel. Consequently, the overall performance of the model is defined by the common area enclosed by the curves of all wheels. Figures 7.3 and 7.4, show the performance curves for conventional model with nominal parameters as well as variation in primary yaw stiffness (k_{ψ_p}), and effective wheel conicity (λ). Each portion of the curve is labelled with the particular wheel that slips first. As the results show, both the parameters (k_{ψ_p}, λ) have significant effect on the maximum curvature which can be negotiated without slip. The maximum cant deficiency

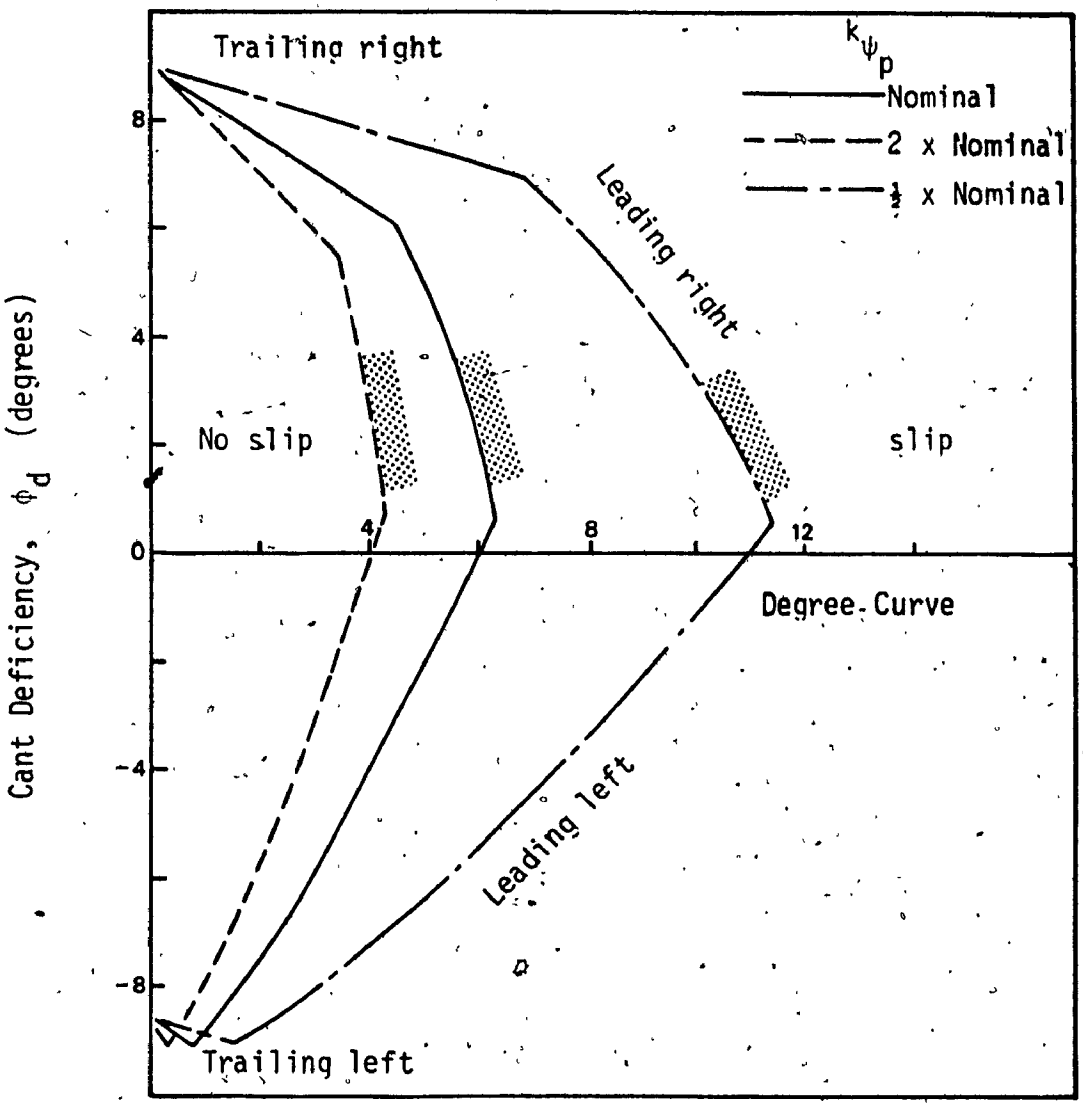

Figure 7.3 Steady-state curving performance (slip boundary) of conventional model, and its sesitivity to primary yaw stiffness.

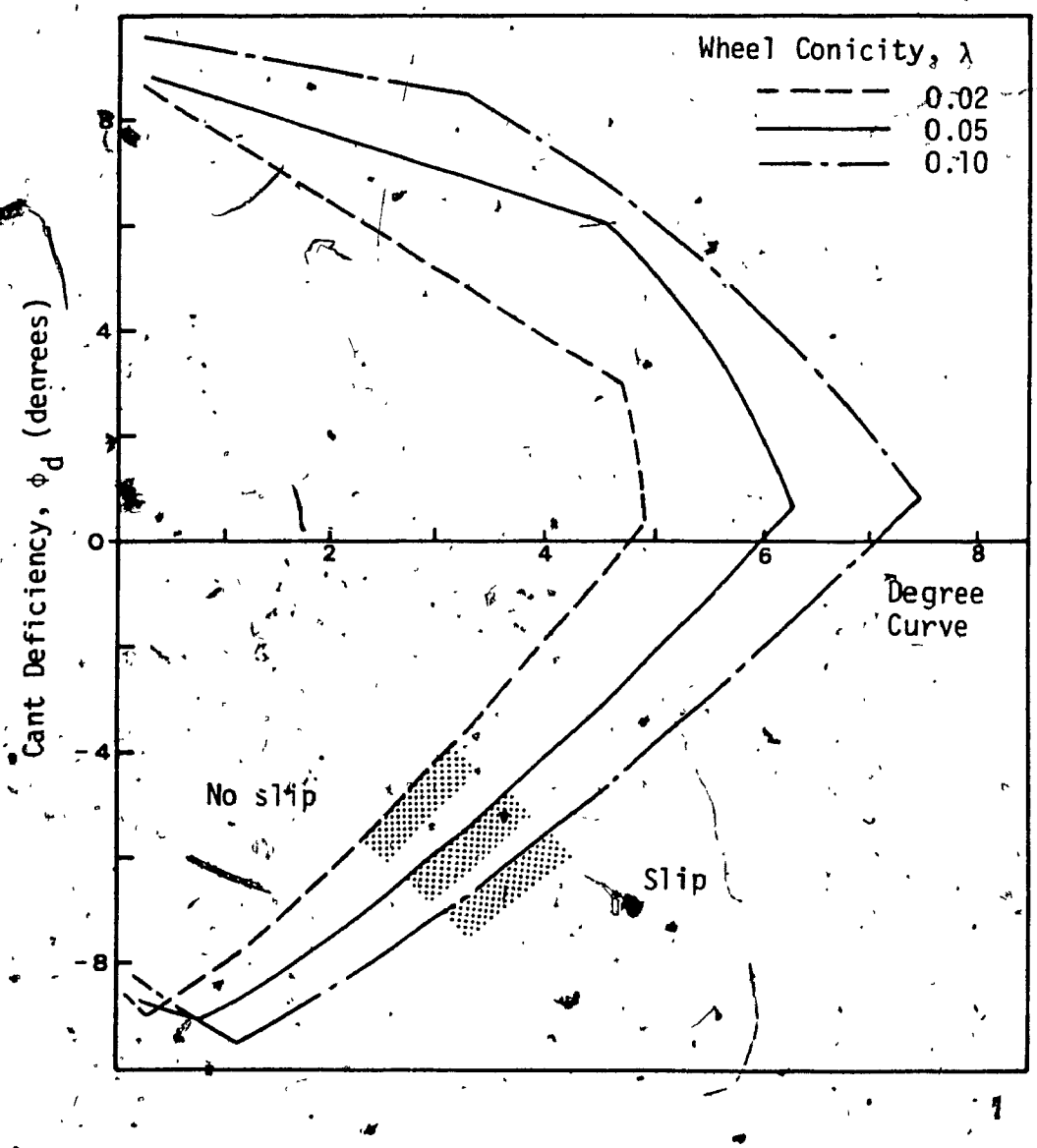

Figure 7.4. Effect of wheel conicity on the curving performance (slip boundary) of conventional model.

sustainable without slip is only slightly affected. These figures also indicate that maximum curvature can be negotiated without slip, for a cant deficiency between zero and one degree, at which point both the wheels on the leading axle slip together.

The flange boundary on the other hand is obtained directly by equating absolute value of lateral displacement to flange clearance. For all cases, flange clearance is taken to be 1.9×10^{-3} m (6.25×10^{-3} ft), which is rather large, but it is reasonable since in practice track can also move in the lateral direction allowing additional displacement before flange contact takes place. Similar to the case of lateral response, cant deficiency has very little effect on the flange boundary. Figures 7.5 to 7.7, show the flange and slip boundaries as well as tangent track critical speeds for variation in primary stiffness (k_{ψ_p}, k_{y_p}), and wheel conicity (λ) for balanced running ($\phi_d = 0$) condition. These figures clearly demonstrate the extent of conflict in parametric requirements between tangent track stability and curving performance of conventional system.

For EDCW system, the coupler between the wheels effectively reduces the longitudinal component of creep force. Therefore, it is necessary to study the influence of variation in creep coefficients on the curving performance of conventional system. Figure 7.8 shows the slip and flange boundaries as a function of the creep coefficients. Results are shown for variation of all creep coefficients together, as well as lateral and longitudinal creep coefficient alone, while the other parameters are kept constant and equal to their nominal values. When all the creep

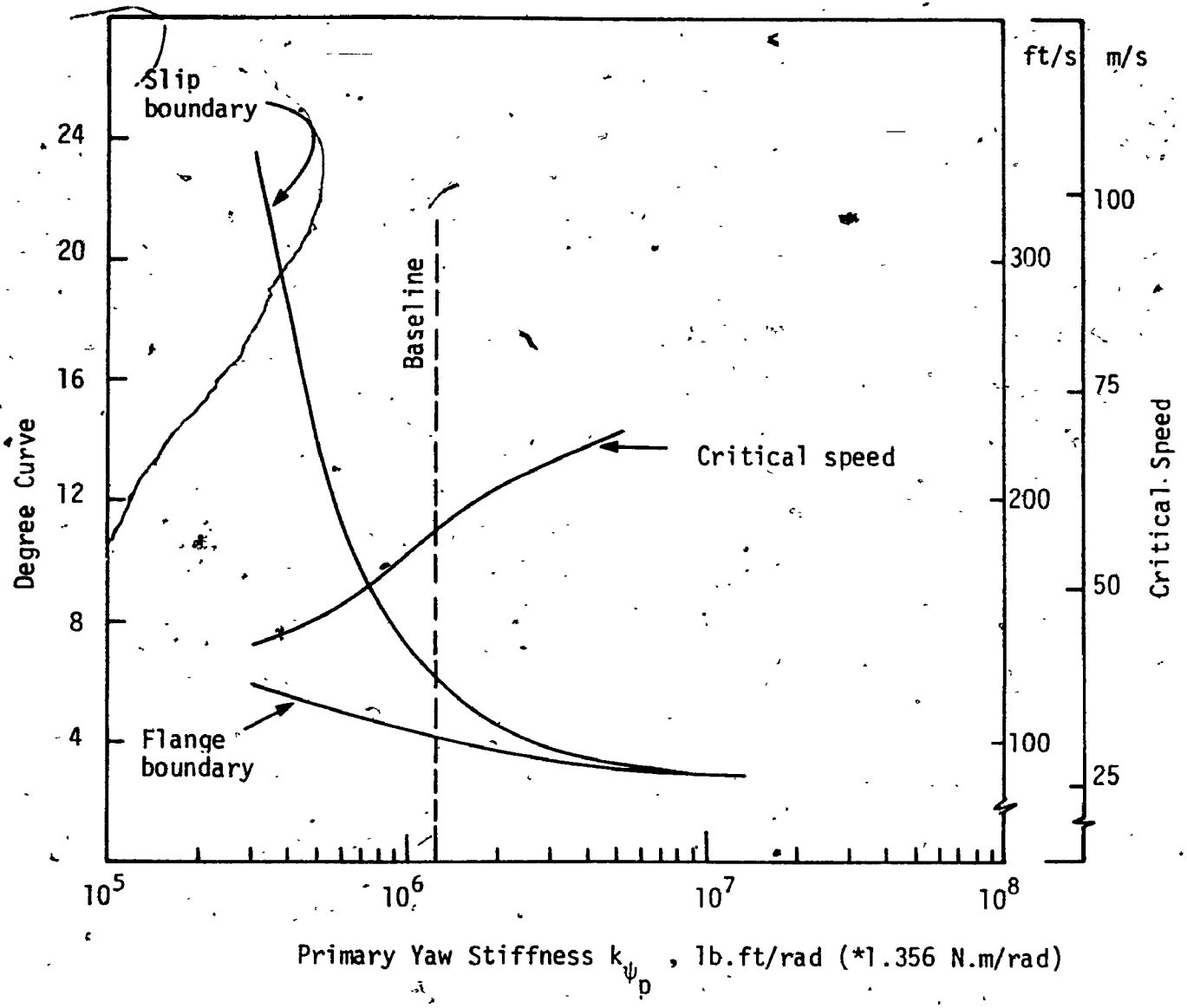

Figure 7.5 Sensitivity of curving performance and tangent track critical speed of conventional system to variation in primary yaw stiffness, (ϕ_d=0)

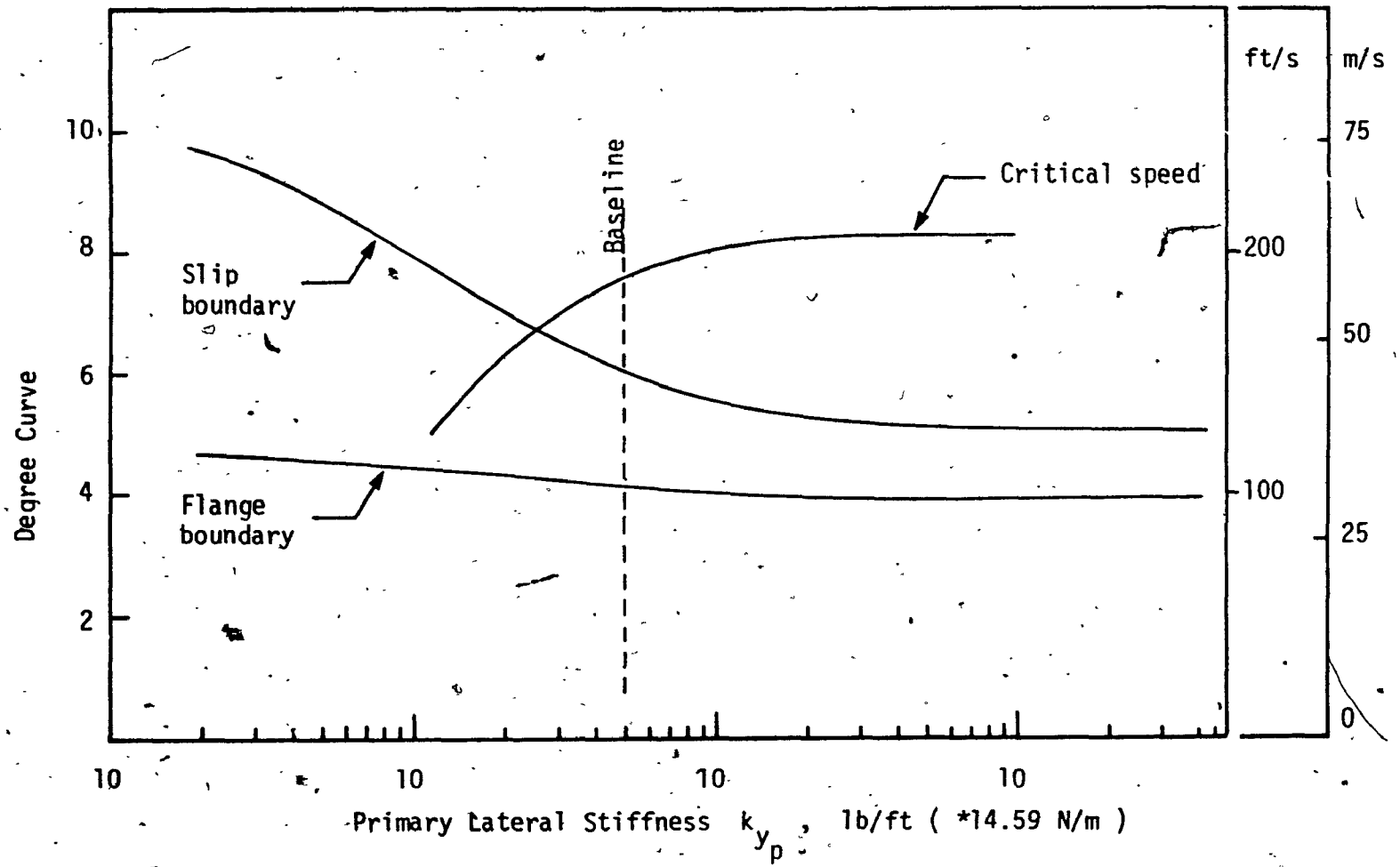

Figure 7.6 Sensitivity of curving performance and tangent track critical speed of conventional system to variation in primary lateral stiffness, (ϕ_d=0)

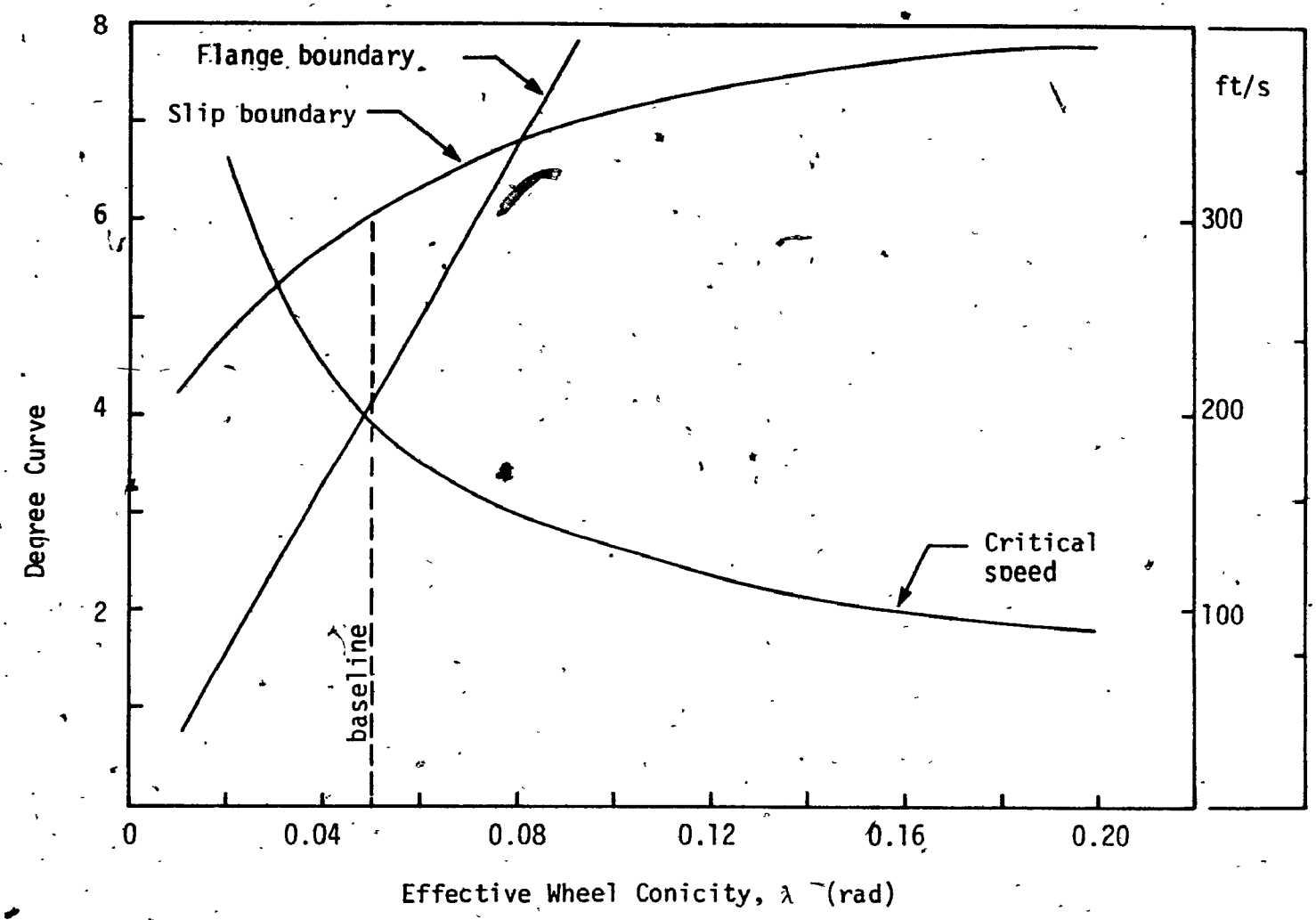

Figure 7.7 Sensitivity of curving performance and tangent track critical speed of conventional system to variation in effective wheel conicity, (ϕ_d=0)

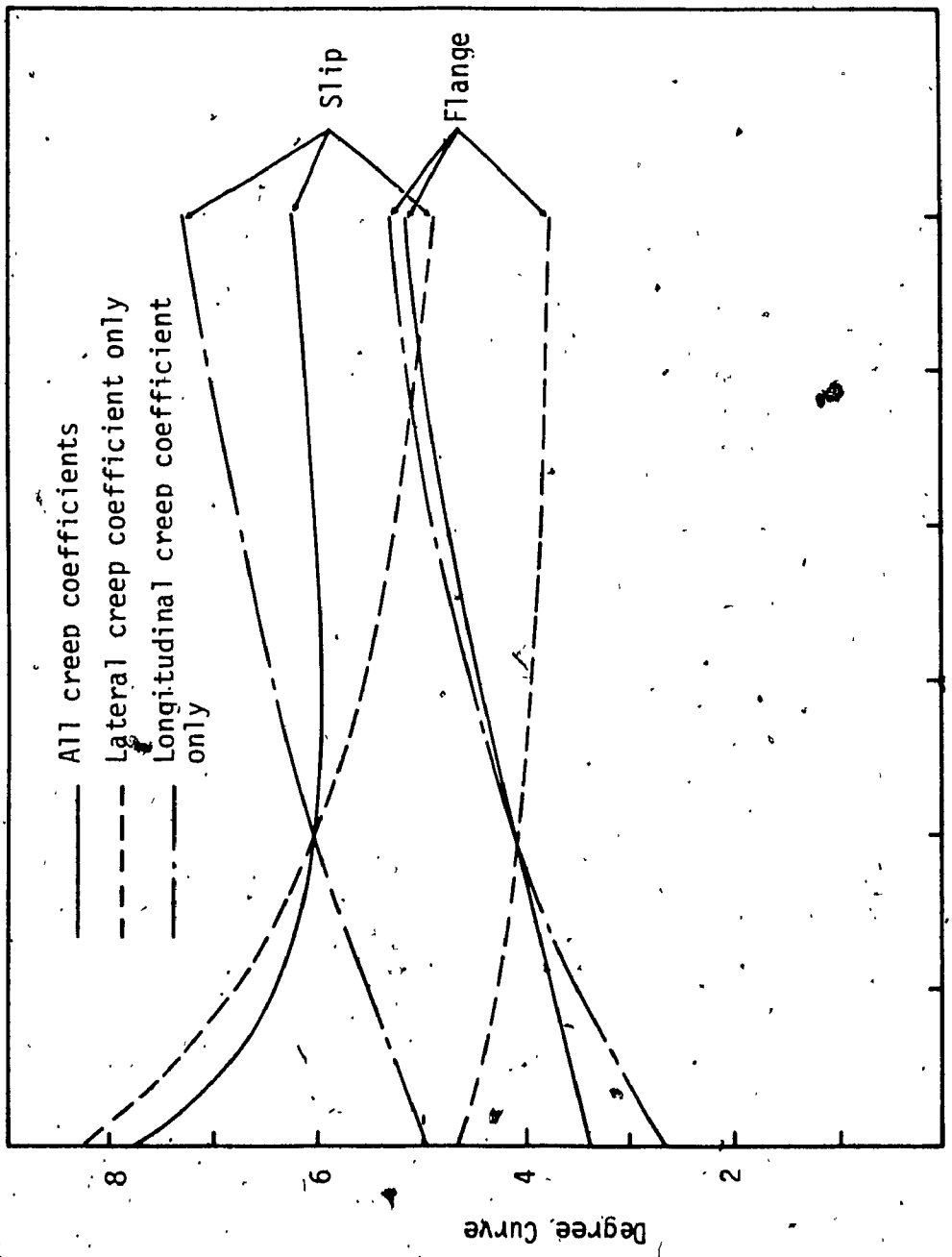

Figure 7.8 Effect of creep coefficients on the slip and flange boundaries of conventional system.

coefficients are increased, the slip boundary in not significantly affected. But when reduced, the slip performance improves in terms of ability to negotiate tighter curve. For the same variation, flange boundary on the other hand reduces with the reduced creep coefficients. This indicates that reduction in creep force results in greater wheelset displacement in order to generate the creep force necessary to negotiate a curve under the guidance of creep.

As Figure 7.8 indicates, when lateral creep coefficient alone is reduced while other creep coefficients are kept equal to their nominal values, the slip boundary improves significantly while flange boundary remains relatively unaffected. The effect of varying longitudinal creep coefficient alone, results on the other hand, in a significant variation of both slip and flange boundaries. However, in this case, curving performance in terms of both slip and flange boundary deteriorates with reduced longitudinal creep coefficient. This behaviour results from loss of longitudinal creep force, to cause the wheelsets to yaw for radial alignment, and leads to greater tracking error. As a result, the wheelsets tend to slip and flange on a less tighter curve.

Hence, it appears that, for improving curving performance of conventional system, reduction in longitudinal creep force is undesirable. In the following sub-section, detailed results from steady-state curving analysis of the truck model with EDCW are presented and discussed.

7.4.2 Truck Model with EDCW

In this section, the truck model with EDCW is considered to

determine the effect of wheelset coupler on the curving behaviour. The various steps used in this analysis are identical to those followed in the analysis of conventional system. Both unrestrained and restrained wheelsets are first considered under balanced running condition, to examine the influence of wheelset coupler damping on the steady-state curving response. The response is computed in terms of tracking error (lateral displacement) and misalignment (angle of attack). The effect of coupler parameter on the curving performance of baseline truck model is then determined in the presence of cant deficiency. Finally, limited but detailed parametric study is carried out to study the influence of important model parameters on the curving performance of the EDCW system.

7.4.2.1 Influence of Wheelset Coupler on Curving Behaviour

For an unrestrained ($k_{y_p} = k_{\psi_p} = 0$) EDCW under balanced running condition ($\phi_d = 0$), results are obtained in terms of lateral and yaw responses to track curvature as coupler damping parameter $C_{D_{AX}}$ is varied. Figure 7.9 shows the lateral response to track curvature versus $C_{D_{AX}}$ for various wheel conicities. As the figure indicates, when there is no coupling (IRW), the loss of guidance results in excessive lateral response. Further, for very small values of $C_{D_{AX}}$, the lateral response of leading wheelset is greater than that of trailing wheelset. As $C_{D_{AX}}$ is increased, the lateral response rapidly decreases and approaches the value corresponding to rigid axle wheelset. The results further indicate, that as wheel conicity is increased the influence of $C_{D_{AX}}$ on the lateral response is reduced. For the unrestrained EDCW, $C_{D_{AX}}$ on the other hand, has no influence on the wheelset yaw response. For all values of $C_{D_{AX}}$ leading and trailing wheelsets yaw in opposite directions

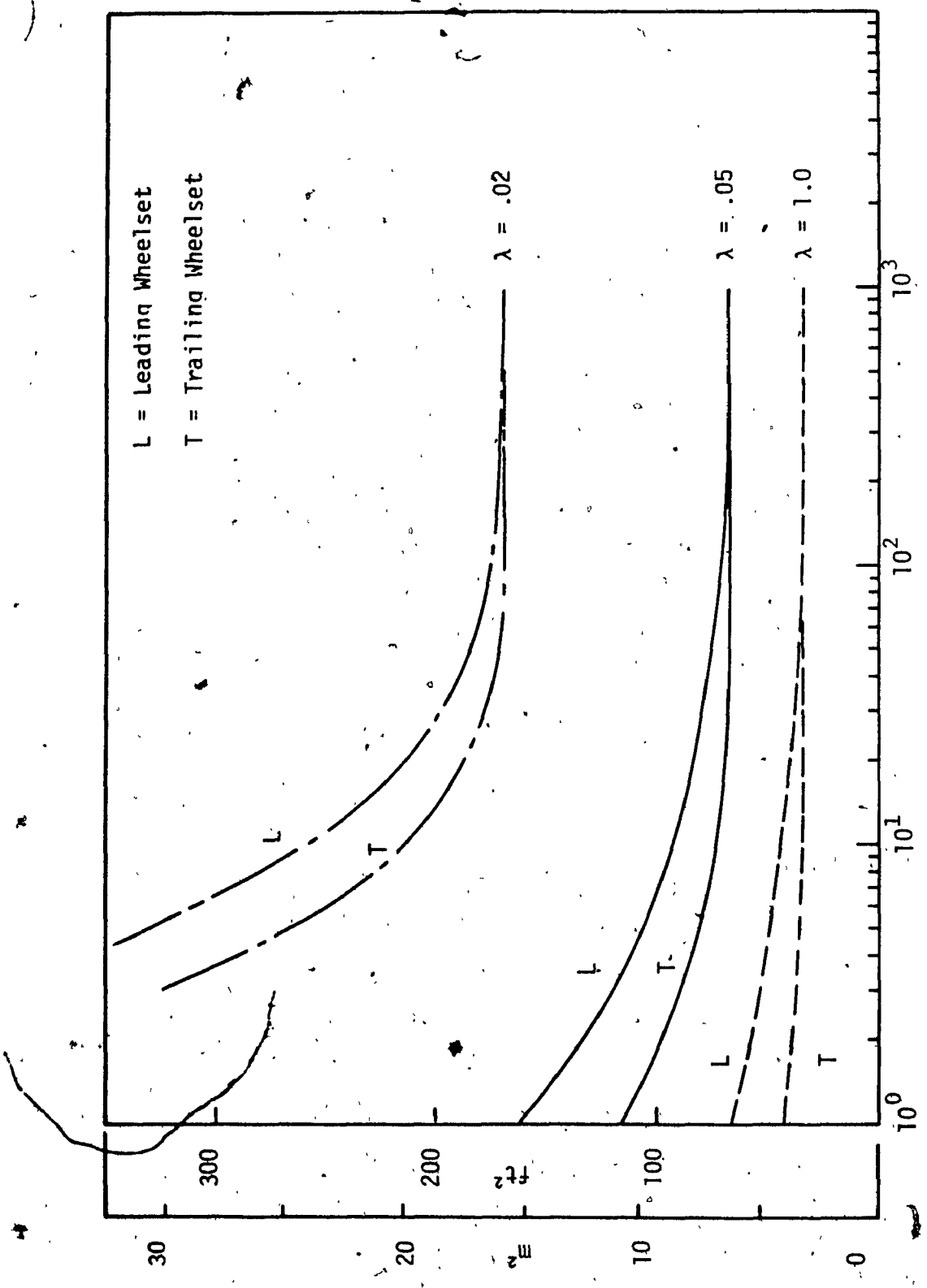

Figure 7.9 Influence of coupler parameter ($C_{D_{AX}}$) on the unrestrained wheelset lateral response to track curvature, for different values of wheel conicity, ($\phi_d = 0$).

to align themself radially with the track.

For a restrained EDCW, in the presence of finite primary suspension stiffness, the influence of $C_{D_{AX}}$ on the lateral and yaw responses to track curvature are next examined. Figure 7.10 shows lateral response versus $C_{D_{AX}}$ for various values of k_{ψ_p}, while all the other parameters are equal to their nominal values. In general, as $C_{D_{AX}}$ is increased, the lateral response reduces, and approaches the value corresponding to conventional system for a very large value of $C_{D_{AX}}$, where the lateral response to track curvature is a minimum. For identical variation of parameters, Figure 7.11 shows the yaw response to track curvature. In this case for smaller values of $C_{D_{AX}}$, yaw misalignment for both leading and trailing wheelsets are in the same direction. Further, the misalignment of leading wheelset is significantly greater than that of trailing wheelset. As $C_{D_{AX}}$ is increased, the leading wheelset misalignment reduces, while that of trailing wheelset first reduces to zero and then increases in the negative direction. For very large values of $C_{D_{AX}}$, misalignment of both wheelsets reduces and approaches the values corresponding to rigid axle. From Figure 7.11 it is also evident that k_{ψ_p} has significantly less influence on misalignment for smaller values of $C_{D_{AX}}$. The results further show that misalignment for both wheelsets are minimum for rigid axle system with soft primary yaw stiffness.

To examine the influence of primary lateral stiffness (k_{y_p}) similar results are also obtained for various values of k_{y_p}. Figures 7.12 and 7.13 show lateral and yaw misalignment responses, respectively, to track curvature as $C_{D_{AX}}$ is increased, for various values of k_{y_p}. The effects are very similar but are less than that of k_{ψ_p} variation presented in

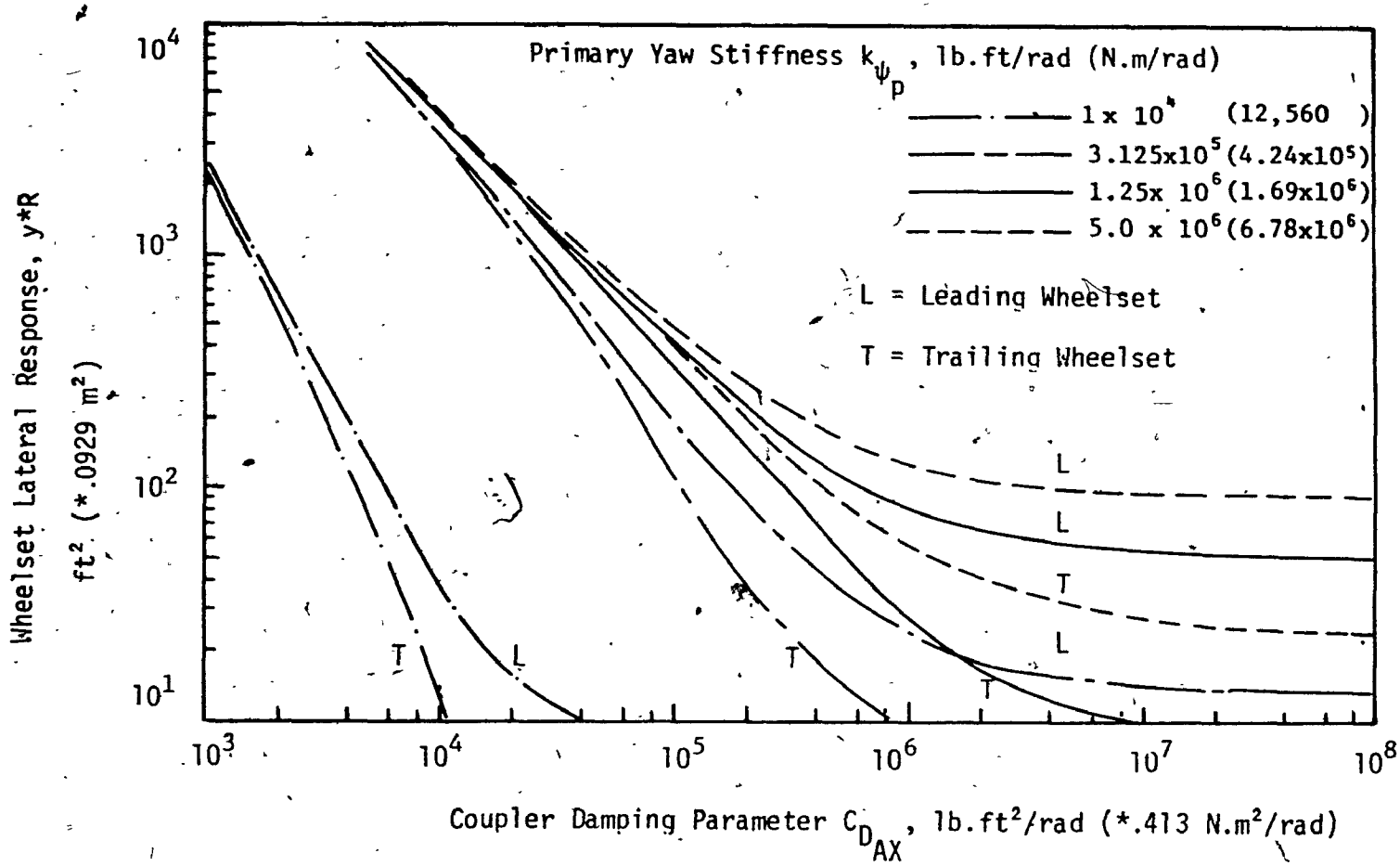

Figure 7.10 Influence of coupler parameter $C_{D_{AX}}$ on the restrained wheelset lateral response to track curvature, for different values of primary yaw stiffness, ($\phi_d = 0$).

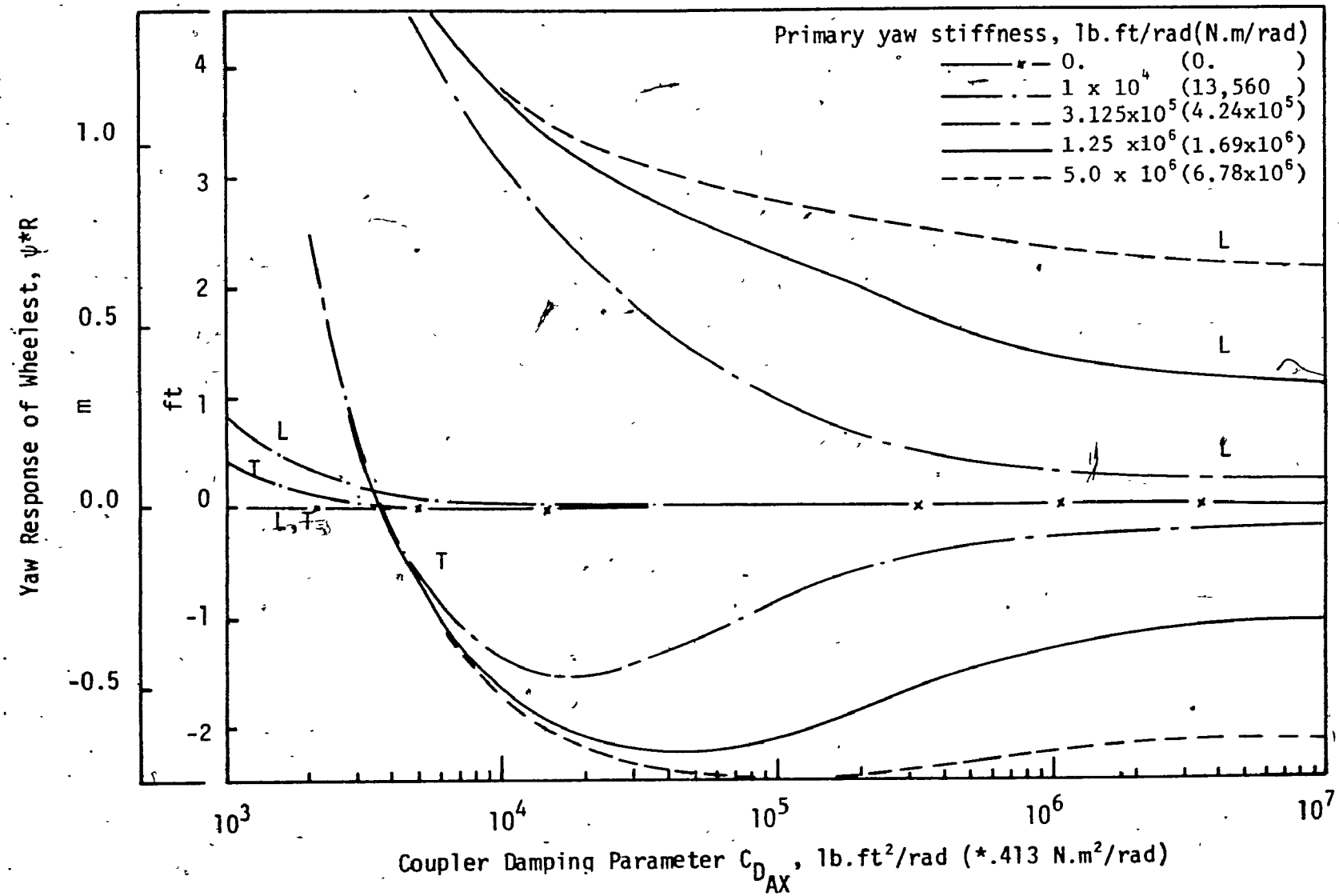

Figure 7.11 Influence of coupler parameter $C_{D_{AX}}$ on the restrained wheelset yaw response to track curvature, for different values of primary yaw stiffness, ($\phi_d = 0$).

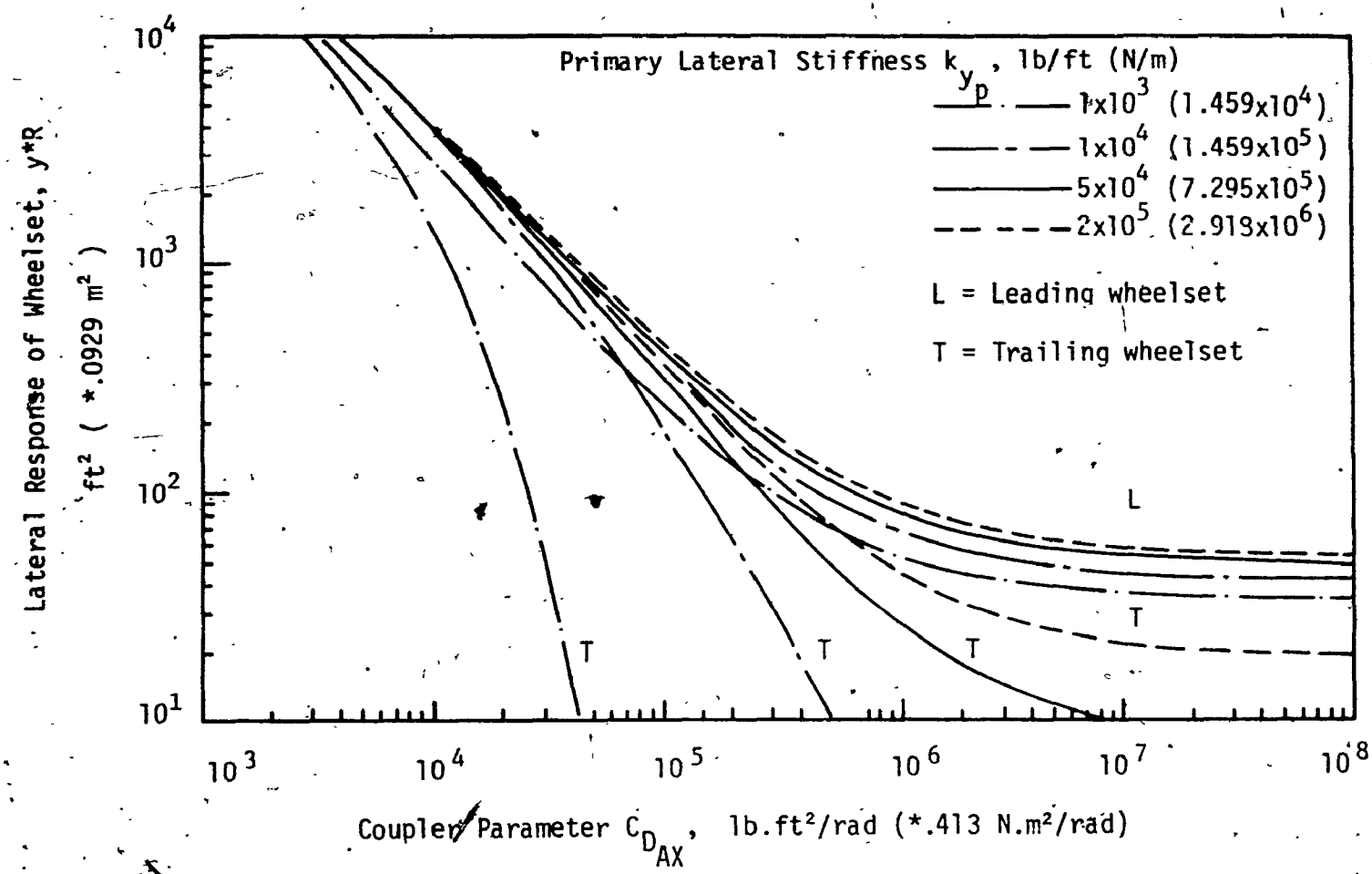

Figure 7.12 Influence of coupler parameter $C_{D_{AX}}$ on the wheelset lateral response to track curvature, for different values of primary lateral stiffness, ($\phi_d = 0$).

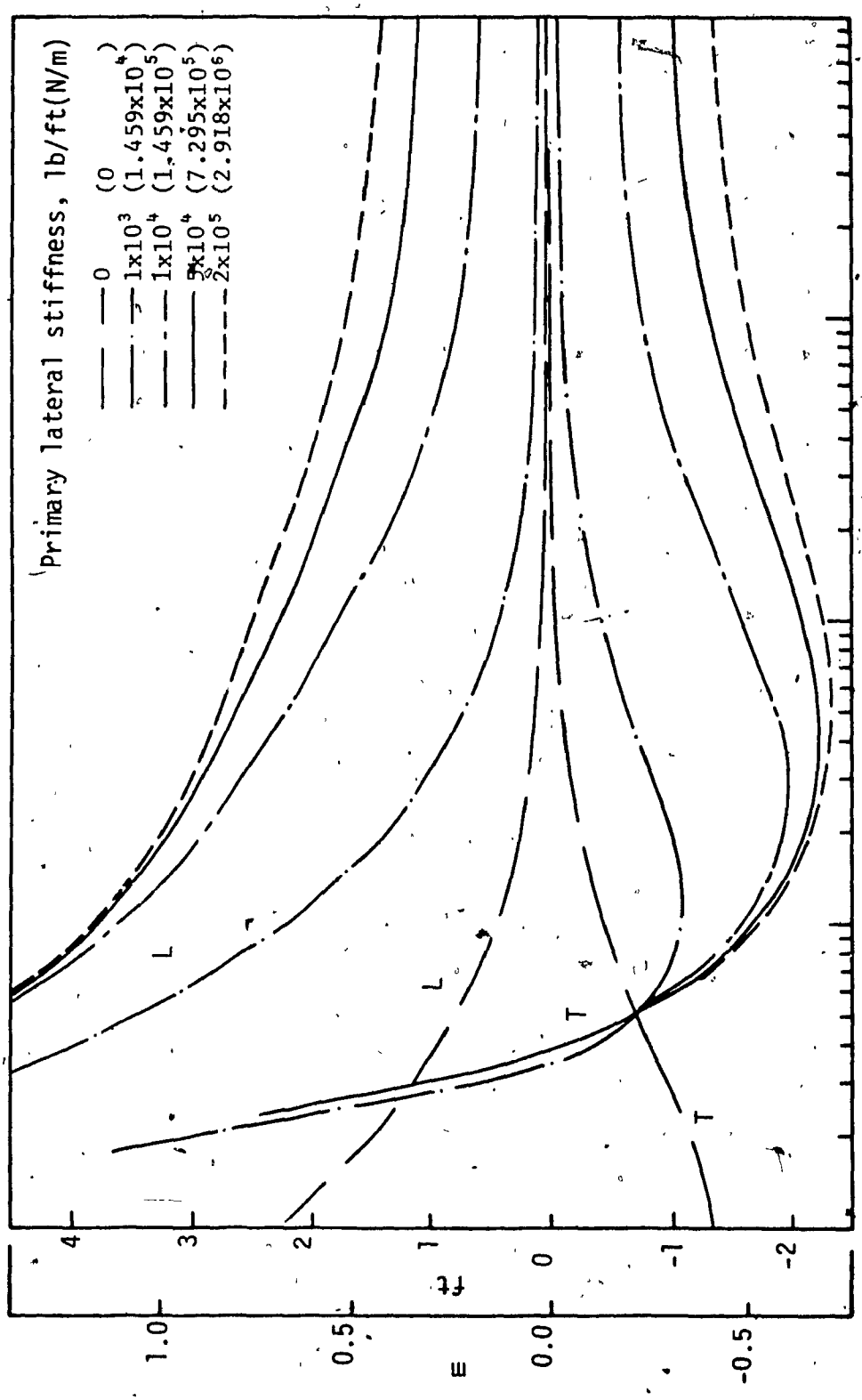

Figure 7.13 Influence of coupler parameter $C_{D_{AX}}$ on the wheelset yaw response to track curvature, for different values of primary lateral stiffness, ($\phi_d = 0$).

Figures 7.10 and 7.11.

The influence of $C_{D_{AX}}$ on curving response examined so far are for balanced running ($\phi_d = 0$) condition. Figures 7.14 and 7.15 show the effect of cant deficiency, ϕ_d on the lateral and yaw response of wheelsets as $C_{D_{AX}}$ is varied. These results are obtained for ϕ_d in the range of $\pm 4^o$, and for 2 degree curve. As Figure 7.14 indicates, lateral response of trailing wheelset is only affected by ϕ_d, where positive cant deficiency increases the response while negative cant deficiency reduces the response significantly. In all cases, lateral response is minimum for large value of $C_{D_{AX}}$. For all values of $C_{D_{AX}}$ the influence of ϕ_d on yaw misalignment on the other hand, is identical for both leading and trailing wheelsets. For positive cant deficiency leading wheelset misalignment decreases, while that of trailing wheelset increases, and vice-versa.

The effects of $C_{D_{AX}}$ on curving response indicate, that lateral response is minimum for rigid axle wheelsets (for large value of $C_{D_{AX}}$). The same is true for yaw misalignment except for $C_{D_{AX}}$ in the vicinity of 1.45×10^3 N.m^2/rad (3.5×10^3 lb.ft^2/rad), at which for balanced running, the trailing wheelset misalignment is zero. But for leading wheelset minimum misalignment is provided by rigid axle.

Finally, in this section, curving performance of the truck model with EDCW is determined for various values of $C_{D_{AX}}$. Figure 7.16 shows the slip boundaries as track curvature that can be negotiated for a cant deficiency without any of the wheels sliping. As the results indicate, reduction in the value of $C_{D_{AX}}$ causes significant reduction in the curving performance. The effect of reducing $C_{D_{AX}}$ is, however, less for

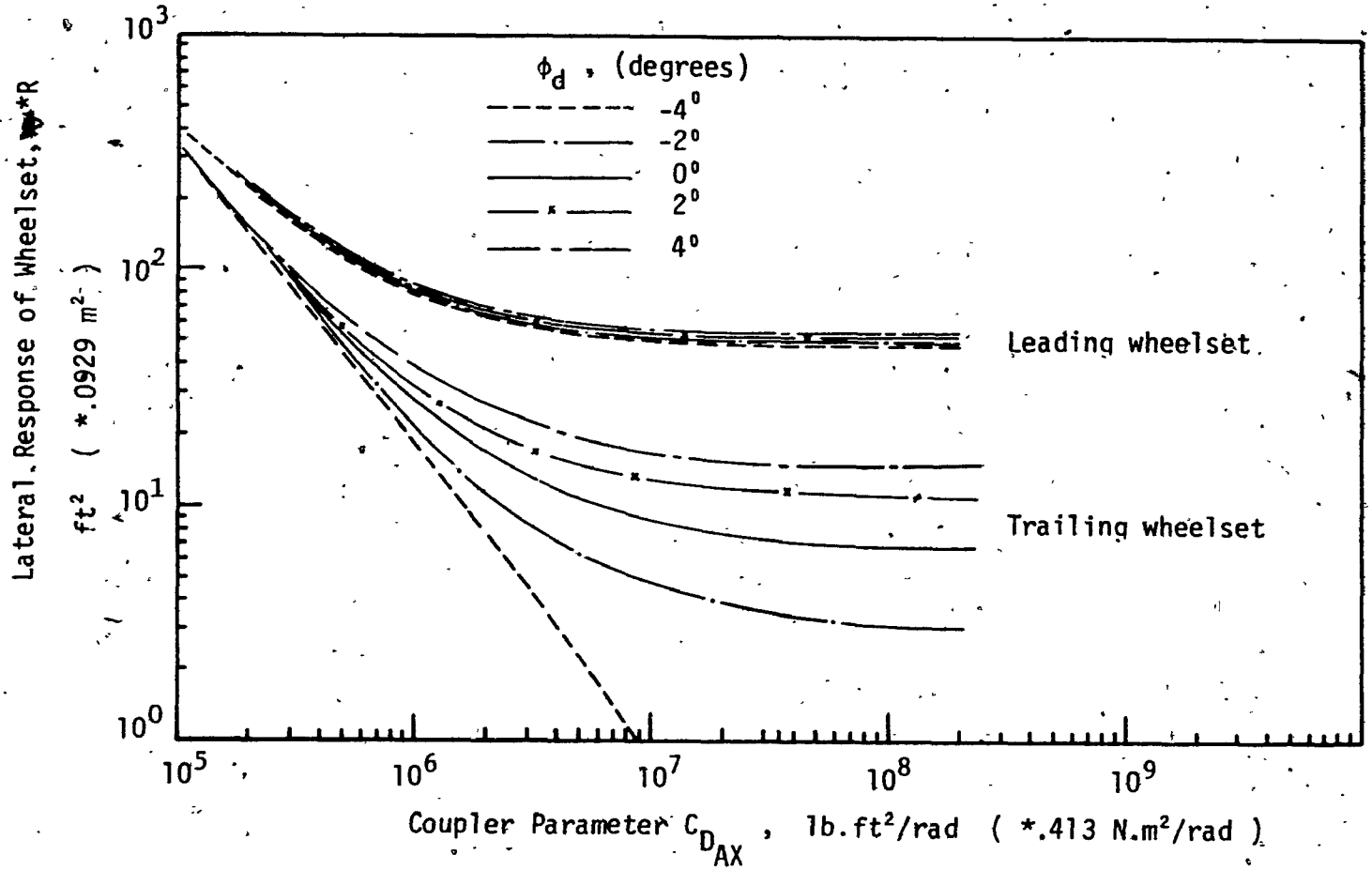

Figure 7.14 Influence of cant deficiency ϕ_d on the wheelset lateral response as coupler parameter $C_{D_{AX}}$ is increased, (R = 2°).

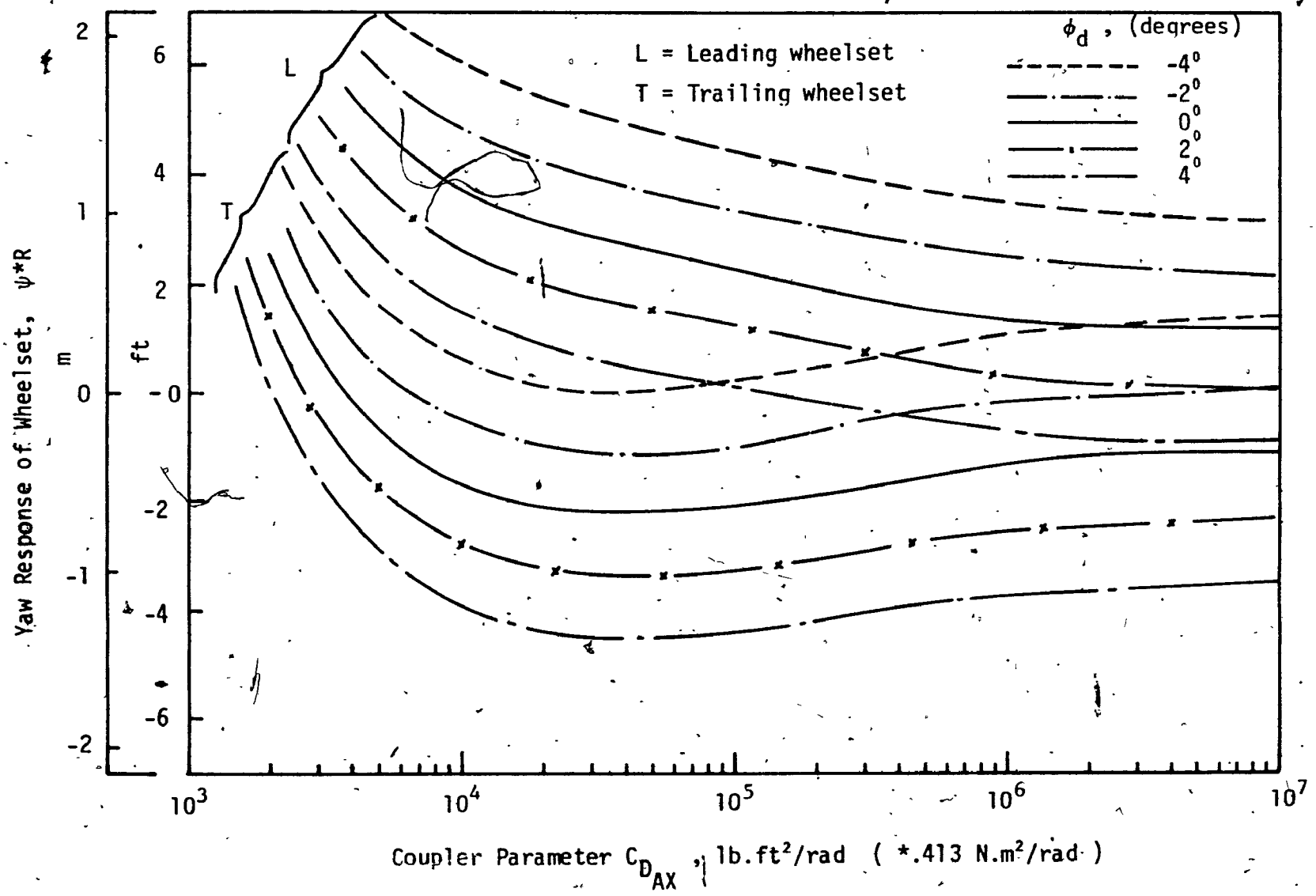

Figuer 7.15 Influence of cant deficiency ϕ_d on the wheelset yaw response as coupler parameter $C_{D_{AX}}$ is increased, (R = 2°)

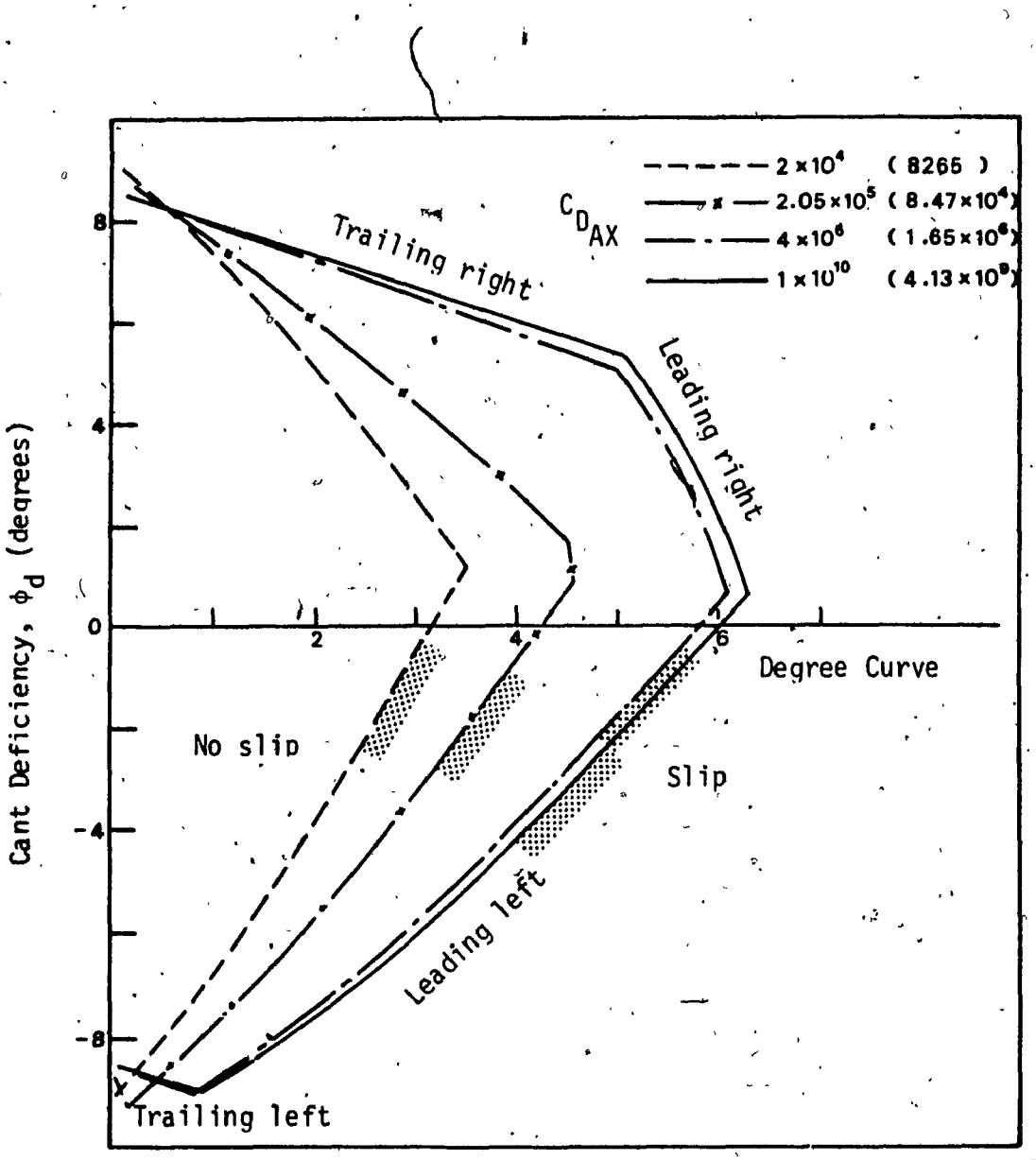

Figure 7.16 Steady-state curving performance (slip boundary) of truck model with SDCW for various values of coupler parameter $C_{D_{AX}}$

larger values of cant deficiency. For the values of $C_{D_{AX}}$ considered, flange boundary is not affected by ϕ_d. The slip boundary as well as flange boundary for balanced running, as a function of $C_{D_{AX}}$ is presented in Figure 7.17. The sensitivity of both slip and flange boundaries to $C_{D_{AX}}$ are very similar, where very large value of $C_{D_{AX}}$ aids in negotiating a curve of minimum radius (maximum degree curve) without flanging or wheel slip taking place.

7.4.2.2 Influence of Model Parameters

In this section, the influences of selected model parameters on the curving performance of truck model with EDCW are examined. Results are obtained for variation in one parameter at a time, for various values of $C_{D_{AX}}$. The parametric sensitivity of curving performance for the model with optimal coupler parameter corresponding to tangent track stability is examined. Results of parametric sensitivity of curving performance are compared to those of stability on tangent track. The results are further compared with those corresponding to conventional wheelset system.

The parameters considered are, primary yaw and lateral stiffness, and effective wheel conicity. The results are obtained for values of $C_{D_{AX}}$ in the range of 4.13×10^3 to 4.13×10^9 N.m^2/rad (10^4 to 10^{10} lb.ft^2/rad), where the largest value simulates rigid axle, giving identical results to those obtained earlier for conventional model. In this section, the optimal wheelset coupler parameter is the speed dependent coupler damping constant $C_{D_{AX}} = 8.47 \times 10^4$ N.m^2/rad (2.05×10^5 lb.ft^2/rad), which corresponds to the maximum critical speed of the

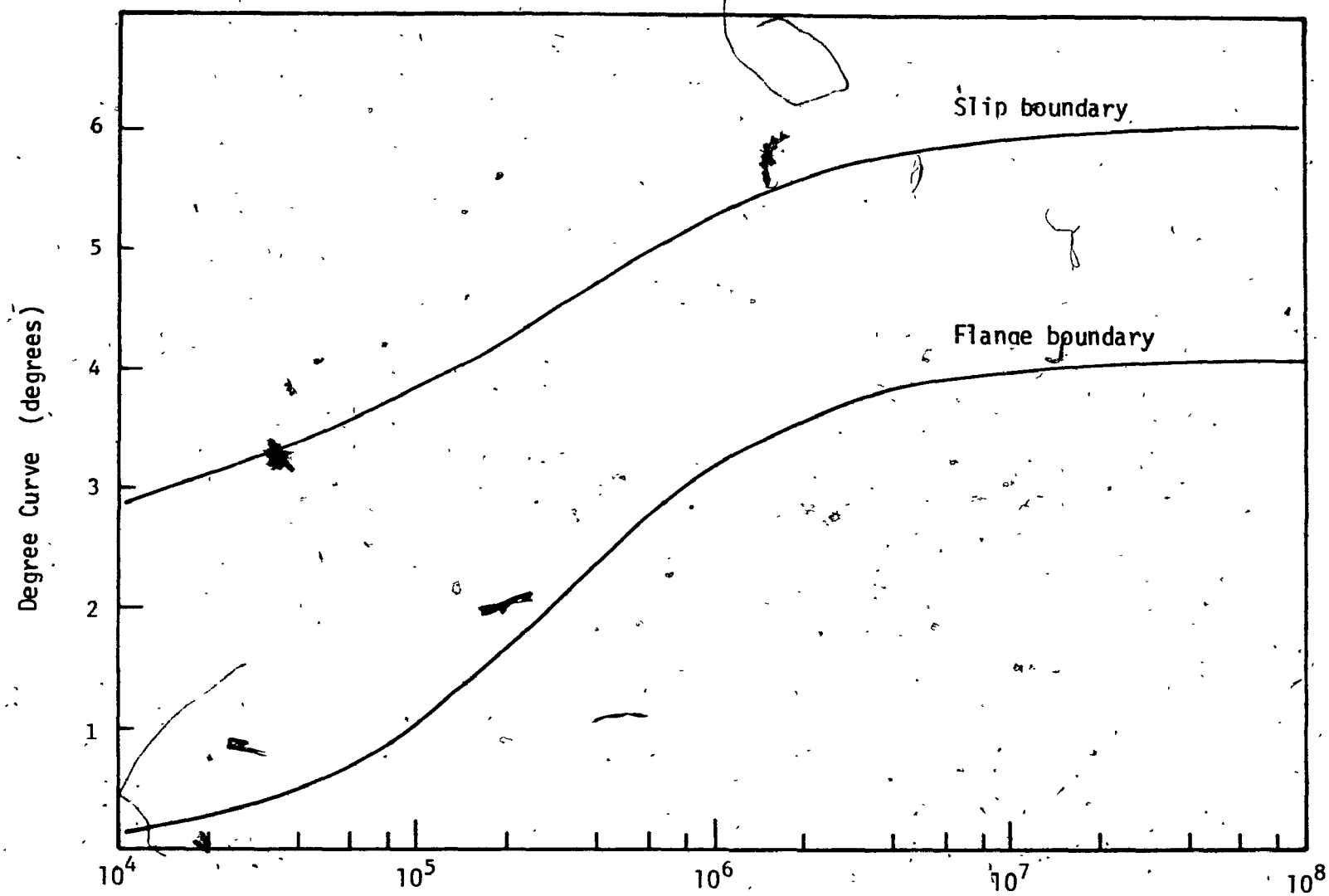

Figure 7.17 Influence of coupler parameter $C_{D_{AX}}$ on the track curvature that can be negotiated without wheel slip and flange contact, for balanced running.

baseline truck model on tangent track. In the following studies balanced running is only considered.

Influence of Primary Yaw Stiffness (k_{ψ_p})

As identified earlier, k_{ψ_p} is one of the most important parameters with regard to both curving and stability performance. Figures 7.18 and 7.19 show the sensitivity of lateral and yaw responses to track curvature, respectively, as k_{ψ_p} is varied, for various values of $C_{D_{AX}}$. Both lateral and yaw responses to track curvature increase with increase in k_{ψ_p}. When $C_{D_{AX}}$ is reduced from rigid coupler, the lateral response increases significantly in comparison to rigid coupler. The yaw response on the other hand, is somewhat less sensitive to decrease in $C_{D_{AX}}$, as k_{ψ_p} is varied. Reduction of coupler parameter $C_{D_{AX}}$ from a large to optimal value, has significantly less influence on misalignment, compared to lateral response as shown in Figures 7.18 and 7.19.

The sensitivity of slip and flange boundaries to variation in k_{ψ_p}, for various values of $C_{D_{AX}}$ are shown in Figures 7.20 and 7.21, respectively. When k_{ψ_p} is increased, the curving performance decreases with regard to both slip and flange boundaries. When $C_{D_{AX}}$ is reduced (Figure 7.20), the slip boundary reduces for relatively smaller values of k_{ψ_p}, and increases slightly for larger values of k_{ψ_p}. Whereas, the flange boundary (Figure 7.21) shows a large decrease as $C_{D_{AX}}$ is reduced, for all values of k_{ψ_p}. These results further show, that the curving performance sensitivity to k_{ψ_p} reduces with reduction in $C_{D_{AX}}$. Figure 7.22 shows both slip and flange boundaries for the truck model with rigid wheelset coupler, as well as for optimal value of coupler parameter

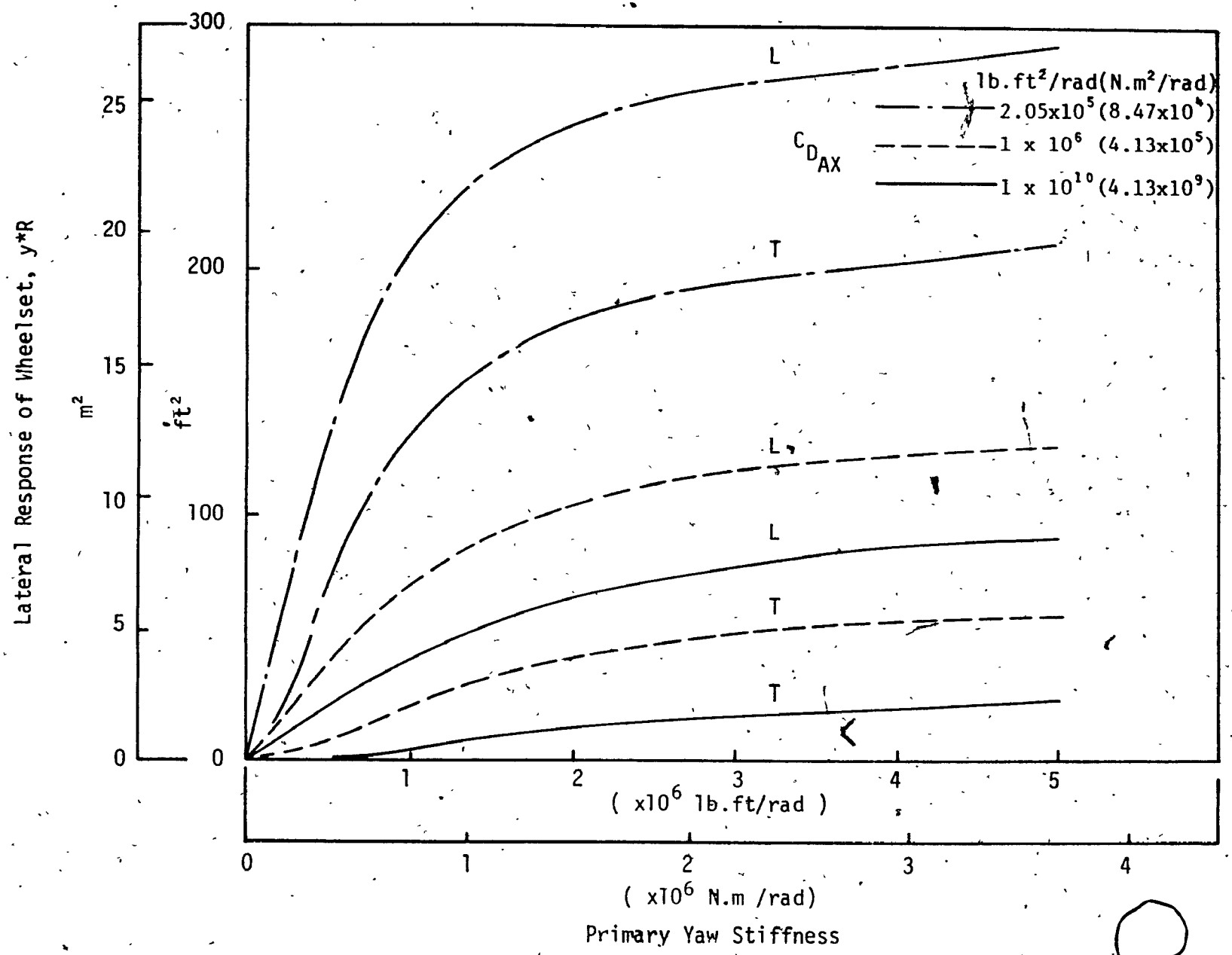

Figure 7.18 Effect of primary yaw stiffness variation on the wheelset lateral response to track curvature for various values of $C_{D_{AX}}$, ($\phi_d = 0$)

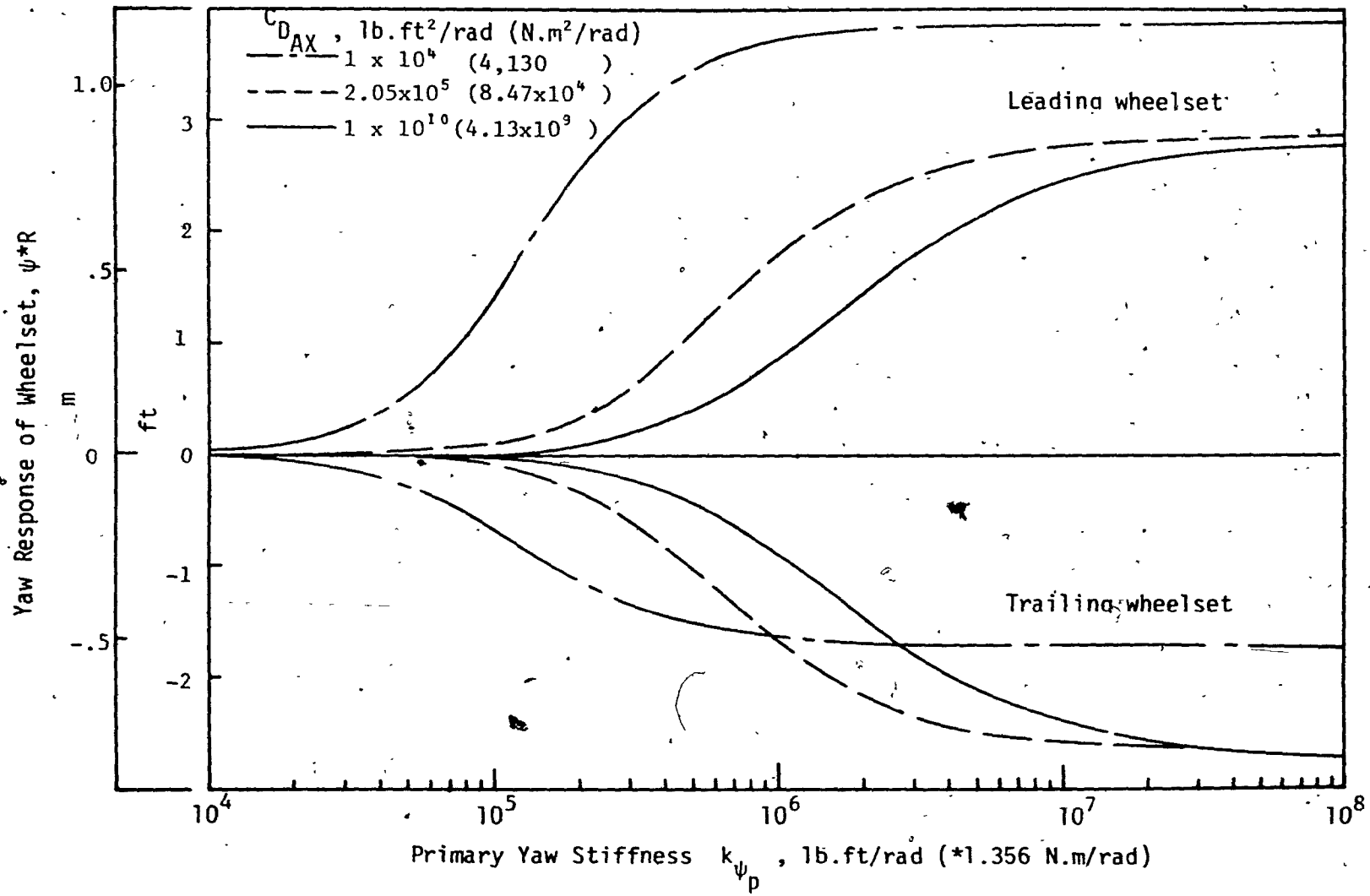

Figure 7.19 Effect of primary yaw stiffness variation on the wheelset yaw response to track curvature for various values of $C_{D_{AX}}$, ($\phi_d = 0$).

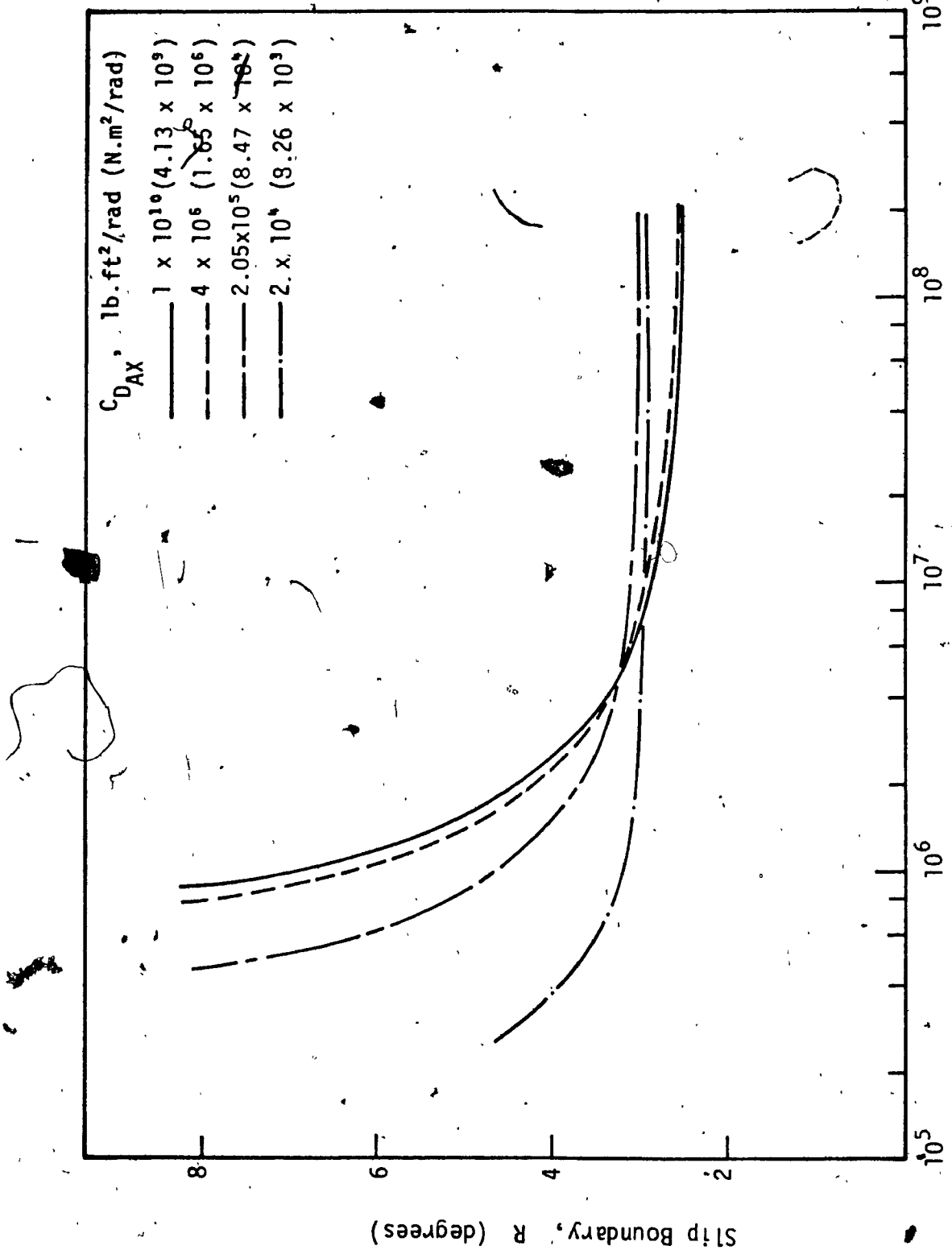

Figure 7.20 Slip boundary versus primary yaw stiffness for various values of wheelset coupler parameter $C_{D_{AX}}$ ($\phi_d = 0$).

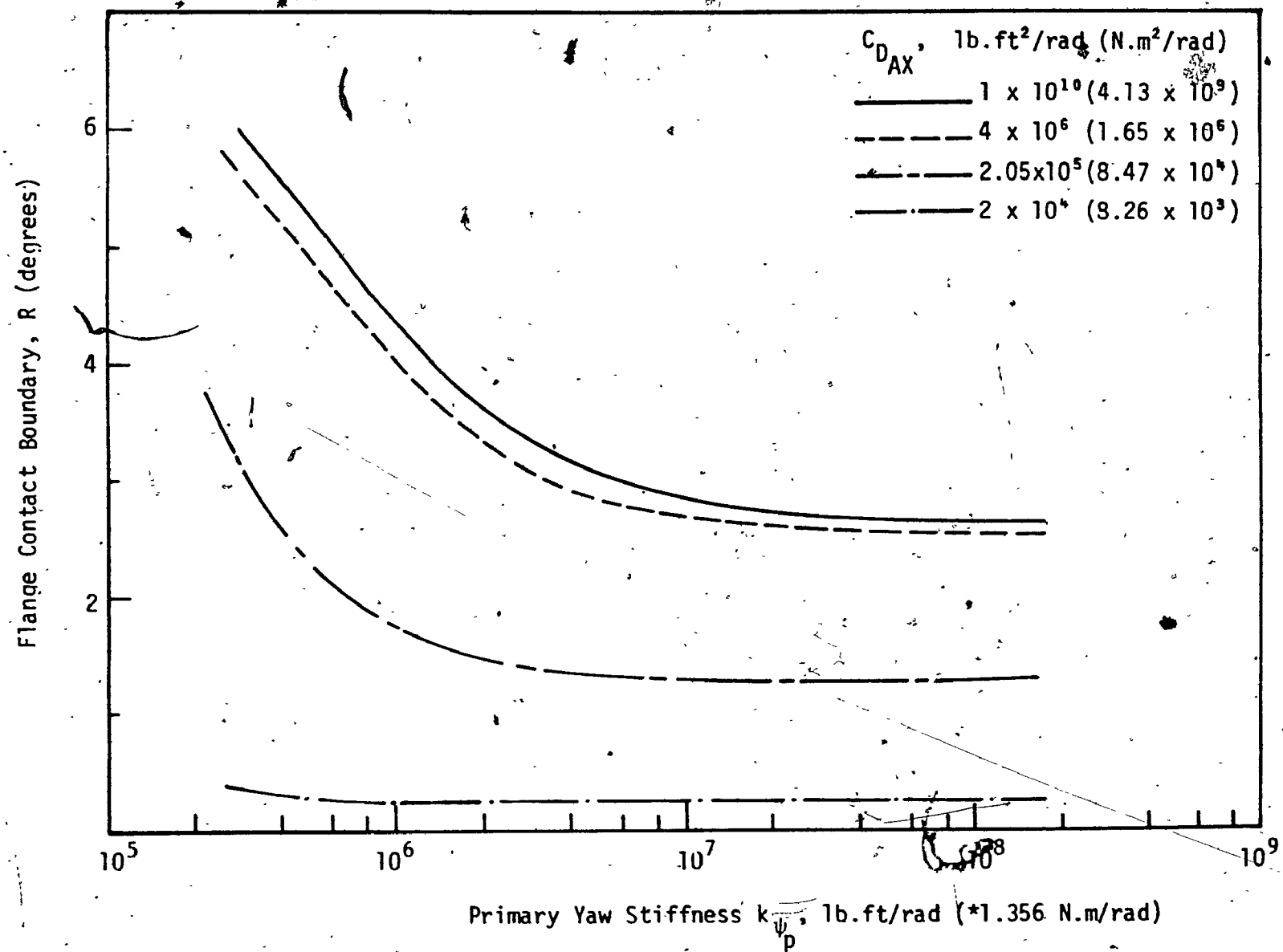

Figure 7.21 Flange contact boundary versus primary yaw stiffness for various values of wheelset coupler parameter $C_{D_{AX}}$.

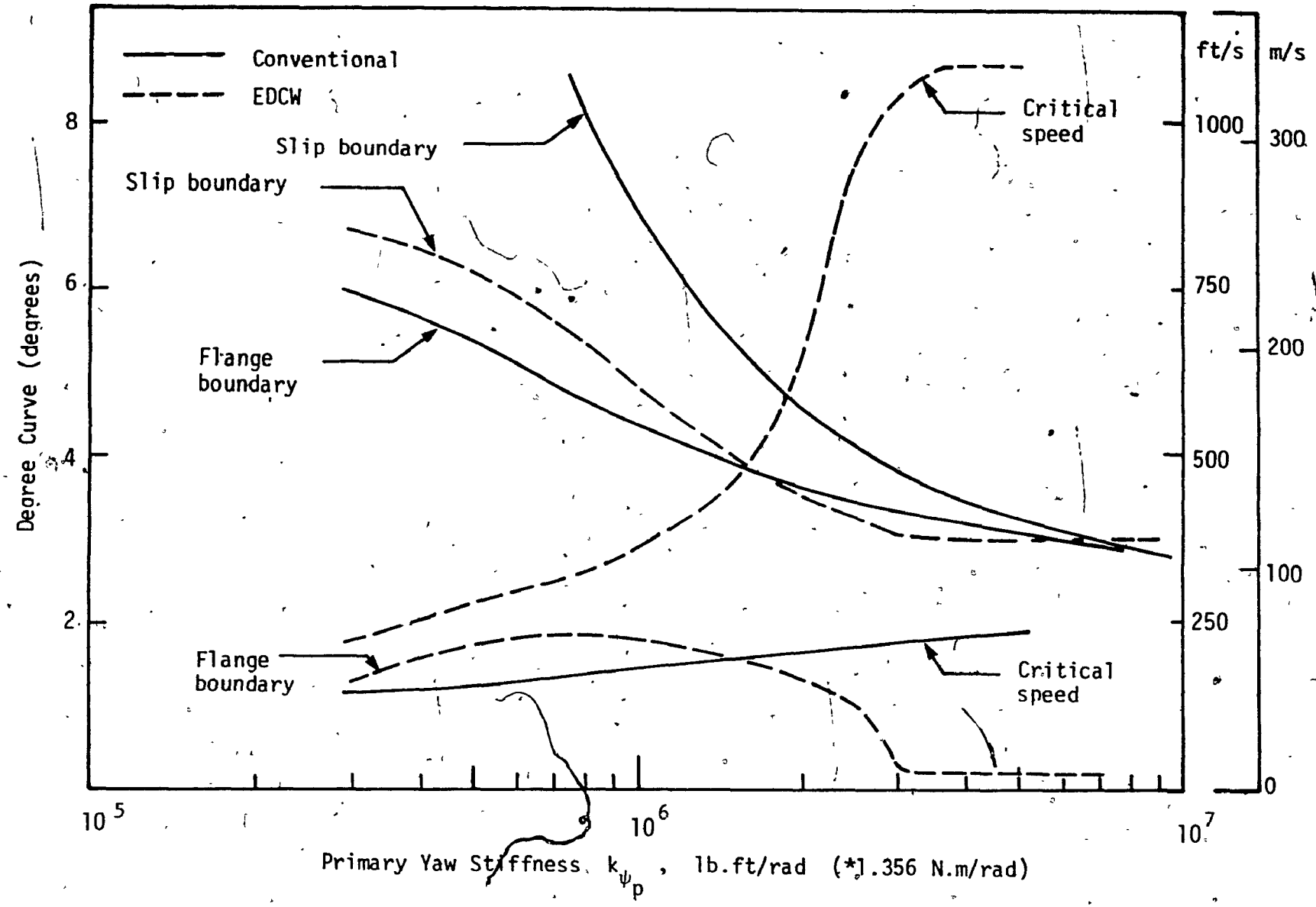

Figure 7.22 Sensitivity of curving performance and tangent track critical speed of truck model with EDCW and rigid axle wheelsets to variation in yaw stiffness, (ϕ_d=0).

$C_{D_{AX}}$, as k_{ψ_p} is varied. On the same figure, the tangent track critical speed sensitivity to k_{ψ_p} for both the models are plotted for total performance comparison. As the results show, the conventional system can negotiate tighter curve without wheel slip or flanging than that of EDCW system with optimal coupler. It is evident that EDCW will tend to flange on a very soft curve. Therefore, unless greater flange clearance is allowed, the curving will take place under the guidance of flange. As discussed earlier, this study cannot predict the ability of the truck model to negotiate a curve under flange guidance. If curving performance is compared in terms of slip boundary, the results(Figure 7.22) show that by utilizing EDCW, the critical speed can be increased dramatically with a small loss in slip curving performance for larger values of k_{ψ_p}.

Influence of Primary Lateral Stiffness (K_{y_p})

The influence of k_{y_p} on the steady-state curving response of truck model is similar to that of the influence of k_{ψ_p}. Figures 7.23 and 7.24 show the influence of k_{y_p} on the wheelsets lateral and yaw response to track curvature, respectively, for various values of $C_{D_{AX}}$. As the results indicate, the responses are more sensitive to k_{y_p} for smaller values of $C_{D_{AX}}$. The sensitivity of curving performance (slip and flange boundaries) to variation in k_{y_p} is shown in Figures 7.25 and 7.26. These results indicate, that best performance is provided by rigid axle (large $C_{D_{AX}}$), and that only slip boundary is sensitive to k_{y_p} for large values of $C_{D_{AX}}$.

Figure 7.27 shows the slip and flange boundaries as well as critical speed sensitivity to k_{y_p} for both conventional system and EDCW

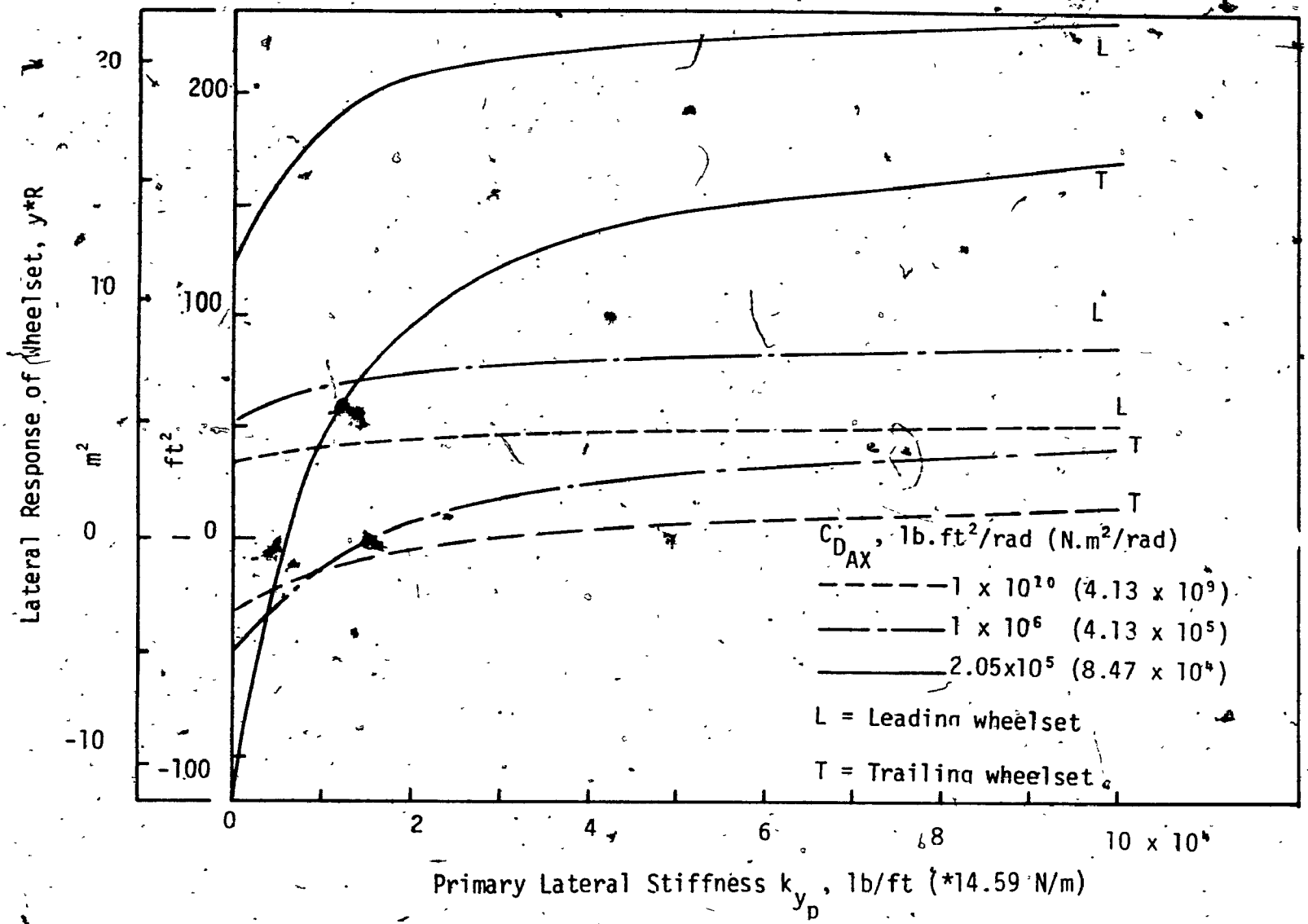

Figure 7.23 Effect of primary lateral stiffness variation on the wheelset lateral response to track curvature for various values of $C_{D_{AX}}$, ($\phi_d = 0$).

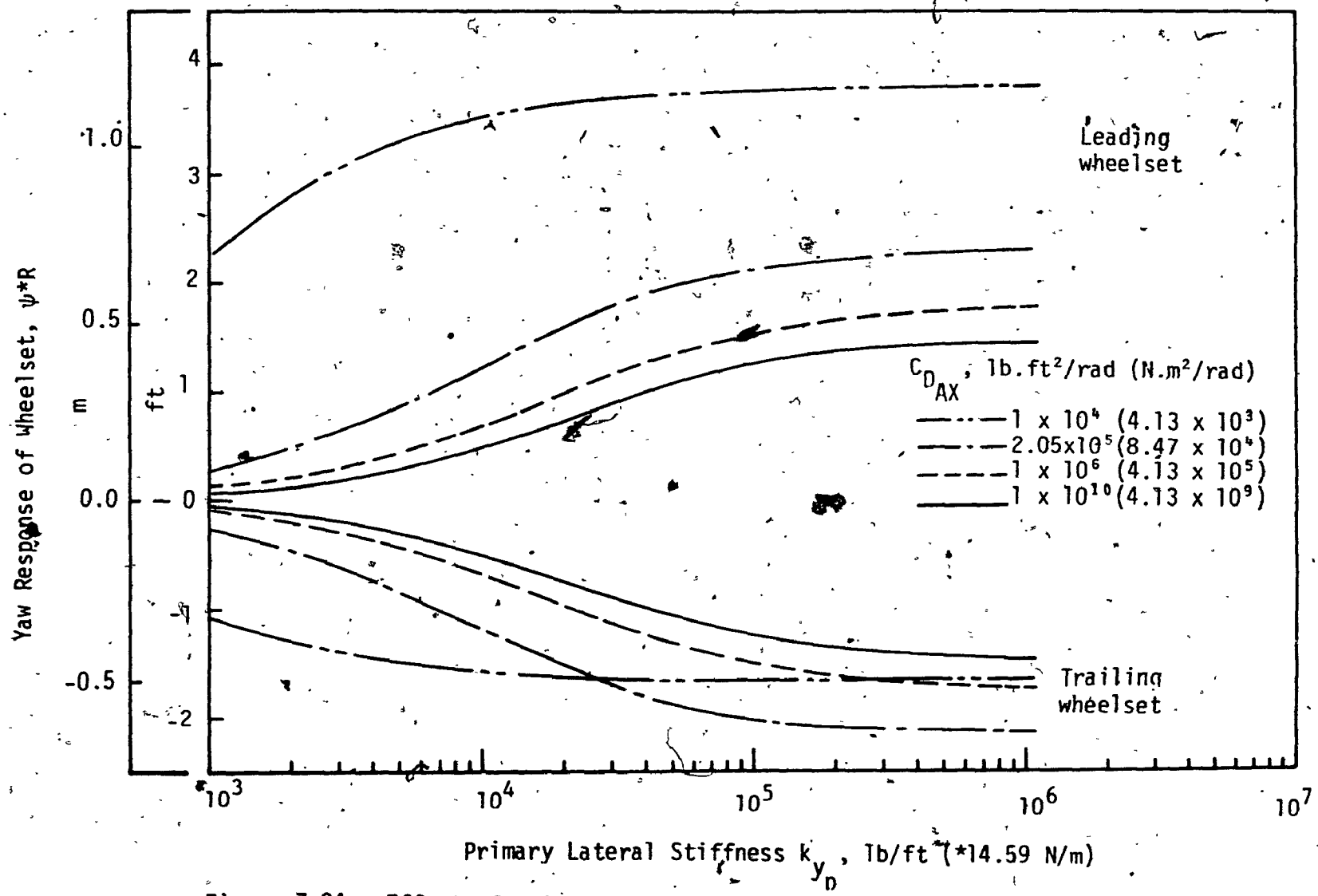

Figure 7.24 Effect of primary lateral stiffness variation of the wheelset yaw response to track curvature for various values of $C_{D_{AX}}$, ($\phi_d = 0$).

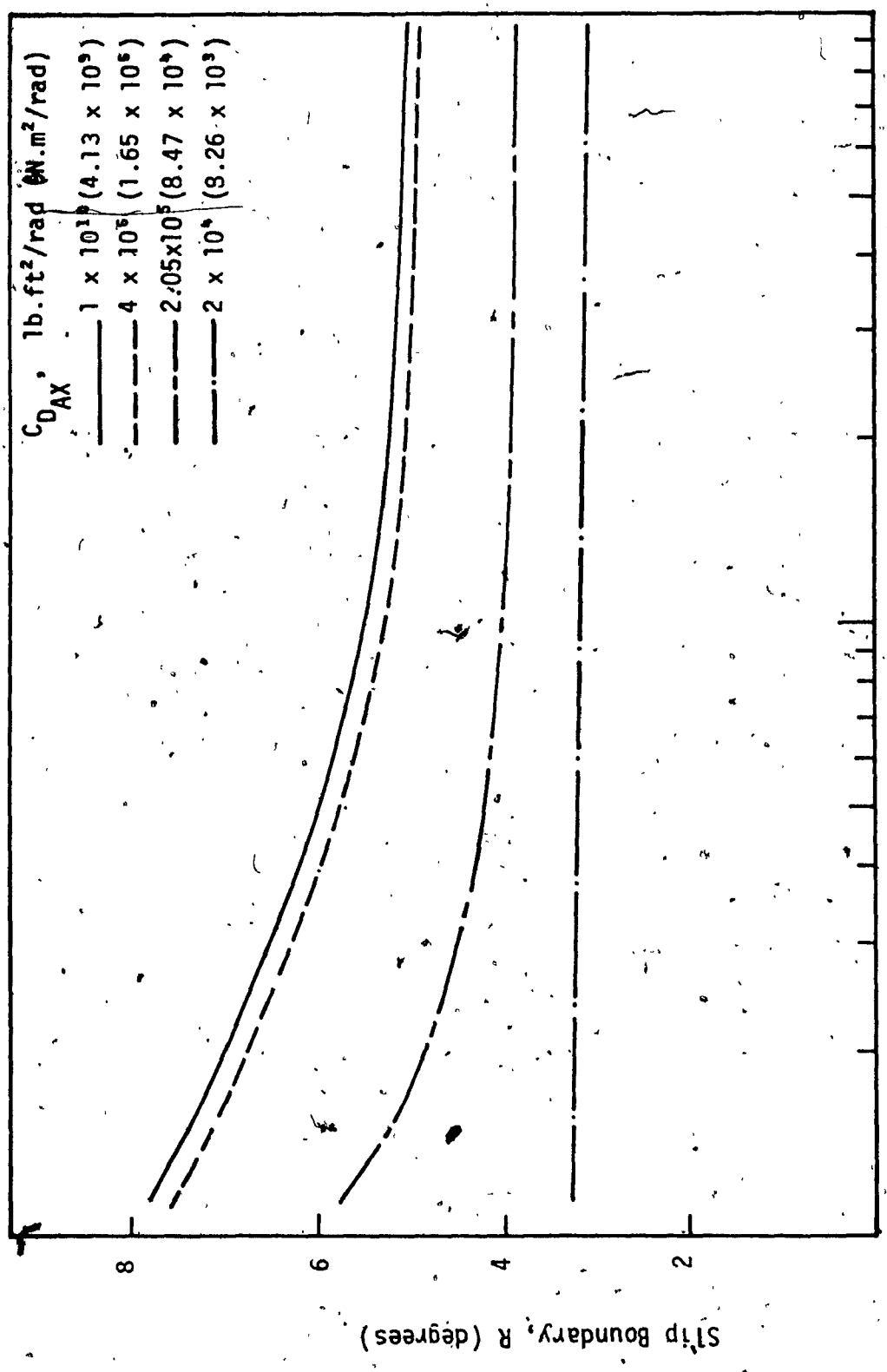

Figure 7.25 Slip boundary versus primary lateral stiffness for various values of wheelset coupler parameter $C_{D_{AX}}$.

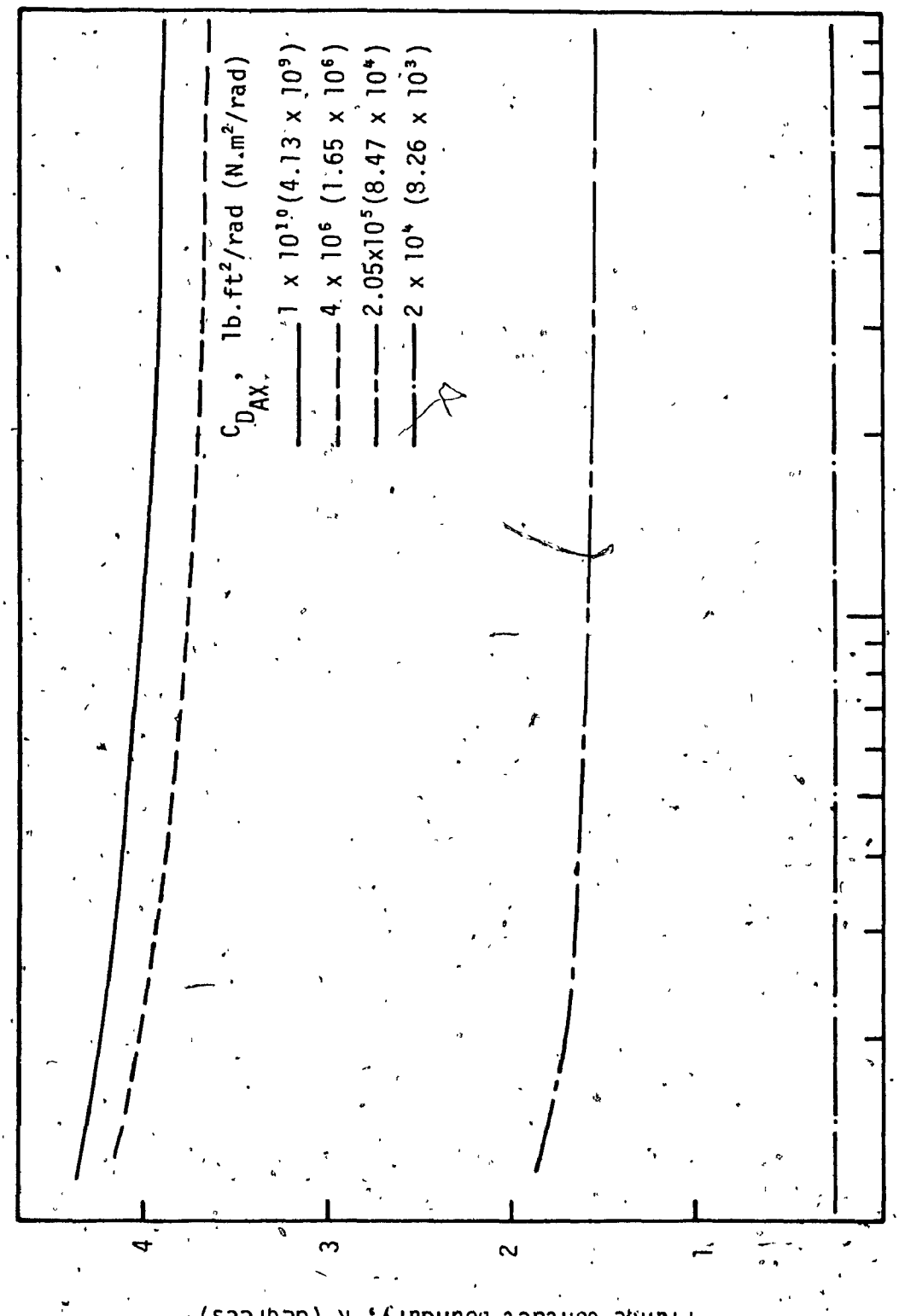

Figure 7.26 Flange boundary versus primary lateral stiffness for various values of wheelset coupler parameter $C_{D_{AX}}$

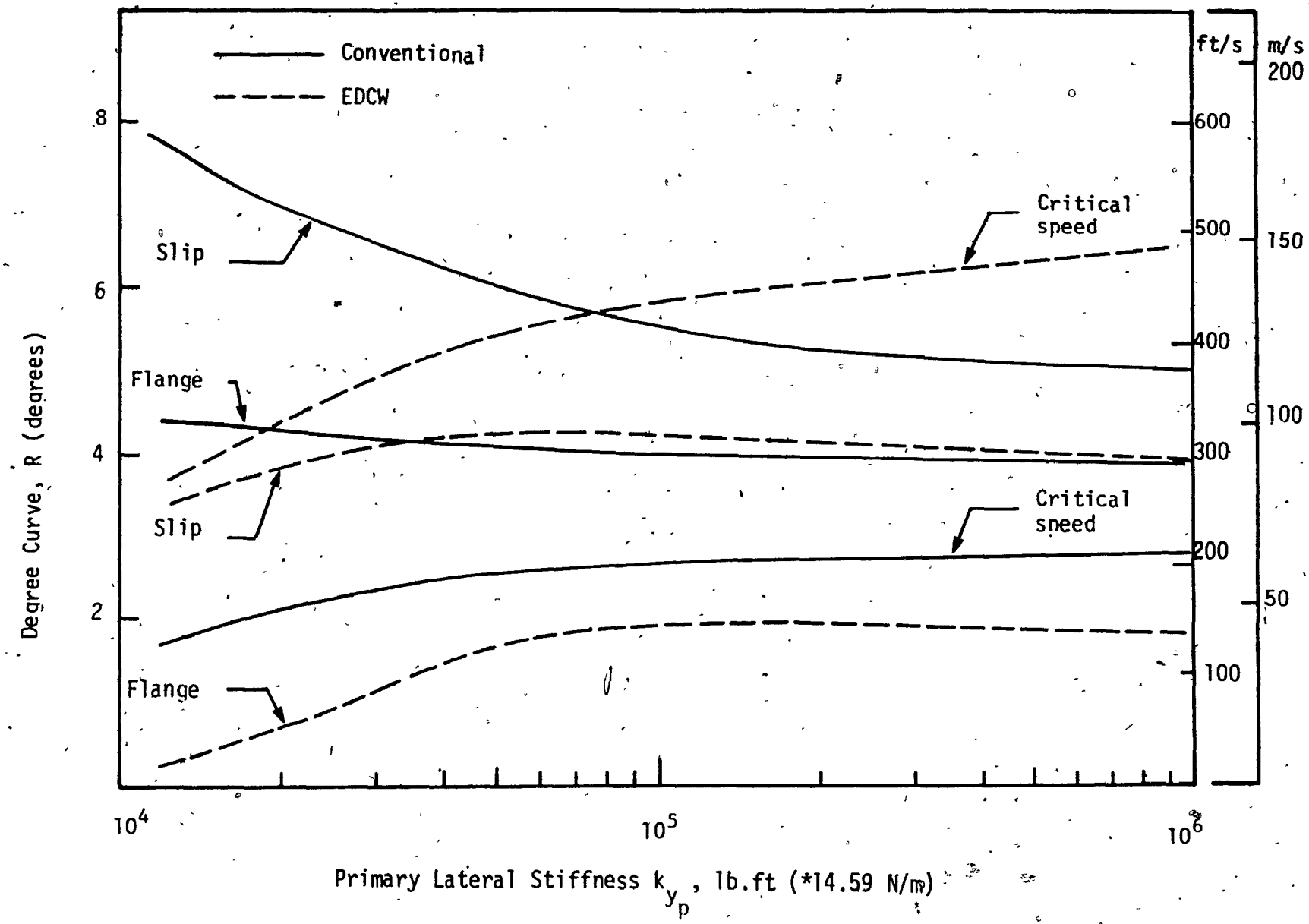

Figure 7.27 Sensitivity of curving performance and tangent track critical speed of truck model with EDCW and rigid axle wheelsets to variation in primary lateral stiffness, ($\phi_d = 0$).

system with optimal $C_{D_{AX}}$. In this case unlike conventional rigid axle system, the EDCW system does not have conflicting requirement between stability and curving. For both stability and curving improvement of truck model with EDCW, larger value of k_{y_p} is desirable.

Influence of Effective Wheel Conicity (λ)

Effective wheel conicity is one of the most sensitive parameters, for which distinct trade-off between the conventional vehicle dynamic stability and steady-state curving performance exists. In Figure 7.28, the curving performance in terms of both slip and flange contact boundaries are shown for various values of coupler parameter $C_{D_{AX}}$. For conventional rigid axle (large value of $C_{D_{AX}}$), wheel conicity has similar effect on both slip and flange boundaries, where the influence on flange boundary is more significant. This is primarily due to the role of conicity in determining the distance of the pure rolling line from the track centerline, where for smaller wheel conicity, greater lateral displacement is required to assume pure rolling.

From the results in Figure 7.28, it is evident, that when $C_{D_{AX}}$ is reduced the sensitivity of both slip and flange boundaries to wheel conicity reduces drastically. When greater differential spin is allowed between the wheels of an axle, the wheelset in no longer dependent on conicity to provide pure rolling line. At the same time loss of guidance causes the wheelset to flange on a less tighter curve.

The sensitivity of curving performance and tangent track critical speed to wheel conicity for both conventional and EDCW truck systems are shown in Figure 7.29. Clearly, the conflict between curving and

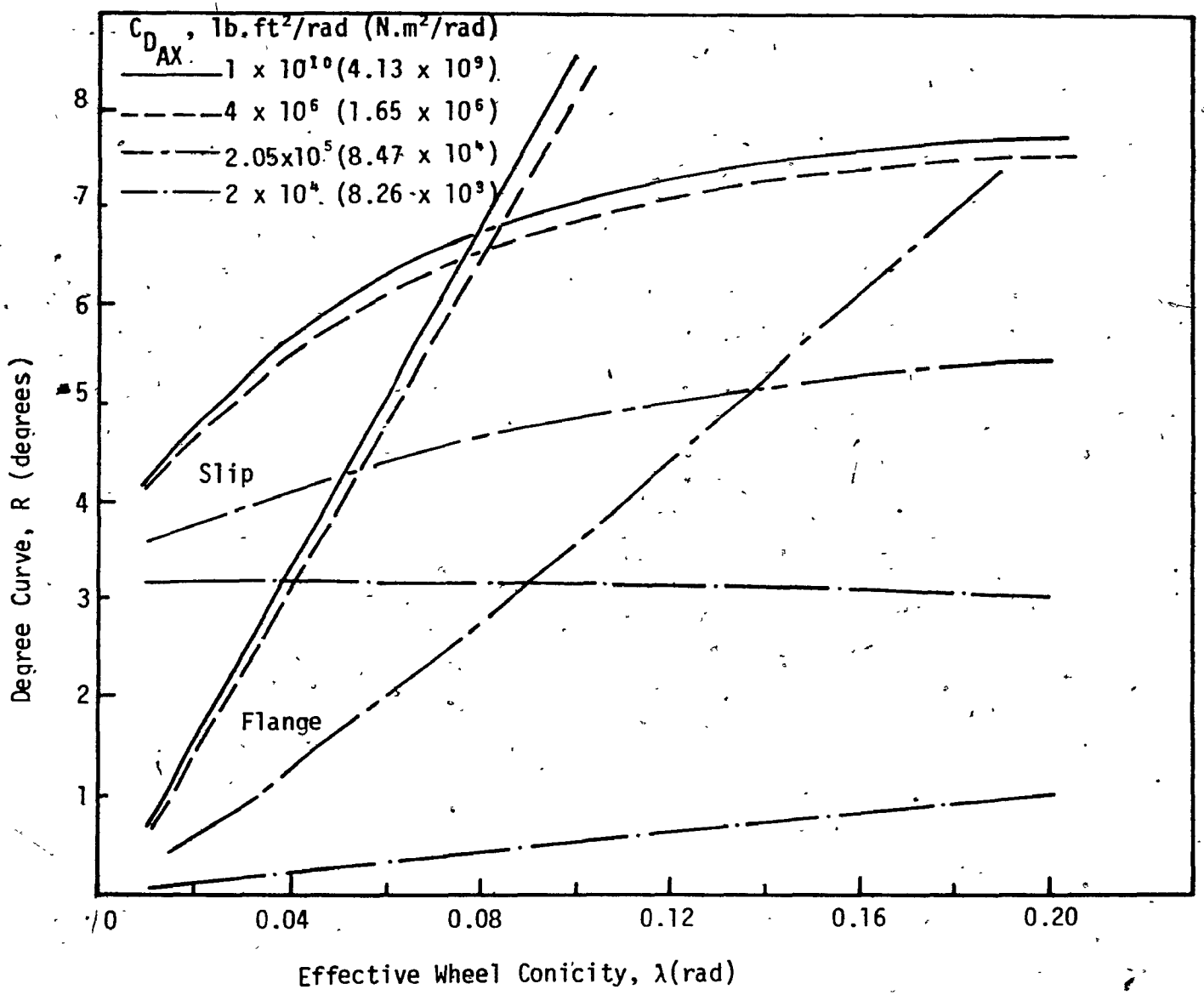

Figure 7.28 Curving performance (slip and flange boundaries) versus effective wheel conicity for various values of coupler parameter $C_{D_{AX}}$.

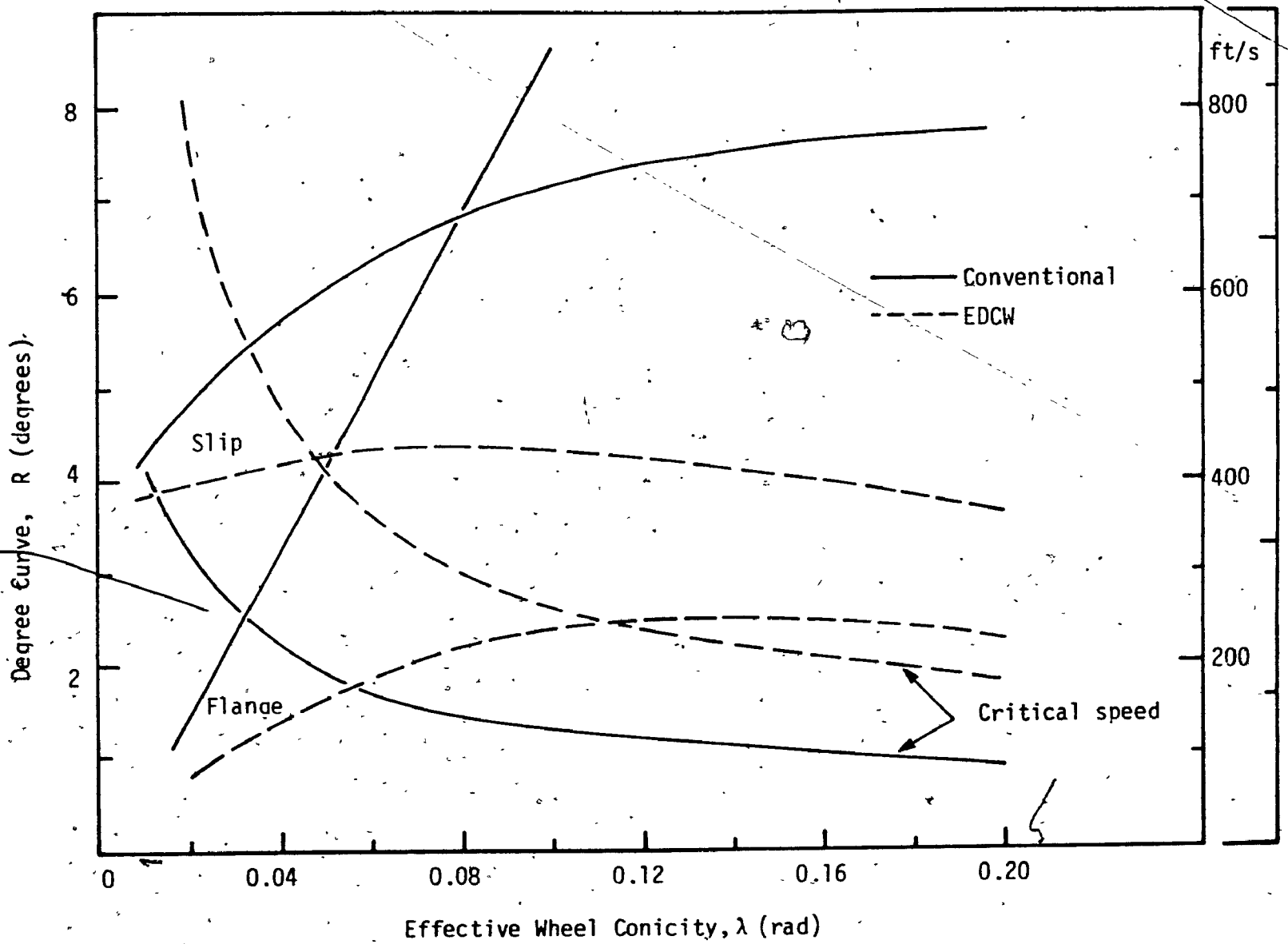

Figure 7.29 Sensitivity of curving performance and tangent track critical speed of truck model with EDCW and rigid axle wheelsets to variation in effective wheel conicity, ($\Phi_d = 0$).

stability is reduced by the EDCW system. But at the same time curving performance is reduced to some extent in comparison to rigid axle wheelset system. For very small values of wheel conicity, however, the curving performance is very similar for both rigid and EDCW truck model, where the critical speed of the truck model with EDCW is significantly greater than that of truck model with conventional wheelsets.

7.5 Summary and Conclusion

Steady-state curving analysis of railway freight truck with EDCW and rigid axle wheelsets are presented in this chapter. The freight truck model with conventional wheelset is first considered to validate the model and to obtain in depth understanding of the freight car steady-state curving behaviour. The results of conventional system demonstrated its well known curving behaviour, and the distinct trade-off between the vehicle dynamic stability and steady-state curving performance for several model parameters.

The stability analysis of truck model with EDCW showed that there is an optimal coupler parameter to maximize the critical speed on tangent track. The optimal coupler parameter is found to be velocity dependent torsional damping with small value of torsional stiffness. Consequently, in this chapter, the influence of coupler damping parameter ($C_{D_{AX}}$) on the curving behaviour of truck model is primarily examined. The truck model with EDCW, for all cases produced identical results to that of conventional model for very large value of $C_{D_{AX}}$. Extensive results are obtained to study the influence of $C_{D_{AX}}$ on the curving response and performance of the truck. Curving performance is primarily determined in

terms of slip boundary, which is the limiting value of track curvature that can be negotiated without any of the wheels slipping. The curving performance is also determined in terms of flange boundary, which is the limiting value of track curvature that can be negotiated without any of the wheels experiencing flange contact.

In general, the results indicated that when the value of coupler parameter $C_{D_{AX}}$ is reduced, the wheelset response to track curvature increases. This is due to combination of loss of guidance and reduction in effective longitudinal creep force. Reduction in longitudinal creep force results in greater wheelset misalignment. And loss of guidance results in greater lateral response or tracking error. As a result, curving performance is reduced by reducing the value of $C_{D_{AX}}$ from rigid axle simulation.

The sensitivity of curving performance as well as stability (critical speed) to variation in important parameters are also examined in this study. Results are obtained for conventional rigid axle truck model, and EDCW truck model with optimal value of $C_{D_{AX}}$, where the optimal value of $C_{D_{AX}}$ corresponds to the maximum critical speed on tangent track. The parameters examined are primary suspension stiffness and effective wheel conicity. The results, in general, showed that due to torsional compliance of EDCW, there is some loss of curving performance in term of radius of track curvature that can be negotiated without wheel slip, in comparison to rigid axle. But the loss is not that significant in comparison to the gain in critical speed. The comparison of flange boundary on the other hand show very significant decrease for EDCW. The results indicate that the baseline truck model with EDCW will tend to

flange on curves with $R > 1.7^0$ for existing flange clearance, but will not slip until $R > 4.25^0$ is reached for balanced running. The problem of EDCW flanging on curves can be overcome either by increasing flange clearance or by restricting minimum radius of mainline track curvature. Another alternative is to allow negotiation of a curve under the guidance of flange. As discussed earlier, flange contact, although undesirable, does not necessarily mean inability to negotiate a curve. The curving performance of the truck model under the flange guidance cannot be predicted from this investigation, since it does not include flange contact and associated flange force.

CHAPTER 8

CONCLUSION AND RECOMMENDATIONS FOR FUTURE WORK

8.1 General

The primary objective of this thesis is to investigate the influence of elasto-damper coupling between the wheels of an axle, on the lateral dynamic behaviour of railway freight car system. The study also includes steady-state curving analysis of the system. For all the various models developed in this study, considerable time and effort is devoted to validate the models. The primary validation is achieved by comparing the results of the Elasto-Damper Coupled Wheelset (EDCW) models to that of conventional system, when wheelset coupler parameters simulate rigid axle. For this, in some cases mathematical model of conventional system having similar complexity to that of the model with EDCW are formulated and studied. The models with EDCW in their limiting case, simulating a conventional wheelset, showed excellent correlation for both experimental and observed trends with that of conventional system. Such validation is required to gain confidence in the developed model, which also aided in quantitative comparison of results with conventional system.

In this investigation, a single EDCW model is first developed and analyzed for its stability behaviour on tangent track. Effects of various arrangements of the coupler elements, and values of coupler element parameters are studied. The results showed that both coupler torsional stiffness and damping have significant influence on the wheelset stability behaviour. For small values of coupler stiffness, the

critical mode is the wheelset relative speed, where coupler damping has greater influence. Where as, for large values of coupler stiffness, the critical mode is the wheelset lateral motion, where coupler damping has little or no influence. When coupler stiffness is swept from small to large value, at the intersection of spin and lateral stability boundaries, there exist a value of the coupler torsional stiffness for which the wheelset critical speed is a maximum.

As a representative of the freight car system, a truck model is next developed, where the EDCW model is extended to incorporate truck motions. The 11-DOF truck model included a pseudo-car body with lateral and roll degrees of freedom. The results of truck stability analysis on tangent track showed that due to strong coupling in the system, the wheelset coupler parameters have strong influence on wheelset as well as car body and truck lateral modes. Extensive analysis of the model showed, that for very small values of wheelset coupler stiffness, there is an optimal value of coupler damping, that maximizes the critical speed of freight car system. The optimal coupler damping maximizes the critical speed by moving the wheelset and truck lateral stability boundaries to coincide (identical critical speed for both the modes). However, for this optimal value of coupler damping, the wheelset spin mode in unstable for a small range of initial velocities. To overcome this, a velocity dependent coupler damping is proposed, that provides large damping for low velocities and optimal damping for velocity corresponding to the system critical speed. With such an EDCW, the baseline truck model showed over 100% improvement of the critical speed in comparison to conventional system. The parametric study of the truck model also showed overall superiority of the EDCW system, where the

critical speed is most sensitive to primary yaw stiffness and wheel conicity.

To examine the influence of EDCW on the curving ability of freight car, a steady-state curving model of freight truck with EDCW is developed. A model of conventional system with same complexity is also developed to obtain an understanding of its curving behaviour, and for the purpose of model validation and comparison. The results of steady-state curving performance for the truck with EDCW is not as encouraging as that of stability performance on tangent track. For flange-free curving, conventional rigid axle wheelsets largely depend on the guidance provided by di-cone arrangement of the wheelsets. In general, for EDCW the guidance to a certain degree is lost, and the longitudinal component of the creep force is reduced. This results in greater wheelset response to track curvature and consequently the EDCW slips and flanges on less tighter curves than that for rigid axle wheelset.

For optimal EDCW corresponding to stability, the loss in curving performance in terms of wheel slip condition is not as significant as that of flanging of wheelset in response to track curvature. The conflict between stability and curving, however, is significantly less for the system with EDCW, in comparison to that of conventional system.

8.2 Specific Conclusions

From the results of this study, highlights and specific conclusions drawn in each of the three phases are outlined as follows:

8.2.1 Wheelset Stability on Tangent Track

- The wheelset model includes lateral, yaw and relative spin degrees-of-freedom, where the elasto-damper coupler primarily have influence on the lateral and spin modes.

- When wheelset coupler consists of a damper element only, the mathematical model always has a consistent zero eigenvalue corresponding to lateral mode. Besides this, the spin mode becomes unstable as forward velocity is increased. The critical speed of spin mode increases with increased coupler damping and approaches the critical speed of rigid axle conventional wheelset.

- For parallel stiffness-damper configuration of the coupler, when torsional stiffness is small, relative spin is the critical mode that becomes unstable as speed is increased, where the lateral mode is stable. For large values of torsional stiffness, lateral mode becomes unstable as speed is increased, where spin mode is stable. When torsional stiffness is small, coupler damping has significant influence only on spin mode.

- As coupler stiffness is varied, there exists a peak critical speed for zero damping, at the intersection of spin and lateral stability boundaries. This critical speed is 64% greater than that of conventional rigid axle wheelset of identical parameters.

- The results of series and parallel configuration of coupler elements showed, that peak critical speed can be obtained in the

presence of stiffness alone, and is a function of total torsional stiffness between the wheels.

- The peak critical speed of EDCW is highly sensitive to variation in primary yaw stiffness and effective wheel conicity. For both conventional and EDCW models, critical speed increases with decrease in wheel conicity and increase in primary yaw stiffness.

- The critical speed of EDCW is sensitive to creep coefficients for values greater than the nominal values. Whereas, the rigid axle wheelset is sensitive to decrease in the creep coefficients. In general, decrease in creep coefficients increases the critical speed slightly. For very small values of creep coefficients, the peak critical speed of EDCW approaches close to rigid axle critical speed, indicating less influence of wheelset coupler in this case.

- Sensitivity of critical speed to axle load is negligible for EDCW, however, the optimal value of torsional stiffness is highly sensitive to axle load. The results indicate, that larger torsional stiffness is required in the presence of larger creep forces.

8.2.2 Truck Stability on Tangent Track

- Influence of wheelset coupler parameters on the stability behaviour of truck model is different to that of single wheelset. In the case of single wheelset, the truck frame is employed as fixed reference, which provides additional guidance.

- For the truck model, when wheelset torsional stiffness is small, depending on the value of torsional stiffness, critical modes are either relative spin or car body lateral motion, for a range of initial forward velocities. While, for large coupler stiffness representing conventional system, the critical mode is truck lateral motion, where the critical speed corresponding to wheelset lateral mode is significantly greater than that of truck lateral mode.

- For small values of coupler stiffness, wheelset coupler damping has significant influence on relative spin as well as wheelset, truck, and car lateral modes. When the stiffness is small, for small or no damping, the truck lateral critical speed is much greater than that of wheelset lateral mode. As the coupler damping is increased, the critical speed boundaries of these two modes approaches each other and eventually switches over. And for very large values of damping the situation becomes identical to that of conventional system. Increase in coupler damping also reduces the unstable region of spin and car lateral modes.

- In the absence of coupler damping, the only major stable region for the truck model is for relatively large values of coupler stiffness, where critical speed is maximum for rigid axle. This finding is very similar to the results obtained in previous investigations [86, 94].

- For very small values of coupler stiffness, there is an optimal value of coupler damping, for which the critical speed boundaries of wheelset and truck lateral modes coincide. The optimal

coupler damping, however, is not large enough to eliminate the initial spin unstable region. Therefore, in order to avail the maximum critical speed through EDCW, a damper is required such that, it provides large damping at slow speeds and optimal damping at the critical speed. For this purpose, a velocity dependent damper, having damping parameter $^{C}D_{AX}$ is proposed, such that $D_{AX} = {}^{C}D_{AX}/V$. The wheelset coupler providing such a damping is referred to as optimal coupler.

- The EDCW truck model with optimal coupler provides significantly superior stability performance in comparison to rigid axle system, where the critical speed can be improved by over 100%. This improvement of truck hunting behaviour is obtained at the expense of effective damping ratio corresponding to wheelset lateral mode, but without affecting the overall stability of the system.

- The trends of critical speed sensitivity to model parameters are found to be similar for both truck models with EDCW and rigid axle wheelset. For the truck model with EDCW, the optimal coupler parameter is also sensitive to other model parameters. The stability performance of truck model with optimal wheelset coupler showed overall superiority, over the conventional system for all parameter ranges.

- In comparison to conventional system, the critical speed of EDCW system is significantly more sensitive to primary yaw stiffness and effective wheel conicity. For both the system, critical speed increases with reduced wheel conicity and increase in

primary yaw stiffness.

. The limited study on the influence of worn wheel profile on the critical speed showed, that the critical speed of EDCW is less sensitive to profiled wheels in comparison to rigid axle system. Worn profiled wheels, however, seem to aid the stability behaviour of truck model with EDCW by reducing wheelset spin and car lateral instability regions.

. Similar to wheelset behaviour, the critical speed of truck model with EDCW is less sensitive to axle load in comparison to conventional truck. However, car body lateral stability or primary hunting performance is superior for the model with EDCW. The baseline conventional system exhibit primary hunting for increased axle load.

. Among the secondary suspension parameters, the influence of lateral damping on the stability behaviour is examined to study its effect on primary hunting (car lateral instability) phenomenon. When secondary lateral damping is increased, the coupling between truck and car lateral modes increases and as a result primary hunting behaviour worsens for both conventional and EDCW truck systems. However, with increase in lateral damping, the primary hunting phenomenon is more critical for the conventional system.

8.2.3. Truck Steady-State Curving

. Steady-state curving analysis is carried out using 9-DOF truck

models with EDCW and conventional wheelset. For both the models, spin velocity terms are retained, where for conventional system $\beta_L = \beta_R$. For the EDCW system, influence of only coupler damping is examined, where damping coefficient (D_{AX}) is velocity dependent, defined as $D_{AX} = C_{D_{AX}}/V$. The coupler damping term $C_{D_{AX}}$ has strong influence on the steady-state curving performance of truck model.

- The results of conventional wheelset system demonstrated the well known conflicting parameter requirement and trade-off between vehicle dynamic stability on tangent track and steady-state curving performance.

- The sensitivity of conventional system curving ability to creep coefficient is maximum for longitudinal creep coefficient, where curving ability is reduced by reduced longitudinal creep force.

- When influence of $C_{D_{AX}}$ is examined on the curving ability of the truck with EDCW, the results are not as encouraging as stability performance. In the case of steady-state curving, as $C_{D_{AX}}$ is reduced from rigid coupler, the curving performance continuously worsens in terms of wheelset response to track curvature.

- For optimal $C_{D_{AX}}$ corresponding to tangent track stability, the curving performance in terms of wheel slip on curved track is reduced to some extent. The reduction in slip performance is not as significant as that of reduction in flange performance due to optimal $C_{D_{AX}}$, in comparison to rigid axle system.

- For both the systems, cant deficiency (ϕ_d) or unbalance have

influence on slip boundary only, where slip takes place on larger radius curves as unbalance is introduced. Minimum radius of track without wheel slip, is for ϕ_d in the range of 0 to + 1°. For balanced running, as track radius is reduced (degree curve increased), in general, flanging takes place well before wheel slip condition is reached.

- The conflicting requirements of wheel conicity and primary stiffness between stability and curving are considerably less for the truck model with EDCW in comparison to conventional system.

- Unlike conventional system, both stability and curving performance of EDCW system improves with increase in primary lateral stiffness. The sensitivity to this parameter is however, not that significant.

- If optimal value of $C_{D_{AX}}$ corresponding to tangent track stability is used on curved track, the results show that wheelsets will tend to flange even on existing mainline curves unless flange clearance is increased.

- Flange contact during curving is not necessarily an indication of curving limitation. Although not desirable, curved track can be negotiated under the guidance of flange, provided excessive flange forces are not developed. This study does not include flange contact and associated forces, and hence, cannot predict the ability of the truck to perform flange guided curving.

In summary, the results of this investigation show that EDCW with coupler primarily consisting of a speed dependent damper, can improve the

stability behaviour of freight car system significantly. But like various other parameters, coupler damping introduces conflict between stability and curving performance. It can therefore be concluded, that in order to utilize the benefits of EDCW on tangent track stability performance, some restriction has to be imposed on radii of mainline curved tracks. Assuming that freight car with EDCW can negotiate a mainline curve under the guidance of flange, the loss in curving performance in terms of wheel slip condition in response to track curvature is not significant in comparison to the improvement of stability performance. Before implementation of such concept, however, further studies are required into various aspects of freight car dynamics. In the following section, recommendations for future work are outlined.

8.3 Recommendations for Future Work

The study presented in this thesis is primarily to investigate the effectiveness of EDCW concept in improving the lateral stability behaviour of freight car system. Various aspects of study on both stability and steady-state curving can be further investigated without major modification to the developed models. Recommendations are made here, for further investigations and follow-up studies, which are:

- To study the effect of flange contact in terms of flange forces and flange clearance.
- To evaluate the influence of profiled wheels on both stability and curving.
- To study the effect of track gage, wheel base, and wheel radius

on the performance of truck model with EDCW.

- To examine the effect of relative motions between the left and right wheels of EDCW, in lateral, yaw and roll directions.
- To evaluate the lateral response of the model subjected to lateral track inputs.
- To carry out an investigation on the building of a laboratory prototype freight truck with EDCW, and to carry out an experimental testing on a roller-rig for validation, and to observe physical limitations of the unit.
- To study the influence of system non-linearities due to suspension and wheel-rail geometry, as well as non-linear torsional damper element of the EDCW.
- To study the dynamics of a radial truck model with EDCW, for the evaluation of its stability as well as curving performance.
- To develop a model of complete freight car system with EDCW to investigate stability, response, as well as curving performance.
- To carry out dynamic curving analysis for examining curve entry and exit behaviour, and derailment tendency of the freight car system with EDCW.
- To undertake a comprehensive optimization of freight car system with EDCW, to maximize the operating speed with constraints on ride quality and curving ability.

REFERENCES

[1] Law, E.H., and Cooperrider, N.K., "A Survey of Rail Vehicle Dynamic Research", Trans. ASME, J. of Dyn. Systems, Measurement, and Control, June 1974, pp. 132-146.

[2] Garg, V.K., and Dukkipati, R.V., "Dynamics of Railway Vehicle Systems", Academic Press, N.Y., 1984.

[3] Bhatti, M.H., and Garg, V.K., "A Review of Railway Vehicle Performance and Design Criteria", Int. J. of Vehicle Design, Vol. 5, Nos. 1/2, 1984, pp. 232-254.

[4] Hamid, A., and Yang, T.L., "Analytical Description of Track Geometry Variation", ENSCO, Transportation Tech., Engineering Division, Springfield, Virginia, 1981.

[5] Corbin, J.C., "Statistical Characterization of Railway Track Behaviour", ASME/IEEE Joint Railway Conference, Pittsburg, Pennsylvania, IEEE Paper C 74903-31A, 1974.

[6] Kenn, A.D., "The Stress and Stability Analysis of Railroad Track", Trans. ASME, J. of Applied Mech., No. 41, Dec. 1974, pp. 841-848.

[7] Grassie, S.L., Gregory, R.W., and Johnson, K.L., "The Dynamic Response of Railway Track to High Frequency Lateral Excitation", 1982, pp. 91-95.

[8] Grassie, S.L., Gregory, R.W, and Johnson, K. L., "The Dynamic Response of Railway Track to High Frequency Longitudinal Excitation", J. of Mech. Eng. Science, I. Mech. Eng., Vol. 24, No. 2, 1982, pp. 97-102.

[9] Meinke, P., Hehenberger, W., Perger, K. and Gruber, J., "Track Dynamics at High Vehicle Speeds", Proceedings of 6th IAVSD-Symposium held at Tech. University Berlin, Sept. 1979.

[10] Ahlbeck, D.A., "Predicting the Load Environment on Railroad Track", ASME paper No. 80-RT-7, 1980.

[11] Bhatti, M.H., "Vertical and Lateral Dynamic Response of Railway Bridges Due to Non-Linear Vehicle and Track Irregularities", Ph. D. Dissertation, Illinois Institute of Tech., Chicago, 1982.

[12] Carter, F.W., "On the Action of Locomotive Driving Wheel", Proceeding of the Royal Society of London, Series A, Vol. 112, 1926, pp. 151-157.

[13] Johnson, K.L., and Vermenlen, P.J., "Contact of Non-Spherical Bodies Transmitting Tangential Force", J. Applied Mechanics. 31, 1964, pp. 338-340.

[14] Kalker, J.J., "On the Rolling Contact of Two Elastic Bodies in the Presence of Dry Friction", Doctoral Dissertation, Delft University of Tech., Delft, Netherlands, 1967.

[15] Kalker, J.J., "Survey of Wheel-Rail Rolling Contact Theory", Vehicle System Dynamics, 8, 1979, pp. 317-358.

[16] Kalker, J.J., "Review of Wheel-Rail Rolling Contact Theory the General Problem of Rolling Contact", Applied Mech. Division, ASME, Vol. 40, 1980, pp. 72-92.

[17] Leffler, B.R., "The Relation Between the Swaying of Hopper Car and Stagger of Rail Joint in Track", AREA Proceeding, Vol. 27, 1926.

[18] Manos, W.P., and Shang, J.C., "Dynamic Analysis of Rolling Freight Cars", ASME Anthology of Rail Vehicle Dynamics", Vol. 2,

1972, pp. 135-145.

[19] Henderson, K.A., and Johnson, J., "A Criterion for the Control of 100-Ton Hopper Car Roll Motion", Trans. ASME, Vol. 90-B, No. 4, 1968, pp. 717-724.

[20] Reynolds, D.J., and Blank, R.W., "A Car Rocking Mechanism", ASME paper No. 77-WA/RT-11, 1977.

[21] Liepins, A.A., "Digital Computer Simulation of Railroad Freight Car Rocking", Trans. ASME, Vol. 90-B, No. 4, 1968, pp. 701-707.

[22] Mecham, H.C., and Ahlbeck, D.R., "A Computer Study of Dynamic Loads Caused by Vehicle-Track Interaction", Trans. ASME, J. of Eng. for Industry, 1969, pp. 808-816.

[23] Samaha, M., "Dynamic Response and Optimization of Rail Road Freight Car Under Periodic and Stochastic Excitations", Ph. D. Thesis, Concordia University, 1978.

[24] "Harmonic Roll Series", Track Train Dynamics Project Report, Association of American Railroads, 1975.

[25] Willis, T., and Shum, K., "A Non-Linear Mathematical Model of the Dynamics of a Railroad Freight Car/Freight Element", ASME paper No. 76-DE-42, April 1976.

[26] Healy, M.J., "A Computer Method for Calculating Dynamic Responses of Non-Linear Flexible Rail Vehicles", ASME paper No. 76-RT-5, April 1976.

[27] Hedrick, J.K., Wormley, D.N., Kar, A.K., Murray, W., and Baum, W., "Performance Limits of Rail Passenger Vehicles: Evaluation and Optimization", Report DOT-RSPA-DPB-50-79-32, U.S. Dept. of Transportation, Washington, D.C., 1979

[28] Carter, F.W., "On the Stability of Running of Locomotives",

Proceedings of the Royal Society of London, Series A, Vol. 121, 1928, pp. A-30 to A-36.

[29] Brann, R.P., "Some Aspects of the Hunting of a Railway Axle", Journal of Sound and Vibration, Vol. 4, No. 1, 1966, pp. 18-32.

[30] Wickens, A.H., "The Dynamic Stability of Railway Vehicle Wheelsets and Bogies Having Profiled Wheels", Int. J. of Solids and Structures, Vol. 1, 1965, pp. 319-341.

[31] Wickens, A.H., "Static and Dynamic Stability of Railway Vehicle Wheelsets Having Profiled and Coned Wheels", Technical Note, DYN/90, British Railway Research Dept., 1968.

[32] Law, E.H., and Brand, R.S., "Analysis of the Non-Linear Dynamics of a Railway Vehicle Wheelset", J. of Dynamic Systems, Measurement, and Control, Trans. ASME, Series G, Vol. 95, No. 1, 1973, pp. 28-35.

[33] Law, E.H., "Analysis of the Non-Linear Dynamics of a Railway Vehicle Wheelset", Ph. D. Thesis, University of Connecticut, Storrs, Conn., 1971.

[34] Clark, J.W., and Law E.H., "Investigation of the Truck Hunting Instability Problem of High-Speed Trains", ASME paper No. 67-Tran-17, 1967.

[35] Cooperrider, N.K., "High Speed Dynamics of Conventional Railway Trucks", Ph. D. Thesis, Stanford University, Stanford, Calif., 1968.

[36] Cooperrider, N.K., "The Hunting Behaviour of Conventional Railway Trucks", J. of Eng. for Industry, Trans. ASME, Series B, Vol. 94, 1972, pp. 752-762.

[37] Matsudaira, T., "Hunting Problem of High-Speed Railway Vehicles

with Special Reference to Bogie Design for the New Tokaido Line", Proceedings of the Inst. of Mech. Eng., London, Vol. 180, Part 3F, 1966, pp. 58-66.

[38] Scheffel, H., " The Influence of the Suspension on the Hunting Stability of Railway Vehicle", Rail International, 1979, pp. 662-696.

[39] Hannebrink, D.N., Lee, H.S.H., Wainstock, H., and Hedrick, J.K., "Influence of Axle Load, Track Gage, and Wheel Profile on Rail Vehicle Hunting", ASME Trans. J. of Eng. for Industry, 1977, pp. 186-195.

[40] Tuten, J.M., Law, E.H., and Cooperrider, N.K., "Lateral Stability of Freight Cars with Axles-Having Different Wheel Profile and Asymmetric Loading", Trans. ASME, J. of Eng. for Industry, Vol. 101, 1979, pp. 1-16.

[41] Law, E.H., "Non-Linear Wheelset Dynamic Response to Lateral Rail Irregularities", Trans. ASME, J. of Eng. for Industry, 1974, pp. 1168-1176.

[42] D'Souza, A.F., and Caravavatna, P., "Analysis of Non-Linear Hunting Vibration of Rail Vehicle Trucks", Trans. ASME, J. of Mech. Design, Vol. 102, 1980, pp. 77-85.

[43] Hedrick, J.K., and Arslan, A.V., "Non-Linear Analysis of Rail Vehicle Forced Lateral Response and Stability", Trans. ASME, J. of Dynamic Systems, Measurement, and Control, 1979, pp. 230-236.

[44] Hadden, J.A., "The Effects of Truck Design and Component Flexibility on the Lateral Stability of Railway Freight Vehicle", Masters Thesis, Clemson University, Dec. 1976.

[45] Sweet, L.M., and Karmel, A., "Spectral Analysis of Freight Car

Truck Lateral Response", Trans. ASME J. of Dyn. Systems, Measurement, and Control, Vol. 104, 1983, pp. 297-303.

[46] Fries, R.H., Cooperrider, N.K., and Law, E.H., "Experimental Investigation of Freight Car Lateral Dynamics", Trans. ASME, J. of Dyn. Systems, Measurement, and Control, Vol. 103, 1981, p.p. 201-210.

[47] Cooperrider, N.K., Cox, J.J., and Hedrick, J.K., "Lateral Dynamic Optimization of Conventional Rail Car", Trans. ASME, J. of Dyn. Systems, Measurement, and Control, 1975, p.p. 293-299.

[48] Cox, J.J., Hedrick, J.K. and Cooperrider, N.K, "Optimization of Rail Vehicle Operating Speed with Practical Constraints", Trans. ASME, J. of Dyn. Systems, Measurement, and Control, 1978, pp. 260-269.

[49] Ramachandran, P.V., Gilchrist, A.J., Elmadany, M.M., and Cappel, K., "Validation of Rail Vehicle System Dynamic Models", Int. J. of Vehicle Design, Vol. 3, No. 2, pp. 202-233.

[50] Law, E.H., Cooperrider, N.K., and Tuten, J.M., "Lateral Stability of Freight Cars with Axles Having Different Wheel Profiles and Asymmetric Loading", ASME paper No. 78-RT-3.

[51] Bronowicki, A., and Hasselman, T.K., "DYNALIST II, a Computer Program for Stability and Dynamic Response Analysis of Rail Vehicle Systems", Report No. FRA/ORD-75-22, 1976.

[52] Wickens, A.H., "General Aspects of the Lateral Dynamics of Railway Vehicles", Trans. ASME, J. of Eng. for Industry, 1969, pp. 869-878.

[53] Pearce, T.G., and May, B.J., "A Study of the Stability and Dynamic Response of Linear Induction Motor Test Vehicle", FRA-RT-

70-25, Office of High Speed Ground Transportation, Washington, D.C. (PB-192718).

[54] Wickens, A.H., "The Effects of Lateral Track Flexibility and Gyroscopic Forces on the Stability of Railway Vehicle Wheelsets", DYN/7, 1965, British Railway Research Dept.

[55] Bell, C.E., Hoark, D., and Hedrick, J.K., "Stability and Curving Mechanics of Railway Vehicle", J. of Dyn. Systems, Measurement, and Control, Trans. ASME, Vol. 103, 1981, pp. 181-190.

[56] Law, E.H., and Cooperrider, N.K., "Non-Linear Dynamic and Steady-State Curving of Rail Vehicles", Presented at the 1978 ASME Winter Annual Meeting, San Francisco, CA., Dec. 1978.

[57] Mackenzie, J., Proceedings of Inst. of Civil Engineers, Vol. LXXIV, 1883, pp. 1-57.

[58] Eksergian, R., "Static Adjustments of Trucks on Gurves", Trans. ASME, Vol. 42, No. 1776, 1921.

[59] Porter, S.R.M., "The Mechanics of a Locomotive on Curved Track", The Railway Gazette, 1935.

[60] Newland, D.E., "Steering Characteristics of Bogies", The Railway Gazette, 1958, pp. 745-750.

[61] Newland, D.E., "Steering a Flexible Railway Truck on Curved Track", Trans. ASME, J. of Eng. for Industry, Series B, Vol 91, 1969, pp. 908-918.

[62] Boocock, D., "The Equations of Motion of an Elastically Restrained Wheelset on Curved Track, and preliminary Study of Steady State Motion", DYN/35, British Railway Research Dept. 1966.

[63] Boocock, D., "Steady State Motion of Railway Vehicle on Curved

Track", J. of Mech. Eng. Science, Vol. 11, No.6, 1969, pp. 556-566.

[64] Nagurka, M.L., Bell, C.E., Hedrick, J.K., and Wormley, D.N., "Computational Methods for Rail Vehicle Steady-State Curving Analysis", Computational Method in Ground Transportation Vehicle, Vol. 50, Presented at ASME Winter Annual meeting at Phoenix, Arizona, Nov. 14-19th, 1982, pp. 153-179.

[65] Hedrick, J.K., Wormley, D.N., Arslan, A.V., and Chin, R., "Non-Linear Analysis as Design Tools for Rail Vehicles: Non-Linear Locomotive Dynamics", AAR Report R-463, Dec. 1980.

[66] Elkins, J.A., and Gostling, R.J., "A General Quasi-Static Curving Theory for Railway Vehicle", Proceedings of 5th VSD 2nd IUTAM Symposium on the Dynamics of Vehicles on Roads and Tracks, 1978, pp. 388-406.

[67] Matsui, N., "A Practical Calculation Method of Quasi-Static Curving Performance of Railway Bogie Vehicles", Proceedings of 6th IAVSD Symposium held at the Technical University, Berlin, Sept. 3-7, 1979, pp. 276-288.

[68] Muller, C., "Dynamics of Railway Vehicles on Curved Track, Interaction Between Vehicle and Track", Proceedings of the Inst. of Mech. Engineers, Vol. 180, Part 3F, 1966, pp 45-57.

[69] Smith, K.R., "Curve Entry and Curve Negotiation Characteristics of Two-Axle Truck", M.S. Thesis, IIT, Chicago, 1975.

[70] Scheffel, H., "The Hunting Stability and Curving Ability of Railway Vehicles", Rail International, No. 2, 1974, pp. 154-177.

[71] Bullock, R.L., "Modified /Three-Piece Truck Reduces Hunting and Improves Curving-Status Report", 12th Annual Railroad Engineering

Conference on the Effect of Heavy Axle Loads on Tracks, 1975, p. 85.

[72] Scheffel, H., "Wheelset Suspension Designed to Eliminate the Detrimental Effects of Wheel Wear on the Hunting Stability of Railroad Vehicles", ASME Symposium on Railroad Equipment Dynamics, Chicago, 1976.

[73] Scheffel, H., "Self-Steering Wheelsets will Reduce Wear and Permit Higher Speeds", Railway Gazette Int., Dec. 1976.

[74] Scales, B.T., "Behaviour of Bogies on Curves", Railway Engineering Journal, Vol. 1, No. 4, 1972, p. 12.

[75] List, H.A., "Design System Approach to Problem Solving", 12th Annual Railroad Engineering Conference on the Effect of Heavy Axle Loads on Track, 1975, p. 79.

[76] List, H.A., Caldwell, W.N., and Marcotte, P., "Proposed Solution to the Freight Car Truck Problems of Flange Wear and Truck Hunting", ASME paper No. 75-WA-RT-8, 1976.

[77] Wickens, A.H., "Steering and Dynamic Stability of Railway Vehicles", Vehicle System Dynamics, Vol. 5, 1976, p. 15.

[78] Horak, D., Bell, C.E., and Hedrick, J.K., "A Comparison of the Stability and Curving Performance of Radial and Conventional Rail Vehicle Trucks", Trans. ASME, J. of Dyn. Systems, Measurement, and Control, Vol. 103, 1981, pp. 191-200.

[79] Hedrick, J.K., and Wormley, D.N., "Active Suspension for Ground Transport Vehicles - A State-of-the-Art Review", Mechanics of Transportation Systems, AMD - Vol. 15, ASME, 1975, pp. 21-40.

[80] Jeffcoat, R.L., and Wormley, D.N., "Improvement of Rail Vehicle Lateral Dynamics Performance Through Active Control", Vehicle

System Dynamics, Vol. 4, No. 2-3, 1975, pp. 169-173.

[81] Sinha, P.K., Wormley, D.N., and Hedrick, J.K., "Rail Passenger Vehicle Lateral Dynamic Performance Improvement Through Active Control", ASME J. of Dyn. Systems, Measurement, and Control, Vol. 100, 1978, 270-283.

[82] Celniker, G.W., and Hedrick, J.K., "Rail Vehicle Active Suspension for Lateral Ride and Stability Improvement", Trans. ASME, J. of Dyn. Systems, Measurement, and Control, Vol. 104, 1982, pp. 100-106.

[83] Hedrick, J.K., "Railway Vehicle Active Suspensions, State-of-the-Art Papers", 7th IAVSD/IUTAM Symposium, Vehicle System Dynamics, 1981.

[84] Dukkipati, R.V., Bowler, E.H., and Garlicki, A.M., "Dynamics of Independently Rotating Railway Wheel Systems, Past Experience and Possible Future Exploration", Proc. Fifth Symposium on Engineering Application of Mechanics, Ottawa, 1980, pp. 259-263.

[85] Becker, P., "On the Use of Individually Supported Free-Rolling Wheels on Railway Vehicles", Eisenbahntechnische Rundschau, No. 11, 1970, pp. 457-463.

[86] Hadden J.A., and Law, E.H., "Effects of Truck Design on Hunting Stability of Railway Vehicles", Trans. ASME, J. of Eng. for Industry, 1977, pp. 162-171.

[87] Kaplan, A., Hasselman, T.K., and Short, S.A., "Independently Rotating Wheels for High Speed Trains", SAE paper No. 700841, 1970.

[88] Koyanagi, S., "The Stability of Motion of the Independently Rotating Wheel-Axle", Japanese National Research, Quarterly

Reports, Vol. 12, No. 1, 1971, pp. 29-33.

[89] Koyanagi, S., "The Stability of Guided Railway Car with Independently Rotating Wheels - Calculation Based on Shinkansen Car Model", Japanese National Research, Quarterly Reports, Vol. 14, No.3, 1973, pp. 168-171.

[90] Koyanagi, S., "A New Guide System for a Wheel-Rail Vehicle", Proceedings of the 5th VSD-2nd IUTAM Symposium held at the Tech. University of Vienna, Austria, Sept. 19-23rd, 1977, pp. 407-415.

[91] Benington, C.K., "The Railway Wheelset and Suspension Unit as a Closed-Loop Guidance Control System, A Method for Performance Improvement", J. of Mech. Eng. Science, Vol. 10, No. 2, 1968, pp. 91-100.

[92] Benington, C.K., and Greenhorn, W.R., "A proposal for Improving the Performance of Two-Axled Rail-Guided Vehicle", J. of Mech. Eng. Science, Vol. 13, No. 3, 1971, pp. 157-167.

[93] Dukkipati, R.V., and Guntur, R.R., "Selection of Suspension Parameters for Stability of Wheelsets", Proceedings of the 10th IMACS World Congress on System Simulation and Scientific Computation, Vol. 3, Aug. 8-13, 1982, pp. 157-158.

[94] Doyle, Jr.G.R., and Prause, R.H., "Hunting Stability of Rail Vehicle with Torsionally Flexible Wheelset", Trans. ASME, J. of Eng. for Industry, 1977, pp. 10-17.

[95] Lovaldi, U., "Railway Bogie with Independently Rotating Wheels", Ball Bearing Journal, No. 205, 1980, pp. 16-18.

[96] Malavasi, G., and Scarponi, P., "Results of Experiment with Independently Rotating Wheels", Ingegneria Ferroviaria, Vol. 33, No. 5, 1979, pp. 757-768.

[97] Kalker, J.J., "Simplified Theory of Rolling Contact", Delft Progress Report, Series C, Mechanical and Aeronautical Engineering and Shipbuilding, 1, 1973, pp. 1-10.

[98] Illingworth, R., "The Mechanism of Railway Vehicle Excitation by Track Irregularities", Doctoral Dissertation, University of Oxford, England, 1973.

[99] Brickle, V.B., "Steady-State Forces and Moments on a Railway Wheelset Including Flange Contact Condition", Doctoral Thesis, Loughborough University of Tech., England, 1973.

[100] Hobbs, A.E.W., "A Survey of Creep", DYN/52, British Railway Research Dept., Derby, England, 1967.

[101] Cooperrider, N.K., and Law, E.H., "A Survey of Rail Vehicle Testing for Validation of Theoretical Dynamic Analysis", Trans. ASME, J. of Dyn. Systems, Measurement, and Control, Vol. 100, 1978, pp. 238-251.

[102] Agrawal, C., "Determination of Creep Force Characteristics of A Railway Vehicle on a Roller Rig", Masters Thesis, Clemson University, 1980.

[103] Cooperrider, N.K., Hull, R., Kadala, P.S., and Tuten, J.M., "Analytical and Experimental Determination of Non-Linear Wheel/Rail Geometric Constraint", Interim Report to U.S. Dept. of Transportation, Federal Railroad Administration, Dec. 1975.

[104] Sherrick, J.W., "Roller Bearing Adaptor Mounting for Rail Cars", ASME, Anthology of Rail Vehicle Dynamics, Vol. II, 1972, pp. 190-196.

[105] Cooperrider, N.K., "Non-Linear Behaviour in Rail Vehicle Dynamic Analysis", New Approach to Non-Linear Problems in

Dynamics. Siam Publ., Philadelphia, 1980, pp. 173-194.

[106] Garg, V.K., Chu, K.H., and Mels, K.D., "Lateral Dynamics of a Railway Vehicle", Symposium on Railroad Equipment Dynamics, Joint ASME-IEEE Railroad Conference, Chicago, Illinois, 1976, pp. 25-40.

[107] Goldstein, H., "Classical Mechanics", Addison-Wesley Publishing Company Inc., London, 1965.

APPENDIX A

WHEELSET VELOCITY AND MOMENTUM IN TERMS OF THE AXIS SYSTEM

A.1 The Axis Systems (Tangent Track)

In the derivation of creep forces, normal forces, and equations of motion of the Elasto-Damper Coupled Wheelset (EDCW), two axis systems are used. One relates the disturbed wheelset axis to the space-fixed axis system of equilibrium. And the other relates the wheel/rail contact plane axis system to the wheelset CG axis system.

The wheelset axis system is shown in Figure A.1. At equilibrium, the space-fixed axis system is designated by "triple-prime". The $\hat{i}'''$ unit vector is directed coincident to the track centerline pointing forward along the track. The $\hat{j}'''$ unit vector is directed perpendicular to the track centerline pointing to the left. And $\hat{k}'''$ unit vector is normal to the plane of the track pointing up.

When the wheelset yaw about $\hat{k}'''$, and roll about $\hat{i}'''$, it finally gives axis system designated by "prime", which denotes wheelset body coordinate system. The $\hat{i}'$ vector is parallel to the rail plane, directed toward the direction of motion. The $\hat{j}'$ vector is coincident with the axle centerline, and $\hat{k}'$ is normal to $\hat{i}'$ and $\hat{j}'$.

The expressions relating the space-fixed and the wheelset unit vectors can be derived using concept of Eulerian angles [107]:

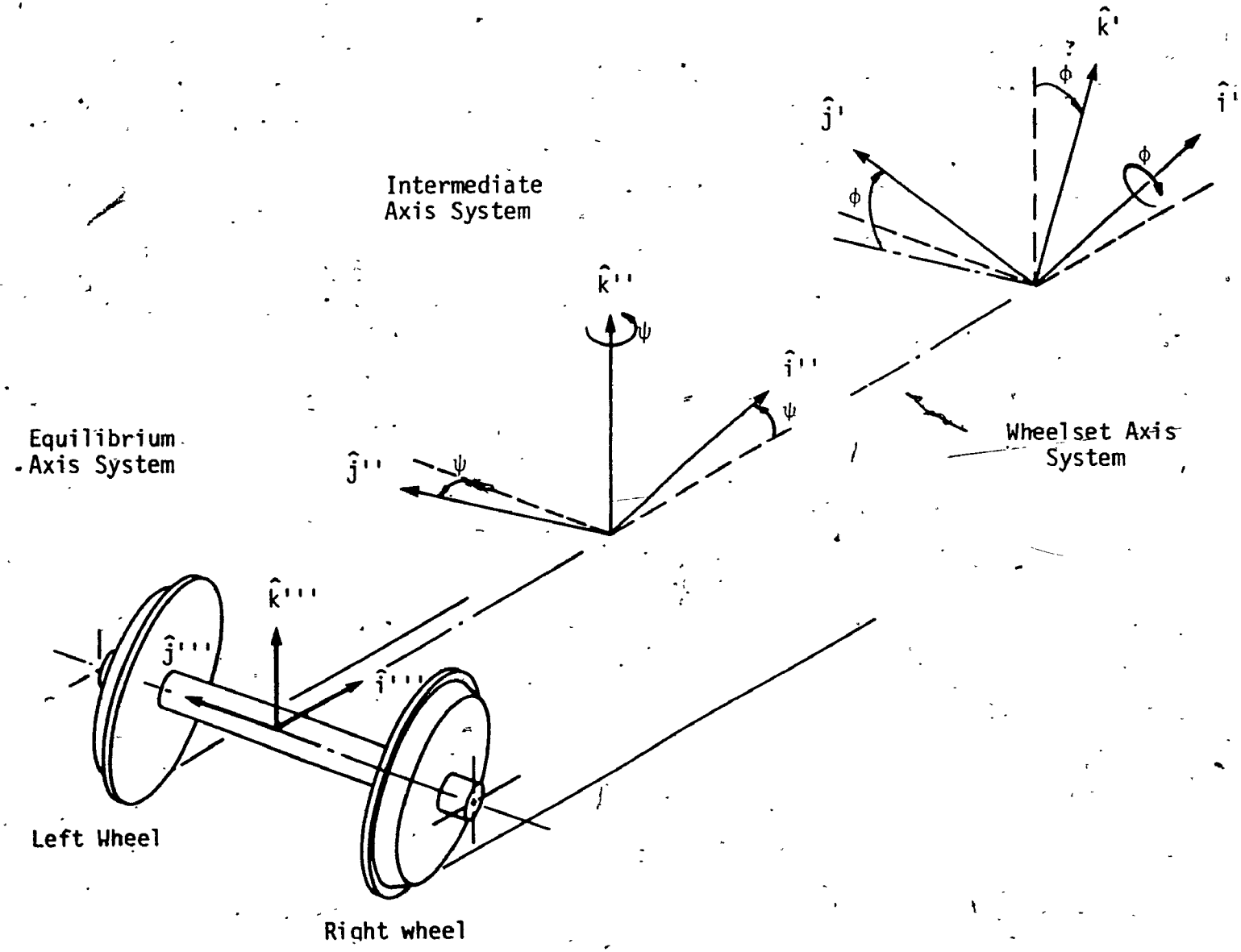

Figure A.1 Axis system for the wheelset model on tangent track.

$$\begin{Bmatrix} \hat{i}''' \\ \hat{j}''' \\ \hat{k}''' \end{Bmatrix} = \begin{bmatrix} \cos(\psi) & -\sin(\psi)\cos(\phi) & \sin(\psi)\sin(\phi) \\ \sin(\psi) & \cos(\psi)\cos(\phi) & -\cos(\psi)\sin(\phi) \\ 0 & \sin(\phi) & \cos(\phi) \end{bmatrix} \begin{Bmatrix} \hat{i}' \\ \hat{j}' \\ \hat{k}' \end{Bmatrix} \quad \text{(A.1)}$$

And for small angles:

$$\begin{Bmatrix} \hat{i}''' \\ \hat{j}''' \\ \hat{k}''' \end{Bmatrix} = \begin{bmatrix} 1 & -\psi & 0 \\ \psi & 1 & -\phi \\ 0 & \phi & 1 \end{bmatrix} \begin{Bmatrix} \hat{i}' \\ \hat{j}' \\ \hat{k}' \end{Bmatrix} \quad \text{(A.2)}$$

or

$$\begin{Bmatrix} \hat{i}' \\ \hat{j}' \\ \hat{k}' \end{Bmatrix} = \begin{bmatrix} 1 & \psi & 0 \\ -\psi & 1 & \phi \\ 0 & -\phi & 1 \end{bmatrix} \begin{Bmatrix} \hat{i}''' \\ \hat{j}''' \\ \hat{k}''' \end{Bmatrix} \quad \text{(A.3)}$$

Also, the axis system for wheel/rail contact plane is required to be defined, so that the forces at the contact plane can be expressed in terms of fixed axis system.

Figure A.2 shows the contact plane axis system designated by $(\hat{e}_1, \hat{e}_2, \hat{e}_3)$. The unit vectors for the left wheel, $\hat{e}_{1_L}$, $\hat{e}_{2_L}$ and $\hat{e}_{3_L}$, are defined with respect to the plane of contact as tangent in the longitudinal direction, tangent in the lateral direction, and normal, respectively. The unit vectors $\hat{e}_{1_R}$, $\hat{e}_{2_R}$, $\hat{e}_{3_R}$ are defined similarly for the right wheel. The relationship between contact plane axis and axle-axis system for the left wheel is given by:

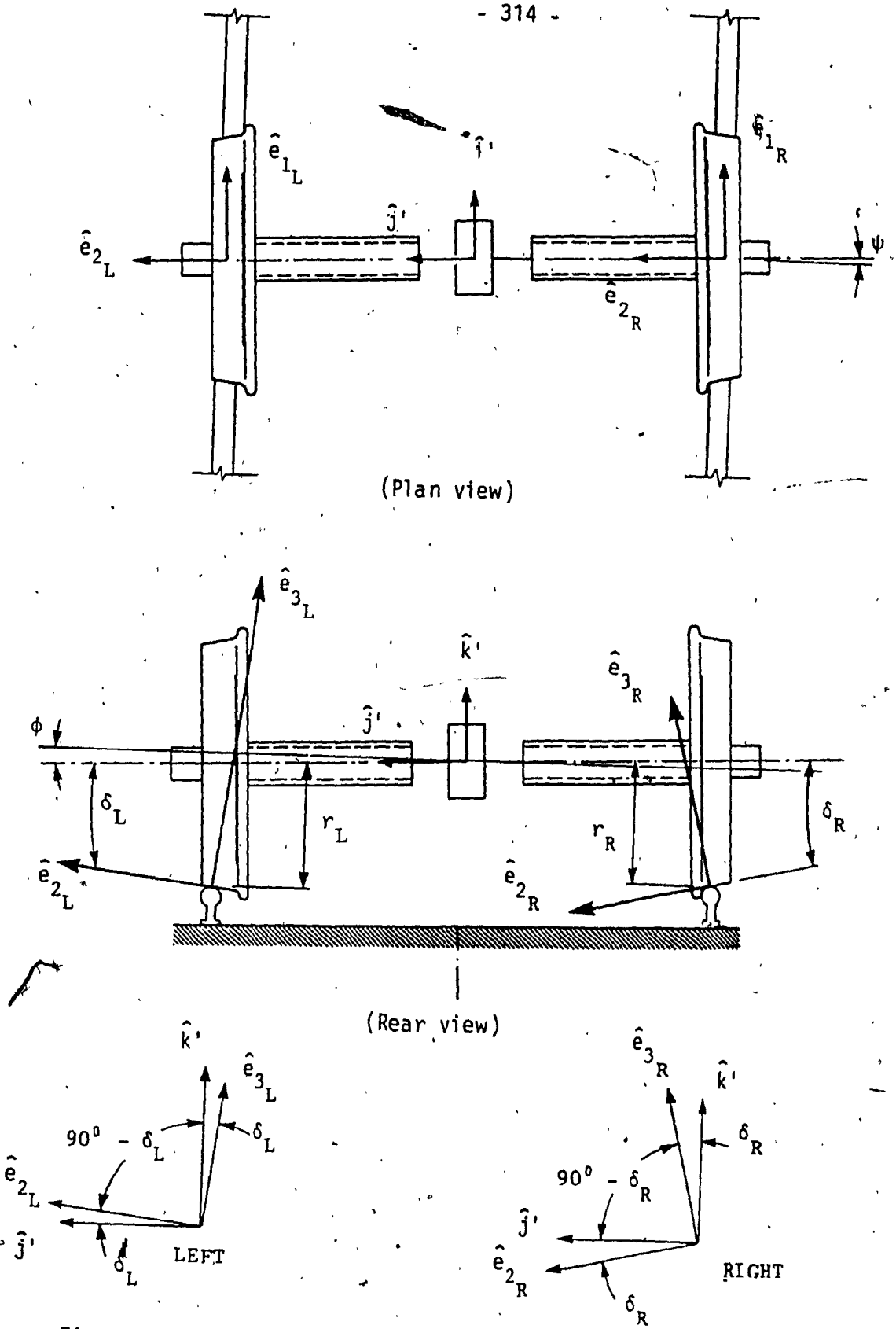

Figure A.2 Axis system at the wheel/rail contact plane.

$$\begin{Bmatrix} \hat{e}_{1_L} \\ \hat{e}_{2_L} \\ \hat{e}_{3_L} \end{Bmatrix} = \begin{bmatrix} 1 & 0 & 0 \\ 0 & \cos(\delta_L) & \cos(90-\delta_L) \\ 0 & \cos(90+\delta_L) & \cos(\delta_L) \end{bmatrix} \begin{Bmatrix} \hat{i}' \\ \hat{j}' \\ \hat{k}' \end{Bmatrix}$$

$$= \begin{bmatrix} 1 & 0 & 0 \\ 0 & \cos(\delta_L) & \sin(\delta_L) \\ 0 & -\sin(\delta_L) & \cos(\delta_L) \end{bmatrix} \begin{Bmatrix} \hat{i}' \\ \hat{j}' \\ \hat{k}' \end{Bmatrix} \qquad (A.4)$$

For small angles, substituting for axle-axis (prime) system from Equation (A.3), the expression for transformation from left wheel contact plane axes to wheelset equilibrium axis system is:

$$\begin{Bmatrix} \hat{e}_{1_L} \\ \hat{e}_{2_L} \\ \hat{e}_{3_L} \end{Bmatrix} = \begin{bmatrix} 1 & \psi & 0 \\ -\psi & 1 & \delta_L + \phi \\ 0 & -(\delta_L + \phi) & 1 \end{bmatrix} \begin{Bmatrix} \hat{i}''' \\ \hat{j}''' \\ \hat{k}''' \end{Bmatrix} \qquad (A.5)$$

Similarly for the right wheel:

$$\begin{Bmatrix} \hat{e}_{1_R} \\ \hat{e}_{2_R} \\ \hat{e}_{3_R} \end{Bmatrix} = \begin{bmatrix} 1 & 0 & 0 \\ 0 & \cos(\delta_R) & -\sin(\delta_R) \\ 0 & \sin(\delta_R) & \cos(\delta_R) \end{bmatrix} \begin{Bmatrix} \hat{i}' \\ \hat{j}' \\ \hat{k}' \end{Bmatrix} \qquad (A.6)$$

Similar to that of left wheel, the final expression relating right wheel contact plane axes to equilibrium axis system is:

$$\begin{Bmatrix} \hat{e}_{1_R} \\ \hat{e}_{2_R} \\ \hat{e}_{3_R} \end{Bmatrix} = \begin{bmatrix} 1 & \psi & 0 \\ -\psi & 1 & -(\delta_R - \phi) \\ 0 & (\delta_R - \phi) & 1 \end{bmatrix} \begin{Bmatrix} \hat{i}''' \\ \hat{j}''' \\ \hat{k}''' \end{Bmatrix} \tag{A.7}$$

Using the described axis system, the position, velocity and acceleration of the wheelset center of gravity are:

$$\bar{r}_{CG} = (x + x_0)\hat{i}''' + (y)\hat{j}''' + (z)\hat{k}''' \tag{A.8}$$

$$\dot{\bar{r}}_{CG} = (\dot{x} + V)\hat{i}''' + (\dot{y})\hat{j}''' + (\dot{z})\hat{k}''' \tag{A.9}$$

$$\ddot{\bar{r}}_{CG} = (\ddot{x})\hat{i}''' + (\ddot{y})\hat{j}''' + (\ddot{z})\hat{k}''' \tag{A.10}$$

where x, y and z are longitudinal, lateral and vertical displacements of the wheelset (CG), respectively. And x_0 is the distance wheelset travelled along the track from equilibrium position.

For the EDCW, the total angular velocity of each wheel may be different. The angular velocity of the left wheel in terms of wheelset axis system can be written as:

$$\bar{\omega}_L = (\dot{\phi})\hat{i}' + (\Omega + \dot{\beta}_L)\hat{j}' + (\dot{\psi})\hat{k}' \tag{A.11}$$

Using the transformation Equation (A.3), and neglecting products of small terms, the expression in terms of fixed axis system can be obtained as:

$$\bar{\omega}_L = (\dot{\phi} - \Omega\psi)\hat{i}''' + (\Omega + \dot{\beta}_L)\hat{j}''' + (\Omega\phi + \dot{\psi})\hat{k}''' \tag{A.12}$$

Similarly for the right wheel, the angular velocity is:

$$\bar{\omega}_R = (\dot{\phi} - \Omega\psi)\hat{i}''' + (\Omega + \dot{\beta}_R)\hat{j}''' + (\Omega\phi + \dot{\psi})\hat{k}''' \tag{A.13}$$

The angular velocity of the wheelset can be taken as the average of the left and right wheel angular velocities as:

$$\bar{\omega} = \tfrac{1}{2}(\bar{\omega}_L + \bar{\omega}_R) \tag{A.14}$$

Therefore, substituting for $\bar{\omega}_L$ and $\bar{\omega}_R$, and for spin motion of the left and right wheels being antisymmetric, the angular velocity of the wheelset is:

$$\bar{\omega} = (\dot{\phi} - \Omega\psi)\hat{i}''' + (\Omega)\hat{j}''' + (\phi\Omega + \dot{\psi})\hat{k}''' \tag{A.15}$$

or in terms of wheelset body axis system:

$$\bar{\omega} = (\dot{\phi})\hat{i}' + (\Omega)\hat{j}' + (\dot{\psi})\hat{k}' \tag{A.16}$$

For the wheelset, the moment of inertia about the center of gravity is:

$$\bar{I}_W = (I_{W_1})\hat{i}' + (I_{W_2})\hat{j}' + (I_{W_1})\hat{k}' \tag{A.17}$$

since $I_{W_3} = I_{W_1}$. The angular momentum for the wheelset can be found from:

$$\bar{H}_G = (I_{W_1}\dot{\phi})\hat{i}' + (I_{W_2}\Omega)\hat{j}' + (I_{W_1}\dot{\psi})\hat{k}' \qquad (A.18)$$

The time rate change of angular momentum for the wheelset can be obtained from the relation:

$$\dot{\bar{H}}_G = \frac{d}{dt}\bar{H}_G + \bar{\omega}_{axis} \times \bar{H}_G \qquad (A.19)$$

where, $\bar{\omega}_{axis} = (\dot{\phi})\hat{i}' + (\dot{\psi})\hat{k}'$

substitution of the terms into Equation (A.19), leads to the expression for rate of change of angular momentum, which with respect to equilibrium axis is:

$$\dot{\bar{H}}_G = (I_{W_1}\ddot{\phi} - I_{W_2}\Omega\dot{\psi})\hat{i}''' + (I_{W_2}\Omega\dot{\phi} + I_{W_1}\ddot{\psi})\hat{k}''' \qquad (A.20)$$

In addition to this, the rates of change of angular momentum are also required for left and right wheels about the j' axis. Following the above procedure, these required expressions can be obtained as:

$$\dot{\bar{H}}_{G_L} \cdot \hat{j}' = \tfrac{1}{2}(I_{W_2}\ddot{\beta}_L) \qquad (A.21)$$

$$\dot{\bar{H}}_{G_R} \cdot \hat{j}' = \tfrac{1}{2}(I_{W_2}\ddot{\beta}_R) \qquad (A.22)$$

where for each wheel assembly, moment of inertia about $\hat{j}'$ is taken as $\frac{1}{2} I_{W_2}$.

A.2 The Axis System (Curved Track)

For curving analysis, two wheelsets connected through the truck frame are considered. In this case, wheelset axis system can be defined similarly to the tangent track. In Figure A.3, two wheelsets on a curved track is shown, where distance between the wheelset center is denoted by 2l. The fixed axis system in this case is referred to the truck reference frame denoted by "triple prime". If the axis systems are taken parallel to the plane of the tracks, the only difference between this and tangent track is the additional term l^*/R in the yaw direction. The l^*/R term is a result of the chosen coordinate system, which has the wheelset radially aligned with the track when $(\psi + l^*/R)$ is zero. As defined in Figure (A.3), the term $-l^*/R$ is equal to $+l/R$ for the leading (front) wheelset and $-l/R$ for the trailing (rear) wheelset.

Therefore, for curved track, the transformation matrices presented in (A.1) to (A.7) can be rewritten as:

$$\begin{Bmatrix} \hat{i}''' \\ \hat{j}''' \\ \hat{k}''' \end{Bmatrix} = \begin{bmatrix} 1 & -(\psi + \frac{l^*}{R}) & 0 \\ (\psi + \frac{l^*}{R}) & 1 & -\phi \\ 0 & \phi & 1 \end{bmatrix} \begin{Bmatrix} \hat{i}' \\ \hat{j}' \\ \hat{k}' \end{Bmatrix} \qquad (A.23)$$

$$\begin{Bmatrix} \hat{i}' \\ \hat{j}' \\ \hat{k}' \end{Bmatrix} = \begin{bmatrix} 1 & (\psi + \frac{l^*}{R}) & 0 \\ -(\psi + \frac{l^*}{R}) & 1 & \phi \\ 0 & -\phi & 1 \end{bmatrix} \begin{Bmatrix} \hat{i}''' \\ \hat{j}''' \\ \hat{k}''' \end{Bmatrix} \qquad (A.24)$$

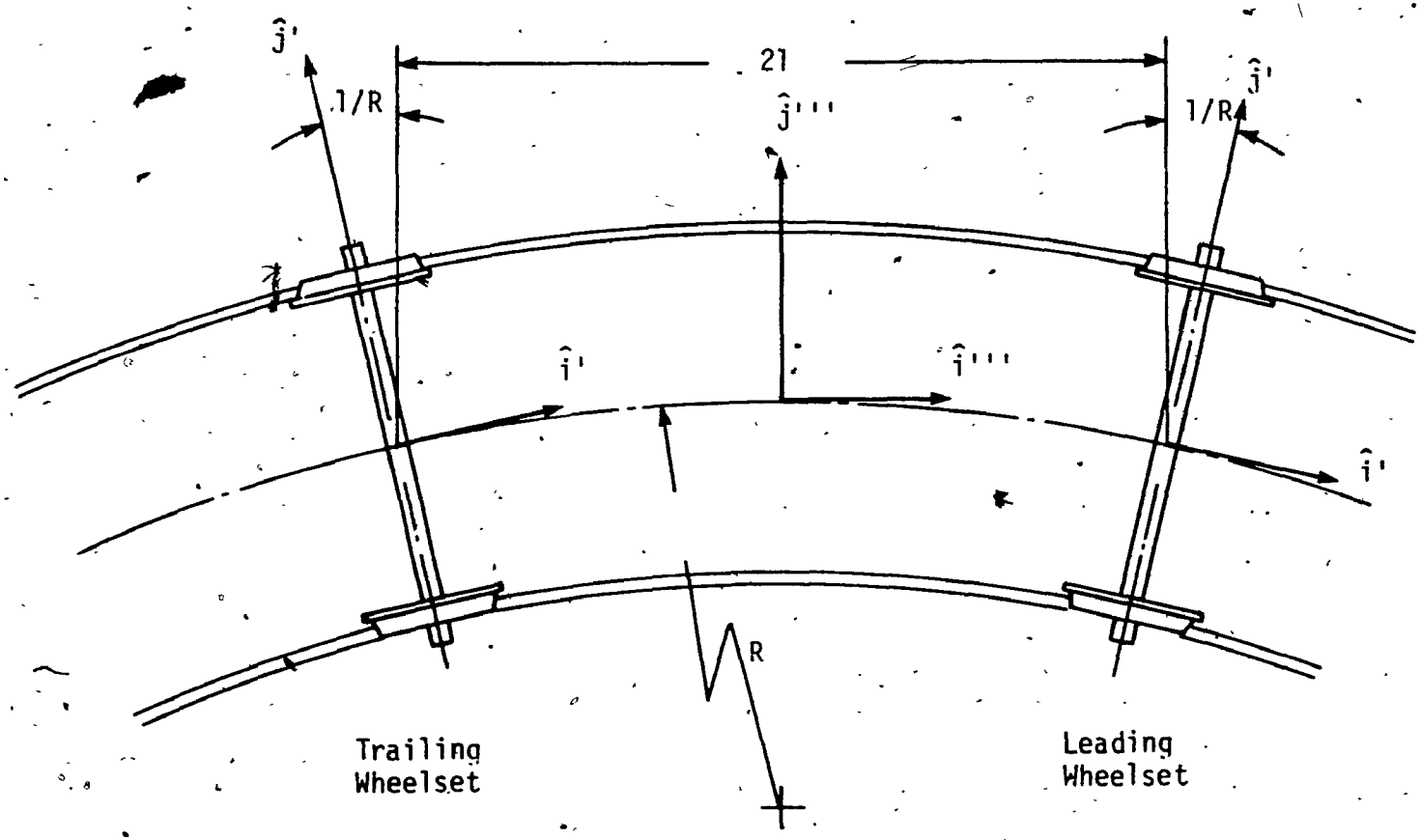

Figure A.3 Axis system for wheelsets on curved track.

$$\begin{Bmatrix} \hat{e}_{1_L} \\ \hat{e}_{2_L} \\ \hat{e}_{3_L} \end{Bmatrix} = \begin{bmatrix} 1 & (\psi + \frac{1^*}{R}) & 0 \\ -(\psi + \frac{1^*}{R}) & 1 & (\delta_L + \phi) \\ 0 & -(\delta_L + \phi) & 1 \end{bmatrix} \begin{Bmatrix} \hat{i}' \\ \hat{j}' \\ \hat{k}' \end{Bmatrix} \qquad (A.25)$$

and

$$\begin{Bmatrix} \hat{e}_{1_R} \\ \hat{e}_{2_R} \\ \hat{e}_{3_R} \end{Bmatrix} = \begin{bmatrix} 1 & (\psi + \frac{1^*}{R}) & 0 \\ -(\psi + \frac{1^*}{R}) & 1 & -(\delta_R - \phi) \\ 0 & (\delta_R - \phi) & 1 \end{bmatrix} \begin{Bmatrix} \hat{i}''' \\ \hat{j}''' \\ \hat{k}''' \end{Bmatrix} \qquad (A.26)$$

The other terms that will differ from tangent track are $\bar{\omega}_L$, $\bar{\omega}_R$, $\bar{\omega}$ and $\dot{\bar{H}}_G$. In the case of curved track, precision velocity V/R has to be included. Therefore angular velocity of the left and right wheels are:

$$\bar{\omega}_L = (\dot{\phi})\hat{i}' + (\Omega + \dot{\beta}_L)\hat{j}' + (\dot{\psi} - \frac{V}{R})\hat{k}' \qquad (A.27)$$

$$\bar{\omega}_R = (\dot{\phi})\hat{i}' + (\Omega + \dot{\beta}_R)\hat{j}' + (\dot{\psi} - \frac{V}{R})\hat{k}' \qquad (A.28)$$

And the angular velocity of the wheelset, similar to (A.16) is:

$$\bar{\omega} = (\dot{\phi})\hat{i}' + (\Omega)\hat{j}' + (\dot{\psi} - \frac{V}{R})\hat{k}' \qquad (A.29)$$

Therefore, in this case:

$$\dot{\bar{H}}_G = (I_{w_1}\dot{\phi})\hat{i}' + (I_{w_2}\Omega)\hat{j}' + [I_{w_1}(\dot{\psi} - \frac{V}{R})]\hat{k}' \qquad (A.30)$$

and $$\dot{\bar{H}}_G = \frac{d}{dt}\bar{H}_G + \dot{\bar{\omega}}_{axis} \times \bar{H}_G \qquad (A.31)$$

where, $$\bar{\omega}_{axis} = (\dot{\phi})\hat{i}' + (\psi - \frac{V}{R})\hat{k}'$$

Substitution of the terms into Equation (A.31) and transformation of axes leads to the angular momentum expression for the wheelset as:

$$\bar{H}_G = [I_{w_1}\ddot{\phi} - I_{w_2}\Omega(\dot{\psi} - \frac{V}{R})]\hat{i}''' + [I_{w_1}\ddot{\psi} + I_{w_2}\Omega\dot{\phi}]\hat{k}''' \qquad (A.32)$$

APPENDIX B

DERIVATION OF CREEP FORCES AND MOMENTS

In this section, the general expressions for creep forces and moments are derived for a curved track, where by setting R to infinity, will result in the expressions for tangent track. In Section 2.3.1, creep forces and moments for left and right wheels are defined by Equations (2.8) to (2.11) as:

$$\bar{F}_L = \left[\frac{f_{22}}{V}\left(-\dot{\bar{r}}_{L_c} \cdot \hat{e}_{2_L}\right) + \frac{f_{23}}{V}\left(-\bar{\omega}_{L_c} \cdot \hat{e}_{3_L}\right)\right]\hat{e}_{2_L} + \frac{f_{11}}{V}\left(-\dot{\bar{r}}_{L_c} \cdot \hat{e}_{1_L}\right)\hat{e}_{1_L} \quad (B.1)$$

$$\bar{M}_L = \left[\frac{f_{23}}{V}\left(\dot{\bar{r}}_{L_c} \cdot \hat{e}_{2_L}\right) + \frac{f_{33}}{V}\left(-\bar{\omega}_{L_c} \cdot \hat{e}_{3_L}\right)\right]\hat{e}_{3_L} \quad (B.2)$$

$$\bar{F}_R = \left[\frac{f_{22}}{V}\left(-\dot{\bar{r}}_{R_c} \cdot \hat{e}_{2_R}\right) + \frac{f_{23}}{V}\left(-\bar{\omega}_{R_c} \cdot \hat{e}_{3_R}\right)\right]\hat{e}_{2_R} + \frac{f_{11}}{V}\left(-\dot{\bar{r}}_{R_c} \cdot \hat{e}_{1_R}\right)\hat{e}_{1_R} \quad (B.3)$$

$$\bar{M}_R = \left[\frac{f_{23}}{V}\left(\dot{\bar{r}}_{R_c} \cdot \hat{e}_{2_R}\right) + \frac{f_{33}}{V}\left(-\bar{\omega}_{R_c} \cdot \hat{e}_{3_R}\right)\right]\hat{e}_{3_R} \quad (B.4)$$

The position vector at the left wheel point of contact is:

$$\bar{r}_{L_c} = \bar{r}_{CG} + \left[(a + \Delta l_w)\hat{j}' - r_L\right] \quad (B.5)$$

where Δl_w is the lateral displacement of contact point from equilibrium. $\bar{r}_{CG}$ is the position vector of wheelset center of gravity defined by Equation (A.8). Since the absolute velocity of the rail is zero, $\bar{\omega}_{L_c} = \bar{\omega}_L$ and $\bar{\omega}_{R_c} = \bar{\omega}_R$. Therefore, velocity of the left wheel contact point is:

$$\dot{\bar{r}}_{L_c} = \dot{\bar{r}}_{CG} + \bar{\omega}_L \times [(a + \Delta l_w)\hat{j}' - (r_L)\hat{k}'] \tag{B.6}$$

Substituting for $\dot{\bar{r}}_{CG}$ from Equation (A.9) and for $\bar{\omega}_L$ from Equation (A.27), performing the cross product, and transformation to equilibrium axis system, lead to the expression for left wheel contact point velocity as:

$$\dot{\bar{r}}_{L_c} = (\dot{x} + V - r_L\Omega - r_L\dot{\beta}_L - a\dot{\psi} + \frac{Va}{R})\hat{i}''' +$$

$$(\dot{y} + r_L\dot{\phi} - r_L\Omega\psi - r_L\Omega\frac{l^*}{R})\hat{j}''' + (\dot{z} + a\dot{\phi})\hat{k}''' \tag{B.7}$$

where, it is assumed that $(a + \Delta l_w) \simeq a$. Further, the products of perturbations as well as product of perturbation and 1/R are neglected as small. Similarly, for the right wheel contact point:

$$\dot{\bar{r}}_{R_c} = \dot{\bar{r}}_{CG} + \bar{\omega}_R \times [-(a + \Delta l_w)\hat{j}' - (r_R)\hat{k}'] \tag{B.8}$$

Substitution of $\dot{\bar{r}}_{CG}$ from Equation (A.9) and $\bar{\omega}_R$ from (A.28), and identical treatment as that of left wheel, lead to the expression for right wheel contact point velocity as:

$$\dot{\bar{r}}_{R_c} = (\dot{x} + V - r_R\Omega - r_R\dot{\beta}_R + a\dot{\psi} - \frac{Va}{R})\hat{i}''' +$$

$$(\dot{y} + r_R\dot{\phi} - r_R\Omega\psi - r_R\Omega\frac{l^*}{R})\hat{j}''' + (\dot{z} - a\dot{\phi})\hat{k}''' \tag{B.9}$$

Substituting for $\dot{\bar{r}}_{L_C}$, $\dot{\bar{r}}_{R_C}$, $\bar{\omega}_{L_C}$ and $\bar{\omega}_{R_C}$ from (B.7), (B.9), (A.27)

and (A.28), respectively, in to Equations (B.1) (to B.4), the general expressions for creep forces and moments can be obtained. Transformation of axis system from wheel/rail contact point to fixed equilibrium axis system using (A.25), and performing the dot products, the expressions for creep force and moment are obtained for left wheel as:

$$\bar{F}_L = \left[-\frac{f_{11}}{V}\left(\dot{x} + V - r_L\Omega - r_L\dot{\beta}_L - a\dot{\psi} + \frac{Va}{R}\right)\right]\hat{i}''' +$$

$$\left[-\frac{f_{22}}{V}\left(\dot{y} - V\psi - \frac{Vl^*}{R} + r_L\dot{\phi}\right) - \frac{f_{23}}{V}\left(\dot{\psi} - \frac{V}{R} - \delta_L\Omega\right) -\right.$$

$$\left.\frac{f_{11}}{V}\left(V\psi - r_L\Omega\psi + \frac{Vl^*}{R} - r_L\Omega\frac{l^*}{R}\right)\right]\hat{j}''' \qquad \text{(B.10)}$$

$$\bar{M}_L = \left[\frac{f_{23}}{V}\left(\dot{y} - V\psi - \frac{Vl^*}{R} + r_L\dot{\phi}\right) - \frac{f_{33}}{V}\left(\dot{\psi} - \frac{V}{R} - \delta_L\Omega\right)\right]\hat{k}''' \qquad \text{(B.11)}$$

(B.11)

Similarly for right wheel:

$$\bar{F}_R = \left[-\frac{f_{11}}{V}\left(\dot{x} + V - r_R\Omega - r_R\dot{\beta}_R + a\dot{\psi} - \frac{Va}{R}\right)\right]\hat{i}''' +$$

$$\left[-\frac{f_{22}}{V}\left(\dot{y} - V\psi - \frac{Vl^*}{R} + r_R\dot{\phi}\right) - \frac{f_{23}}{V}\left(\dot{\psi} - \frac{V}{R} + \delta_R\Omega\right) -\right.$$

$$\left.\frac{f_{11}}{V}\left(V\psi - r_R\Omega\psi + \frac{Vl^*}{R} - r_R\Omega\frac{l^*}{R}\right)\right]\hat{j}''' \qquad \text{(B.12)}$$

$$\bar{M}_R = \left[\frac{f_{23}}{V}\left(\dot{y} - V\psi - \frac{Vl^*}{R} + r_R\dot{\phi}\right) - \frac{f_{33}}{V}\left(\dot{\psi} - \frac{V}{R} + \delta_R\Omega\right)\right]\hat{k}''' \qquad \text{(B.13)}$$

In these derivations, it is maintained that the angles are small, the creep coefficients are constant, and the rails are rigid. The Equations (B.10) to (B.13) are the general expressions for creep forces and moments for curved track of radius R. For tangent track, R is

infinite, and for curved track, the term 1*/R is + 1/R for the leading wheelset and -1/R for the trailing wheelset.

APPENDIX C

SIMPLIFICATION OF LONGITUDINAL, ROLL, AND VERTICAL EQUATIONS

C.1 Longitudinal Equation

In this section, it is shown that the wheelset longitudinal equation of motion simply reduces to a kinematic relation. The longitudinal equation of the EDCW model obtained in Chapter 2 as Equation (2.27) is:

$$m_w\ddot{x} + \frac{f_{11}}{V}\left[\dot{2x} + 2V - \Omega(r_L + r_R) - r_L\dot{\beta}_L - r_R\dot{\beta}_R\right] + F_{s_{p_x}} = 0 \qquad (C.1)$$

Since it is assumed that the wheelset is travelling at constant velocity without any longitudinal perturbation,

$$x = \dot{x} = \ddot{x} = 0 \qquad \text{and} \qquad F_{s_{p_x}} = 0$$

Also, the spin motion of left and right wheels about $\hat{j}'$ is antisymmetric, i.e., $\beta_L = -\beta_R$. Therefore, the longitudinal Equation (C.1) can be simplified to:

$$2V = \Omega(r_L + r_R) \qquad (C.2)$$

Substituting $\Omega = V/r_o$, results in:

$$(r_L + r_R) = 2r_o \qquad (C.3)$$

Letting $r_L = r_o + \Delta r_L$ and $r_R = r_o + \Delta r_R$, where Δr_L and Δr_R are the

changes in rolling radii, Equation (C.3) becomes:

$$r_0 + \Delta r_L + r_0 + \Delta r_R = 2r_0$$

$$\text{or} \quad \Delta r_L = -\Delta r_R \tag{C.4}$$

which simply states that the rolling radius of one wheel will decrease by the same amount the other increases. From another point of view, antisymmetry of the spin motion can be shown by substituting for $(r_L + r_R)$ by $2r_0$ in Equation (C.1).

C.2 Roll and Vertical Equations

In this section, the vertical and roll equations of wheelset are used to obtain an expression for normal force terms in the wheelset lateral Equation (2.31), which is:

$$(N_L + N_R)\phi + N_L\delta_L - N_R\delta_R \tag{C.5}$$

Multiplying the vertical Equation (2.29) by 'a':

$$(N_L + N_R)a = (m_w\ddot{z} + m_w g + W'_{APP} + F_{s_{p_z}})a \tag{C.6}$$

Adding Equation (C.6) to the roll Equation (2.33) gives

$$N_L = \frac{1}{2a}\{(m_w\ddot{z} + m_w g + W'_{APP} + F_{s_{p_z}})a + [I_{w_1}\ddot{\phi} - I_{w_2}\Omega\dot{\psi} + \frac{2f_{22}r_0}{V}(\dot{y} + r_0\dot{\phi} - V\psi) + f_{23}(\frac{2r_0}{V}\dot{\phi} + \delta_R - \delta_L) - M_{s_{p_x}}]\} \tag{C.7}$$

And subtracting Equation (C.6) from the roll Equation (2.33) results in:

$$N_R = \frac{1}{2a}\{(m_w\ddot{z} + m_w\eta + W'_{APP} + F_{s_{p_z}})a - [I_{w_1}\ddot{\phi} - I_{w_2}\Omega\dot{\psi} + \frac{-2f_{22}r_0}{V}(\dot{y} + r_0\dot{\phi} - V\psi) + f_{23}(\frac{2r_0}{V}\dot{\phi} + \delta_R - \delta_L) - M_{s_{p_x}}]\} \quad (C.8)$$

From Equation (C.6):

$$(N_L + N_R)\phi = (m_w g + W'_{APP})\phi \quad (C.9)$$

and from Equations (C.7) and (C.8):

$$(N_L\delta_L - N_R\delta_R) = (m_w g + W'_{APP})(\frac{\delta_L - \delta_R}{2}) - I_{w_2}\Omega\dot{\psi}(\frac{\delta_L + \delta_R}{2a}) \quad (C.10)$$

where all the product of small quantities are neglected. The second term in the right hand side of (C.10) is retained, which represents dynamic effect. The expression for (C.5) can now be obtained from (C.9) and (C.10) as:

$$(N_L + N_R)\phi + N_L\delta_L - N_R\delta_R = W_{APP}(\phi + \frac{\delta_L - \delta_R}{2}) - I_{w_2}\Omega\dot{\psi}(\frac{\delta_L + \delta_R}{2a}) \quad (C.11)$$